Distribution Agreement

In presenting this thesis or dissertation as a partial fulfillment of the requirements for an advanced degree from Emory University, I hereby grant to Emory University and its agents the non-exclusive license to archive, make accessible, and display my thesis or dissertation in whole or in part in all forms of media, now or hereafter known, including display on the world wide web. I understand that I may select some access restrictions as part of the online submission of this thesis or dissertation. I retain all ownership rights to the copyright of the thesis or dissertation. I also retain the right to use in future works (such as articles or books) all or part of this thesis or dissertation.

Signature:

_____ _____

Charles B. Wright Date

Evaluation of *Rpe65* mutant mice as models for Leber congenital amaurosis, type 2, an early onset blindness

By

Charles B. Wright, B.S.

Graduate Division of Biological and Biomedical Science
Genetics and Molecular Biology

_____
Advisor: John M. Nickerson, Ph.D.

_____
Committee Member: Jeffrey H. Boatright, Ph.D.

_____
Committee Member: Machelle T. Pardue, Ph.D.

_____
Committee Member: Erwin Van Meir, Ph.D.

_____
Committee Member: Anthony W. Chan, Ph.D.

Accepted:

_____
Lisa A. Tedesco, Ph.D.
Dean of the James T. Laney School of Graduate Studies

_____
Date

Evaluation of *Rpe65* mutant mice as models for Leber congenital amaurosis, type 2, an early onset blindness

By

Charles B. Wright

B.S., Clemson University, 2007

Advisor: John M. Nickerson, Ph.D.

An abstract of
A dissertation submitted to the Faculty of the
James T. Laney School of Graduate Studies of Emory University
in partial fulfillment of the requirements for the degree of
Doctor of Philosophy
in Graduate Division of Biological and Biomedical Sciences,
Genetics and Molecular Biology, 2013

Abstract

Evaluation of *Rpe65* mutant mice as models for Leber congenital amaurosis, type 2, an early onset blindness

By

Charles B. Wright

The initial steps in vision start with light detection by visual pigment located in the neural retina and recycling of the visual pigment in the adjacent retinal pigment epithelium (RPE). RPE65 is a critical enzyme in the recycling of 11-*cis*-retinal, a cofactor that is required for light-sensitivity in the retina. When RPE65 is mutated, it causes a severe childhood-onset blindness called Leber congenital amaurosis, type 2 (LCA2). The *Rpe65* gene knockout (KO) mouse was developed for the study and treatment of LCA2 and resembles the human disease in many important ways, but the KO mouse has a large *Rpe65* gene deletion and such mutations are rarely found in humans. New mouse models, tvrm148 and rd12, contain point mutations in the *Rpe65* gene that are similar to, or identical to, mutations found in humans. I hypothesized that the tvrm148 or rd12 point mutations would result in visual phenotypes different from the KO. I found that the tvrm148 mutation in *Rpe65* caused a loss in visual function that was virtually identical to the KO because of low levels of RPE65 protein that had no enzymatic activity. In contrast, the rd12 mutation caused a much faster loss of visual function compared to tvrm148 or KO mice and inherited in a semidominant fashion, unlike the KO and many typical LCA2 patients. These mice produced no detectable RPE65 protein and no RPE65 enzymatic activity. The rd12 mice accumulated mutant *Rpe65* mRNA that inefficiently associated with ribosomes for translation, and I conclude this contributes to the unusually aggressive form of blindness. These findings supported my hypothesis that point mutations could produce visual defects that differed from the KO mutation. These findings are important because treatments being developed for the disease are based on work in the KO mouse, and my work suggests that these treatments may not be as effective for all human mutations. Furthermore, because the rd12 mutation is found in humans and because my findings showed that it produced a more aggressive blindness, I recommend these patients need to be monitored for an unusually aggressive form of LCA2 that might be more difficult to treat.

Evaluation of *Rpe65* mutant mice as models for Leber congenital amaurosis, type 2, an early onset blindness

By

Charles B. Wright

Advisor: John M. Nickerson, Ph.D.

A dissertation submitted to the Faculty of the
James T. Laney School of Graduate Studies of Emory University
in partial fulfillment of the requirements for the degree of
Doctor of Philosophy
in Graduate Division of Biological and Biomedical Sciences,
Genetics and Molecular Biology, 2013

Table of Contents

List of Figures

List of Tables

List of Abbreviations

A2E—2-[2,6-dimethyl-8-(2,6,6-trimethyl-1-cyclohexen-1-yl)-1*E*,3*E*,5*E*,7*E*-octatetraenyl]-1-(2-hydroxylethyl)-4-[4-methyl-6-(2,6,6-trimethyl-1-cyclohexen-1-yl)-1*E*,3*E*,5*E*-hexatrienyl]-pyridinium

ACHM—Achromatopsia

adRP—Autosomal dominant retinitis pigmentosa

AIM2—Absent in melanoma 2

Albino C57BL/6J—C57BL/6J$^{c\text{-}2J}$

ANOVA—Analysis of variance

AOS—Accessory optic system

AP—Activator protein

arCSRD—Autosomal recessive childhood-onset severe retinal dystrophy

ARPE-19—Adult retinal pigment epithelial cell 19

arRP—Autosomal recessive retinitis pigmentosa

ARVO—Association for Research in Vision and Ophthalmology

BAD—Bcl-2-associated death promoter protein

BAX—Bcl-2-associated X protein

BCA—Bicinchoninic acid

BCL-2—B-cell lymphoma 2

BCMO1—Beta-carotene 15,15′-monooxygenase 1

BMF—Bcl-2-modifying factor

CASP1—Caspase-1

CathS—Cathepsin S

CNGA1—Cyclic nucleotide gated channel alpha 1

CSNB—Congenital stationary night blindness

CPFL1—Cone photoreceptor function loss 1

DFT—Discrete Fourier Transform

DM1—Myotonic dystrophy, type 1

DNA—Deoxyribonucleic acid

dsRNA—Double-stranded ribonucleic acid

DTT—Dithiothreitol

E—Embryonic day

EDTA—Ethylenediaminetetraacetic acid

ENU—*N*-ethyl-*N*-nitrosourea

ER—Endoplasmic reticulum

ERG—Electroretinogram

FISH—Fluorescence *in situ* hybridiziation

FMR1—Fragile X mental retardation 1

fMRI—Functional magnetic resonance imaging

FA—Fundus albipunctatus

FXTAS—Fragile X-associated tremor ataxia syndrome

GA—Geographic atrophy

GCL—Ganglion cell layer

GNAT—Guanine nucleotide-binding protein, alpha transducing activity polypeptide

GRK1—G protein-coupled receptor kinase 1

HEK293—Human embryonic kidney 293

HPLC—High-performance liquid chromatography

HRP—Horseradish peroxidase

IACUC—Institutional Animal Care and Use Committee

IFN—Interferon

IFNAR—Interferon alpha receptor

IFNGR—Interferon gamma receptor

IL—Interleukin

INL—Inner nuclear layer

ipRGC—Intrinsically photosensitive retinal ganglion cell

IRBP—Interphotoreceptor retinoid-binding protein

IRES—Internal ribosome entry site

IRF—Interferon response factor

IS—Inner segment

ISH—*In situ* hybridization

KO/+—$Rpe65^{KO/+}$

KO/KO—$Rpe65^{KO/KO}$

KO/rd12—$Rpe65^{KO/rd12}$

LAMP2—Lysozyme-associated membrane protein 2

LCA—Leber congenital amaurosis

LRAT—Lecithin retinol acyltransferase

M cone—Green-sensitive cone

MAVS—Mitochondrial antiviral signaling protein

miRNA—microRNA

mRNA—Messenger ribonucleic acid

mRNP—Messenger ribonucleoprotein

MWL—Middle wavelength

MyD88—Myeloid differentiation primary response gene 88

NAS—Nonsense-associated altered splicing

NCL—Neural ceroid lipofuscinosis

NF—Nuclear factor

NFKB1—Nuclear factor kappa light polypeptide gene enhancer in B-cells 1

NLR—Nucleotide-binding domain and leucine-rich repeat containing

NLRC4—NLR family, CARD domain containing 4

NLRP3—NLR family, pyrin domain containing 3

NMD—Nonsense-mediated decay

NOD—Nucleotide-binding oligomerization domain containing

OKR—Optokinetic response

OKT—Optokinetic tracking

OMIM—Online Mendelian Inheritance in Man

ONH—Optic nerve hypoplasia

ONL—Outer nuclear layer

OP—Oscillatory potential

OS—Outer segment

P—Postnatal day

P body—Processing body

PANTHER—Protein Analysis Through Evolutionary Relationships

PCR—Polymerase chain reaction

PDE6—Phosphodiesterase 6

PhD-SNP—Predictor of Human Deleterious Single Nucleotide Polymorphisms

PLR—Pupillary light response

polyPhen 2.0—Polymorphism Phenotyping 2.0

PROVEAN—Protein Variation Effect Analyzer

PTC—Premature termination codon

qRT-PCR—Quantitative real time polymerase chain reaction

QTL—Quantitative trait locus

R91W—*Rpe65*^{R91W}

rAAV—Recombinant adeno-associated viral vector

RAL—Retinal

RAR—Retinoic acid receptor

rd12—retinal degeneration 12

rd12/+—*Rpe65*$^{rd12/+}$

rd12/rd12—*Rpe65*$^{rd12/rd12}$

RDH—Retinol dehydrogenase

RE—Retinyl ester

REST—Retinyl ester storage particle

RGC—Retinal ganglion cell

RGR—Retinal G protein-coupled receptor

Rho—Rhodopsin

RIPA buffer—Radioimmunoprecipitation assay buffer

RLR—RIG-1-like receptor

RM-ANOVA—Repeated measures analysis of variance

RNA—Ribonucleic acid

ROL—Retinol

RP—Retinitis pigmentosa

RPE—Retinal pigment epithelium

RPE65—Retinal pigment epithelium-specific protein 65 kDa

RRH—Retinal pigment epithelium-derived rhodopsin homolog

RT-PCR—Reverse transcriptase polymerase chain reaction

RTC—Read through compound

RXR—Retinoid X receptor

tvrm148/+—*Rpe65*$^{tvrm148/+}$

tvrm148/KO—*Rpe65*$^{tvrm148/KO}$

tvrm148/tvrm148—*Rpe65*$^{tvrm148/tvrm148}$

S cone—UV-sensitive cone

S/MAR—Scaffold/matrix attachment region

SDS—Sodium dodecyl sulfate

SDS-PAGE—Sodium dodecyl sulfate polyacrylamide gel electrophoresis

SIFT—Sorting Intolerant from Tolerant

SMD—Staufen-mediated decay

SNAP—Screening for Non-Acceptable Polymorphisms

SNK—Student-Newman-Keuls

SNP—Single nucleotide polymorphism

SOPA—Summed oscillatory potential amplitude

ssRNA—Single-stranded ribonucleic acid

SWL—Short wavelength

TEM—Transmission electron microscopy

Ticam1—Toll-like receptor adaptor molecule 1

TLR—Toll-like receptor

TVRM—Translational Vision Research Model

UNC93B1—Unc-93 homolog B1 (C. elegans)

UTR—Untranslated region

UV—Ultraviolet

VAD—Vitamin A-deficient

VEP—Visual-evoked potential

VMD2—Vitelliform macular dystrophy 2

VWT—Visual water task

Wild type or +/+—*Rpe65*$^{+/+}$

I: Introduction

This chapter is currently being prepared as a review article.

Key questions to be addressed in this section:

1. What are the eye, retina, and retinal pigment epithelium (RPE)?
2. What is the visual cycle?
3. What is RPE65?
4. What happens to visual function when RPE65 is not working?
5. What are some known (or suspected) mutations occurring in the mouse *Rpe65* gene?
6. How have mouse *Rpe65* gene mutations helped to develop treatments for patients in the clinic?
7. Why is it important to study other mouse *Rpe65* gene mutations?

1.1—PURPOSE AND CENTRAL HYPOTHESIS

RPE65 is a protein that serves a vital role in maintaining healthy vision in humans. It is found in a single cell layer, called the retinal pigment epithelium (RPE), which sits underneath the retina (the light-sensitive tissue in the eye). The *RPE65* gene encodes the information to make the protein, and when mutated, leads to a severe visual impairment, Leber congenital amaurosis (LCA); often, children are born with severe visual impairment and are completely blind by childhood or early adulthood. Most human *RPE65* gene mutations result in reduced RPE65 enzymatic activity. To develop treatments for this disease, researchers have turned to mice, using their similar anatomy, physiology, and biochemistry to create therapies that are currently being tested in the clinic for safety and efficacy. Most work that has been conducted in mice has been performed in a single lineage (the *Rpe65* gene knockout mouse, a.k.a. KO). It accurately models many LCA cases, but the variety of human mutations (most are point mutations rather than the large deletions used to create the KO mouse) seen in the clinic raises the question of whether all *RPE65* mutations produce similar physiological and biochemical phenotypes in all cases of LCA. This project aimed to test whether two other mouse *Rpe65* gene mutations, tvrm148 and rd12 (analogous to known human *RPE65* mutations), produced similar effects with respect to visual function and cell biology as the well-studied KO mouse. This study is important with respect to modeling LCA.

The central purpose of this project was to test whether different mouse mutations produced similar phenotypic outcomes as the KO mouse line, and by extension, whether all human *RPE65* gene mutations could be expected to produce similar phenotypic outcomes. My central hypothesis was that different mouse *Rpe65*

gene mutations would behave differently from the KO mutation with respect to phenotype and molecular biology. This work was significant to the study of the disease and to treatment development because the information presented here could allow for the use of mouse models that more accurately model the human disease. The tvrm148 mutation is located in a region of the gene that is rich in pathogenic mutations in humans. The rd12 mutation is actually found in humans. If the tvrm148 and rd12 mutations were found to not produce phenotypes like the KO mutation in mice, humans with similar or identical mutations could be suspected of responding differently to treatments now being tested in the clinic. Hypotheses testing different aspects of each mutation's manifestation, along with whether these hypotheses were supported or rejected and the data interpreted to support or reject those hypotheses, are located in Table 1.1 (tvrm148) and Table 1.2 (rd12).

This dissertation is divided into five sections. The first section (this one, **I: Introduction**) is an introduction that will provide basic information necessary for the basic comprehension of the research being presented in later sections. The second section (**II: Cellular pathologies in RPE65-deficient mice**) will provide in-depth information concerning RPE65 deficiency in mice that will be useful for experts in the field. The third (**III: Complementation test of *Rpe65* knockout and tvrm148**) and fourth (**IV: The rd12 allele exerts a semidominant negative effect on visual function in mice**) sections will report my findings with the tvrm148 and rd12 mutations, respectively. The final section (**V: Discussion and future directions**) will provide preliminary data that will form the foundation for future studies with these mutations and will discuss the

shortcomings and significance of my work. Before and after each section are questions and key points that will guide readers in their understanding of the project.

Table 1.1—Hypotheses tested concerning the tvrm148 mutation

Hypothesis	Supported?	Data Figure
tvrm148 is in *Rpe65*	YES	3.4, 3.5
tvrm148 is recessively-inheriting	YES	3.6, 3.7
tvrm148 leads to visual function loss	YES	3.6, 3.7
tvrm148 visual phenotype is similar to KO	YES	3.5, 3.8
tvrm148 produces hallmark LCA2 morphology seen in human patients (slight retina thinning, intact retina architecture, cone nuclei loss, lipid droplets in RPE)	YES	3.9, 3.10, 3.11, 3.12
tvrm148 produces non-functional gene product	YES	3.13, 3.14, Table 3.3

Table 1.2—Hypotheses tested concerning the rd12 mutation

Hypothesis	Supported?	Data Figure
rd12 is in *Rpe65*	YES	4.3, 4.5
rd12 is recessively-inheriting	NO	4.6, 4.9
rd12 leads to visual function loss	YES	4.5, 4.6, 4.7, 4.8
rd12 visual phenotype is similar to KO	NO	4.5, 4.6
rd12 produces non-functional gene product	YES	Table 4.2
rd12 produces hallmark LCA2 morphology (slight retina thinning, intact retina architecture, cone nuclei loss)	YES	4.11, 4.12, 4.13
rd12 produces truncated toxic peptide	NO	4.14
rd12 mRNA expressed but sequestered in nucleus	NO	4.15
rd12 mRNA contains splicing errors or other mutations	NO	Table 4.3
rd12 mRNA adopts abnormal secondary structure	NO	4.16
rd12 mRNA localized differently with respect to RPE (in cytoplasm or extracellularly)	NO	4.17
rd12 mRNA has abnormal association with ribosomes	YES	4.19, 4.20, 4.21

1.2—THE VISUAL SYSTEM: ANATOMY, BIOCHEMISTRY, AND VISUAL ASSESSMENT

1.2.1—Anatomy of the eye

The eye is the organ that allows for vision, the ability to see the world (Fig. 1.1). The globe shape of the eye is maintained mostly by the sclera, a fibrous, protective outer layer of the eye that is white in color. Light enters through the transparent cornea and passes through the lens, which further focuses the light onto the light sensitive tissue of the eye, the neural retina (Fig. 1.1). The neural retina processes the light it detects into a neural signal that can pass through the optic nerve to the brain. The retina (Fig. 1.2) contains three types of photoreceptor cells: rods, which mediate colorless vision and operate under dim light conditions; cones, which mediate color vision and operate under bright light conditions; and, intrinsically photosensitive retinal ganglion cells (ipRGCs), which, among other functions, help set the body's internal clock for daily biological rhythms (i.e. circadian rhythms) (Masland 2012). Rod and cone photoreceptors, which have their nuclei in the ONL, have the majority of their mitochondria located in the inner segments (IS) and stacks of light-sensitive rhodopsin and cone opsin proteins in outer segments (OS), respectively (Fig. 1.2). Layers of the retina include the outer nuclear layer (ONL; contains photoreceptor cell nuclei), inner nuclear layer (INL; contains bipolar, horizontal, and amacrine cells), and the ganglion cell layer (GCL; contains ganglion cells) (Masland 2012). Müller cells (Fig. 1.2) extend through many layers of the retina; they largely serve a structural role for supporting the retina but may also be involved in retinoid processing for cone photoreceptors. Rhodopsin and cone opsin proteins detect light and cause the photoreceptors to send the visual signal to the INL, which contains horizontal cells,

bipolar cells, and amacrine cells (Masland 2012). The cells in the INL help to amplify, process, and integrate the visual signal so it can then be sent to the GCL. In the GCL, other ganglion cells (not the ipRGCs that are also present in the GCL) further coordinate and send the visual signal along the nerve fiber layer (NFL) to the optic nerve so it can then be sent to the brain (Masland 2012). Underneath the retina is the retinal pigment epithelium (RPE), a pigmented cell type that is one cell layer thick, and that derives its blood supply from the choroid (Fig. 1.1). The RPE serves many purposes (Strauss 2005), but it is primarily involved in maintaining the health of the neural retina, providing a physical barrier that separates neural tissue from systemic blood circulation, and participating in vital biochemical pathways like the visual cycle (Fig. 1.1B) (Strauss 2005). The biochemistry of the visual cycle is discussed below.

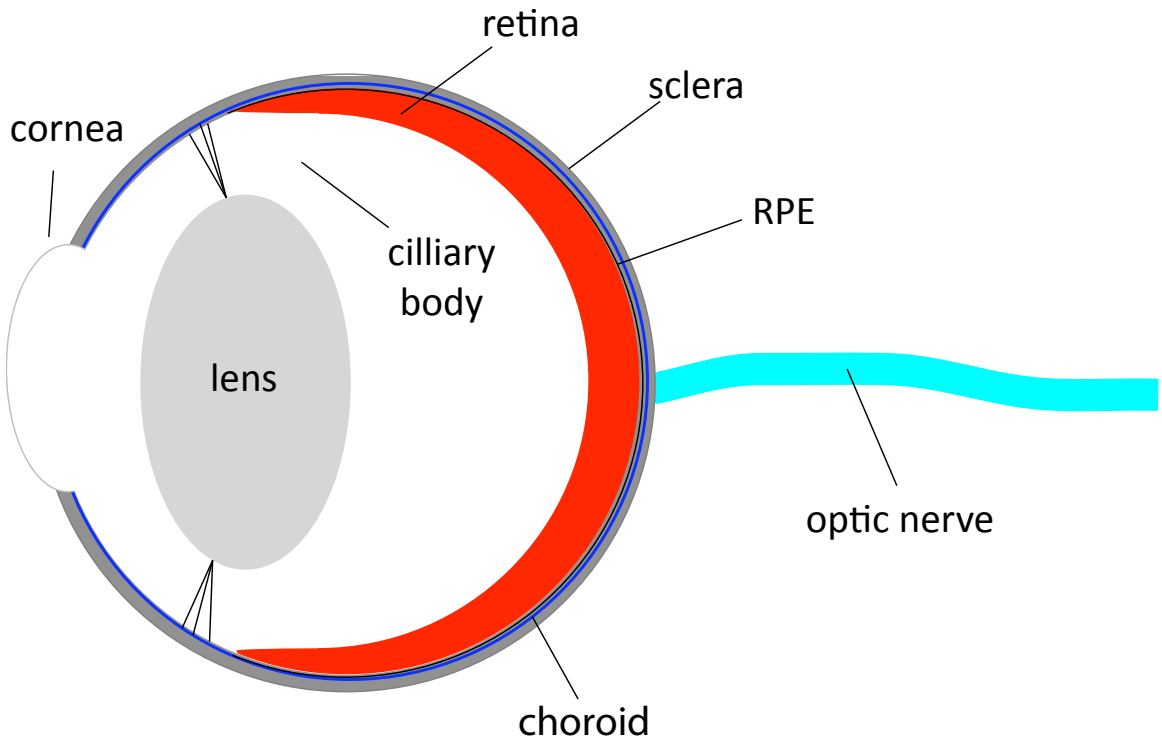

Figure 1.1—Anatomy of the eye. Simplified anatomy of the eye with basic structures shown. The cornea is the transparent tissue in the front of the eye that light passes through. The lens helps to further focus light on the retina, which is the light sensitive tissue in the eye. The ciliary body connects to the lens and helps it to better focus light. Underneath the retina is the RPE, which helps provide support for retinal health. The visual signal in response to light is passed through the optic nerve to the brain for processing. Surrounding the eye is the sclera, which helps form the exterior of the eye and maintains globe shape. The choroid lies between the sclera and the RPE and provides the RPE with blood supply (so the RPE can then pass oxygen and other nutrients to the outer retina).

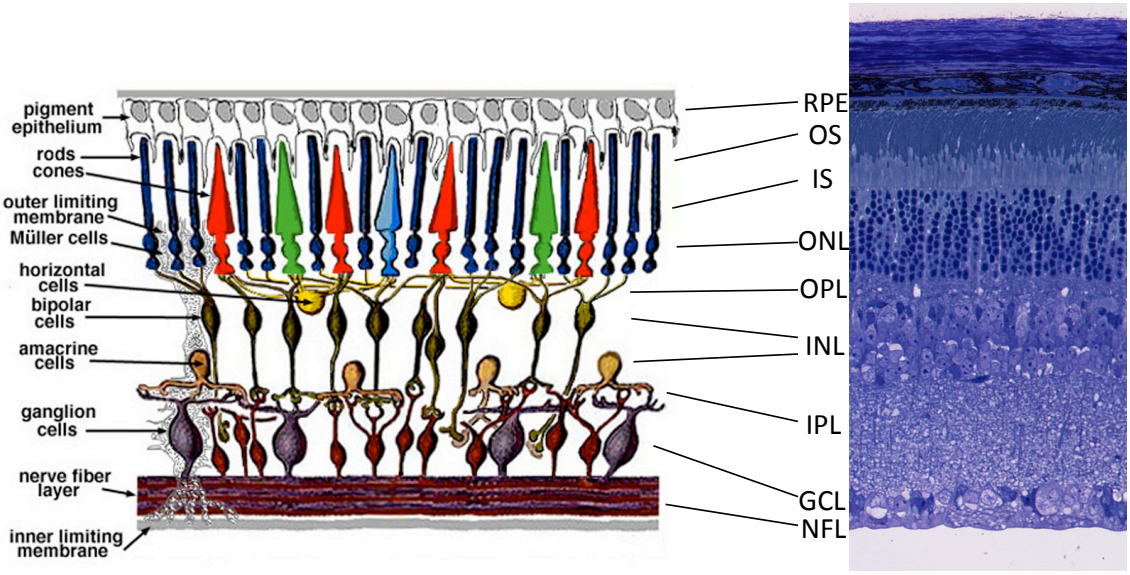

Figure 1.2—Anatomy of the mammalian retina. On the left, a diagram of the cells in the mammalian retina is shown; a typical wild type mouse retina at P60 is shown for comparison. At the top is the RPE, a cell layer that participates in the visual cycle (discussed in detail below). Figure adapted from Webvision (http://webvision.med.utah.edu/) for noncommercial purposes and reproduced under an Attribution, Noncommercial, No Derivative Works Creative Commons license. RPE, retinal pigment epithelium; OS, outer segments; IS, inner segments; ONL, outer nuclear layer; OPL, outer plexiform layer; INL, inner nuclear layer; IPL, inner plexiform layer; GCL, ganglion cell layer; NFL, nerve fiber layer.

1.2.2—Biochemistry

The visual cycle (Fig. 1.3) is essential for maintaining healthy vision. Rod photoreceptor cells contain a light-sensitive protein called rhodopsin (found in outer segments; OS), which is capable of detecting a single photon of light. In order to be sensitive to light, rhodopsin has a light-sensitive molecule, 11-*cis*-retinal (11-*cis*-RAL), covalently bound to it as a cofactor (Saari 2012). Upon exposure to light (Fig. 1.3), 11-*cis*-RAL spontaneously isomerizes to all-*trans*-retinal (all-*trans*-RAL), which then separates from rhodopsin (rhodopsin without a retinoid cofactor is called rod opsin protein). This first step initiates the phototransduction cascade (Fig. 1.4). Retinol dehydrogenase 8 (RDH8) in the rod photoreceptor converts all-*trans*-RAL to all-*trans*-retinol (all-*trans*-ROL; Fig. 1.3) (Saari 2012). Interphotoreceptor retinoid binding protein (IRBP) binds all-*trans*-ROL (Saari 2012) from the rod photoreceptor cell and releases it to the RPE (known to be at least partially mediated by IRBP). Lecithin-retinol acyltransferase (LRAT) converts all-*trans*-ROL to all-*trans*-retinyl ester (all-*trans*-RE), and retinal pigment epithelium-specific protein 65 kDa (RPE65) is responsible for regeneration of the 11-*cis* double bond (Saari 2012) by isomerizing all-*trans*-RE to 11-*cis*-retinol (11-*cis*-ROL; Fig. 1.3). Retinol dehydrogenase 5 (RDH5) converts 11-*cis*-ROL to 11-*cis*-RAL, and IRBP protects the light-sensitive 11-*cis* double bond while 11-*cis*-RAL is transported back to the rod photoreceptor (Fig. 1.3) (Saari 2012). 11-*cis*-RAL then covalently bonds with rod opsin protein to reform functional rhodopsin protein (which is then capable of detecting another photon). 11-*cis*-RAL is absolutely necessary for rod and cone opsin sensitivity to light. Blocks in 11-*cis*-RAL synthesis result in blindness. Mutations in *RPE65* and *LRAT* result in LCA, but mutations in other genes in the visual cycle may result in less severe visual

deficits. The important findings that lead to the modern understanding of the visual cycle will be discussed in detail below in "*1.3—History of the visual cycle*."

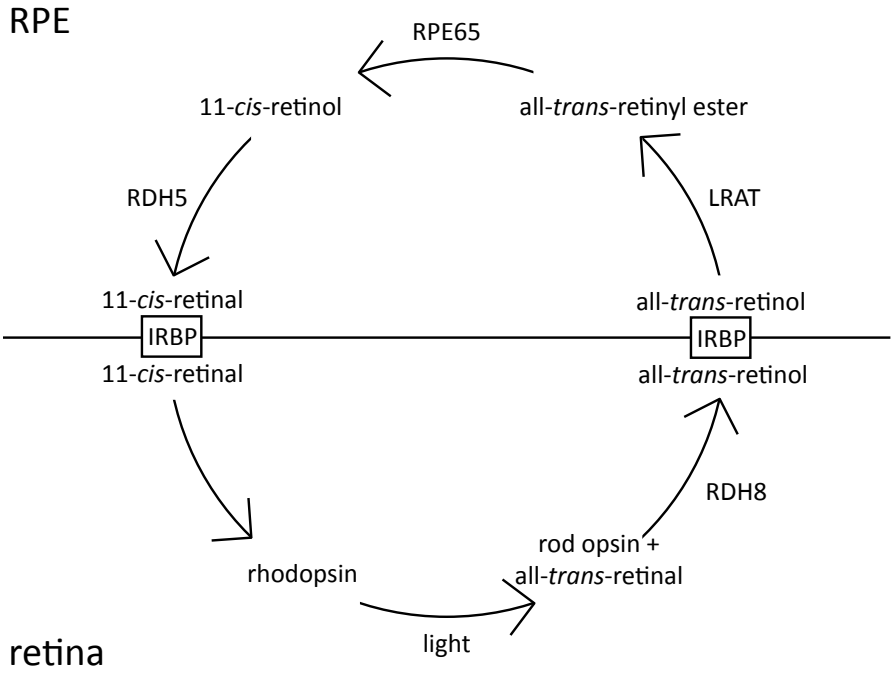

Figure 1.3. Biochemistry of the visual cycle. The retina and RPE contain components necessary for the visual cycle, which recycles all-*trans*-retinol to 11-*cis*-retinal to continuously replenish the supply of functional, light sensitive opsin proteins in photoreceptors.

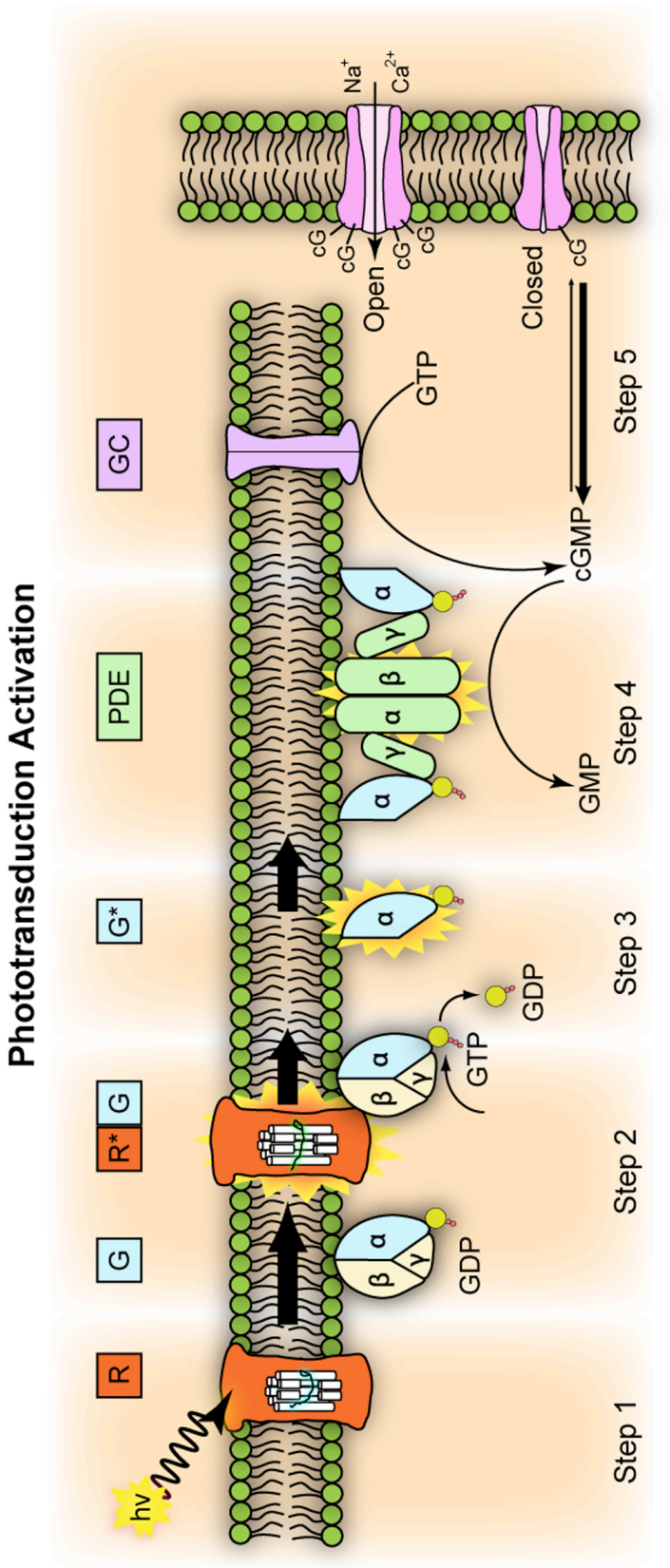
Phototransduction Activation
R
G
R*
G
G*
PDE
GC
hν
GDP
GTP
GDP
GTP
cGMP
GMP
Open
Closed
cG
Na+
Ca2+
Step 1
Step 2
Step 3
Step 4
Step 5

Figure 1.4—The isomerization of 11-*cis*-RAL to all-*trans*-RAL by light initiates the phototransduction cascade. The phototransduction cascade is the series of steps that culminates in the hyperpolarization of the rod photoreceptor membrane so the visual signal can be sent to the INL (Fig. 1.2). In Step 1, a photon of light (hv) causes the spontaneous isomerization of 11-*cis*-RAL to all-*trans*-RAL (11-*cis*-RAL then has to be recycled by the visual cycle). Rhodopsin protein (R) then undergoes a conformational change to form R*. During Step 2, R* activates multiple transducin (G) proteins to G* that then exchange GDP for GTP. Alpha and beta subunits are released from G*. During Step 3, G* binds the gamma subunits of phosphodiesterase (PDE); the gamma subunits inhibit the alpha and beta subunits, so PDE becomes active. Step 4 of the phototransduction cascade consists of activated PDE hydrolyzing cyclic GMP (cGMP) to form GMP. Finally, in Step 5, with decreased levels of cGMP, cGMP-gated channels close to prevent the further influx of sodium and calcium ions. This causes the rod cell membrane to hyperpolarize and send the visual signal to bipolar cells in the INL (Fig. 1.2). This figure was adapted (Leskov, Klenchin et al. 2000) and reproduced with permission under the terms of the GNU Free Documentation License, version 1.2.

1.2.3—Visual assessment techniques

Optokinetic tracking (OKT; Fig. 1.5A) and electroretinography (ERG; Fig. 1.5B) are two methods for measuring visual function in mice, each one measuring the function of a different aspect of the visual system. OKTs are a behavioral measurement of visual function, and ERGs are a physiological measure of retinal function. One form of measurement does not supplant the other, but rather complement each other to provide information about visual function at different levels.

OKT measures the spatial vision of the mouse by measuring its ability to detect a moving striped gradient (either virtual or physical) that moves across the mouse's field of vision (Fig. 1.5A). A mouse sits on a platform in the middle of four computer screens facing inward that project a virtual rotating striped gradient (Prusky, Alam et al. 2004; Douglas, Alam et al. 2005). When the visual signal passes through the optic nerve, some of the axons cross the optic chiasm and continue to the visual cortex in the brain (Fig. 1.5A), while other axons carry the visual signal to the accessory optic system (AOS). In the AOS, neurons sensitive to directional movement detect the movement of the spatial gradient. The AOS then sends efferent signals to muscles to track the movement (Fig. 1.5A). Using the head tracking movement (otherwise known as optokinetic tracking, or OKT) to detect the mouse's ability to see the gradient, the thickness of the lines on the gradient (measured in cycles per degree, or c/d) can be reduced until the mouse can no longer detect it. The point at which the mouse can no longer detect the gradient is known as the visual threshold (Prusky, Alam et al. 2004; Douglas, Alam et al. 2005). The OKT measures behavioral vision (i.e. a measureable behavioral response to visual stimulus), not physiological function. For physiological measurement, we must turn to ERGs.

ERGs measure physiological function of the retina and can be used to assess rod, cone, and inner retinal function. When light enters the retina, it is detected by photoreceptor cells. In response to light, the photoreceptor cell membrane hyperpolarizes, producing the a-wave (Fig. 1.5B) in the ERG response (Wachtmeister 1998). Bipolar cells in the inner nuclear layer (INL) depolarize in response to the photoreceptors and transmit the visual signal to retinal ganglion cells (RGCs), producing the b-wave (Wachtmeister 1998). Oscillatory potentials (OPs) are wavelets on the leading edge of the b-wave (Fig. 1.5B). OPs are generated by amacrine cells in the retina and are not entirely understood (Wachtmeister 1998). The OPs can be filtered (Fig. 1.5B) and their amplitudes and implicit times (the time it takes for them to appear after the retina is exposed to a flash of light) measured. Mice that are dark-adapted (left in the dark for an extended period of time to attain maximum sensitivity to light) can have scotopic (dim light, rod photoreceptor response) ERG measurements taken. Rod photoreceptors can be completely saturated with light by leaving mice in bright light for several minutes. This is known as light-adaptation, and it is a necessary prerequisite for measuring photopic (bright light, cone photoreceptor response) ERGs.

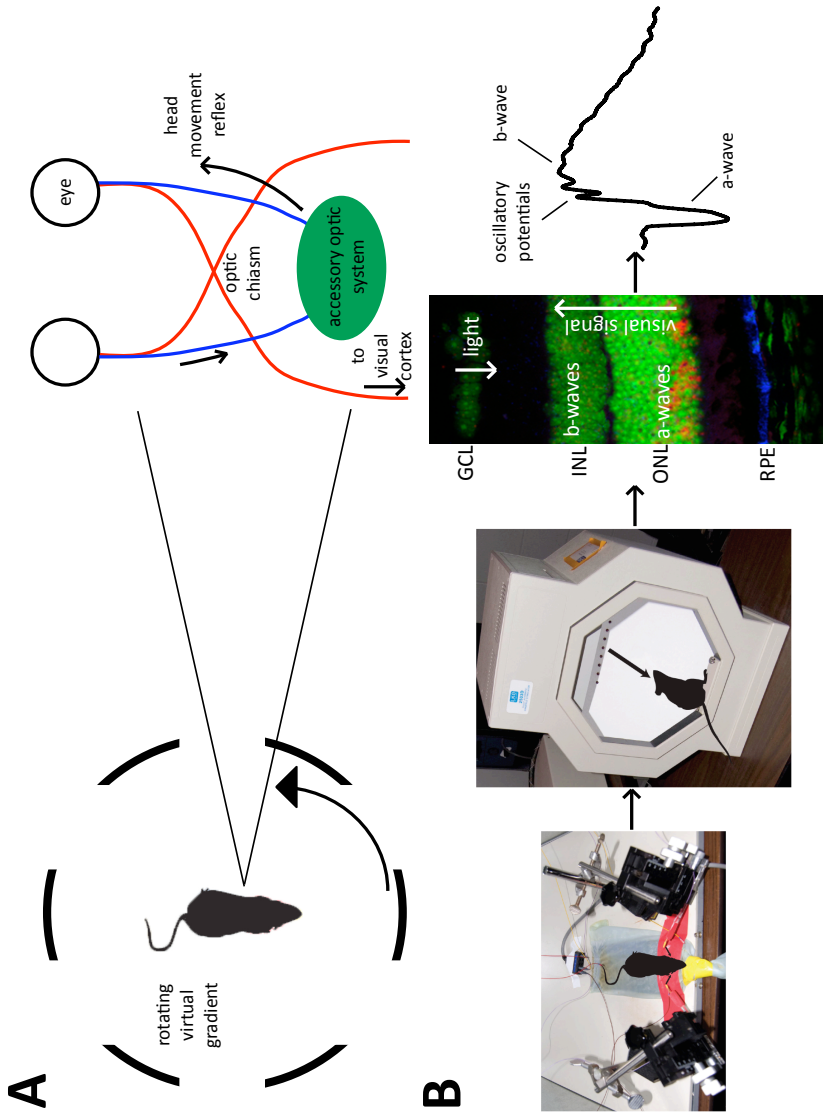

Figure 1.5—OKTs and ERGs are visual assessment methods for mice. OKTs and ERGs, and the visual components they measure, are labeled. (**A**) The rotating virtual gradient produces an optokinetic response that is manifested by head movement in the direction of the gradient rotation. It is an involuntary reflex response mediated by the accessory optic system. Upon exposure to the moving gradient, axons in the optic nerve direct the visual signal to both the visual cortex and to the accessory optic system (AOS). In the AOS, neurons sensitive to directional movement detect the motion of the spatial gradient. The AOS then sends an efferent signal to extraocular muscles and other muscles so the mouse can use its head to track the movement. This movement is observed and scored by the researcher performing the test. (**B**) Mice have to be anesthetized to measure retina function by ERG. Once a mouse is anesthetized, it is placed on a heating pad; electrodes are placed so they touch the cornea (left image). A Ganzfeld apparatus (center left image)

exposes the mouse to a flash of light (a mouse is shown in the image to demonstrate where the light stimulus is generated, but the mouse does not actually sit on the Ganzfeld during the procedure). The ERG response is produced in the retina (center right image) and produces an electrical trace that contains a-wave, oscillatory potential, and b-wave components (right image). Oscillatory potentials can be filtered from the raw electrical trace and analyzed further.

1.3—HISTORY OF THE VISUAL CYCLE

The first work with the visual cycle began in 1876 with the work of Franz Boll, who observed and described a light-sensitive part of the eye that changed color when exposed to light and turned back into its original color when left in the dark. This became known as Boll's Phenomenon (Baumann 1977; Marmor and Martin 1978). In 1878, Willy Kühne reported that visual purple (now known as light-sensitive rhodopsin which absorbs light in the green-yellow portion of the visual spectrum) (Kühne 1878), when dissected in the dark and exposed to light, bleached to form visual yellow (now known as bleached free opsin without chromophore) (Kühne 1878). Visual yellow could again become the light-sensitive visual purple if the retina was left on top of the retinal epithelium (now called the RPE); this recovery of visual purple, though, would not occur if the retina was dissected away from the RPE (Kühne and Sewall 1880) (Fig. 1.6). The recovery of visual purple in the presence of the RPE, (Kühne and Sewall 1880) would form the foundation of the modern understanding of the visual cycle and the critical role the RPE plays in its maintenance.

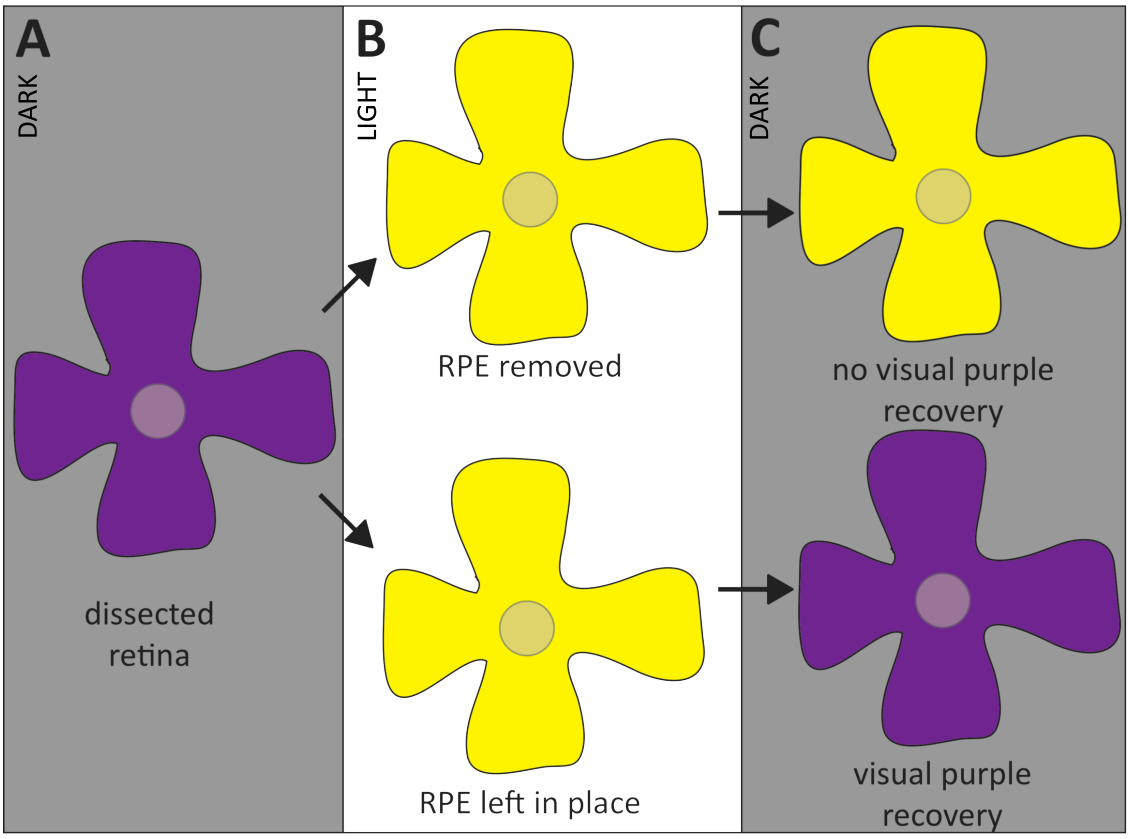

Figure 1.6—The retina only recovers sensitivity to light if the RPE is left attached. The initial importance of the RPE to visual sensitivity and the visual cycle was first described by Boll and Kühne in the 19th century. (**A**) If the retina, RPE, and choroid are dissected in the dark, the retina will appear a reddish-purple color because of visual purple (i.e. rhodopsin). (**B**) If exposed to light, visual purple will bleach to form visual yellow (i.e. bleached rhodopsin). Visual yellow will form even if the RPE is not attached. (**C**) If the RPE is dissected away from the retina, though, visual purple will not reappear if the retina is placed back in the dark. The RPE is required for recovery of visual sensitivity to light.

Despite the early contributions by Boll and Kühne in the late nineteenth century, the advance of the modern molecular understanding of the visual cycle would not occur until 1935. When George Wald exposed the visual purple to light, it allowed vitamin A (which he referred to as retinene) to be freely released from the retina; likewise, when visual yellow was restored to visual purple, retinene was lost (Wald 1935). Wald concluded that vitamin A was a prosthetic group on visual purple, and that its continuous replacement was necessary for continued vision (Wald 1935). In 1937, Wald used the concept of the visual cycle to explain dark- and light-adaptation (Wald and Clark 1937). By 1953, Wald established the chief importance of the visual cycle to be the conversion of all-*trans*-vitamin A (retinal) to 11-*cis*-vitamin A for the regeneration of visual pigment (Wald and Brown 1953). The recognition of the importance of regeneration of the 11-*cis* double bond for visual pigment sensitivity to light by Wald in 1953 resulted in the molecular description of bleaching ten years later (Matthews, Hubbard et al. 1963). By 1963, Wald's laboratory had discovered 11-*cis*-retinal (RAL) was bound to opsin by a Schiff base to form light-sensitive rhodopsin; after exposure to light, all-*trans*-RAL was discovered to dissociate from rhodopsin to leave free opsin apoprotein, and the necessary recycling of the 11-*cis* double bond did not occur directly on the protein (Matthews, Hubbard et al. 1963). Four years later, the importance and value of Wald's contributions to the molecular understanding of vision were recognized with the 1967 Nobel Prize in Physiology or Medicine (Wald 1968). A full understanding of the visual cycle still lacked the roles the RPE fulfilled.

The understanding of the RPE's importance in the visual cycle (Fig. 1.3) built upon Kühne's and Boll's qualitative observations concerning visual purple and the retinal

epithelium (Kühne and Sewall 1880). All-*trans*-RAL could be converted to all-*trans*-ROL by the retinol dehydrogenases RDH8 and/or RDH12 (Janecke, Thompson et al. 2004; Maeda, Maeda et al. 2005; Parker and Crouch 2010) in the rod OS. Further work on all-*trans*-retinoids indicated all-*trans*-ROL was esterified in the RPE (now known to be performed by lecithin retinol acyltransferase, LRAT) (Andrews and Futterman 1964; Zimmerman 1974). Bernstein and Rando discovered the isomerase activity was localized to RPE membranes, and this isomerase activity was abolished if the RPE was dissociated with detergents. However, the direct substrate for the isomerase reaction was still not understood (Bernstein, Law et al. 1987).

Initially, the importance of vitamin A esterification was not well understood in the context of the visual cycle because 11-*cis*-RAL (Perlman, Nodes et al. 1982), not all-*trans*-retinyl ester (RE) or 11-*cis*-RE, could restore functional rhodopsin (Canada, Law et al. 1990). By 1990, though, all-*trans*-RE was recognized as being a critical intermediate to the reformation of 11-*cis*-vitamin A in the RPE (Trehan, Canada et al. 1990). Eventually, it was widely understood an isomerase-like enzyme performed a one-step conversion of all-*trans*-retinyl ester to 11-*cis*-ROL (later identified as RPE65). 11-*cis*-ROL would subsequently be enzymatically converted to 11-*cis*-RAL by RDH5 in the RPE (Yamamoto, Simon et al. 1999).Wiggert and Chader in 1977 described retinol receptors in both the outer retina and RPE, suggesting the existence of a protein that was capable of shuttling retinoids in the subretinal space (the subretinal space is a misnomer because it simply refers to the boundary between the retina and RPE) (Abe, Wiggert et al. 1977). This protein, interphotoreceptor retinol-binding protein (IRBP), was isolated in 1983 (Adler and Evans 1983). IRBP was found to be localized in the interphotoreceptor

space and binds retinoids in the subretinal space (Adler and Evans 1983; Bridges, Alvarez et al. 1984). At this point, it was clear the isomerase was in the RPE, but there was a gap in understanding between the retinyl ester substrate and the 11-*cis*-ROL product.

Before the retinol isomerase was identified, it was known the isomerase activity was localized in and around the RPE cell membrane (Bernstein, Law et al. 1987; Bernstein, Law et al. 1987). A possible candidate protein for this isomerase-like activity would not emerge until 1991, when a monoclonal antibody to chicken RPE cell antigens identified a protein that ran at a 65 kDa size by sodium dodecyl sulfate polyacrylamide gel electrophoresis (SDS-PAGE) (Sagara and Hirosawa 1991). Although another group isolated a candidate for the retinol isomerase, this group identified it in the nuclear membrane of the RPE, which we now know to be incorrect (Livrea, Tesoriere et al. 1991). Because this protein appeared to be RPE-specific, the protein was named RPE65, and subsequent work indicated this protein's localization coincided with the expected location of retinoid isomerization (Bernstein, Law et al. 1987; Bernstein, Law et al. 1987; Sagara and Hirosawa 1991). RPE65 was finally confirmed as the long-sought retinal isomerase in 2005 when cell culture experiments demonstrated all-*trans*-RE could be directly converted to 11-*cis*-ROL upon introduction of RPE65 gene expression (Moiseyev, Chen et al. 2005).

1.4—RPE65: STRUCTURE, FUNCTION, AND MECHANISM

RPE65 was first described in 1991 as a 63 kDa RPE-specific protein (Sagara and Hirosawa 1991; Kiser and Palczewski 2010) and was first successfully cloned in 1993 (Hamel, Tsilou et al. 1993). Initial work with bovine RPE65 indicated the protein was 533 amino acids in length with a computed molecular weight of 61 kDa, and the mRNA had a length of approximately 3.2 kb (Hamel, Tsilou et al. 1993). In this study, it was noted the mRNA was relatively abundant while the protein was less abundant than would be expected for that amount of mRNA. The authors attributed this difference in levels of mRNA and protein to the fact that the mRNA was much longer than it would be if it just contained the coding sequence. They speculated that length of the 3'-untranslated region (UTR) of the mRNA might contain elements key to its translational regulation (Hamel, Tsilou et al. 1993), an observation that was later supported by increased protein levels after deletion of the 3'-UTR region in the mRNA (Liu and Redmond 1998). The fact that the protein had an expected size of 61 kDa based on its amino acid composition but a molecular weight of 63-65 kDa when subjected to SDS-PAGE suggested posttranslational modifications might be important to the function and stability of the protein (Hamel, Tsilou et al. 1993). Furthermore, although the protein was shown to localize to the RPE microsomal membrane (Sagara and Hirosawa 1991; Hamel, Tsilou et al. 1993), the amino acid sequence of the protein suggested RPE65 had no transmembrane domains, suggests it was associated with the lipid membrane instead of being embedded within it (Hamel, Tsilou et al. 1993).

RPE65 was initially reported to be expressed in an RPE-specific manner (Hamel, Tsilou et al. 1993; Nicoletti, Wong et al. 1995), but more recent evidence suggests it may

be expressed in a wider variety of cell types. Aberrant *RPE65* expression has been reported in cancer patients with transformed kidney cells (Ma, Zhang et al. 1999) and in human embryonic kidney 293 (HEK293) cells (Ma, Zhang et al. 1999; Chen, Moiseyev et al. 2003), but it is important to note *RPE65* expression was undetectable in human kidneys without renal tumors (Ma, Zhang et al. 1999). Also, dermatological journals report that *RPE65* expression is present in healthy human keratinocytes (Hinterhuber, Cauza et al. 2004; Hinterhuber, Cauza et al. 2005) and nonmelanocytic skin tumors (Hinterhuber, Cauza et al. 2005). Furthermore, RPE65 may be expressed in normal cone photoreceptor cells in mammals as well. Although many older reports show amphibians with a cone-dominant retina express RPE65 in cone photoreceptors (Ma, Xu et al. 1998), RPE65 expression in rod-dominant mammalian retina tissue (Znoiko, Crouch et al. 2002; Tang, Buhusi et al. 2011) is just now being identified. At this time, RPE65's role is only understood in the context of the RPE. Its exact function in cones, skin, and kidney cancers is still being investigated.

RPE65 structure has been resolved to a 1.9 angstrom resolution by x-ray crystallography. Like all proteins, the overall protein structure can be divided into primary, secondary, tertiary, and quaternary structures. RPE65 at its primary structure is 533 amino acids in length and, as previously mentioned, shows no evidence (based on sequence) of any transmembrane domains (Hamel, Tsilou et al. 1993); information about the tertiary structure is described below). The amino acid sequence of the RPE65 protein, though, did provide evidence of its ability to metabolize retinoids. RPE65 is similar to the human enzyme beta-carotene 15,15'-monooxygenase 1 (BCMO1, Fig. 1.7) (Redmond, Gentleman et al. 2001). BCMO1 belongs to a family of proteins that is known for

retinoid metabolism and provided indirect evidence for the possible role of RPE65 in the visual cycle, possibly as a retinoid isomerase (Redmond, Gentleman et al. 2001). Because BCMO1 was known to convert carotenoids into vitamin A and had a similar protein sequence (40% identity between BCMO1 and RPE65; Fig. 1.7), it suggested a strong possibility that RPE65 was the retinoid isomerase in the visual cycle (Redmond, Gentleman et al. 2001). As previously mentioned, this hypothesis would later be supported.

In terms of secondary structure, RPE65 consists mostly of beta strands that arrange in an antiparallel fashion to form beta sheets (each beta sheet containing at least four beta strands), which make up seven beta propeller blades (Kiser, Golczak et al. 2009; Golczak, Kiser et al. 2010). To form the tertiary structure (Fig. 1.8), the seven beta propeller blades of RPE65, in addition to an iron cofactor, fold together to form a structure with a mostly hydrophilic exterior (Kiser, Golczak et al. 2009; Golczak, Kiser et al. 2010). One face of RPE65, though, is hydrophobic, and it is this portion of the protein that is thought to associate with the microsomal membrane in the RPE (Golczak, Kiser et al. 2010). Upon associating with the microsomal membrane, the protein undergoes a conformational change that is required for enzymatic activity (Kiser, Farquhar et al. 2012). From the hydrophobic face, a hydrophobic tunnel leads to the interior of the protein to where the iron cofactor-containing active site resides (Kiser, Golczak et al. 2009; Golczak, Kiser et al. 2010). The knowledge of the quaternary structure of the protein is still largely theoretical, but RPE65 is capable of forming homodimers when

Score	Expect	Method	Identities	Positives	Gaps
407 bits (1047)	1e-139	Compositional matrix adjust.	206/519 (40%)	321/519 (61%)	19/519 (3%)

```
RPE65   20   EELSSPLTAHVTGRIPLWLTGSLLRCGPGLFEVGSEPFYHLFDGQALLHKFDFKEGHVTY  79
             +E   P+ A VTG+IP WL G+LLR GPG+  VG   + H FDG ALLH F  ++G V Y
BCMO1   10   KEQLEPVRAKVTGKIPAWLQGTLLRNGPGMHTVGESRYNHWFDGLALLHSFTIRDGEVYY  69

RPE65   80   HRRFIRTDAYVRAMTEKRIVITEFGTCAFPDPCKNIFSRFFSYFRGV--EVTDNALVNVY  137
               +++R+D Y   +   RIV++EFGT A+PDPCKNIFS+ FSY      + TDN L+N+
BCMO1   70   RSKYLRSDTYNTNIEANRIVVSEFGTMAYPDPCKNIFSKAFSYLSHTIPDFTDNCLINIM  129

RPE65   138  PVGEDYYACTETNFITKINPETLETIKQVDLCNYVSVNGATAHPHIENDGTVYNIGNCFG  197
               GED+YA +ETN+I KINP+TLET+++VD   YV+VN AT+HPH +  G V N+G
BCMO1   130  KCGEDFYATSETNYIRKINPQTLETLEKVDYRKYVAVNLATSHPHYDEAGNVLNMGTSIV  189

RPE65   198  KNFSIAYNIVKIPPL----QADKEDPISKSEIVVQFPCSDRFKPSYVHSFGLTPNYIVFV  253
             +     Y I KIP      +   + P   +E+    P      PSY HSFG+T NY++F+
BCMO1   190  EKGKTKYVIFKIPATVPEGKKQGKSPWKHTEVFCSIPSRSLLSPSYYHSFGVTENYVIFL  249

RPE65   254  ETPVKINLFKFLSSWSLWGANYMDCFESNETMGVWLHIADKKRKKYLNNKYRTSPFNLFH  313
             E P ++++ K  +++ +   ++  C   +     ++HI D++ ++ +  K+ T    +FH
BCMO1   250  EQPFRLDILKMATAY-IRRMSWASCLAFHREEKTYIHIIDQRTRQPVQTKFYTDAMVVFH  308

RPE65   314  HINTYEDNGFLIVDLCCWKGFEFVYNYLYLANLRENWEEVKKNARKAPQPEVRRYVLPLN  373
             H+N YE++G ++ D+  ++    +Y   YLANL ++++E   N+R    P +RR+ +PL+
BCMO1   309  HVNAYEEDGCIVFDVIAYED-NSLYQLFYLANLNQDFKE---NSRLTSVPTLRRFAVPLH  364

RPE65   374  IDK-ADTGKNLVTLPNTTATAILCSDETIWLEPEVLFSGPRQAFEFPQINYQKYCGKPYT  432
             +DK A+ G NL+ + +TTATA+   D  ++ +PE L+ G     E P++NY  + GK Y
BCMO1   365  VDKNAEVGTNLIKVASTTATALKEEDGQVYCQPEFLYEG----LELPRVNY-AHNGKQYR  419

RPE65   433  YAYGLGLN-HFVPDRLCKLNVKTKETWVWQEPDSYPSEPIFVSHPDALEEDDGVVLSVVV  491
             Y +  G+    +P ++ K ++ TK +  W+E D +P+EP+FV  P A +EDDGV+LS +V
BCMO1   420  YVFATGVQWSPIPTKIIKYDILTKSSLKWREDDCWPAEPLFVPAPGAKDEDDGVILSAIV  479

RPE65   492  SPGAGQKPAYLLILNAKDLSEVARAEVEINIPVTFHGLF  530
             S    QK  +LLIL+AK  +E+ARA V++++ +  HGLF
BCMO1   480  STDP-QKLPFLLILDAKSFTELARASVDVDMHMDLHGLF  517
```

Figure 1.7—Alignment of human RPE65 and BCMO1 protein sequences. RPE65 shares significant sequence identity (40%) with BCMO1, a protein that cleaves beta-carotene to yield two vitamin A molecules. The loose sequence similarity of RPE65 with other retinoid metabolism proteins, combined with observations in KO mice that 11-*cis*-retinoid (isomerase product) levels were not detectable and all-*trans*-RE (retinoid substrate) levels were elevated indicated that RPE65 might be the retinol isomerase in the visual cycle (because the absence of RPE65 produced a block in the visual cycle). The mouse nonsense R44X mutation and missense R91W and F229S mutations are highlighted in red on the protein sequence. Idnetical amino acid residues are indicated between RPE65 and BCMO1 sequences; (+) indicates amino acids with similar biochemical properties.

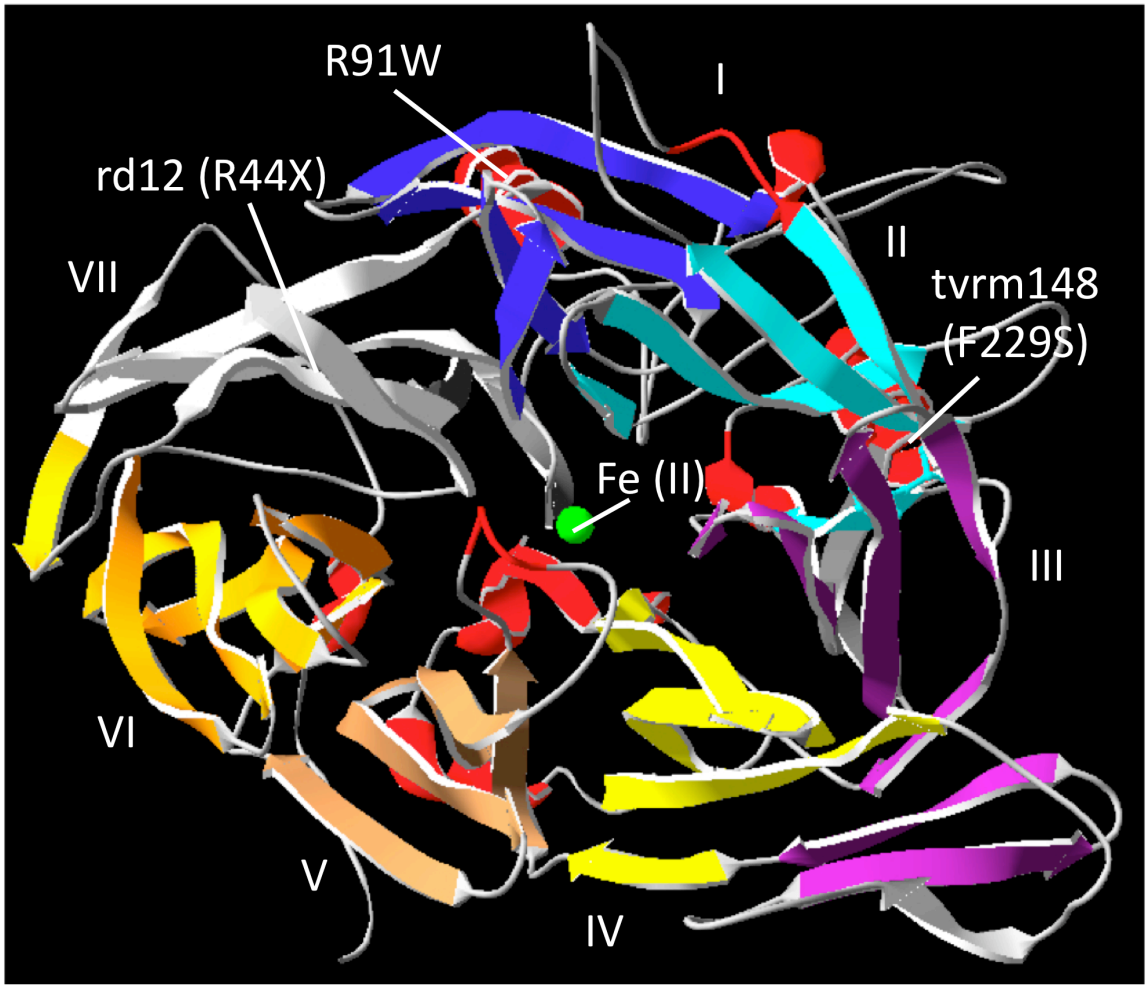

Figure 1.8—Tertiary structure of RPE65 with iron (II) cofactor and mouse mutations labeled. RPE65 has a hydrophobic tunnel that leads to the interior of the protein for the isomerization of all-*trans*-RE substrate to 11-*cis*-ROL product. This one tunnel is the only channel that leads from the exterior of the protein to the interior. The tunnel opens on the RPE membrane but is closed on the other (where the active site is located). For another molecule of substrate to enter, a molecule of product must leave first. Mouse missense mutations R44X, R91W, and F229S are labeled. The seven beta-propeller blade structures (I-VII) are also labeled.

crystallized (Golczak, Kiser et al. 2010), and it is predicted that RPE65 may form a multiprotein complex with 11-*cis*-retinol dehydrogenase (RDH5) and retinal G protein-coupled receptor (RGR) at the microsomal membrane in the RPE (Golczak, Kiser et al. 2010). It should be noted that RPE65 has only been observed to form homodimers in crystals; this has never been reported *in vivo*. These and other protein interactions have been proposed, but as of yet, no direct protein interactions have been confirmed. These structural data have aided in the mechanistic understanding of RPE65 isomerase activity.

Experimental data have suggested that posttranslational modifications are necessary for RPE65 association with the microsomal membrane (Ma, Zhang et al. 2001), and it is now known that RPE65 requires association with a lipid membrane for its enzymatic activity (Kiser, Farquhar et al. 2012). Initial work suggested palmitoylation might be required for RPE65 association with the plasma membrane, because mutation of Cys residues (which can be sites for palmitoylation) C231, C329, and C330 of the human protein resulted in a decrease in RPE65 activity (Takahashi, Moiseyev et al. 2006). More recent data, though, suggests that although membrane association is necessary for RPE65 activity (Nikolaeva, Moiseyev et al. 2011), palmitoylation of those Cys residues is not necessary for membrane association (Trudel, Beaufils et al. 2006; Jin, Yuan et al. 2007; Golczak, Kiser et al. 2010). C112 palmitoylation does appear to be necessary for appropriate membrane association and enzymatic activity (Takahashi, Moiseyev et al. 2009). These data suggest that proper protein folding alone is not sufficient for RPE65 function.

In addition to posttranslational modifications, the iron cofactor previously mentioned is critical for the isomerase activity of RPE65; chelation of iron with either

2,2′-bipyridine or 1,10-phenanthroline abolishes all enzymatic activity (Moiseyev, Takahashi et al. 2006; Kiser, Golczak et al. 2009). The iron cofactor sits in the active site of RPE65 and is held in an iron coordination motif by four His residues (Kiser, Farquhar et al. 2012). Mutation of any one of the His-binding residues H180, H241, H417, or H527 in bovine RPE65 abolishes enzymatic activity (Redmond, Poliakov et al. 2005; Takahashi, Moiseyev et al. 2005). In the active site, it is currently thought that the iron cofactor plays an important role in the initial catalysis of the isomerization by acting as a Lewis acid (Kiser, Farquhar et al. 2012), implying the Fe(II) cofactor is temporarily oxidized to Fe(III) during the conversion of all-*trans*-RE to 11-*cis*-ROL (Kiser, Farquhar et al. 2012).

The actual mechanism of RPE65 isomerase activity was unresolved for several years as two different mechanisms for all-*trans* to 11-*cis* isomerization seemed possible. The first mechanism proposed that an S_N2' mechanism of nucleophilic addition to the C_{11} carbon could result in 11-*cis* production (Deigner, Law et al. 1989). The second mechanism proposed all-*trans* to 11-*cis* isomerization proceeded through the formation of a carbocation intermediate that results from protonation of the substrate and subsequent bond rearrangement because of electron delocalization (McBee, Kuksa et al. 2000). Eventual resolution of the isomerization mechanism came in 2010, and relied on predictions concerning 11-*cis* retinoid production from each mechanistic proposal. If the isomerization proceeded through the proposed S_N2' nucleophilic substitution, then RPE65 would produce only 11-*cis*-ROL without any 13-*cis*-ROL byproduct formed (Redmond, Poliakov et al. 2010). If, on the other hand, the isomerization proceeded through formation of a carbocation intermediate, it would be expected some 13-*cis*-ROL

would be produced by RPE65 as well (Redmond, Poliakov et al. 2010). When the canine RPE65 residues Thr147 and Phe103, which both reside in the active site but are not involved in iron coordination, were mutated, RPE65 specificity for 11-*cis* and 13-*cis*-ROL production is altered (Redmond, Poliakov et al. 2010). These data suggest that the isomerization proceeds through the formation of a carbocation intermediate.

In summary, RPE65 is a 533 amino acid protein with a structure that consists of seven beta propellers that fold together to form a hydrophobic cave that leads from the exterior of the protein to the interior where an iron(II) factor is coordinated by four histidine residues to form the active site (Kiser, Golczak et al. 2009; Golczak, Kiser et al. 2010; Kiser, Farquhar et al. 2012). The entire exterior of the protein, with the exception of residues 126-250 that form a hydrophobic face, is hydrophilic (Trudel, Beaufils et al. 2006). Posttranslational palmitoylation of C112 in both bovine and human RPE65 is necessary for association of the protein with the RPE microsomal membrane (Takahashi, Moiseyev et al. 2009), where it is hypothesized to directly interact with RDH5 and RGR (Golczak, Kiser et al. 2010). The association of the hydrophobic face with the microsomal membrane is thought to allow for the passage of retinoids to and from the active site of RPE65 (Mata, Moghrabi et al. 2004; Nikolaeva, Takahashi et al. 2009). At the active site, the iron(II) cofactor acts as a Lewis acid (Kiser, Farquhar et al. 2012) to protonate the all-*trans*-RE substrate, where isomerization proceeds through formation of a carbocation intermediate to form 11-*cis*-ROL with trace amounts of 13-*cis*-ROL as a byproduct (Redmond, Poliakov et al. 2010). The possible interactions of RPE65 with other visual cycle proteins at the microsomal membrane of the RPE (Golczak, Kiser et al.

2010) may allow for efficient processing of hydrophobic retinoids in an assembly line-like fashion.

Even if an "assembly line" of retinoid processing does exist in the RPE, the rate of 11-*cis*-ROL synthesis is too slow to account for the rate of regeneration needed for light-adapted vision (Wang and Kefalov 2011). In order to operate in a bright environment, cone photoreceptors require a more rapid synthesis of chromophore to compensate for the higher demand (Wang and Kefalov 2011). Given the structure of RPE65 and the fact that substrate and product must proceed deep into the protein structure to bind to the active site, RPE65 may not be able to synthesize product fast enough for cone photoreceptor demand. Other work, which is beyond the scope of this dissertation to explore in necessary detail, suggests a cone visual cycle (with a Müller cell retinoid isomerase) may supplement chromophore generation in the retina for light-adapted vision (Wang and Kefalov 2011).

1.5—RPE65 AND ITS ASSOCIATION WITH LEBER CONGENITAL AMAUROSIS (LCA)

Leber congenital amaurosis (LCA) is an inherited genetic disease that affects approximately 1 in 80,000 people (Cideciyan 2010) and 20% of students in schools for blind children (Ahmed and Loewenstein 2008). Currently, LCA is a disease known to originate from mutations in different genes (Table 1.3), accounting for >70% of all diagnosed cases of LCA (the other 30% of LCA cases still have no associated gene mutations at this time) (den Hollander, Roepman et al. 2008). The disease was originally (and sometimes still) considered a severe, congenital form of retinitis pigmentosa (RP)

when it was first formally described by Leber in 1869 (den Hollander, Roepman et al. 2008), with four criteria that must be met by patients for the diagnosis of LCA: 1) severe, early childhood vision loss, 2) nystagmus, 3) severely reduced pupillary responses, and 4) nearly complete abolishment of ERG response (den Hollander, Roepman et al. 2008). Many diseases are misdiagnosed in the clinic based on these criteria. Albinism, optic nerve hypoplasia (ONH), complete and incomplete achromatopsia (ACHM), congenital stationary night blindness (CSNB), Alström syndrome, neuronal ceroid lipofuscinosis (NCL), and Joubert syndrome can all resemble LCA at very early ages and can only be properly distinguished from LCA as patients get older (den Hollander, Roepman et al. 2008).

Table 1.3—Mutations in different genes can cause LCA

LCA Variant	Gene Mutated	% of LCA Cases (if known)
LCA1	*GUCY2D*	11.7
LCA2	*RPE65*	6.0
LCA3	*SPATA7*	unknown
LCA4	*AIPL1*	5.3
LCA5	*LCA5*	1.8
LCA6	*RPGRIP1*	4.2
LCA7	*CRX*	1.0
LCA8	*CRB1*	9.9
LCA9	*NMNAT1*	unknown
LCA10	*CEP290*	15.0
LCA11	*IMPDH1*	8.3
LCA12	*RD3*	0.1
LCA13	*RDH12*	2.7
LCA14	*LRAT*	0.5
LCA15	*TULP1*	0.8
LCA16	*KCNJ13*	unknown
LCA17	*GDF6*	unknown

This table lists all the known genes that can cause LCA when mutated. Gene mutation percentages are shown (den Hollander, Roepman et al. 2008). Genes associated with LCA1 – LCA17 are found on OMIM (omim.org).

Before it was established that RPE65 was the isomerase in the visual cycle (Moiseyev, Chen et al. 2005), it became apparent that *RPE65* mutations could have profound impacts on vision. Mutations in *RPE65* are mostly associated with LCA2, but they have been found to play a role in other human visual dystrophies such as autosomal recessive childhood-onset severe retinal dystrophy (arCSRD) (Gu, Thompson et al. 1997), autosomal recessive retinitis pigmentosa (arRP) (Poehner, Fossarello et al. 2000), and fundus albipunctatus (FA) (Schatz, Preising et al. 2011). In dogs, *RPE65* mutations are linked to LCA2 (Veske, Nilsson et al. 1999), congenital stationary night blindness (CSNB) (Aguirre, Baldwin et al. 1998) and autosomal recessive retinal dystrophy (Veske, Nilsson et al. 1999). Multiple *RPE65* mutations have been identified in humans (Gu, Thompson et al. 1997; Marlhens, Bareil et al. 1997; Morimura, Fishman et al. 1998; Hanein, Perrault et al. 2004; Chen, Moiseyev et al. 2006; Stone 2007; Philp, Jin et al. 2009; Sundaresan, Vijayalakshmi et al. 2009; Xu, Dong et al. 2012), and all inherit in an autosomal recessive fashion, except one dominant-negative mutant, $RPE65^{D477G}$, identified in 2011 (Bowne, Humphries et al. 2011). It is not yet understood how the $RPE65^{D477G}$ mutation induces a dominant-negative effect on vision or even if protein-protein interactions are involved in the dominantly inheriting negative effects on vision. Mouse models have been critical in understanding the disease processes that occur in RPE65 deficiency and have been used to develop promising treatments for humans. Four mouse mutants (KO, rd12, R91W, and tvrm148) are currently available for modeling LCA2 (considered models for LCA2 because they have *Rpe65* mutations and because they resemble the phenotypes seen in patients). Figure 1.9 shows the location of all known human RPE65 gene mutations with mouse mutations labeled. The rd12 and

R91W mutations are found in humans, but the tvrm148 is not (even though multiple human mutations are found four amino acids away at position 225).

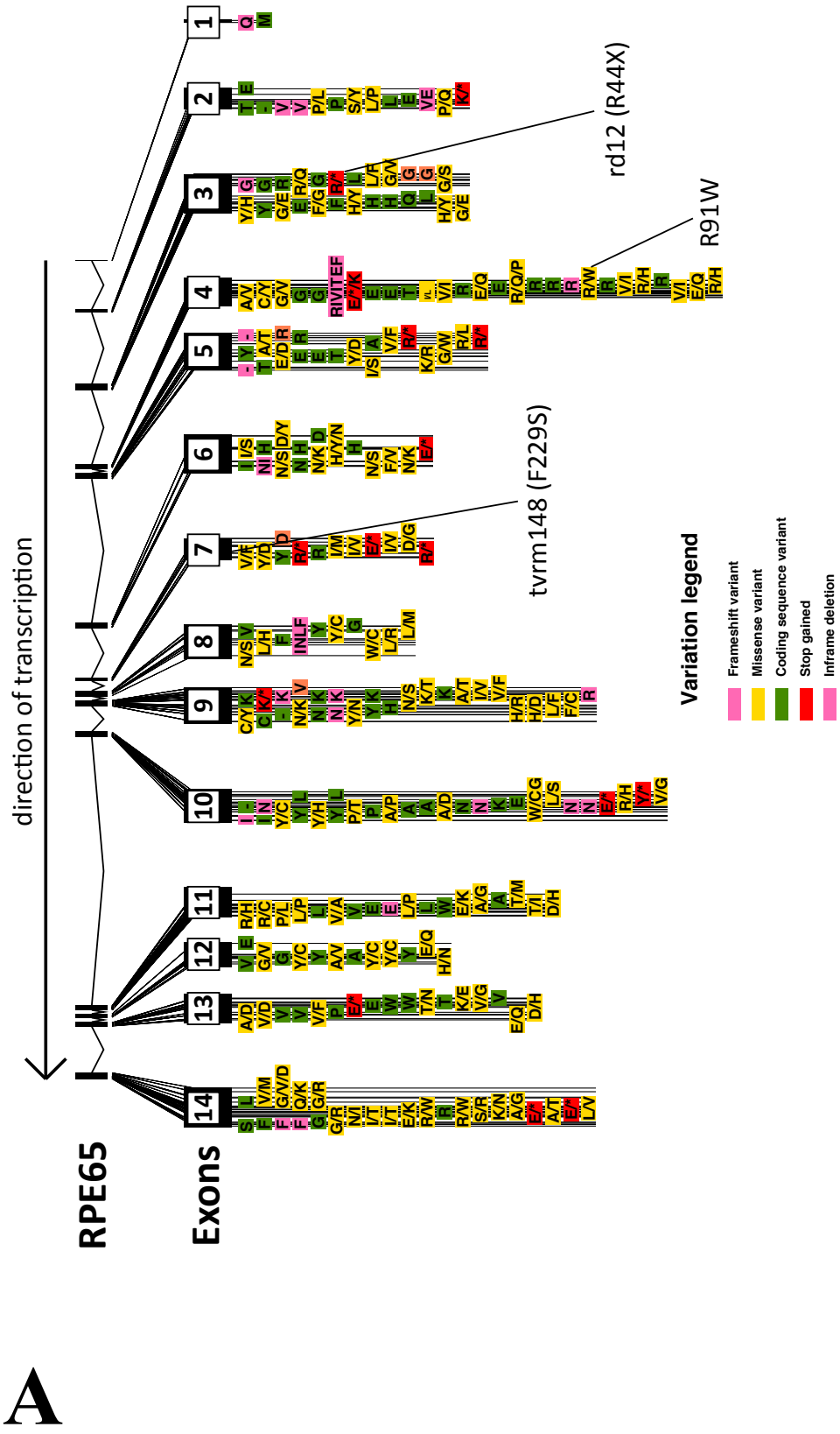
A
RPE65
Exons
direction of transcription
rd12 (R44X)
R91W
tvrm148 (F229S)
Variation legend
Frameshift variant
Missense variant
Coding sequence variant
Stop gained
Inframe deletion

B

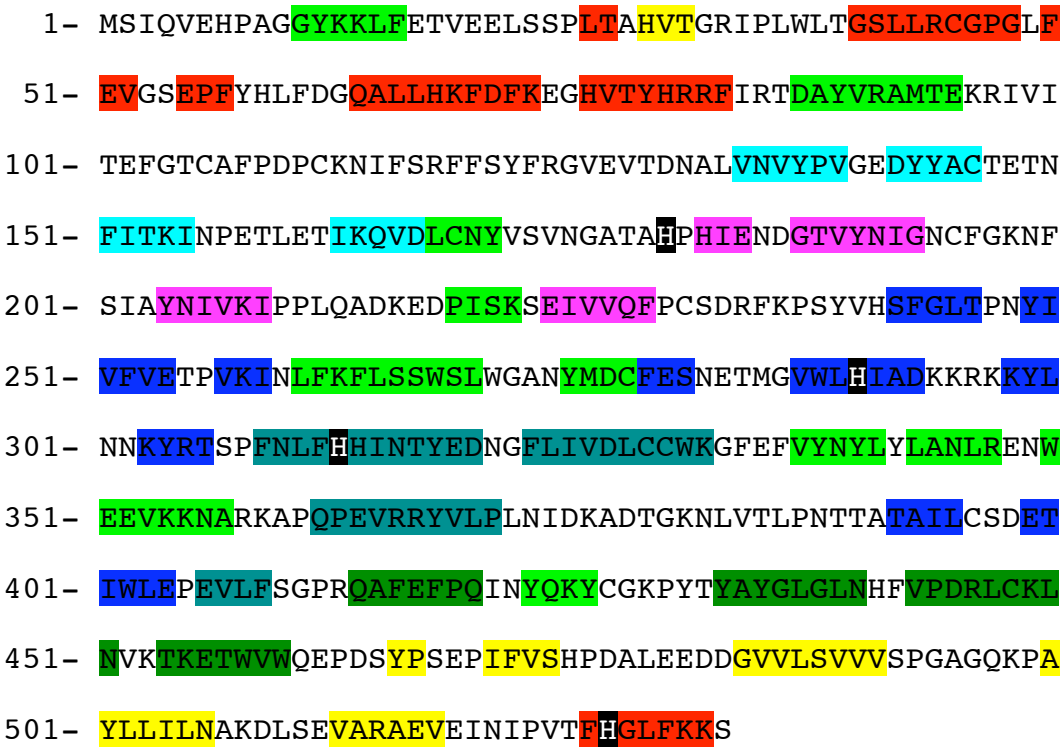

Figure 1.9. Known human and mouse mutations in RPE65. (**A**) The human RPE65 gene is shown above with all known coding, missense, stop, frameshift, and deletion mutations shown. It should be noted that the human RPE65 gene is on chromosome 1 and is on the (-) DNA strand, while the mouse RPE65 gene is on chromosome 3 and is on the (+) DNA strand. (**B**) Human RPE65 protein with known structural motifs in the protein. Alpha helices are highlighted in green, beta propeller I is highlighted in cyan, beta propeller II is highlighted in magenta, beta propeller III is highlighted in blue, beta propeller IV is highlighted in teal, beta propeller V is highlighted in green, beta propeller VI is highlighted in yellow, and beta propeller VII is highlighted in red (Kiser, Golczak et al. 2009). Iron-coordinating histidine residues, which form the active site of the protein, are highlighted in black with white font. The residues that form the active site are H180, H241, H313, and H527 (Redmond, Poliakov et al. 2005).

1.6—MOUSE LINES WITH *RPE65* GENE MUTATIONS

1.6.1—Rpe65^{KO} (KO) mouse

The KO mouse (Redmond, Yu et al. 1998) was created in 1998 because of the association of the mouse *Rpe65* gene with vitamin A metabolism (Båvik, Lévy et al. 1993; Hamel, Tsilou et al. 1993) and because of its association to LCA (Marlhens, Bareil et al. 1997) and arCSRD (Gu, Thompson et al. 1997). This mouse has been used to test many hypotheses, and, in the original breakthrough 1998 article, Redmond et al used the KO mouse to test if it still exhibited isomerase activity, reflected by substrate build up (retinyl palmitate), and absence of product (11-*cis*-RAL). The KO was constructed by recombining a neomycin resistance cassette with the mouse *Rpe65* gene to delete the first three exons and part of the third intron of the gene (Redmond, Yu et al. 1998). At the molecular level, *Rpe65* mRNA and RPE65 protein expression were absent (Redmond, Yu et al. 1998). During phenotypic examination of the KO mice, they were found to have disorganized rod outer segments while still retaining relatively normal retina morphology and sharply diminished dark- and light-adapted electroretinographic (ERG) responses (decrease in retinal sensitivity of about four to five orders of magnitude) (Redmond, Yu et al. 1998). The rod outer segments, despite being disorganized, still contained opsin apoprotein but no endogenous rhodopsin (Redmond, Yu et al. 1998). Antibody staining for rhodopsin indicated it was still present in the outer segments, but the purified opsin protein from the outer segments was incapable of absorbing light in 20-week-old KO mice (Redmond, Yu et al. 1998). Most importantly, high-performance liquid chromatography (HPLC) data showed no detectable amounts of 11-*cis*-RAL but large amounts of all-*trans*-RE (Redmond, Yu et al. 1998), meaning there was a block in the

visual cycle at the isomerization step (Fig. 1.3). Heterozygous mice were reported to have wild type ERG responses, intact rod outer segments, functional rhodopsin, and detectable 11-*cis*-RAL (Redmond, Yu et al. 1998). Based on these data, the authors of the study concluded the KO mutation was a null *Rpe65* gene mutation that inherited in an autosomal recessive manner (Redmond, Yu et al. 1998). The most important conclusions were that RPE65 is necessary for isomerase activity, and that it is either the isomerase, or an essential subunit of a complex that converts retinyl-esters to 11-*cis*-retinoids. Of course, RPE65 was later confirmed to be the retinol isomerase in the visual cycle (Moiseyev, Chen et al. 2005). The KO mouse has since been considered the standard LCA2 model in the field. Properties of the KO mouse with respect to RPE65 and ERG function are summarized in Table 1.4.

Table 1.4—Mouse RPE65 variants and their effects on protein function

Mutation	% *Rpe65* mRNA	% RPE65 protein	% remaining enzymatic activity	Reduced ERG response? (YES/NO)
RPE65 (Balb/c)	100	100	100	NO
$RPE65^{L450M}$ (C57BL/6)	96	50	45	NO
KO	0	0	0	YES
rd12 (R44X)	70	0	0	YES
R91W	62	2.5	3	YES
tvrm148 (F229S)	87	7.3	0	YES

This table shows information about the known RPE65 variants that have been studied. All information presented is relative to the Balb/c RPE65 variant, which contains no known mutations compared to other mouse strains. For the $RPE65^{L450M}$ variant, this information was assumed to be true for all C57BL/6 strains (Wenzel, Reme et al. 2001; Lyubarsky, Savchenko et al. 2005), including C57BL/6J, which is the genetic background for the KO (Wright, Chrenek et al. 2013), rd12 (data presented in Chapter 4), R91W (Samardzija, von Lintig et al. 2008), and tvrm148 strains (Wright, Chrenek et al. 2013).

1.6.2—Rpe65^{rd12} (rd12) mouse (R44X)

The rd12 mouse was the first spontaneous *Rpe65* gene mutant isolated in mouse (Pang, Chang et al. 2005). During a fundus examination of the B6.A-*H2-T18*^{a}/BoyEg mouse line at The Jackson Laboratories, a 10-month-old mouse presented with discrete white dots throughout the fundus (Pang, Chang et al. 2005). This male mouse was subsequently mated to a C57BL/6J female and then to females of the resulting litter to found the rd12 line (Pang, Chang et al. 2005). During the foundation of the rd12 line, the mice were backcrossed to "C57BL/6J until it was inbred congenic with that background (Pang, Chang et al. 2005)," meaning the rd12 mutation was on the C57BL/6J genetic background. Genetic mapping linked the mutant locus to chromosome 3 and microsatellite marker *D3Mit19* (Pang, Chang et al. 2005), and DNA sequencing of the critical region showed a C-to-T base transition that resulted in an R44X nonsense mutation in codon 44 in exon 3 of the mouse *Rpe65* gene (Pang, Chang et al. 2005).

Unlike their KO counterparts (Redmond, Yu et al. 1998), rd12 mice were reported to have white flecks in their fundus (Pang, Chang et al. 2005) similar to those seen in human patients with fundus albipunctatus (FA) (Yamamoto, Simon et al. 1999) and some LCA2 patients with *RPE65* point mutations (Gu, Thompson et al. 1997; Schatz, Preising et al. 2011). Similar to KO mice (Redmond, Yu et al. 1998), ERG responses were only detectable at the highest flash intensities (Pang, Chang et al. 2005). Outer nuclear layer (ONL) and OS thinning were reported in the retina at later ages, but for the most part, retina morphology was relatively preserved (Pang, Chang et al. 2005), which is similar to what was previously reported in KO mice (Redmond, Yu et al. 1998). During the initial report of rd12 mice, investigators did note some OS disorganization at early ages and

lipid droplets in the RPE from retinyl ester accumulation (Redmond, Yu et al. 1998) that increase in size with age (Pang, Chang et al. 2005). RPE65 protein expression was examined through antibody staining of retinal cross sections, but was not detected. The authors speculated that the *Rpe65* mRNA was probably degraded by nonsense mediated decay (NMD) because of the lack of protein staining, *Rpe65* mRNA expression was not measured (Pang, Chang et al. 2005). Similar to KO mice (Redmond, Yu et al. 1998), there was no rhodopsin absorbance detected (rhodopsin with bound retinoid strongly absorbs at 500 nm) in mice homozygous for the rd12 mutation, and 11-*cis*-RAL was undetectable in homozygote mice with retinyl ester accumulation that increased with age (Pang, Chang et al. 2005). Based on this work, it was concluded the rd12 mutation was a nonsense mutation that resulted in a recessively-inherited, null phenotype (Pang, Chang et al. 2005).

The initial similarities of the KO and rd12 mice came into question a few years after the first findings of the rd12 mutation were published. Subsequent work with rd12 mice focused on the use of gentamicin (delivered through subcutaneous injection) as a potential read-through compound (RTC) to rescue the mutant phenotype (Guerin, Gregory-Evans et al. 2008). RTCs can sometimes allow ribosomes to skip over nonsense mutations to produce a protein that may retain some function (Bidou, Allamand et al. 2012) because it interferes with tRNA proofreading by the ribosome (which may allow a random amino acid to be inserted at the PTC during translation), and it was hypothesized that gentamicin could rescue the production of some RPE65 protein. The nonsense codon in rd12 mice was known to respond well to RTC drugs when in other genes, so the authors found it surprising that other stop codons known to be less-responsive responded

well to treatment but the rd12 mutation did not. There was no evidence to suggest that the rd12 allele contained another mutation that would make the treatment ineffective; the authors of the study merely found in surprising the rd12 mutation was resistant to treatment with RTCs. Unlike other nonsense mutations tested, the rd12 mutation was resistant to treatment with gentamicin (Guerin, Gregory-Evans et al. 2008). Also, unlike other nonsense mutations examined, significant *Rpe65* mRNA accumulation was detected by qRT-PCR (but data was not shown in this publication) (Guerin, Gregory-Evans et al. 2008).

My work, which is presented in "**Chapter IV: The rd12 allele exerts a semidominant negative effect on visual function in mice**" of this dissertation, suggests the rd12 mutation is not purely recessive, but is rather a semidominantly inherited mutation that is mediated by the mutant mRNA rather than a mutant protein. Semidominance, also called incomplete dominance, results when a phenotype intermediate between wild type and homozygous mutant is observed with only one copy of the mutation (this is distinct from both haploinsufficiency and codominance). Visual acuity, as measured by optokinetic tracking (OKT) showed that rd12 mice experienced an earlier loss of detectable visual acuity as compared to KO mice, and when rd12 and KO mice were bred together, the resulting offspring exhibited the rd12 homozygote phenotype. Mice with one copy of the rd12 allele and one copy of the wild type allele exhibited slight visual deficits, suggesting a semidominant inheritance. Consistent with earlier work that reported the nonsense rd12 mutation was somehow able to evade NMD (Guerin, Gregory-Evans et al. 2008), I found that rd12 mice had levels of *Rpe65* mRNA comparable to wild type mice even though there was no detectable protein levels. Work

with sucrose gradient density centrifugation, which separated the *Rpe65* mRNA into messenger ribonucleoprotein (mRNP), monoribosome, and polyribosome fractions, suggested the mutant rd12 mRNA may be sequestered on mRNPs. Instead of being bound to ribosomes for translation, this sequestration may form the foundation for the observed semidominant effect on visual function. Properties of the rd12 mouse with respect to RPE65 and ERG function are summarized in Table 1.4.

1.6.3—Rpe65^{R91W} (R91W) mouse

The R91W missense mutation is the most common missense mutation in LCA2 patients with *RPE65* mutations (Thompson, Gyurus et al. 2000) and has been identified in multiple studies since *RPE65* was first linked to visual dysfunction (Gu, Thompson et al. 1997). This amino acid substitution often appears in patients that have compound heterozygous mutations for *RPE65* (Lorenz, Gyurus et al. 2000) and was found to be homozygous in patients from a consanguineous Tunisian family in 2006 (El Matri, Ambresin et al. 2006). Like rd12 mice (Pang, Chang et al. 2005) and other LCA2 patients (Gu, Thompson et al. 1997; Schatz, Preising et al. 2011). Patients with the R91W mutation typically present with white punctate dots in the fundus (El Matri, Ambresin et al. 2006). Because the R91W mutation is the most common *RPE65* missense mutation to present in the clinic (Thompson, Gyurus et al. 2000), there was substantial interest in modeling this particular *RPE65* variant in mouse (Takahashi, Chen et al. 2006). The R91W knock-in mouse was created to study this relatively common *RPE65* mutation and its effects on retinal function and the visual cycle (Samardzija, von Lintig et al. 2008). Initial mouse work with the R91W variant indicated that the allele could not rescue

isomerase activity in KO mice (Takahashi, Chen et al. 2006). *In vitro* activity assays indicated the R91W protein variant was incapable of producing 11-*cis*-RAL (Takahashi, Chen et al. 2006). Furthermore, the half-life of R91W mutant protein is reduced in cell culture. Because mice with this mutation could express *Rpe65* mRNA at wild type levels with little protein present, it suggested the R91W amino acid substitution was capable of destabilizing the RPE65 protein (Takahashi, Chen et al. 2006).

Similar to patients with the R91W mutation (Takahashi, Chen et al. 2006), R91W mice express *Rpe65* mRNA at levels similar to wild type mice but accumulate only small amounts of protein as measured by immunoblotting (Samardzija, von Lintig et al. 2008). Comparing the mRNA and protein expression of RPE65 in mice (Samardzija, von Lintig et al. 2008) with earlier cell culture data presented with the human variant (Takahashi, Chen et al. 2006), it appeared the R91W amino acid substitution was also capable of destabilizing the mouse protein as well (Fig. 1.10) (Samardzija, von Lintig et al. 2008). In contrast to earlier work with the human R91W allele (Takahashi, Chen et al. 2006), the R91W mouse was capable of producing detectable amounts of 11-*cis*-RAL, albeit at low levels compared to wild type mice (Samardzija, von Lintig et al. 2008). At 40 weeks of age, R91W mice produced ~6% as much 11-*cis*-RAL as wild type mice (Samardzija, von Lintig et al. 2008). Consistent with HPLC measurements of all-*trans*-RE accumulation, R91W mice developed lipid inclusions in the RPE as they age (Samardzija, von Lintig et al. 2008) in a fashion similar to KO (Redmond, Yu et al. 1998) and rd12 mice (Pang, Chang et al. 2005). Because of the amount of absorbance at 500 nm in protein preparations (rhodospin with bound chromophore absorbs strongly at 500 nm) in R91W mice, they were reported to have ~6% functional rhodopsin when compared to wild type

mice in steady-state conditions in total darkness (Samardzija, von Lintig et al. 2008). ERG responses showed a large loss of retina sensitivity in scotopic waveforms, but the responses were noticeably higher than what was reported in KO mice (Redmond, Yu et al. 1998; Samardzija, von Lintig et al. 2008). By 8 weeks of age, there was no significant difference in photopic ERG response between R91W and wild type mice (Samardzija, von Lintig et al. 2008). Despite relative preservation of visual function when compared to KO mice (Redmond, Yu et al. 1998), R91W mice experienced similar amounts of ONL thinning and OS disorganization (Samardzija, von Lintig et al. 2008). Cone photoreceptors were found to be lost more slowly in mice with the R91W mutation than with the KO mutation. Mice heterozygous for the R91W knock-in allele had no reported abnormalities when compared to wild type mice (Samardzija, von Lintig et al. 2008). The authors concluded the R91W mutation was a recessive, loss-of-function *Rpe65* allele that was pathological but acted more slowly than the KO allele because of slight residual isomerase activity (Samardzija, von Lintig et al. 2008). Properties of the R91W mouse with respect to RPE65 and ERG function are summarized in Table 1.4.

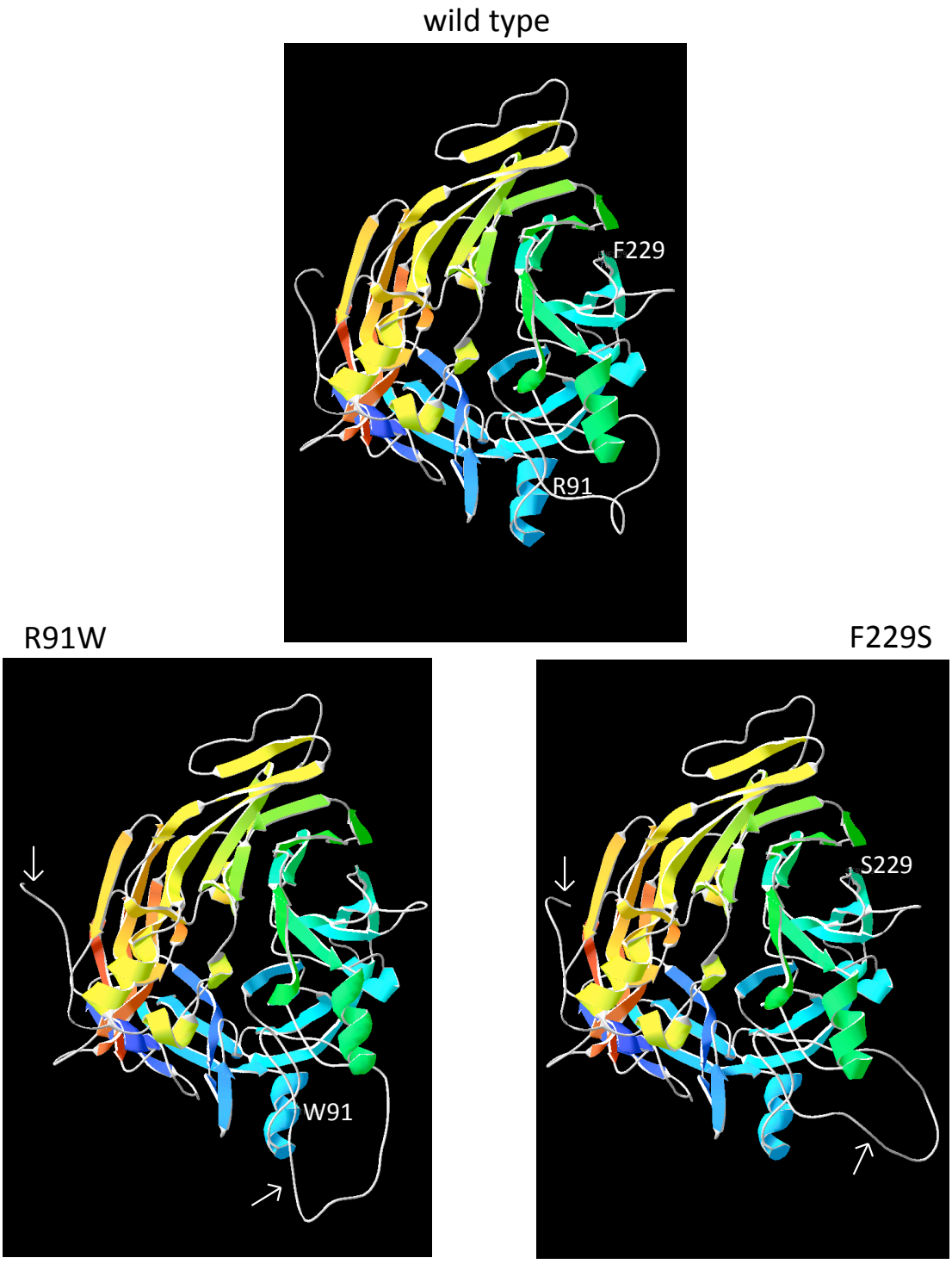

Figure 1.10—The R91W and F229S amino acid substitutions are predicted to distort RPE65 protein tertiary structure. RaptorX protein models of RPE65 structure made by our laboratory that show distortions (arrows) using the Bos taurus 2.1-Å resolution crystal structure (PDB ID 3FSN) template. The

mutations occur in regions of the protein that do not show significant distortions. The R91W mutation occurs in the helix adjacent to the loop indicated by the arrow, and the F229S mutation occurs between two beta-propeller blades and is far removed from the predicted structural distortion. It is possible that the alteration in the loop in the F229S variant (denoted by arrow) is the result of improper folding at the site of the mutation that alters the way other regions of the protein fold. Conversely, it could be the result of problems with the protein modeling. Earlier attempts to model the protein with DeepView were unsuccessful because there was no indication of any structural change (despite thermodynamic calculations performed with PoPMuSiC v2.1 that indicated the protein may not fold correctly). As a result, we performed the modeling with RaptorX.

1.6.4—Rpe65^{tvrm148} (tvrm148) mouse (F229S)

The tvrm148 allele of the *Rpe65* gene was generated as a product of an *N*-ethyl-*N*-nitrosourea (ENU) mutagenesis screen by the Translational Vision Research Models (TVRM) program at The Jackson Laboratory (Won, Shi et al. 2011). Like the rd12 mutation, the tvrm148 mutation was found to map between the microsatellite markers *D3Mit147* and *D3Mit19* (the rd12 mutation only mapped close to *D3Mit19*), and subsequent DNA sequencing of the locus revealed a T-to-C transition in exon 7 of *Rpe65* that resulted in an F229S amino acid substitution (Won, Shi et al. 2011). F229 is an RPE65 residue conserved in most vertebrates, including chicken, zebrafish, and human, but not chimpanzee (which has a tyrosine residue at that position) (Won, Shi et al. 2011). Work showed that tvrm148 mice were found to have reduced dark- and light-adapted ERG response, and retina morphology showed progressive ONL, inner segment (IS), and OS thinning from one month to one year of age (Wright, Chrenek et al. 2013). Won, et al. concluded the tvrm148 allele behaves similarly to the KO allele (Won, Shi et al. 2011). Later work confirmed that the tvrm148 mutation produced a visual phenotype similar to the KO mutation and is presented in "**Chapter III: Complementation test of Rpe65 knockout and tvrm148**" (Wright, Chrenek et al. 2013). The mRNA produced by the mutant tvrm148 allele was present at levels similar to wild type, but mutant protein was present at reduced levels as compared to wild type (Wright, Chrenek et al. 2013). This work suggested that the mutant mRNA is either translated inefficiently or that the mutant protein might be unstable. Protein modeling of the F229S mutation is presented in Fig. 1.10 and indicates the mutant protein may have an altered structure (that could be

destabilizing, although this modeling alone is not conclusive). Properties of the tvrm148 mouse with respect to RPE65 and ERG function are summarized in Table 1.4.

1.6.5—RPE65 polymorphism in C57BL/6 lines

Data in 2000 indicated the C57BL/6J background did not experience photoreceptor damage as the result of light damage (Grimm, Wenzel et al. 2000). Work that same year utilizing C57BL/6J$^{c\text{-}2J}$ (albino C57BL/6J) mice (i.e. albino containing the *Tyr*$^{c\text{-}2J}$ allele on the C57BL/6J background), indicated they received less damage to their photoreceptors following light damage than Balb/c mice (Danciger, Matthes et al. 2000). A highly significant quantitative trait locus (QTL) in albino C57BL/6J mice was found to contribute to almost 50% of the protective effect on photoreceptors following light damage, and genetic mapping identified the *Rpe65* locus as being responsible for the protective effect (Danciger, Matthes et al. 2000). Northern blotting showed *Rpe65* mRNA size correlated well with the size of the 1835 bp nucleotide sequence they reported and expressed at the same level in albino C57BL/6J and Balb/c mice. DNA sequencing of the locus indicated an L450M amino acid substitution in RPE65 protein in albino C57BL/6J mice (Danciger, Matthes et al. 2000). This polymorphism was responsible for the protective effect against light damage.

Later work concerning the L450M allele found in C57BL/6J mice showed the polymorphism was protective by slowing rhodopsin regeneration; slower rhodopsin regeneration ultimately slowed the rate of toxic byproduct production (Grimm, Wenzel et al. 2000), thus protecting the photoreceptors during and following light damage. The L450M allele produced less RPE65 protein in steady-state conditions when compared to

other mouse strains, despite similar mRNA levels, and the mutant protein had 45% of the enzymatic activity of RPE65 protein found in Balb/c mice (Redmond, Weber et al. 2007). All four previously mentioned *Rpe65* mutant mouse lines (KO, rd12, R91W, and tvrm148) are backcrossed to the C57BL/6J mouse line (Redmond, Yu et al. 1998; Pang, Chang et al. 2005; Samardzija, von Lintig et al. 2008; Won, Shi et al. 2011). It should be noted that when authors refer to wild type *Rpe65* (*Rpe65*$^{+}$), they may be referring to the L450M mutant (methionine in place of leucine at amino acid position 450 in RPE65 protein) which is found in C57BL/6J strains. Properties of the RPE65^{L450M} mutation with respect to RPE65 and ERG function are summarized in Table 1.4.

1.6.6—Comparison of the KO mouse with the diet-induced vitamin A-deficient (VAD) mouse

Before the KO mouse was first generated (Redmond, Yu et al. 1998), it was hoped by some researchers vitamin A deficiency could model visual cycle defects in the eye. Comparison of *Rpe65* KO and VAD mice (mice deprived of vitamin A in their diet) showed significant differences between them that may ultimately preclude the use of the KO mouse as a model for vitamin A deficiency. VAD mice showed a much greater degree of OS disorganization than KO mice in addition to a lack of lipid inclusions in the RPE (after all, RPE lipid inclusions in RPE65-deficient mice contain all-*trans*-RE, which could only be present if vitamin A was present) (Hu, Chen et al. 2011). VAD mice had a much higher cone density in the central retina when compared to KO mice, but a lower cone density in the peripheral retina than in KO mice (Hu, Chen et al. 2011), which could affect residual visual function in VAD mice when compared to KO mice. At the

molecular level, cone-specific markers *Gnat2* and short wavelength (SWL)-opsin had much lower expression levels in KO mice when compared to VAD mice, but middle wavelength (MWL)-opsin and the rod-specific markers *Gnat1* and *Rho* had similar expression levels (Hu, Chen et al. 2011). Obviously, there were substantial differences in the retinoid profile of the VAD retina when compared to KO mice. VAD mice, which had been exposed to vitamin A at early ages prior to deprivation, had appreciable amounts of all-*trans*-RAL and 11-*cis*-RAL when compared to KO mice, but KO mice had much higher levels of all-*trans*-RE (Hu, Chen et al. 2011). RPE65 protein, but not LRAT protein (recall LRAT is the protein just upstream in the visual cycle; Fig. 1.3), was expressed in VAD mice; the opposite protein expression profile was seen in KO mice (Hu, Chen et al. 2011). Perhaps more importantly, LRAT protein expression was not rescued after VAD mice were reintroduced to dietary vitamin A (Hu, Chen et al. 2011). Because of the number of important differences observed between VAD and KO mice, which are most likely due to other systemic problems caused by vitamin A deprivation, the KO mouse may not be an appropriate model of vitamin A deficiency in the eye.

1.7—PHENOTYPIC RESCUE OF RPE65-DEFICIENT MICE

Ultimately, the purpose of understanding the basic biology in *Rpe65* mutant mice is to aid in the development of treatments for human LCA2 patients. There are many approaches for the treatment of human LCA2 that are currently in development and being tested in *Rpe65* mutant mice, but only two approaches are in clinical trials at the moment (Table 1.5). The first approach is *RPE65* gene augmentation through the use of viral vectors (injected into the subretinal space between the retina and RPE) to supply the missing retinoid isomerase activity, and the second approach makes use of an oral synthetic 9-*cis*-retinoid to replace missing 11-*cis*-RAL. Work in *Rpe65* mutant mice suggests both methods are safe and effective, and this section of the review will investigate these treatments to replace the missing 11-*cis*-RAL required to form functional visual pigments.

Table 1.5—Current clinical trials for patients with *RPE65* mutations

Method	Drug/Biological	Trial Phase	Trial ID	Active?	Outcome
Viral	rAAV2/4.hRPE65	1, 2	NCT01496040	YES	Pending
Viral	rAAV2-hRPE65	1	NCT00821340	YES	Pending
Viral	rAAV2-CB-hRPE65	1, 2	NCT00749957	YES	Pending
Viral	rAAV-CBSB-hRPE65	1	NCT00481546	YES	Pending
Retinoid	QLT091001	1	NCT01543906	YES	Pending
Viral	AAV2-hRPE65v2	3	NCT00999609	YES	Pending
Retinoid	QLT091001	1	NCT01014052	NO	Successful
Viral	tgAAG76 (rAAV 2/2. hRPE65p.hRPE65)	1,2	NCT00643747	?	Unknown; last updated July 2010
Viral	AAV2-hRPE65v2	1	NCT00516477	YES	Pending
Viral	AAV2-hRPE65v2	1,2	NCT01208389	YES	Pending
Retinoid	QLT091001	1	NCT01521793	YES	Pending

This table shows all the active or completed clinical trials listed on the FDA clinical trials website (clinicaltrials.gov) that aim to treat LCA2 patients.

1.7.1—Viral vector delivery of RPE65

RPE65-expressing vectors can be delivered to the RPE by subretinal injection to partially restore visual function. Many of these vectors are delivered to the subretinal space (between the outer segments of the retina and the RPE) and use RPE-specific promoters to ensure expression of the transgene only in the RPE. After success with recombinant adeno-associated viral (rAAV)-*RPE65* vectors in Briard dogs (Acland, Aguirre et al. 2001; Narfström, Katz et al. 2003; Acland, Aguirre et al. 2005), which carry a spontaneous *RPE65* mutation (4-bp deletion in exon 5 of *RPE65*), work began in parallel with KO mice (Rakoczy, Lai et al. 2003). It is unfortunately beyond the scope of this chapter to discuss Briard dogs in full because the primary focus of the work presented in the dissertation is mouse models of LCA2. Human studies of have LCA indicated that infants have severe visual deficits (Cremers, van den Hurk et al. 2002) and fetuses (Porto, Perrault et al. 2002) have retinal histological aberrations. By adolescence, the retinal degeneration appreciably progresses (Jacobson, Cideciyan et al. 2003), and it was doubtful that older patients could make substantial recovery after gene augmentation because of the degree of visual function loss by that point (Lorenz, Gyurus et al. 2000) (a concern that later was found to be false, as patients into their mid-twenties were successfully treated).

The first rAAV-*RPE65* administration in *Rpe65* mutant mice was made at embryonic day (E) 18 through *in utero* gene therapy, and this treatment successfully preserved visual function in mice (Dejneka, Surace et al. 2004). Soon after successful visual recovery was demonstrated in KO mice, other studies followed, demonstrating rAAV-*RPE65* vectors could rescue isomerase activity and allow for appreciable 11-*cis*-

RAL production (Pang, Chang et al. 2006). Around this time, studies of rAAV-*RPE65* vector administration in the then recently-isolated rd12 mice were being performed. Some of these studies showed visual recovery as measured by ERG correlated with improvements in visual-dependent behavior in the Morris water maze, which is normally used to assess learning and memory but was modified to test behavioral vision (Pang, Chang et al. 2006). These early experiments performed in young mice, before weaning age (Chen, Moiseyev et al. 2006; Pang, Chang et al. 2006), showed that they were amenable to therapy shortly after birth. *In utero* treatments, although successful, were technically demanding, and success in young postnatal mice allowed for easier successful treatment. It was not clear from these studies how old mice could be before they no longer responded to treatment.

The treatment window for effective gene augmentation was further defined in rd12 mice. Postnatal day (P) 18 mice showed that cortical visual function, measured through visual-evoked potentials (VEP), is rescued with vector treatment (Nusinowitz, Ridder et al. 2006). 13-month-old mice showed no improvement in cortical visual function, but 6-month-old mice still recover some function post-treatment (Nusinowitz, Ridder et al. 2006). These results supported speculation that younger LCA2 patients would receive the greatest treatment benefit, and later studies showed ample visual recovery in the 3-month-old rd12 mouse (an age that models LCA2 midcourse pathology in humans) (Li, Li et al. 2011). A comparison of P14- and P35-treated KO and rd12 mice showed similar levels of visual recovery (Pang, Boye et al. 2010). Long-term recoveries of the two mutant lines were not compared, so at this time it is unclear whether similar treatment outcomes persist to later ages. Because patients may have different mutations,

the long-term recovery (>15 months) of both KO and rd12 mice needs to be investigated in mice more fully.

Although the majority of LCA2 treatment with viral vectors has focused on rAAV vectors, other laboratories developed lentiviral vector delivery systems. KO and R91W mice were both responsive to lentiviral-mediated gene transfer of *RPE65* (Bemelmans, Kostic et al. 2006; Bemelmans, Kostic et al. 2008; Kostic, Crippa et al. 2011). Perhaps most importantly, R91W mice showed extensive recovery after treatment at 1 month of age, suggesting many patients (with *RPE65* mutations that retain some enzymatic activity) could have a longer treatment window (Kostic, Crippa et al. 2011). *RPE65* administration to R91W mice rescued cone-specific gene expression (Bemelmans, Kostic et al. 2006; Kostic, Crippa et al. 2011), suggesting human patients could reactivate dormant cone photoreceptors with treatment and open an effective treatment window even further. This evidence has been recently reinforced by more recent work in Briard dogs, which also show protection against cone loss after gene therapy treatment (Mowat, Breuwer et al. 2013).

Some *Rpe65* mutant mice may exhibit long-term visual recovery, but human patients may need multiple administrations. Work in both KO (Li, Kong et al. 2009) and rd12 mice (Barker, Broderick et al. 2009) suggested minimal immune response took place after treating mice a second time, increasing the likelihood of safe multiple treatments in humans, if needed.

As reviewed in Bush, et al, this extensive field of research in RPE65-deficient dog and mouse models ultimately allowed *RPE65* gene therapy to proceed to clinical trials (Buch, Bainbridge et al. 2008). Initial safety trials conducted in a handful of patients

between 17 and 26 years of age (Bainbridge, Smith et al. 2008; Hauswirth, Aleman et al. 2008; Maguire, Simonelli et al. 2008) showed only a marginal increase in immune response markers in treated patients (Maguire, Simonelli et al. 2008) but showed increased pupil responses to light (Maguire, Simonelli et al. 2008), increased visual acuity (Maguire, Simonelli et al. 2008), gains in abilities to navigate an obstacle course (Bainbridge, Smith et al. 2008), and subjective improvements in visual function as reported by the patients, despite insignificant improvements in ERG responses (Bainbridge, Smith et al. 2008; Hauswirth, Aleman et al. 2008; Maguire, Simonelli et al. 2008). The results from these studies prompted researchers to develop plans to treat a larger number of younger patients, to administer higher dosages of the rAAV-*RPE65* vector (Koenekoop 2008), and to better define the treatment window in humans (Stieger and Lorenz 2008). Future work would test visual recovery several months after treatment.

Follow-up studies on patients from clinical trials indicated recovery of visual kinetics. In treated regions of eyes, there was a 50-fold increase in cone photoreceptor sensitivity and a 63,000-fold increase in rod photoreceptor sensitivity (Cideciyan, Aleman et al. 2008). Despite improvements in photoreceptor sensitivity, recovery of rod photoreceptor sensitivity after light exposure was slow. Treated patients may have had a slower 11-*cis*-RAL synthesis (which is needed for remaking light-sensitive rod and cone photoreceptors) as compared to patients without visual cycle defects because they still have lower levels of RPE65 protein (Cideciyan, Aleman et al. 2008). Functional magnetic resonance imaging (fMRI) studies of visual cortex function in treated patients showed an increased cortical activation upon exposure to visual stimulus (Ashtari, Cyckowski et al. 2011), a particularly important finding because it showed LCA2 patients

are capable of having restoration of the entire visual pathway, not just recovery of retinal biochemistry. As was suggested by mouse studies, patients treated in childhood were much more likely to make a greater visual recovery after treatment than older patients (Maguire, High et al. 2009). Fortunately, long-term improvements to visual function were conferred by rAAV-*RPE65* treatment in LCA2 patients; patients assessed for visual recovery at 1 year (Cideciyan, Hauswirth et al. 2009), 1.5 years (Simonelli, Maguire et al. 2010), and 3 years post-treatment (Jacobson, Cideciyan et al. 2012) continued to have the same visual improvement that was first reported 3 months post-treatment (Bainbridge, Smith et al. 2008; Hauswirth, Aleman et al. 2008; Maguire, Simonelli et al. 2008). Hopefully, upon successful completion of Phase 3 clinical trials, these rAAV treatments will be able to help other patients restore functional vision in patients worldwide. It is unclear at this time how much visual recovery will be conferred by these treatments or whether it will be sufficient to allow these patients to live normal lives, but these clinical trials are certainly important steps in the treatment of this disease.

1.7.2—9-cis-*retinoid supplementation*

As mentioned earlier, KO mice retained appreciable residual visual function at younger ages as measured by ERG (Redmond, Yu et al. 1998). KO mice that were kept in the dark for up to 12 weeks after being reared in cyclic light experienced a steady increase in visual function as measured by ERG, and this visual function recovery correlated with an increase in endogenous 9-*cis*-RAL levels (Fan, Rohrer et al. 2003). Although the mechanistic pathway for 9-*cis*-retinoid generation in the eye is not currently understood, mice harboring the KO allele were capable of greater 9-*cis*-RAL generation

if they had a tan coat color instead of the normal black coat color (Fan, Wu et al. 2006). Because RPE65-deficient mice could still generate 9-*cis*-RAL and therefore regenerate functional isoforms of light-sensitive pigment in the form of isorhodopsin (Fan, Rohrer et al. 2003), treatment of RPE65 deficiency with 9-*cis*-retinoids instead of gene therapy vectors is an attractive alternate treatment strategy. Again, researchers reasoned treatment success in LCA2 mouse models could translate into successful treatment in humans.

Early efforts to treat KO mice with 9-*cis*-RAL administration met with rapid success, presumably because of its increased stability compared to 11-*cis*-RAL and its resistance to breakdown in the mouse digestive tract (Van Hooser, Aleman et al. 2000; Van Hooser, Liang et al. 2002). Treatment with oral 9-*cis*-RAL allowed for some visual recovery in KO mice within 48 hours of treatment because of isorhodopsin pigment formation in rods (Van Hooser, Aleman et al. 2000; Van Hooser, Liang et al. 2002). Perhaps more important was the fact that treatment with high doses of 9-*cis*-RAL allowed for full rod photoreceptor recovery when the mice were treated at a relatively young age (2-3 months), and that this visual recovery persisted for more than 6-months post-treatment (Van Hooser, Liang et al. 2002). High doses of 9-*cis*-retinoid supplementation have been demonstrated to be safe in mice (Maeda, Dong et al. 2012).

Young LCA2 patients experience foveal morphological disturbances (Maeda, Cideciyan et al. 2009), suggesting early cone photoreceptor loss is a hallmark of disease progression in humans. KO and *Lrat*$^{-/-}$ mice (recall LRAT is another protein in the visual cycle; Fig. 1.3), which are considered comparable models of LCA because of similarities in visual and molecular phenotypes (Fan, Rohrer et al. 2008), experience early cone photoreceptor death, and treatment with 9-*cis*-retinyl acetate improved visual function in

addition to slowing cone photoreceptor cell loss (Maeda, Cideciyan et al. 2009; Maeda, Maeda et al. 2009). Restoration of cone photoreceptor function and protection from cell death by 9-*cis*-retinoid treatment are both important findings because recent work indicated that cone photoreceptor cell loss defines the effective treatment window for LCA2 (Zhang, Zhang et al. 2011). Furthermore, intravitreal injection of 9-*cis*-RAL in Briard dogs with *RPE65* mutations helped restore visual function (Gearhart, Gearhart et al. 2010), which helped pave the way for more human clinical trials, this time with the 9-*cis*-retinoid QLT091001. Clinical trial (Table 1.5) data publication will be forthcoming.

1.7.3 nanoparticle vector and electroporation gene delivery

Other methods that show promise for treatment of LCA2 that have not reached clinical trials are nanoparticle-mediated vector delivery and *in vivo* electroporation of RPE. Recent work with nanoparticles containing scaffold/matrix attachment regions (S/MARs) showed that they aid in transport of the expression vector to the nucleus for enhanced expression of transgene (Koirala, Makkia et al. 2013). S/MAR-containing nanoparticles have allowed for successful restoration of *RPE65* expression in mice when driven by the vitelliform macular dystrophy 2 (VMD2, an RPE-specific gene) promoter (Koirala, Makkia et al. 2013). *RPE65* expression was detectable in mice for up to 2 years after treatment with the nanoparticle-complexed vector, and visual recovery was noted in both dark-adapted, green sensitive (M)-cone, and UV-sensitive (S)-cone specific ERGs (Koirala, Makkia et al. 2013). Also, work is currently being developed for *in vivo* electroporation of *RPE65* expression vectors (Johnson, Berglin et al. 2008). Work with reporter plasmids have shown that subretinal injection of vector followed by *in vivo*

electroporation could allow for fairly widespread expression of transgene (Johnson, Berglin et al. 2008). Such nonviral methods of gene delivery could be valuable because of a potential for lower treatment costs and reduced risk of immunological response.

1.8—INTRODUCTION SUMMARY

RPE65 is the enzyme responsible for the all-*trans*-vitamin A to 11-*cis*-vitamin A isomerization critical to visual cycle function. Although the visual cycle was first observed in 1878 by Kühne (Kühne 1878) and first described in 1935 by George Wald (Wald 1935), the protein directly responsible for the critical all-*trans* to 11-*cis* conversion of vitamin A would not be definitively identified for another seventy years (Moiseyev, Chen et al. 2005). The creation and identification of several animal models of RPE65 deficiency, particularly in the mouse, has greatly contributed to the field's understanding of visual cycle biochemistry, clinical presentation, and most importantly, avenues of treatment for patients afflicted with LCA2. In addition, the RPE65-deficient mouse lines have provided biomedical research with an ideal model system for the further development and refinement of gene therapy methods currently used in human clinical trials.

Despite initial reports that suggested that many *Rpe65* mutations may have similar visual and biochemical phenotypes, subsequent work with R91W, rd12, and tvrm148 mutations indicated that each mutation might have subtle nuances in their manifestations. The purpose of the work presented in this dissertation was to test whether the tvrm148 and rd12 mutations had phenotypes distinct from the KO mice. Because the KO mouse is the primary strain used to model LCA2, it is possible that aspects of LCA2 presentation

in humans are not being accurately modeled in these mice. The similarities of the tvrm148 and rd12 mutations to human *RPE65* mutations (single nucleotide substitutions in regions or positions in the *RPE65* gene known to be deleterious to visual function; Fig. 1.9) suggests the findings of the studies presented in this dissertation could have an impact in our understanding and treatment of patients in the clinic.

Key points presented in this section:

1. The eye is the organ that allows us to see the world around us. The light-sensitive part of the eye is the retina, which contains rod photoreceptor cells for colorless dim light vision, cone photoreceptor cells for color bright light vision, and intrinsically photosensitive retinal ganglion cells (ipRGCs) that entrain the body's internal clock to daily biological rhythms. The RPE is a single cell layer in the back of the eye that keeps the overlying retina healthy.
2. The visual cycle is the metabolic pathway that recycles 11-*cis*-retinal, the necessary cofactor for the function of light-sensitive proteins in the retina. Binding of 11-*cis*-retinal to opsin creates rhodopsin, and when exposed to light, the 11-*cis*-retinal is isomerized to all-trans-retinal. This activates rhodopsin for visual transduction. Components of the visual cycle are found in the retina and the underlying RPE.
3. RPE65 is a protein found in the RPE that is critical to recycling the 11-*cis* double bond in the light-sensitive form of vitamin A.
4. When RPE65 does not work, patients suffer from a disease called Leber congenital amaurosis, type 2 (LCA2) that is characterized by blindness from birth or early childhood. LCA occurs in 2-3 births per 100,000 births, and approximately 6% of those individuals have mutations in *RPE65*.
5. The *Rpe65* gene knockout (KO), rd12, R91W, and tvrm148 mutations are mutations that occur within the mouse *Rpe65* gene. This dissertation shows work that definitively proves the tvrm148 and rd12 mutations occur in the *Rpe65* gene by complementation test (which is considered the gold standard for determining if

a mutation is in a gene but was not performed previously for either the tvrm148 or rd12 mutations).

6. *Rpe65* mouse mutations have aided in the development of treatments for patients in the clinic by providing models to study how the disease progresses and what methods show promise in treating the disease.
7. All mouse *Rpe65* gene mutations may not produce the same mutant phenotype. Understanding how different mutations may affect gene function and cell biology can aid in the creation of new or more refined treatments for patients in the clinic.

II: Cellular pathologies in RPE65-deficient mice

This chapter is currently being prepared as a review article.

Key questions to be addressed in this section:

1. Which photoreceptors contribute the most to visual function in mice with *Rpe65* gene mutations?
2. How do rod photoreceptors die in *Rpe65* mutant mice?
3. How do cone photoreceptors die in *Rpe65* mutant mice?
4. What abnormalities do RPE cells show in *Rpe65* mutant mice?

2.1—CELLS MEDIATING RESIDUAL VISUAL FUNCTION IN RPE65-DEFICIENT MICE

The understanding of the photoreceptors responsible for residual visual function in *Rpe65* mutant mice has evolved considerably over time. When the KO mouse was first generated, it was assumed RPE65-deficient mice retained visual function through cone photoreceptors because dark-adapted ERG responses were almost undetectable in KO mice but were partially preserved at high light levels (Redmond, Yu et al. 1998). Both rd12 (Pang, Chang et al. 2005; Roman, Boye et al. 2007) and tvrm148 mice (Won, Shi et al. 2011) lose ERG responses in a similar pattern. Follow-up work examined cone-specific ERG responses, and data from KO mice indicated there was very little response from S cones and an abnormal M cone response at early ages (Ekesten, Gouras et al. 2001). It should be noted that mice only have two types of cones (Szél, Röhlich et al. 1992). A logical interpretation of this work concluded that residual visual function in *Rpe65*-deficient mice was attributable to M-cone photoreceptors and not S-cone photoreceptors or rod photoreceptors (Ekesten, Gouras et al. 2001). We now know this interpretation to be incorrect. Follow-up work from another laboratory (Seeliger, Grimm et al. 2001) suggested that rods, not cones, were primarily responsible for residual visual function. Crosses of KO mice with $Rho^{-/-}$ (cone vision only) and $Cnga1^{-/-}$ (rod vision only) mice showed that KO:$Rho^{-/-}$ mice did not retain vision but KO:$Cnga1^{-/-}$ mice did (Seeliger, Grimm et al. 2001). This work strongly suggested rods, not cones, were the photoreceptors that mediate residual visual function. It was proposed rods might respond only in bright light conditions (Seeliger, Grimm et al. 2001). If this was the case, then it meant that visual function in RPE65-deficient mice was rod-mediated.

Rod-mediated visual function in *Rpe65* mutant mice is directly related to the fact that the overall scotopic sensitivity of the retina in these mice is diminished by roughly 10,000-fold (Ablonczy, Crouch et al. 2002; Woodruff, Wang et al. 2003). Little functional rhodopsin is regenerated in RPE65-deficient mice, and it was speculated that unliganded rod opsin may constitutively activate the phototransduction cascade because there is no bound 11-*cis*-RAL ligand (Woodruff, Wang et al. 2003). The quantum catch capability of rods for photons depends on large amounts of functional rhodopsin being present so that a single photon can activate the phototransduction cascade (Ablonczy, Crouch et al. 2002), as is the case in a dark-adapted wild type retina. Because there is so little functional rhodopsin that is capable of catching a photon, it takes far more light to completely saturate the rod photoreceptors still functional in the retina (Dell'Orco, Schmidt et al. 2009). Furthermore, ERG results from Seeliger et al. (Seeliger, Grimm et al. 2001) were later confirmed in visually-evoked behavioral assays measuring optokinetic motor responses in KO and KO*:Rho*$^{-/-}$ mice (Cachafeiro, Bemelmans et al. 2010). KO mice only had an optomotor response if rod photoreceptors were still present (Cachafeiro, Bemelmans et al. 2010). Further evidence arguing for rod-mediated residual visual function in RPE65-deficient mice came from studies showing an early loss (before P30) of S-cone photoreceptors (and a slower loss of M-cone photoreceptors) (Kunchithapautham, Coughlin et al. 2009; Pang, Boye et al. 2010; Fan, Crouch et al. 2011; Tang, Buhusi et al. 2011). Cones cannot mediate residual visual function if they are not present.

In addition to rods and cones, recent work has shown that intrinsically photosensitive retinal ganglion cells (ipRGCs) could possibly contribute to visual and

non-visual responses in mice (Ecker, Dumitrescu et al. 2010). Mice lacking both rod and cone photoreceptors still retained some ability to discriminate patterns in vision as shown through experiments using the visual water task (VWT), another behavioral test of vision. It should be noted that OKT testing cannot detect the ipRGC contribution to visual acuity (Ecker, Dumitrescu et al. 2010). ipRGCs also play a role in circadian rhythm entrainment, pupillary light response (PLR), and light aversion behavior (Fu, Zhong et al. 2005; Thompson, Recober et al. 2010), and KO mice have a reduced PLR similar to that found in human LCA2 patients (Aleman, Jacobson et al. 2004). Reduced PLR in KO mice seems to be due to slow melanopsin regeneration (Doyle, Castrucci et al. 2006), but melanopsin regeneration can be restored to a certain degree if rod photoreceptors in KO mice are lost (because rods scavenge chromophore from the retina to the detriment of other cells in KO mice) (Doyle, Castrucci et al. 2006). There is evidence in the literature that suggests that RPE65 is not directly involved in melanopsin regeneration, and that the melanopsin photocycle is independent of the rod visual cycle (Tu, Owens et al. 2006). Taken together, these data suggest that: 1) rod photoreceptors in RPE65-deficient mice outcompete other cell types (including ipRGCs) for free chromophore in the retina, and that 2) ipRGCs most likely do not contribute to pattern discrimination (visual acuity) in *Rpe65* mutant mice because rods rob them of chromophore needed for their function. What is currently unclear is how the retina has any chromophore (light-sensitive retinoid) if RPE65 is not present.

Because KO and rd12 mice have no detectable levels of 11-*cis*-RAL in the eye (Redmond, Yu et al. 1998; Pang, Chang et al. 2005), the source of rod photoreceptor chromophore is unclear at this time. It might be expected that these mice would not have

any appreciable visual function remaining at any age because 11-*cis*-RAL is undetectable (the lower limit of detection for this assay being 1 pmol), but several possibilities for the chromophore source exist. For example, 11-*cis*-RAL could be obtained in low levels through diet. Most mouse chow formulations contain vitamin A. The cone-specific visual cycle, which operates independently of the RPE and its associated proteins (Fleisch and Neuhauss 2010; Wang and Kefalov 2011; Saari 2012), could account for some chromophore that the rod photoreceptors could then scavenge. There is increasing evidence in the literature to support the role of dihydroceramide desaturase (DES-1), which is typically known for inserting double bonds into its widely known substrate (dehydroceramide, a lipid), in Müller cells as the retinoid isomerase in the cone visual cycle (Kaylor, Yuan et al. 2013). Also, KO mice are capable of generating 9-*cis*-RAL when they are dark-reared (9-*cis*-retinoids are now currently being investigated as a treatment option in humans in clinical trials, please refer back to Section 1.7.2), and this chromophore can form the alternative photopigment isorhodopsin (Fan, Rohrer et al. 2003). The generation of 9-*cis*-RAL was later confirmed in another study (Fan, Woodruff et al. 2005), but it is still not currently known which proteins or pathways are responsible for 9-*cis*-RAL regeneration, but evidence from zebrafish points to another possible retinoid isomerase that operates independently of both RPE65 and DES1 (Takahashi, Moiseyev et al. 2011) that could play an as-of-yet undiscovered role in mice. 9-*cis*-RAL regeneration was reported to be increased in knockout mice with lighter coat color (Fan, Wu et al. 2006). We speculate that mouse skin melanocytes may have unexpected properties involved in the metabolism of retinoids, and this idea is supported by the fact

that visual cycle proteins have been reported in skin cells previously (Amann, Luo et al. 2012).

2.2—ROD PHOTORECEPTOR CELL DEATH

In contrast to the rapid death of cones, retinal morphology indicates rod photoreceptor cell death occurs slowly in KO mice (Redmond, Yu et al. 1998; Pang, Chang et al. 2005; Samardzija, von Lintig et al. 2008; Won, Shi et al. 2011). In the RPE65-deficient rod photoreceptor, opsin apoprotein has little to no access to chromophore, and what little chromophore does traffic to the retina seems to be immediately scavenged by rod photoreceptors to the detriment of other cells that require chromophore, such as cones (Samardzija, Tanimoto et al. 2009) and ipRGCs (Doyle, Castrucci et al. 2006). Rod photoreceptors ultimately die as the result of a constitutively active phototransduction cascade (Rohrer, Ablonczy et al. 2003). The hypothesis that a constitutively active phototransduction cascade could induce rod apoptosis was supported by the fact that GRK1 (a protein involved in the initiation of the phototransduction cascade) was protective against rod cell death in RPE65-deficient mice (Fan, Sakurai et al. 2010). If the phototransduction cascade is not initiated in KO mice (which requires GRK1), then rods seem to be protected against damage. A constitutively-active phototransduction cascade as a pathological mechanism is only one hypothesis for rod cell death.

Some researchers have hypothesized that the absence of chromophore in RPE65-deficient animals and humans could cause rhodopsin mislocalization and contribute to rod cell death. Although rhodopsin localizes appropriately to rod photoreceptor outer

segments in mice with 11-*cis*-RAL deficits (Zhang, Fan et al. 2008), dogs with *RPE65* mutations experience profound rhodopsin trafficking defects (Hernández, Pearce-Kelling et al. 2010). It is currently not understood why localization of rhodopsin is impaired in RPE65-deficient dogs but not RPE65-deficient mice. These data make it likely the consitituvely-active phototransduction cascade may be primarily responsible for rod cell death.

BCL-2, BAX, BAD, and BMF all appear to play a role in rod apoptosis in KO mice. BCL-2 was implicated in rod apoptosis because *Bcl-2* mRNA levels were reduced in the retina of KO mice (Cottet, Michaut et al. 2006). In addition to downregulated Bcl-2, there was a parallel upregulation of proapoptotic genes *Bax*, *Bad*, and *Bmf* (Cottet, Michaut et al. 2006). Roles of BCL-2 and BAX in mediating rod apoptosis were confirmed in mice that were mutant for both *Rpe65* and *Bax* (Hamann, Schorderet et al. 2009). Further evidence of a constitutively active phototransduction cascade directly causing rod cell death in *Rpe65* mutant mice was confirmed when it was also found that KO*:Gnat1*$^{-/-}$ (i.e. deficient in RPE65 and a protein involved in phototransduction) mouse rods were resistant to apoptosis (Hamann, Schorderet et al. 2009). Later work shows that although rod apoptosis is mediated through Bax induction, apoptosis of rods in *Rpe65* mutant mice does not require caspase activation (Métrailler, Schorderet et al. 2012). Furthermore, an early, rapid wave of rod cell death (Fig. 2.1A) between P7 and P25 was found in RPE65-deficient mice (Métrailler, Schorderet et al. 2012). The early wave of apoptosis occurs through BAX induction but coincides with increased expression of autophagy markers *Cathepsin S* (*CathS*), *Lysozyme*, and *Lamp2*, which all have neuroprotective effects (Métrailler, Schorderet et al. 2012). Autophagy gene upregulation

protects most rods from cell death for quite some time, but eventually, BAX-induced apoptosis causes the cells to die (Fig. 2.1B) (Métrailler, Schorderet et al. 2012). In summary, rod cell death (at least in KO mice) is caused by constitutive activation of the phototransduction cascade that results in downregulation of BCL-2 alongside BAX activation, and these proapoptotic events are locked in a tug-of-war with antiapoptotic autophagy markers. It should be noted that data presented in later chapters indicates that although rod photoreceptors are lost, this loss is very slow and does not affect all rod photoreceptors.

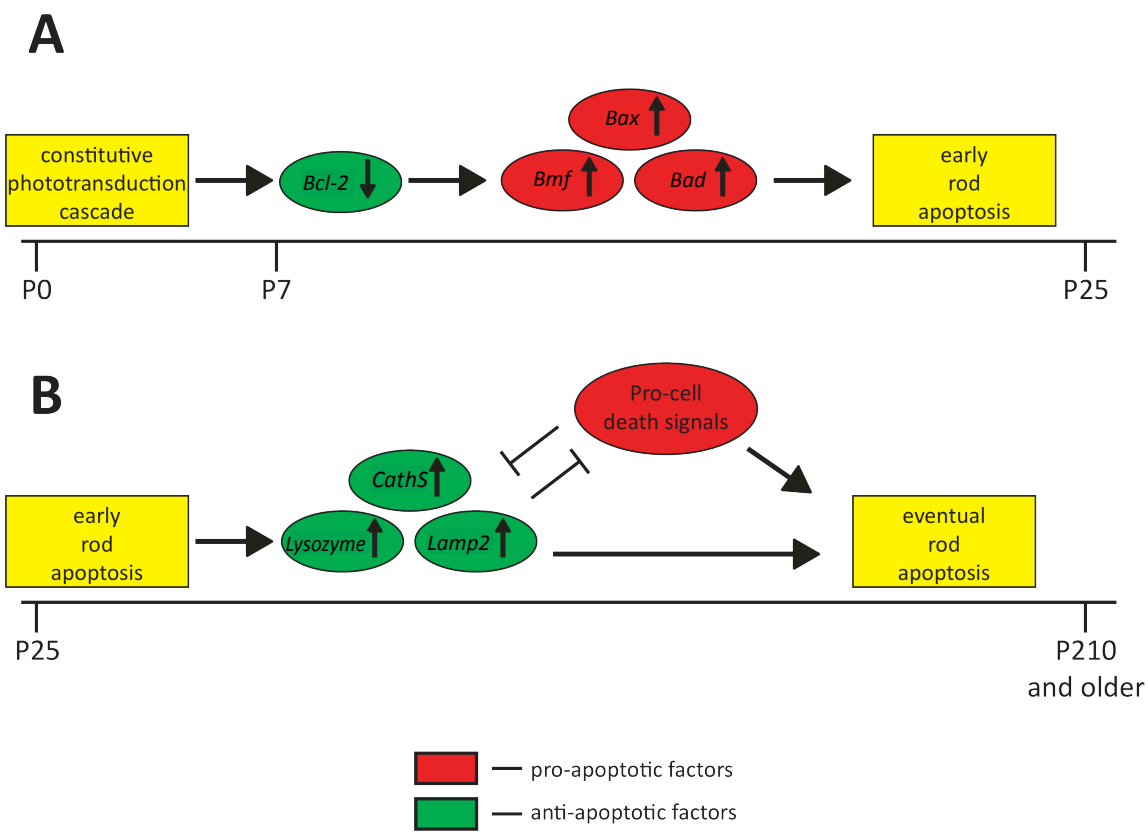

Figure 2.1—Rod photoreceptors are subject to two phases of cell death. The primary driving factor of rod cell apoptosis in RPE65-deficient mice is a constitutively active phototransduction cascade that occurs in the absence of 11-*cis*-RAL. (**A**) An early wave of cell death (P7-P25) occurs because the constitutively active phototransduction cascade is associated with a decreased levels of the anti-apoptotic factor BCL-2. Low BCL-2 levels leads to higher levels of the pro-apoptotic factors BAX, BAD, and BMF; although GNAT1 inhibits pro-apoptotic pathway signaling, some rod cells die by P25. (**B**) Most rod photoreceptors survive the initial wave of early apoptosis because the death between P7 and P25 leads to upregulation of anti-apoptotic autophagy markers *CathS*, *Lysozyme*, and *Lamp2*. Eventually, pro-apoptotic signaling overcomes any protective effects offered by these autophagy markers, and rod cells die. In addition to GRK1 deficiency being protective in RPE65 mutant mice, mice mutant for BAX in addition to RPE65 are also protected against retinal degeneration (Métrailler, Schorderet et al. 2012).

2.3—CONE PHOTORECEPTOR CELL DEATH

By P30, the majority of residual visual function in RPE65-deficient mice comes from rods, not cones (Seeliger, Grimm et al. 2001). It was clear from early work with KO mice that the cone ERG response from mutant mice was minimal by P30 (Ekesten, Gouras et al. 2001), and that this cone function reduction coincided with reductions in cone-specific gene marker expression (Znoiko, Rohrer et al. 2005). Cone degeneration was detectable as early as two weeks of age in KO and rd12 mice (Znoiko, Rohrer et al. 2005; Pang, Boye et al. 2010). S-opsin expression is reduced before M-opsin expression in the retina of RPE65-deficient mice (Znoiko, Rohrer et al. 2005), and cone photoreceptors begin to disappear in the central retina by two weeks of age (faster S-cone loss correlates with increased opsin mislocalization) (Pang, Boye et al. 2010). Consistent with earlier downregulation of S-opsin in the retina, cone photoreceptors are lost in the central and ventral retina (where S-cones are found), (Znoiko, Rohrer et al. 2005) before they are lost in the dorsal and temporal regions (where M-cones are found) (Pang, Boye et al. 2010). At 4 weeks of age, S-cone responses (measured by recording the retinal electrical response to UV-flashes) are undetectable in KO mice, but M-cone responses are fairly robust (Ekesten, Gouras et al. 2001). Later work with R91W mice, indicated that cone protein expression could be recovered after lentiviral delivery of human *RPE65* up to 1 month of age (Kostic, Crippa et al. 2011), suggesting that some cone photoreceptors could become dormant until chromophore becomes available. All of these data indicate that most cone photoreceptors are lost at early ages, while residual rod photoreceptors can persist for months to years in RPE65-deficient mice.

Despite emerging evidence for a cone-specific visual cycle that relies on a retinoid isomerase in Müller cells distinct from RPE65 (Wang and Kefalov 2011; Kaylor, Yuan et al. 2013) cone photoreceptors still rely on RPE65-generated 11-*cis*-RAL for proper function because of rod competition for chromophore (Samardzija, Tanimoto et al. 2009). Adenoviral-mediated delivery of human *RPE65* in KO mice at two weeks of age was able to prevent most cone photoreceptor degeneration (Chen, Moiseyev et al. 2006), suggesting that RPE65 plays a vital role in cone photoreceptor health, however indirectly. Instead of being a phenomenon specific to mice, human LCA2 patients show early cone degeneration (Jacobson, Aleman et al. 2007). Early cone loss in human and mouse can be rescued with administration of 9-*cis*-retinyl acetate (Maeda, Cideciyan et al. 2009), suggesting that KO mice accurately model human LCA2 and that a cone-specific retinoid isomerase alone cannot preserve cone health (perhaps because the cone-specific retinoid isomerase cannot produce enough 11-*cis*-RAL to rescue cones). Mice deficient in both RPE65 and rod photoreceptors retain small amounts of ipRGC and cone function, because rods are not present to outcompete other cell types for chromophore (Samardzija, Tanimoto et al. 2009). Because cone photoreceptors can still die in KO and rd12 mice even if rods are absent, cones may die through a separate mechanism.

Unlike rod photoreceptors in *Rpe65* mutant mice, which are protected from cell death in *Bax* mutant mice, cone photoreceptors still experience an early wave of cell death (Hamann, Schorderet et al. 2009), which suggests that cone photoreceptors die through a different pathway than rod photoreceptors. Staining for M-opsin and S-opsin revealed 11-*cis*-RAL deficiency induced mislocalization of cone opsin proteins; instead of being found in the outer segment, cone opsins are found in other regions of the cell

(Rohrer, Lohr et al. 2005). M-opsin does not have the same degree of mislocalization as S-opsin (Rohrer, Lohr et al. 2005), providing an insight into why S-cones die before M-cones. In addition to the mislocalization of cone opsins, other membrane-associated proteins involved in cone transduction, such as guanylate cyclase 1 (GC1), cone T-alpha-subunit (GNAT1), and cone phosphodiesterase 6α (PDE6-alpha), are mislocalized in the absence of 11-*cis*-RAL (Zhang, Fan et al. 2008). The mislocalization of these proteins occurs before cell death (Zhang, Fan et al. 2008) and coincides with downregulation of cone-specific gene expression (Znoiko, Rohrer et al. 2005; Pang, Boye et al. 2010). Cone phototransduction proteins have restored localization upon treatment with 11-*cis*-RAL (Zhang, Fan et al. 2008). Further work confirmed that a greater amount of S-opsin mislocalization ultimately correlates with earlier S-cone death (Zhang, Zhang et al. 2011). Reduced degeneration of opsin proteins may also play a role.

Although M- and S-opsins are both marked for proteasome degradation, only M-opsin is efficiently degraded, providing another reason why M-cones survive longer than S-cones (degradation of inappropriately trafficked or modified proteins aids in the reduction of ER stress; Fig. 2.2) (Zhang, Zhang et al. 2011). Differences in degradation efficiencies could be the result of different posttranslational modifications that occur on M- and S-opsins. S-opsin, unlike M-opsin, has a higher molecular weight in KO mice than wild type mice because N-glycan modifications are not completely processed after translation (Sato, Nakazawa et al. 2010). When treated with retinoid supplementation, complete N-glycan processing occurs for S-opsin, and the mature protein can exit the endoplasmic reticulum (ER) (Sato, Nakazawa et al. 2010). However, M-opsins do not appear to have aberrant N-glycan posttranslational processing (Sato, Nakazawa et al.

2010) and can be degraded by the proteasome at a higher efficiency, thus potentially causing M-cones to cause less ER stress than S-cones (Sato, Ozaki et al. 2012).

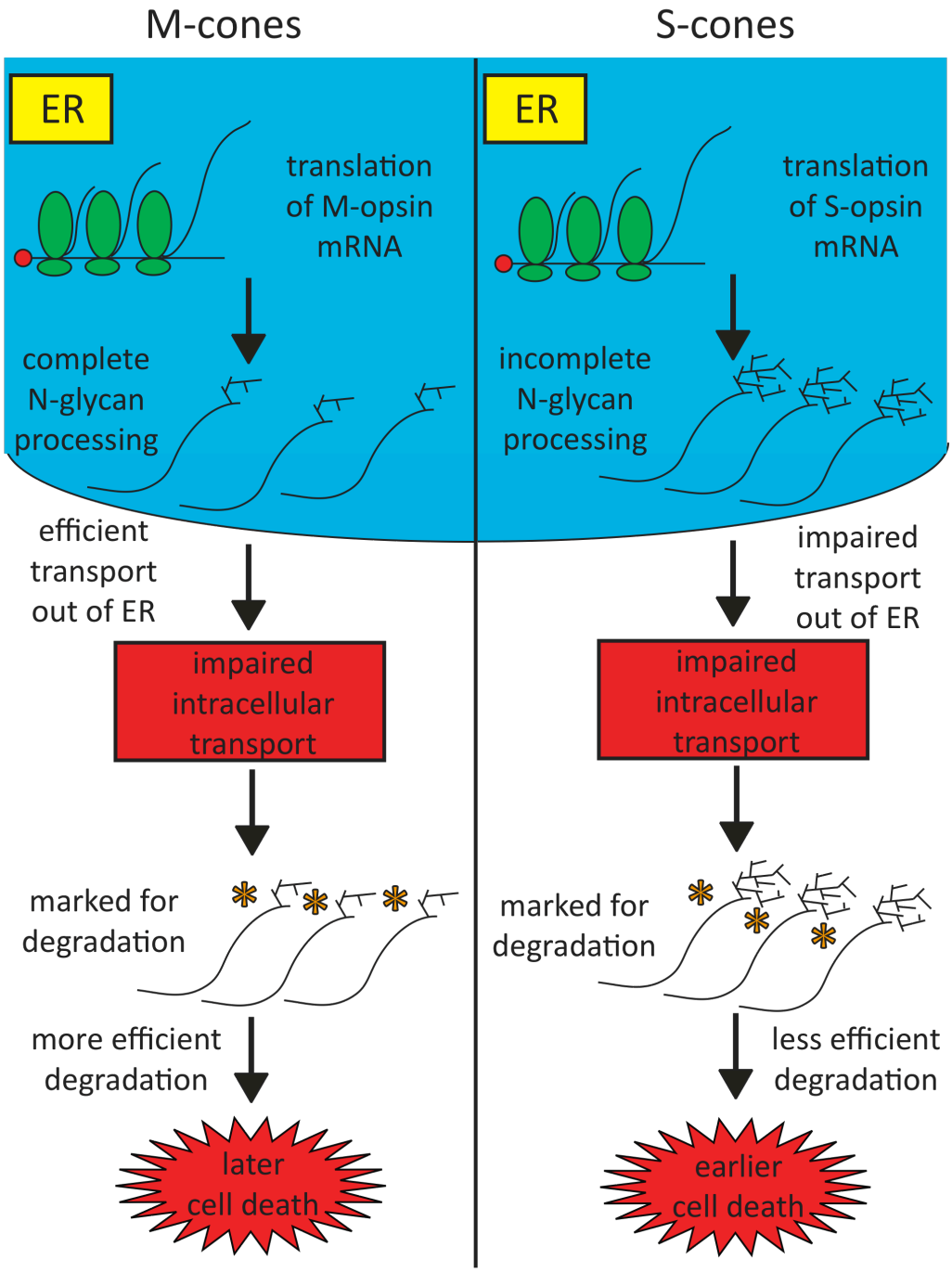
M-cones
S-cones
ER
ER
translation of M-opsin mRNA
translation of S-opsin mRNA
complete N-glycan processing
incomplete N-glycan processing
efficient transport out of ER
impaired transport out of ER
impaired intracellular transport
impaired intracellular transport
marked for degradation
marked for degradation
more efficient degradation
less efficient degradation
later cell death
earlier cell death

Figure 2.2. Cone cell death is associated with altered cone opsin trafficking in the absence of 11-*cis*-RAL. Cone cell death occurs mostly before P30 and is directly related to altered intracellular trafficking of cone opsin proteins. N-linked glycans are covalently attached to the nitrogen-containing side chain in the amino acid asparagine. S-cones die before M-cones. M-opsin has complete N-glycan processing in the ER and is normally trafficked out of the ER. S-cone opsin protein has incomplete N-glycan processing, which increases the protein molecular weight and impairs trafficking of S-opsin out of the ER. Both M- and S-opsin proteins are mistrafficked in cone photoreceptors in the absence of 11-cis-RAL, and both are marked for proteasome degradation. For reasons that are not currently understood, M-opsins are more efficiently degraded than S-opsins. Because of this, M-cones die later than S-cones.

In summary, RPE65-deficient mice experience a rapid, early cone cell death, with S-cones dying before M-cones (<5% S-cones are present by P30, but ~20% of M-cones are present at P60; Fig. 2.2) (Znoiko, Rohrer et al. 2005; Pang, Boye et al. 2010). 11-*cis*-RAL is vital to cone health because it is needed for proper cone opsin localization (Rohrer, Lohr et al. 2005). Rods outcompete cones for available chromophore in the retina of R91W mice (Samardzija, Tanimoto et al. 2009). Cell death may occur via ER stress (Sato, Nakazawa et al. 2010; Sato, Ozaki et al. 2012), and S-cones may die earlier than M-cones because of greater ER stress associated with incomplete maturation of S-opsin as a result of improper posttranslational N-glycan processing (Sato, Nakazawa et al. 2010; Sato, Ozaki et al. 2012). M-opsin N-glycans are processed correctly and leave the ER more efficiently (Sato, Nakazawa et al. 2010; Sato, Ozaki et al. 2012). In addition to potential cell death via ER stress because of improper cone opsin maturation and trafficking, other cone phototransduction proteins are mislocalized (Zhang, Fan et al. 2008). It should be noted that a few cone nuclei are detected in the periphery of the retina until at least P210 (Pang, Boye et al. 2010), but at this time, it is not understood how they remain alive even if they are functionally dormant.

2.4—RPE DYSFUNCTION AND STRESS

Even though RPE65 is by most reports an RPE-specific protein in the eye (Sagara and Hirosawa 1991), the RPE itself seems mostly spared from large amounts of cell death through the life of the KO mouse. Both rd12 and tvrm148 mice exhibit the formation of white spots in the fundus by six months of age (Pang, Chang et al. 2005; Won, Shi et al. 2011). These white-colored areas can also appear in human patients with fundus

albipunctatus, which has been associated with mutations in the visual cycle gene *RDH5* (Yamamoto, Simon et al. 1999) and *RPE65* (Schatz, Preising et al. 2011). It is not currently known how 11-*cis*-retinoid depletion could lead to the accumulation of whitish material in punctate dots on the fundus (under retinal blood vessels). KO mice, on the other hand, were not originally reported to show such formations in the fundus at any age (Redmond, Yu et al. 1998). R91W mice have not been examined for these white fundus spots, at least in reports available in the literature (even though human patients with the R91W mutation have them). Recent results from our laboratory, though, indicate that all *Rpe65* mutant mice have these white fundus spots (Fig 2.3). Other, less obvious, morphological abnormalities have also been reported.

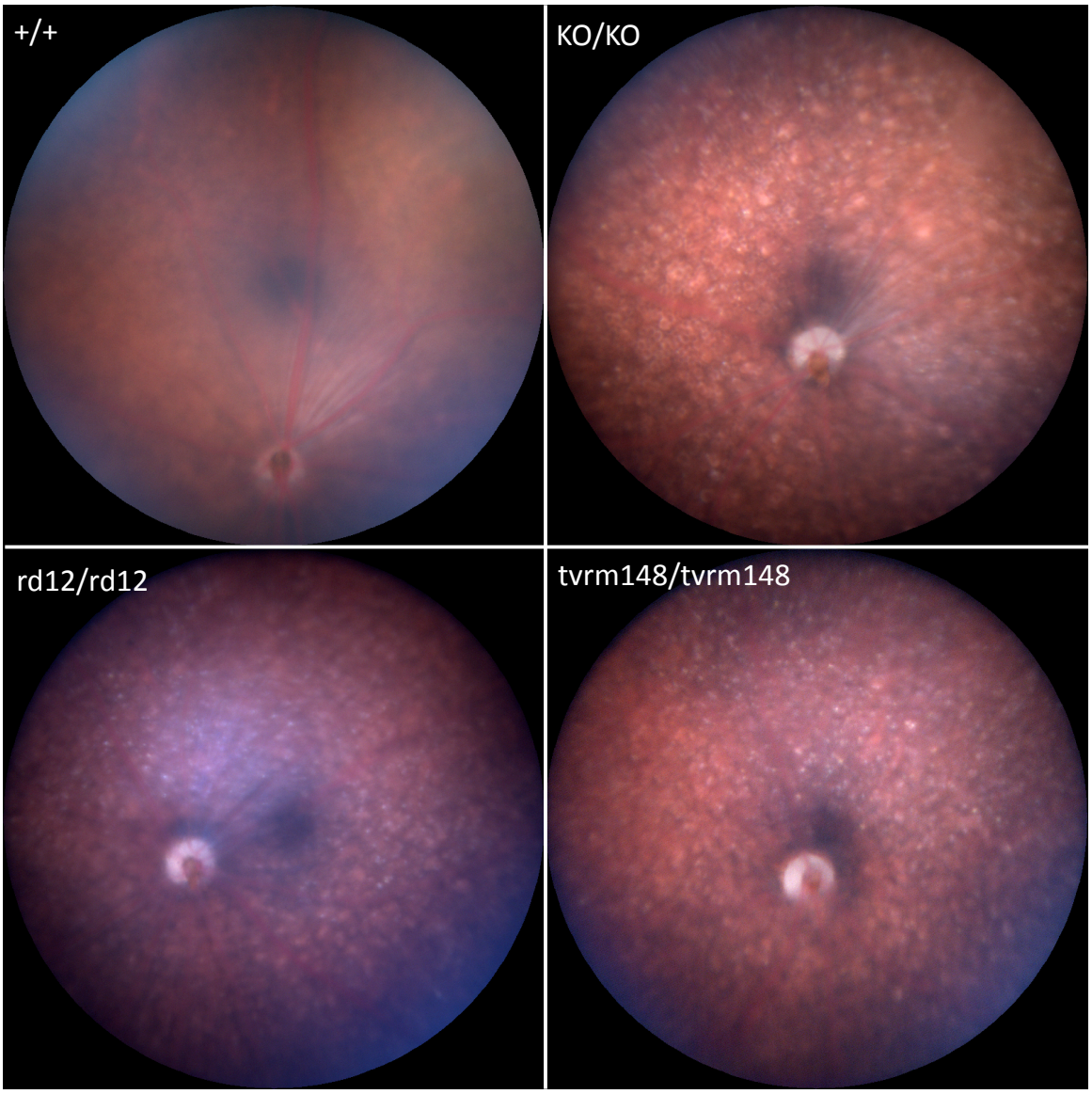

Figure 2.3. Fundus images of wild type and *Rpe65* mutant mice. Fundus photographs of +/+, KO/KO, rd12/rd12, and tvrm148/tvrm148 mice were taken at 4-5 months of age in our laboratory. +/+ mice have no observable abnormalities in the fundus, but all mutant mice show the presence of white punctate dots throughout the fundus. It is not currently known what these white spots consist of in the RPE. The rd12 fundus image will be published along with data and text presented in Chapter 4. This is the first known report of fundus abnormalities in KO/KO mice.

Bruch's membrane is the extracellular matrix that serves as the basement membrane for RPE cells, and some Bruch's membrane abnormalities have been reported. Increasing Bruch's membrane thickness occurs in wild type mice with age, but it occurs earlier in KO mice (by 6 months of age in KO mice versus 1 year of age in wild type) (Ivert, Keldbye et al. 2005). KO mice experience earlier loss of normal plasma membrane basal infoldings than wild type mice and greater intrusions of Bruch's membrane into the basal surface of the RPE (Ivert, Keldbye et al. 2005). RPE basal morphology abnormalities have not been investigated in rd12, R91W, or tvrm148 mice. All RPE65-deficient mice, regardless of mutation, exhibit the formation of lipid vacuoles in the RPE that are widely recognized to be retinyl ester accumulations (Redmond, Yu et al. 1998; Pang, Chang et al. 2005; Samardzija, von Lintig et al. 2008; Won, Shi et al. 2011). The buildup of RPE65 substrate may ultimately cause disruption of other RPE abnormalities.

This buildup of retinoid esters in the RPE forms the foundation for metabolic problems within the RPE. Accumulation of retinyl esters in the RPE occurs through two separate mechanisms: first, through a buildup of all-*trans*-RE (RPE65 substrate) from rod outer segment-supplied all-*trans*-ROL (Redmond, Yu et al. 1998), and second, through a flow of all-*trans*-retinoids to the RPE (Qtaishat, Redmond et al. 2003). In the first mechanism for all-*trans*-RE accumulation, LRAT in the ER first converts all-*trans*-ROL from rod outer segments to all-*trans*-RE, where it then trafficks to retinyl ester storage particles (RESTs) for utilization by RPE65 to produce 11-*cis*-ROL (Imanishi, Batten et al. 2004). Without functional RPE65 to convert substrate to product, the retinosomes swell, because of a block in the visual cycle. For the second mechanism, all-*trans*-

retinoid flow from the RPE to the systemic circulation is impaired in *Rpe65* mutant mice (Qtaishat, Redmond et al. 2003). In *Rpe65* mutant mice, the RPE takes up all-*trans*-ROL from the systemic circulation and converts it to all-*trans*-RE for transport to retinosomes (Imanishi, Batten et al. 2004). All-*trans*-RE cannot be transported from the RPE to systemic circulation, so once all-*trans*-ROL enters the RPE, it becomes trapped (unless it is metabolized to another retinoid product) (Qtaishat, Redmond et al. 2003). As a side note, although different laboratories will use the different terms "lipid vacuole," "REST," "retinosome," and "retinyl ester accumulations," they are all generally considered interchangeable with respect to the RPE. Lipid inclusions will appear as holes in TEM images as the result of histological processing.

The excessive all-*trans*-retinoid accumulation in *Rpe65* mutant mice may ultimately alter gene transcription in the RPE. Work in ARPE-19 cells suggested all-*trans*-retinoids can reduce expression of genes typically transcribed by RPE cells, such as *RPE65*, *RDH5*, and *RRH*; this retinoid accumulation ultimately delays ARPE-19 differentiation in culture (Janssen, Kuhlmann et al. 2000). Work in HEK293 cells, which express genes associated with retinoid metabolism (Chen, Moiseyev et al. 2003), was reported to regulate *RPE65* expression through transcription factors activator protein 1 (AP1), AP4, and nuclear factor 1 (NF1) (Chen, Ma et al. 2003). These transcription factors are in turn regulated by the retinoic acid receptors RARalpha, RARbeta, RARgamma, RXRalpha, RXRbeta, and RXRgamma (Chen, Ma et al. 2003). Addition of all-*trans*-ROL caused retinoic acid receptors to repress AP1, AP4, and NF1 transcription factor binding to the *RPE65* promoter (Chen, Ma et al. 2003). So, if RPE65 enzymatic activity were diminished, it may be possible that accelerated all-*trans*-retinoid

accumulation, brought about by reduced retinoid isomerase activity, could further reduce *RPE65* expression, potentially feeding into a cycle in which an already detrimental situation for the RPE is exacerbated. To date, the direct effects of increased levels of retinoic acid on RPE gene transcription has not been studied *in vivo*.

Unexpectedly, *Rpe65* mutations confer RPE cells with the unexpected benefit of reduced lipofuscin fluorophore accumulation (lipofuscin is a risk factor for age-related macular degeneration) (Katz and Redmond 2001). A2E, a pyridinium bisretinoid that can be formed through the conjugation of two retinaldehydes (Katz, Wendt et al. 2005) in photoreceptor outer segments that accumulate in the RPE after outer segment phagocytosis (Kim, Fishkin et al. 2004), is a major component of lipofuscin fluorophores that cause fundus autofluorescence (Katz and Redmond 2001). Mice homozygous for the KO allele do not accumulate lipofuscin fluorophores, and that KO/+ mice have a significant reduction in fluorophore accumulation with respect to wild type mice (Katz and Redmond 2001). The L450M variant, found in C57BL/6J mice, was found to be protective in terms of the prevention of lipofuscin fluorophore accumulation (Kim, Fishkin et al. 2004). Albino C57BL/6J mice showed significantly less fundus autofluorescence than Balb/c counterparts because C57BL/6J mice have half the isomerase activity compared to Balb/c mice (Kim, Fishkin et al. 2004). Selective abolishment of RPE65 enzymatic activity is sufficient for this inhibition of A2E formation (Maiti, Kong et al. 2006). Interestingly, A2E itself may directly inhibit RPE65 enzymatic activity (Moiseyev, Nikolaeva et al. 2010). Ultimately, it appears KO mice are protected from A2E formation because they cannot accumulate all-*trans*-RAL that is necessary for A2E formation (Katz, Wendt et al. 2005). In summary, although KO mice

suffer from significant photoreceptor and retinal pathology, the RPE, with the exceptions of some slight alterations in morphology and gene transcription (Fig. 2.4), may become resistant to other RPE-associated disease processes.

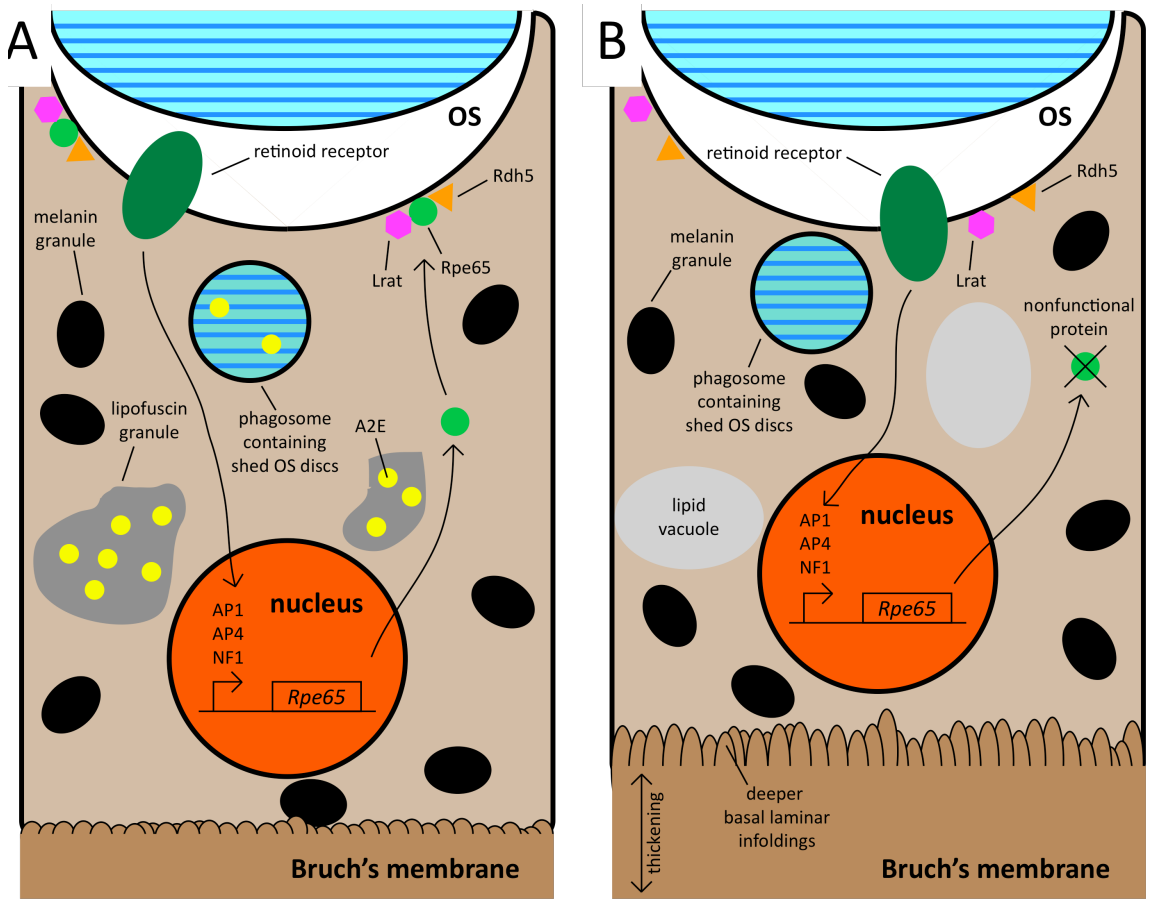

Figure 2.4. RPE cells experience only slight morphological aberrations during RPE65-deficiency. Wild type RPE is shown on the left and RPE65 mutant RPE shown on the right. RPE65-deficient mice experience only small morphological changes with age in the RPE (**B**) compared to wild type mouse RPE (**A**). In the *Rpe65* mutant mouse, lipofuscin granules do not accumulate because A2E bisretinoids cannot form in the rod OS. Lipid vacuoles containing all-*trans*-RE accumulate over time because of the block in the visual cycle caused by absent isomerase activity. RPE cells experience earlier Bruch's membrane thickening and deeper basal laminar infoldings. Retinoid receptors are not shown in either panel but are found on basolateral infoldings.

Key points presented in this section:

1. Rod photoreceptors mediate most of the residual visual function in mice with *Rpe65* mutations.
2. Rod photoreceptors die in *Rpe65* mutant mice because of constitutive activation of the rod phototransduction cascade in the absence of 11-*cis*-RAL. Most rods, though, die only rarely in the retina and usually at later ages.
3. Cone photoreceptors die in *Rpe65* mutant mice because of cell stress induced by errors in the intracellular transport of cone opsin proteins in the absence of 11-*cis*-retinal. S-cones are mostly gone by P30, while M-cones can persist until P60. Some cones can become dormant and survive until several months of age, mostly in the periphery of the retina.
4. When the *Rpe65* gene is mutated in mice, there is a buildup of all-*trans*-retinyl esters (which is substrate for RPE65 protein) that causes swelling of lipid vacuoles in the RPE. No detectable 11-cis-RAL is made in mutant mice.

III: Complementation test of *Rpe65* knockout and tvrm148

This chapter has been published. Wright C. B., Chrenek M. A., Foster S. L., Duncan T., Redmond T. M. Pardue M. T., Boatright J. H., Nickerson J. M. Complementation test of Rpe65 knockout and tvrm148 (2013). Invest Ophthalmol Vis Sci. 54(7):5111-22.

Key questions to be addressed in this section:

1. Does the tvrm148 mutation cause a block in the visual cycle (i.e. abolish enzymatic activity required to recycle retinoids)?
2. How is the tvrm148 mutation inherited (autosomal recessive, autosomal dominant, etc.)?
3. What happens to visual function in mice if they have one or two copies of the tvrm148 mutation?
4. What morphological abnormalities in the eye do tvrm148 mutant mice have?
5. Do tvrm148 mice express *Rpe65* at both the mRNA and protein levels?
6. What relevance does the tvrm148 mutation have with respect to patients in the clinic?

3.1—ABSTRACT

Purpose. A mouse mutation, tvrm148, was previously reported as resulting in retinal degeneration. tvrm148 and *Rpe65* map between markers D3Mit147 and D3Mit19 on a genetic map, but the physical map places *Rpe65* outside the markers. We asked if *Rpe65* or perhaps another nearby gene is mutated and if the mutant reduced 11-cis-retinal levels. We studied the impact of the tvrm148 mutation on visual function, morphology, and retinoid levels.

Methods. Normal phase HPLC was used to measure retinoid levels. C57BL/6J (+/+), tvrm148/+, tvrm148/tvrm148, KO/KO and tvrm148/KO mice visual function was measured by optokinetic tracking (OKT) and electroretinography (ERG). Morphology was assessed by light microscopy and transmission electron microscopy (TEM). qRT-PCR was used to measure *Rpe65* mRNA levels. Immunoblotting measured the size and amount of RPE65 protein.

Results. The knockout and tvrm148 alleles did not complement. No 11-*cis*-retinal was detected in tvrm148/tvrm148 or KO/KO mice. Visual acuity in +/+ and tvrm148/+ mice was ~0.382 c/d, but 0.037 c/d in tvrm148/tvrm148 mice at postnatal day 210 (P210). ERG response in tvrm148/tvrm148 mice was undetectable except at bright flash intensities. Outer nuclear layer (ONL) thickness in tvrm148/tvrm148 mice was ~70% of +/+ by P210. *Rpe65* mRNA levels in tvrm148/tvrm148 mice were unchanged, yet 14.5% of +/+ protein levels was detected. Protein size was unchanged.

Conclusions. A complementation test revealed the KO and tvrm148 alleles do not complement, proving that the tvrm148 mutation is in *Rpe65*. Behavioral, physiological,

molecular, biochemical, and histological approaches indicate that tvrm148 is a null allele of *Rpe65*.

3.2—INTRODUCTION

Recently a catalog of over 160 mouse mutations that cause retinal disease was published (Won, Shi et al. 2011). This collection included a brief description of tvrm148, a putative novel autosomal recessive mutation in the *Rpe65* gene. The tvrm148 lesion was mapped between markers D3Mit147 (at 74.02 cM, corresponding to chr3:148,745,409 - 148,745,542) and D3Mit19 (at 87.60 cM, corresponding to chr3:157,983,038 - 157,983,067), about 9,237,658 bases apart according to the most recent mouse genome sequence assembly, GRCm38 (Fig. 3.1A). This region includes 21 validated genes, but surprisingly, does not include *Rpe65*. Further, *Rpe65* is physically located at chr3:159,599,181-159,625,307 by sequence analysis (Fig. 3.1B). This is about 1.6 Mb further telomeric from the distal end of the mapped disease locus (that is, from D3Mit19; Fig. 3.1B). The region from D3Mit19 to the physical location of the *Rpe65* gene contains another four candidate genes. *Rpe65* is just distal to these genes. Thus, *Rpe65* is not one of the 25 known genes in the mapped locus (Fig. 3.1B). From these two observations arises the potential complication that the gene harboring the tvrm148 lesion is unknown among 25 candidates.

Another potential complication of the tvrm148 assignment is that it is a missense mutation in *Rpe65* (a single base mutation resulting in the change of a wild type Phe codon to a Ser codon). It is often problematic to assign disease causation to missense mutations in the absence of experimental data; after all, chimpanzee contains a Tyr

residue at the same position (Won, Shi et al. 2011) and presumably retains function. For instance, a counter-hypothesis is that tvrm148 is a mutation in a gene close to *Rpe65*, and due to their proximity, a neutral missense mutation in *Rpe65* might be mistaken for the causative lesion. Because the putative causative mutation being a missense mutation that has not been previously detected in mouse, dog, or man, we thought an independent approach to the mutation assignment and additional experiments of tvrm148 as a candidate mutation in *Rpe65* were warranted.

A straightforward way to formally resolve the question of whether tvrm148 is a mutation in the *Rpe65* gene is to perform a complementation test (Fig. 3.2) using a deletion mutation solely within the *Rpe65* gene. Here we used the KO mouse (Redmond, Yu et al. 1998). This knockout is well characterized, has been backcrossed against wild type C57BL/6J for 10 generations, and the knockout of the *Rpe65* gene is well understood both genetically (Redmond, Yu et al. 1998) and biochemically (Redmond, Yu et al. 1998). The *Rpe65* gene was partially deleted in the construction of the knockout (Redmond, Yu et al. 1998), and the resulting gene fragment no longer exhibits any *Rpe65* mRNA (Redmond, Yu et al. 1998) or protein (Redmond, Yu et al. 1998) expression or retinol isomerase enzymatic activity (Redmond, Yu et al. 1998).

The fundamental principles of the complementation test are basic in genetics (Fig. 3.2). Here we perform this test asking if the mutation in tvrm148 is in the same gene as the *Rpe65* knockout. We compared the phenotypes of the homozygous tvrm148 mutation, tvrm148/KO, and KO/KO to wild type C57BL/6J by several histological, behavioral, and biochemical tests. We conclude that tvrm148 does not complement the knockout allele, thus proving unequivocally that this mutation is within the *Rpe65* gene. Given this, we

hypothesized that tvrm148 should manifest as a retinol isomerase mutation. This was confirmed on molecular, biochemical, morphological, and functional levels.

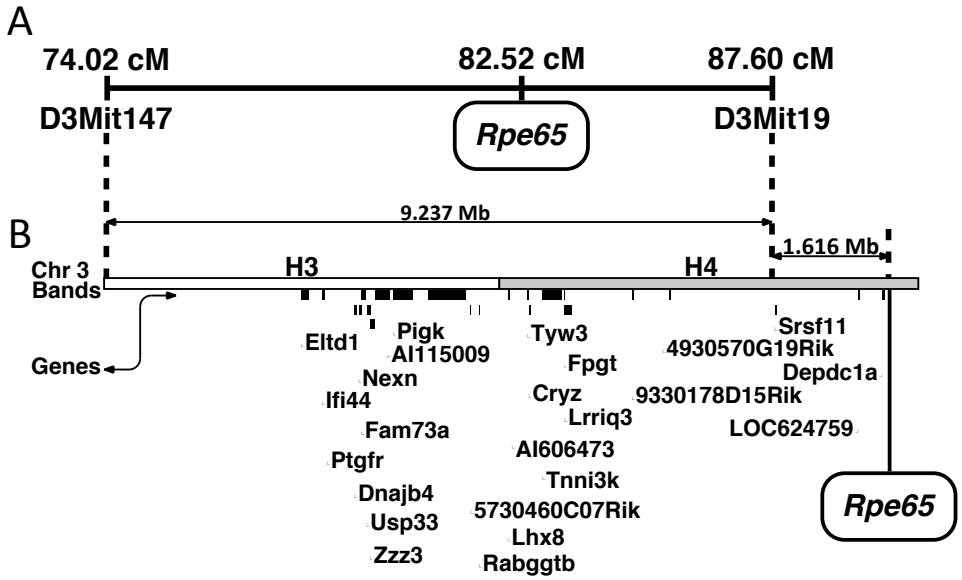

Figure 3.1. *Rpe65* resides outside the markers D3Mit147 and D3Mit19 on the sequence map of chromosome 3. (A) Simplified genetic map of chromosome 3 showing the positions of D3Mit147, D3Mit19, and *Rpe65* **(B)**. Ensembl genome browser map of the critical region neighboring the D3Mit147 and D3Mit19 markers based on the GRCm38 build of the mouse genome released in Dec 2011.

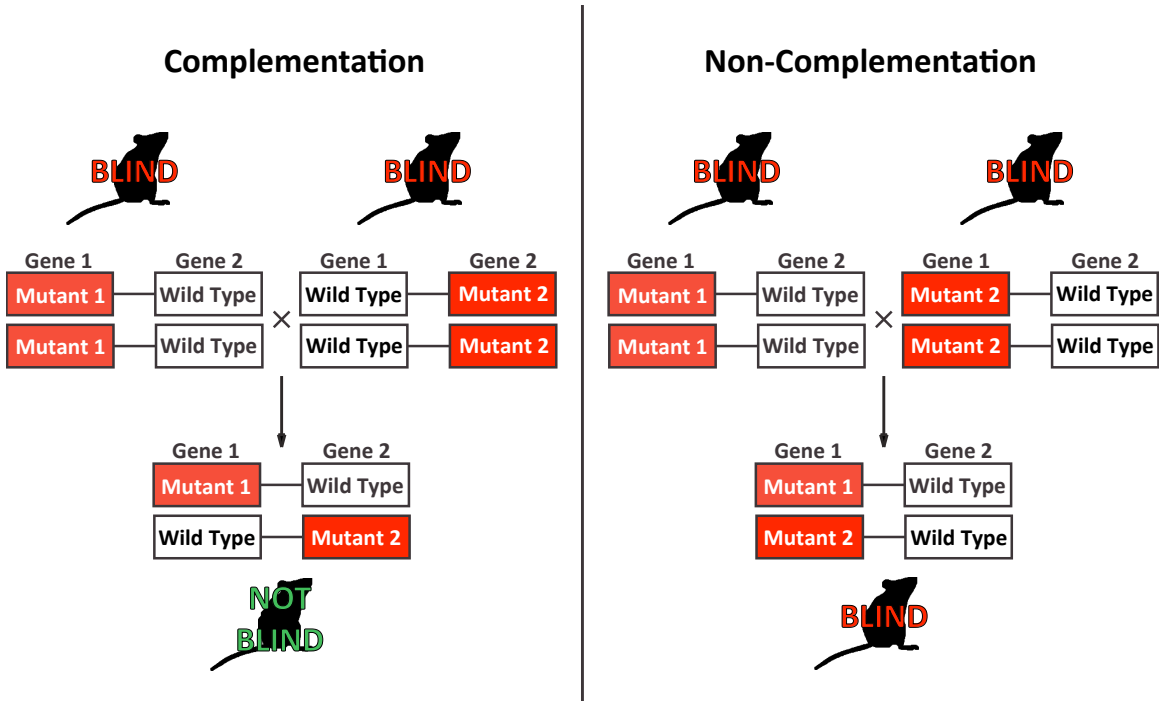

Figure 3.2. The complementation test. The complementation test is used to determine whether two mutations reside in the same gene. In this hypothetical example, there are two mutations, Mutant 1 and Mutant 2 that reside in either Gene 1 or Gene 2, and both mutations are recessive. In the left panel, in which gene complementation occurs, Mutant 1 resides in Gene 1 and Mutant 2 resides in Gene 2. Both mice are blind, and when mated together, the offspring have one copy of both the Mutant 1 and Mutant 2 alleles along with one wild type copy of both Gene 1 and Gene 2. Because both Mutant 1 and Mutant 2 are recessive mutations, the offspring in the left panel are not blind because they have a wild type copy of Gene 1 and Gene 2. In the right panel, though, both Mutant 1 and Mutant 2 reside in the same gene. Both parents are blind, and when mated together, they produce offspring with a copy of Mutant 1 and Mutant 2, both of which are in Gene 1. Because the offspring have no functional copy of Gene 1, the offspring are blind. This is known as non-complementation.

3.3—METHODS

3.3.1—Experimental animals

C57BL/6J (+/+) mice served as wild type in all experiments. tvrm148/tvrm148 mutant mice were induced by ENU mutagenesis at The Jackson Laboratory (Bar Harbor, ME) and were purchased for this study; tvrm148/+ mice were bred by crossing tvrm148/tvrm148 mice with +/+ mice. KO/KO mice were transferred from the National Eye Institute to Emory University, where they were bred and maintained. tvrm148/tvrm148 and KO/KO mice were bred together to create tvrm148/KO mice for the complementation test. Mice were provided food and water ad libitum and maintained in a 12:12 light-dark cycle. Mice were sacrificed with CO_2 gas, and all procedures and care were approved by Emory IACUC and followed ARVO guidelines of animal care and use.

3.3.2—Computer predictions

The web-based computer prediction programs SIFT (Ng and Henikoff 2001; Ng and Henikoff 2003; Ng and Henikoff 2003; Ng and Henikoff 2006; Kumar, Henikoff et al. 2009) (Sorting Intolerant from Tolerant: sift.jcvi.org/www/SIFT_enst_submit.html), polyPhen 2.0 (Sunyaev, Eisenhaber et al. 1999; Ramensky, Bork et al. 2002; Adzhubei, Schmidt et al. 2010) (Polymorphism Phenotyping: genetics.bwh.harvard.edu/pph2/), PANTHER (Mi, Muruganujan et al. 2013) (Protein Analysis Through Evolutionary Relationships: patherdb.org), MutationTaster (Grantham 1974; Altschul, Gish et al. 1990; Reese, Eeckman et al. 1997; Tabaska and Zhang 1999; Gasteiger, Gattiker et al. 2003; Flicek, Aken et al. 2008; Pollard, Hubisz et al. 2010; Abecasis, Auton et al. 2012)

(mutationtaster.org), PMUT (Ferrer-Costa, Gelpi et al. 2005) (mmb2.pcb.ub.es:8080/PMut/), SNAP (Bromberg and Rost 2007) (Screening for Non-Acceptable Polymorphisms: rostlab.org/services/SNAP/), SNPs3D (Yue, Li et al. 2005; Yue, Melamud et al. 2006; Yue and Moult 2006) (snps3d.org), PhD-SNP (Altschul, Madden et al. 1997; Capriotti, Fariselli et al. 2005; Capriotti, Fariselli et al. 2005; Capriotti, Calabrese et al. 2006) (Predictor of Human Deleterious Single Nucleotide Polymorphisms), and PROVEAN (Choi, Sims et al. 2012) (Protein Variation Effect Analyzer: provean.jcvi.org) were used to predict the effect a putative F229S amino acid substitution could have on RPE65 protein.

3.3.3—Electroretinography (ERG)

Mice were dark-adapted overnight prior to ERG measurements. Scotopic recordings were performed after mice were dark-adapted, and photopic recordings were performed after mice had light adapted for 10 minutes under a constant illumination of 30 cd/m^2. Measurements were recorded with a commercial ERG system (UTAS-E3000, LKC, Gaithersburg, MD) (Pardue, McCall et al. 1998; Pardue, Phillips et al. 2005; Chang, Hawes et al. 2007; Jablonski, Dalke et al. 2009) to a range of light intensities from $3x10^{-4}$ $cd \times s/m^2$ to 137 $cd \times s/m^2$. The b-wave amplitudes were measured from the trough of the a-wave to the peak of the positive wave; if the a-wave was not present, b-wave amplitudes were measured from the baseline to the top of the positive wave (Akula, Hansen et al. 2007; Akula, Mocko et al. 2007; Weymouth and Vingrys 2008). Full ERG setup protocol can be found in Section A.1.

3.3.4—Retinoid Analysis

All steps were performed in a darkroom under dim red light. RPE/choroid samples were removed from eyecups and homogenized in 200 µl PBS (pH 7.4, 150 mM NaCl, 1.06 mM KH_2PO_4, 5.60 mM Na_2HPO_4) in a disposable homogenizer. 10 µl homogenate was taken for Bradford Microplate protein assay (Pierce Coomassie Plus kit). The remaining homogenate was transferred to a 15 ml screw-top polypropylene tube (Falcon), and 400 µl methanol was added. Retinoids were extracted two times by adding 1.5 ml hexane and vortex mixing at top speed for 1 minute. Samples were centrifuged at 1424 ×*g* for 3 minutes. Hexane was drawn off the upper phase and transferred to a fresh 15 ml screw-top polypropylene tube. Pooled hexane extracts were dried in a TurboVap (Zymark, Hopkintown, MA). Samples were redissolved in 100 µl hexane by vortex mixing for 1 minute followed by centrifugation at 1424 ×g for 3 minutes. A 50 µl aliquot of each sample was run on a 5-µm particle Lichrospher Si-60 normal phase column on an Agilent 1100/1200 series isocratic HPLC at 1.2 ml/min using HEDO (hexane with 11.2% (V/V) ethyl acetate, 2% (V/V) dioxane, and 1.4% (V/V) octanol) mobile phase (Landers and Olson 1988). Data were analyzed using ChemStation32 software (Agilent). The remaining portion of mutant samples was subjected to saponification with alkaline hydrolysis in ethanolic potassium hydroxide and assayed for isomeric retinols contained in the retinyl esters (Landers and Olson 1988). For analysis of retinals, a pair of mouse retinas were homogenized in 0.5 ml of 50 mM MOPS, pH 6.5, 10 mM NH_2OH, and then transferred to a 15 ml glass screw-cap tube. A further 0.5 ml of 50 mM MOPS, pH 6.5, 10 mM NH_2OH was added along with 1 ml ethanol. The tubes were capped, mixed and incubated at room temperature in the dark for 30 minutes. Retinoids were extracted two

times by addition of 4 ml hexane, vortex mixing and centrifugation, and the hexane upper phases were combined and dried. The dried samples were redissolved in 100 ml hexane. Retinal oxime standards were prepared following Garwin and Saari (Garwin and Saari 2000). Retinal oximes standards and samples (20 µl) were separated using a LiChrospher Si-60, 5µm column running HEDO mobile phase (see above) at 0.7 ml/min.

3.3.5—Optokinetic Tracking (OKT)

Visual acuities of +/+, tvrm148/+, tvrm148/tvrm148, and KO/KO mice were measured at 100% contrast from P30 to P210 using a virtual optokinetic tracking system (OptoMotry 1.7.4; Cerebral Mechanics, Vancouver, British Columbia, Canada). Mice were placed on a central platform where they could freely move; the platform itself was surrounded by four monitors that projected a virtual cylinder with a moving spatial gradient. If at any time during testing the mouse fell off the platform, the mouse was placed back on the platform for further testing. The mouse was monitored on an external computer monitor by a video camera connected to the lid. The mice were first exposed to a gradient frequency of 0.052 cycles per degree (c/d), with the center of the virtual drum (controlled by the user) placed between the mouse's eyes. Tracking of the visual stimulus was assessed by exposing the mice to the gradient and monitoring the mouse to see if the mouse head moved in the direction of the gradient within 5 seconds of exposing the mouse to the stimulus. Visual threshold was obtained through a staircase method for each eye, with the step size halved after each reversal as described in detail in Douglas, et al. (Douglas, Alam et al. 2005). Threshold was identified as the point at which the final set of staircase reversals occurred at least three times. Mice that did not respond to visual

stimulus at any gradient frequency were recorded as having a visual threshold of 0.000 c/d. Values for right and left eye were averaged together to give the average visual threshold for that mouse. The full OKT protocol can be found in Section A.2.

3.3.6—Histology and Morphometrics

+/+, tvrm148/+, and tvrm148/tvrm148 mice were sacrificed at P60 and P210. Eyes were enucleated and fixed in glutaraldehyde (2.5% (W/V) in 0.1 M sodium cacodylate buffer, pH 7.4; Electron Microscopy Sciences, Hatfield PA) for four days at 4 °C. After fixation, the eyes were rinsed three times in 0.1 M sodium cacodylate buffer (Electron Microscopy Sciences). The superior portion of each eye was marked by leaving a small corneal flap after dissecting away the remaining cornea and lens. Eyes were embedded in LX-112 (Ladd Research Industries, Williston, VT) and sectioned at 1 μm thickness on a vertical meridian through the optic nerve head before staining with toluidine blue. Retina cross-sections were imaged at 20X magnification (Nikon Diaphot 300) and photomerged with Adobe Photoshop CS2 (Photoshop; Adobe Systems, Mountain View, CA). Images were imported into Longboard V7.5 (ImagingPlanet, Goleta, CA) for quantitative measures of retina layer thicknesses. Measurements were taken at 500 μm increments superior and inferior to the optic nerve. Nuclei were counted as the number of nuclei on a line perpendicular to the RPE moving through the outer nuclear layer (ONL). Outer nuclear layer (ONL), inner segment (IS), and outer segment (OS) thickness were measured on a line perpendicular to the RPE moving through those respective layers. Cone nuclei were counted in 200 μm areas 0.25 mm, 1 mm, and 2 mm superior and inferior of the optic nerve from retina sections as previously described (Carter-Dawson and LaVail 1979;

Seeliger, Grimm et al. 2001). For transmission electron microscopy (TEM), gray-silver thin sections (700 angstroms) were post fixed in 1% (W/V) osmium tetroxide and stained with 2% (W/V) uranyl acetate and Reynold's lead citrate, and images of +/+, tvrm148/+, and tvrm148/tvrm148 RPE were collected at P60 and P210 at 2,900× and 10,000× magnification.

3.3.7—Quantitative Real Time Polymerase Chain Reaction (qRT-PCR)

Rpe65 mRNA levels were measured by qRT-PCR with P60 +/+ and tvrm148/tvrm148 samples. RNA was isolated from RPE/choroid tissue placed in Trizol (Invitrogen, Grand Island, NY) and extracted using an RNeasy Mini Kit (Qiagen, Valencia, CA). To validate these commercial primers, the PCR product was subcloned into a pDRIVE vector (Qiagen) and DNA sequenced. DNA chromatogram showing the PCR insert (positively identified as *Rpe65* by BLAST) is shown in Figure 3.3. *Rpe65* primers (Qiagen) were used to amplify *Rpe65* mRNA with a one step reaction (Quantitect SYBR Green RT-PCR kit; Qiagen) under these conditions: 30 min at 50 °C, 15 min at 95 °C, 40 cycles at 94 °C for 15 s and 55 °C for 15 s and 72 °C for 40 s, followed by melt curve analysis. Four technical repeats for each reaction were performed in each run of the instrument (iCycler, BioRad, Hercules, CA), and *Rpe65* amplification was normalized to 18S RNA. 18S primers were: forward 5'-GTTGGTTTTCGGAACTGAGGC-3' and reverse 5'-GTCGGCATCGTTTATGGTCG-3'. There were five mice from different litters per sample group.

3.3.8—DNA Sequencing of Rpe65

DNA for sequencing of *Rpe65* was prepared by qRT-PCR of RNA isolated from both +/+ and tvrm148/tvrm148 mice using primers specific to overlapping regions of *Rpe65* (Table 3.1). Resulting DNA samples were sequenced using forward primers from each amplification reaction for qRT-PCR (Eurofins MWG Operon, Huntsville, AL), and tvrm148/tvrm148 samples were compared to +/+ sequence through BLAST (blast.ncbi.nlm.nih.gov/Blast.cgi; Fig. 3.4).

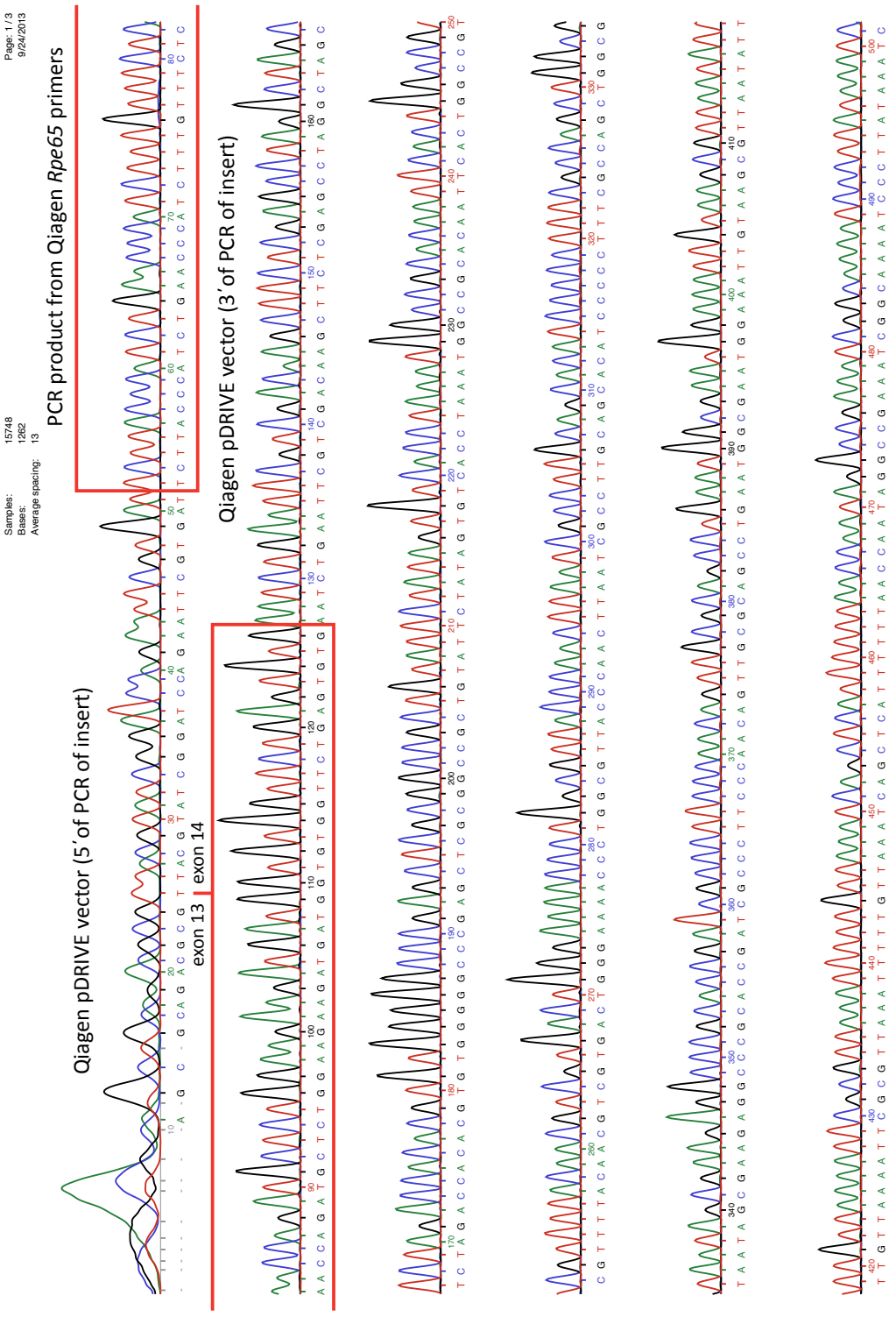

Figure 3.3. Qiagen *Rpe65* primers were validated by DNA sequencing of PCR product. PCR product from Rpe65 primers commercially available from Qiagen was subcloned into a commercially available vector (also from Qiagen). Vector was DNA sequenced using a T7 promoter forward primer. The insert

sequence was compared to *Rpe65* mRNA sequence in BLAST. pDRIVE vector sequence and *Rpe65* PCR product are labeled. It should be noted that the Qiagen *Rpe65* primers amplify exons 13 and 14 instead of exons 12 and 13 that they advertise on their website.

3.3.9—Immunoblotting

RPE/choroid tissue was isolated from P60 +/+, tvrm148/+, and tvrm148/tvrm148 mice in RIPA buffer (Teknova, Hollister, CA). Samples were homogenized by vortex mixing vigorously with stainless steel set screws for five minutes. Following homogenization, samples were centrifuged at 16,000 × *g* for 1 min. Supernatants were collected and protein concentration determined via BCA protein assay (Novagen, Darmstadt, Germany). 1 µg of protein was resolved on a 10% Bis-Tris Criterion gel (Bio-Rad) and transferred to a nitrocellulose membrane (Bio-Rad) with a wet transfer system (Bio-Rad). Western blocking reagent (Roche, Indianapolis, IN) was used. A custom-made N-terminal specific antibody to mouse RPE65 was made by raising antiserum against amino acids 1-43 of RPE65 mouse protein. Primary antibody incubation was performed at a 1:5000 dilution for 1 h at room temperature. A goat anti-rabbit-HRP conjugate secondary antibody (Invitrogen) was incubated at a 1:5000 dilution at room temperature for 1 h. Chemiluminescent detection (ECL Plus; Amersham Biosciences) was used for band visualization. Densitometry of immunoblots with the same protein samples run on different gels (n=3) was performed in Adobe Photoshop CS2 (Adobe Systems).

Table 3.1—Primers for amplification of *Rpe65* cDNA

***Rpe65* amplicon**	**Primer Sequence**
Exons 1-3	F: 5′-AAA TTG AAC ACC CTG CTG GT-3′ R: 5′-AGG GCT TGT CCA TGC AAC AG-3′
Exons 3-4	F: 5′-TGA AGT TGG ATC TGA GCC TT-3′ R: 5′-AAC ATA AGC ATC AGT GCG G-3′
Exons 4-5	F: 5′-TTC ATC CGC ACT GAT GCT TA-3′ R: 5′-CAA GGG CAT TGT CAG TAA CC-3′
Exons 5-6	F: 5′-CCC AGA GAC CTT GGA GAC AA-3′ R: 5′-TGC TTT CAG TGG AGG GAT CT-3′
Exons 6-8	F: 5′-GTC AAT GGT GCC ACT GCT C-3′ R: 5′-CCC ATG CTT TCA TTG GAC TC-3′
Exons 8-9	F: 5′-TTT CGA GTC CAA TGA AAG CA-3′ R: 5′-CCA GCA ACA GAG ATC CAC AA-3′
Exons 9-10	F: 5′-CCT GAC TTC AGG CTG AGG AG-3′ R: 5′-TCC CCT TTC AAT CTC TTC CA-3′
Exons 10-14	F: 5′-AGG CTC CTC AGC CTG AAG TC-3′ R: 5′-AGT CCA TGG AAG GTC ACA GG-3′

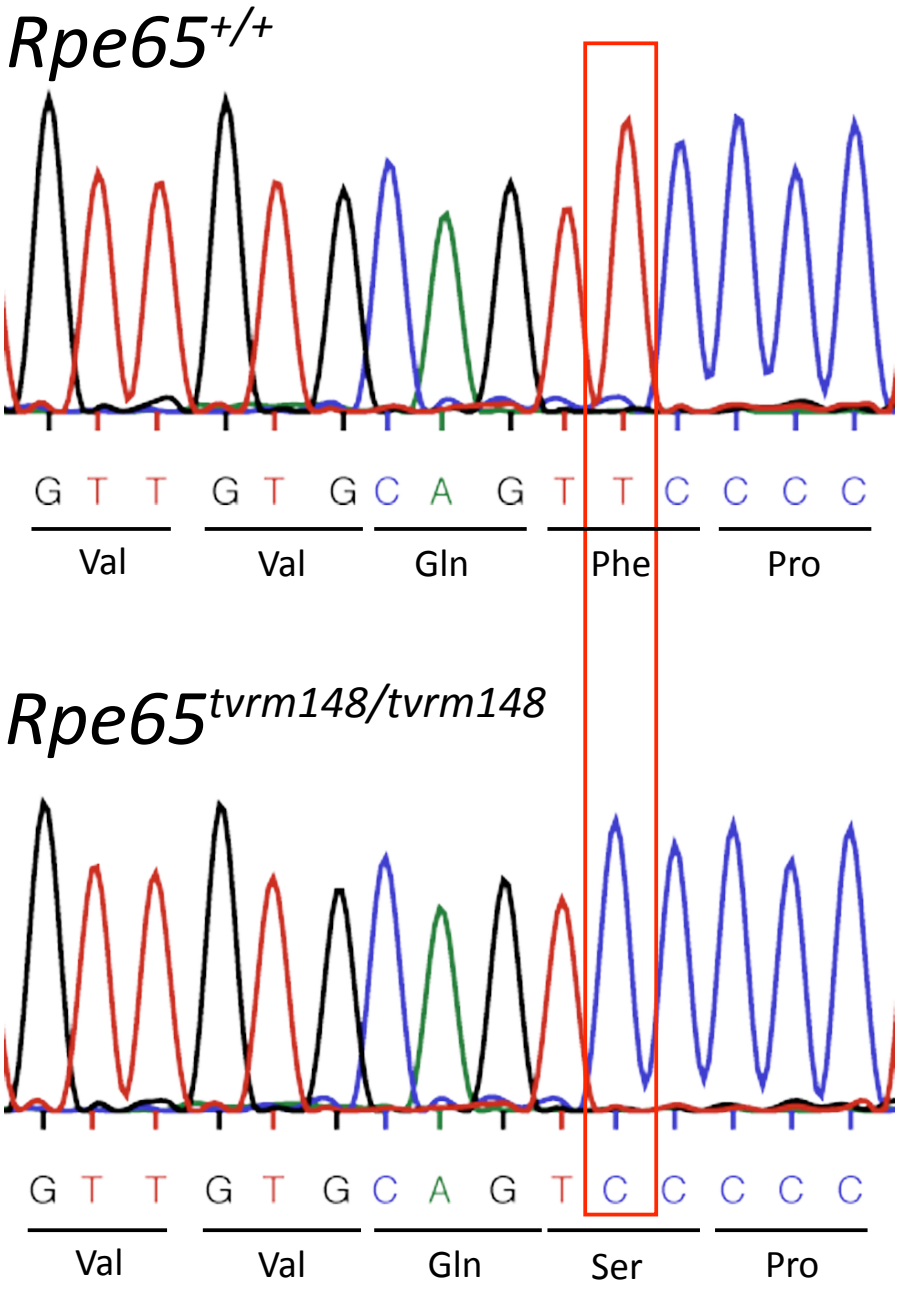

Figure 3.4—There was only one mutation in *Rpe65* in tvrm148 mice. DNA sequencing results showed the *Rpe65* mRNA in tvrm148/tvrm148 mice was identical in sequence to wild type C57BL/6J *Rpe65* mRNA except at the tvrm148 mutation, where there was a single nucleotide substitution of a C for T. This single nucleotide substitution results in the F229S missense mutation. The sequences of each amplicon from C57BL/6J mice were identical to the reference sequence (NCBI Ref Seq NM_029987.2).

3.3.10—Statistical Analysis

Graphs were constructed in Excel 2008 (Microsoft Inc., Redmond, WA). All graphs represent the data as means plus or minus standard deviations. Visual acuity, ERG, and morphometric data were analyzed by two-way repeated measures ANOVA (RM-ANOVA) with post-hoc Student-Newman-Keuls testing. Laser micrometer, OCT, photorefraction, and qRT-PCR data were analyzed by one-way ANOVA with post-hoc Student-Newman-Keuls testing (SigmaPlot 12, Systat, San Jose, CA). Sample sizes are provided in the results. All groups contain at least five mice from different litters.

3.4—RESULTS

3.4.1—Predictions of tvrm148 mutation pathogenicity

Web-based algorithms were used to predict whether the tvrm148 mutation that was previously reported (Won, Shi et al. 2011) could have a potentially harmful effect on RPE65 protein function and could thus have the previously reported effect (Won, Shi et al. 2011) on visual function. The prediction programs SIFT (Ng and Henikoff 2001; Ng and Henikoff 2003; Ng and Henikoff 2003; Ng and Henikoff 2006; Kumar, Henikoff et al. 2009), polyPhen 2.0 (Sunyaev, Eisenhaber et al. 1999; Ramensky, Bork et al. 2002; Adzhubei, Schmidt et al. 2010), PANTHER (Mi, Muruganujan et al. 2013), MutationTaster (Grantham 1974; Altschul, Gish et al. 1990; Reese, Eeckman et al. 1997; Tabaska and Zhang 1999; Gasteiger, Gattiker et al. 2003; Flicek, Aken et al. 2008; Pollard, Hubisz et al. 2010; Abecasis, Auton et al. 2012), PMUT (Ferrer-Costa, Gelpi et al. 2005), SNAP (Bromberg and Rost 2007), SNPs3D (Yue, Li et al. 2005; Yue, Melamud et al. 2006; Yue and Moult 2006), PhD-SNP (Altschul, Madden et al. 1997;

Capriotti, Fariselli et al. 2005; Capriotti, Fariselli et al. 2005; Capriotti, Calabrese et al. 2006), and PROVEAN (Choi, Sims et al. 2012) were used to predict if the putative *Rpe65* mutation could negatively impact visual function in mice. With the exception of PROVEAN, all programs predicted the tvrm148 mutation is responsible for RPE65 dysfunction (Table 3.2). DNA sequencing from tvrm148/tvrm148 mice (Fig. 3.4) confirmed the presence of the tvrm148 mutation that was previously reported (Won, Shi et al. 2011). There were no other sequence differences in any of the other exons or regions sequenced comparing tvrm148 to the C57BL/6J reference sequence.

3.4.2—Complementation test

A complementation test was performed to determine whether the causative mutation driving visual function loss in tvrm148/tvrm148 mice resides in the *Rpe65* locus. By breeding tvrm148/tvrm148 mice and KO/KO mice together, tvrm148/KO offspring were produced. +/+, KO/KO, tvrm148/tvrm148, and tvrm148/KO mice were then screened by ERG at 137 cd×s/m^2 at P30 to assess visual function (Fig. 3.5). All mutant mice had significantly lower responses ($P<0.001$) than +/+ mice [264.7 ± 56.4 μV (n=6), Fig. 3.4, but the a-wave responses of KO/KO, tvrm148/tvrm148, and tvrm148/KO mice were not significantly different when compared to each other alongside wild type mice [KO/KO mice, 24.6 ± 16.2 μV (n=7); tvrm148/tvrm148 mice, 6.1 ± 6.7 μV (n=5); tvrm148/KO mice, 35.1 ± 16.4 μV (n=9)].

Table 3.2—Predictions of putative tvrm148 mutation on RPE65 function

Program	Predicted Damaging Effect?
SIFT	Yes
PolyPHEN 2.0	Yes
PANTHER	Yes
MutationTaster	Yes
PMUT	Yes
SNAP	Yes
SNPs3D	Yes
PhD-SNP	Yes
PROVEAN	No

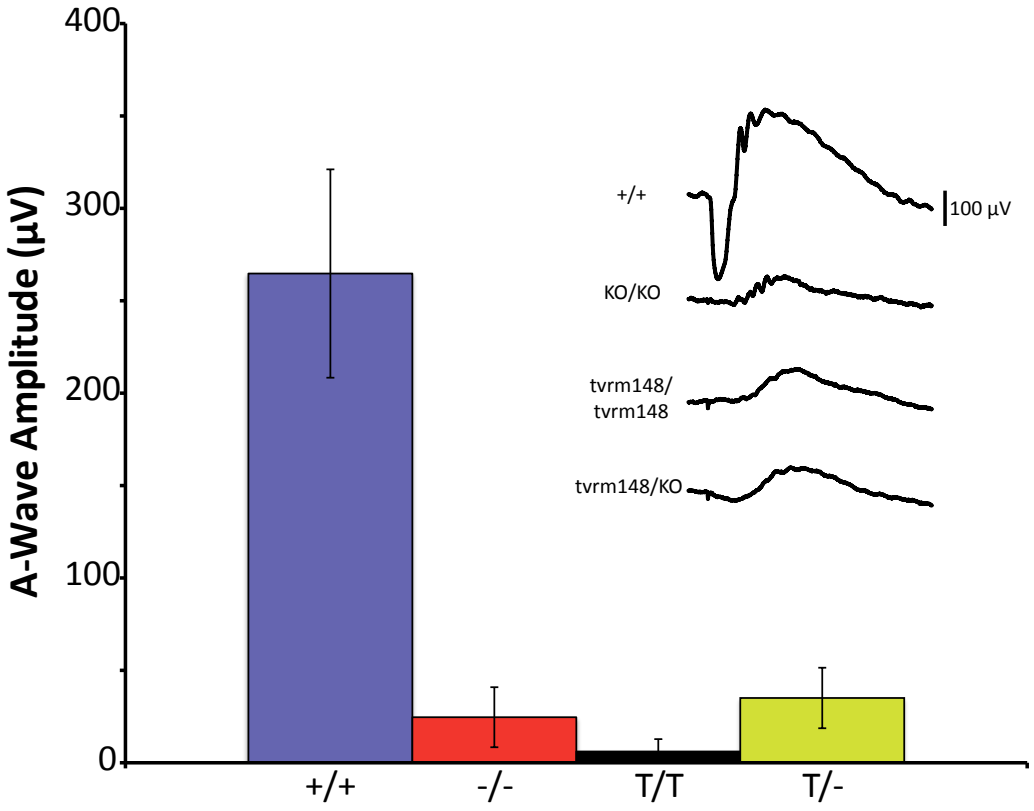

Figure 3.5. The tvrm148 and *Rpe65*^{KO} alleles did not complement. Dark-adapted a-wave amplitudes from a flash stimulus of 137 cd×s/m^2 from +/+ (n=6), KO/KO (n=7), tvrm148/tvrm148 (n=5), and tvrm148/KO (n=9) mice at P30 are shown. KO/KO, tvrm148/tvrm148, and tvrm148/KO mice have significantly lower a-wave amplitudes than +/+ mice, but a-wave amplitudes from KO/KO, tvrm148/tvrm148, and tvrm148/KO mice do not differ significantly from one another, showing the two mutant alleles do not complement one another. Raw ERG waveforms are shown in inset. Recall that a-waves are the first negative trough in the electrical trace. The entire waveform is greatly reduced in mice with two gene mutations. ** $P < 0.001$ compared to +/+. Data are presented as mean ± SD.

3.4.3—Retinoid levels in tvrm148, knockout, and normal mouse eyes

The fact that mutant tvrm148/tvrm148 mice did not have appreciable a-wave responses suggested they lack the ability to produce sufficient amounts of 11-*cis*-ROL (the enzymatic product of RPE65) to support proper photoreceptor function. KO/KO mice have also been shown to harbor excessive amounts of retinyl ester (Redmond, Yu et al. 1998), and we sought to determine if tvrm148/tvrm148 mice shared this canonical chronic loss of 11-*cis*-RAL and increase in retinyl ester content in the RPE/choroid. KO/KO and tvrm148/tvrm148 mice had elevated retinyl esters, while 11-*cis*-RAL was not detected in KO/KO or tvrm148/tvrm148 retinas (Table 3.3). The tvrm148/tvrm148 samples had 22× more retinyl esters than +/+ samples. Retinyl ester content in KO/KO and tvrm148/tvrm148 mice did not differ significantly from one another. Retinol isomers in all samples were below the level of detection prior to saponification of mutant samples. For the saponified portion, only all-*trans*-retinol was detected in the mutant samples and no quantification was attempted.

Table 3.3—Retinol isomerase activity is abolished in KO/KO and tvrm148/tvrm148.

Genotype*	11-*cis*-RAL (pmol/eye)[1]	All-*trans*-RAL (pmol/eye)[2]	Retinyl ester content (pmol/mg protein)[3]
+/+	765.9 ± 70.1	105 ± 13.5	63.40 ± 38.30
KO/KO	None detected	None detected	1826.63 ± 654.34
tvrm148/tvrm148	None detected	None detected	1385.77 ± 629.77

*Number of animals analyzed per genotype ≥3.

1. The lower limit of detection in this assay was 8.79 pmol/mg protein.
2. The lower limit of detection in this assay was 1 pmol.
3. The lower limit of detection in this assay was 8.8 pmol.

3.4.4—Inheritance of tvrm148

We sought to determine how the tvrm148 allele is inherited in mice (alternatively recessive or dominant, autosomal or sex-linked). Longitudinal ERG measurements on dark- and light-adapted +/+, tvrm148/+, and tvrm148/tvrm148 mice were performed at P60 and P180 (Fig. 3.6). While tvrm148/+ mice did not show any reduction in dark-adapted b-wave amplitudes, tvrm148/tvrm148 mice showed depressed dark-adapted b-wave amplitudes at both ages (Fig. 3.6A, C). At P60, in scotopic conditions (0.01551 cd×s/m^2), tvrm148/tvrm148 mice had no measurable (0 ± 0 μV, $P<0.001$) b-wave response, whereas +/+ and tvrm148/+ mice had an average b-wave amplitude of 197.9 ± 62.4 μV and 221.8 ± 59.6 μV, respectively. At the brightest flash intensity tested, 137 cd×s/m^2, tvrm148/tvrm148 mice had an average b-wave response of 132.4 ± 52.4 μV in comparison to 648.2 ± 196.9 μV and 654.3 ± 177.9 μV in +/+ and tvrm148/tvrm148 mice, respectively (Fig. 3.6A). By P180, tvrm148/tvrm148 mice had an average scotopic (0.01551 cd×s/m^2) b-wave amplitude of 0 ± 0 μV compared to 216.0 ± 40.6 μV in +/+ mice and 191.0 ± 39.1 μV in tvrm148/+ mice; at 137 cd×s/m^2, tvrm148/tvrm148 mice had an average b-wave amplitude of 69.1 ± 30.2 μV compared to 526.1 ± 75.1 μV in +/+ mice and 541.3 ± 68.6 μV in tvrm148/+ mice (Fig. 3.6C).

Light-adapted b-wave response was also significantly reduced in tvrm148/tvrm148 mice (Fig. 3B, D). In response to the brightest flash intensity (75 cd×s/m^2) at P60, tvrm148/tvrm148 mice had an average b-wave response of 140.4 ± 58.0 μV compared to 220.4 ± 61.5 μV in +/+ mice and 241.9 ± 76.0 μV in tvrm148/+ mice (Fig. 3.6B), which decreased at P180 in tvrm148/tvrm148 mice to 91.6 ± 19.5 μV compared to 196.5 ± 42.8 μV in +/+ mice and 217.5 ± 29.8 μV in tvrm148/+ mice at

P180 (Fig. 3.6D). There was a significant loss of b-wave amplitudes between P60 and P180 in tvrm148/tvrm148 mice in both scotopic and photopic ERG amplitudes (data not shown).

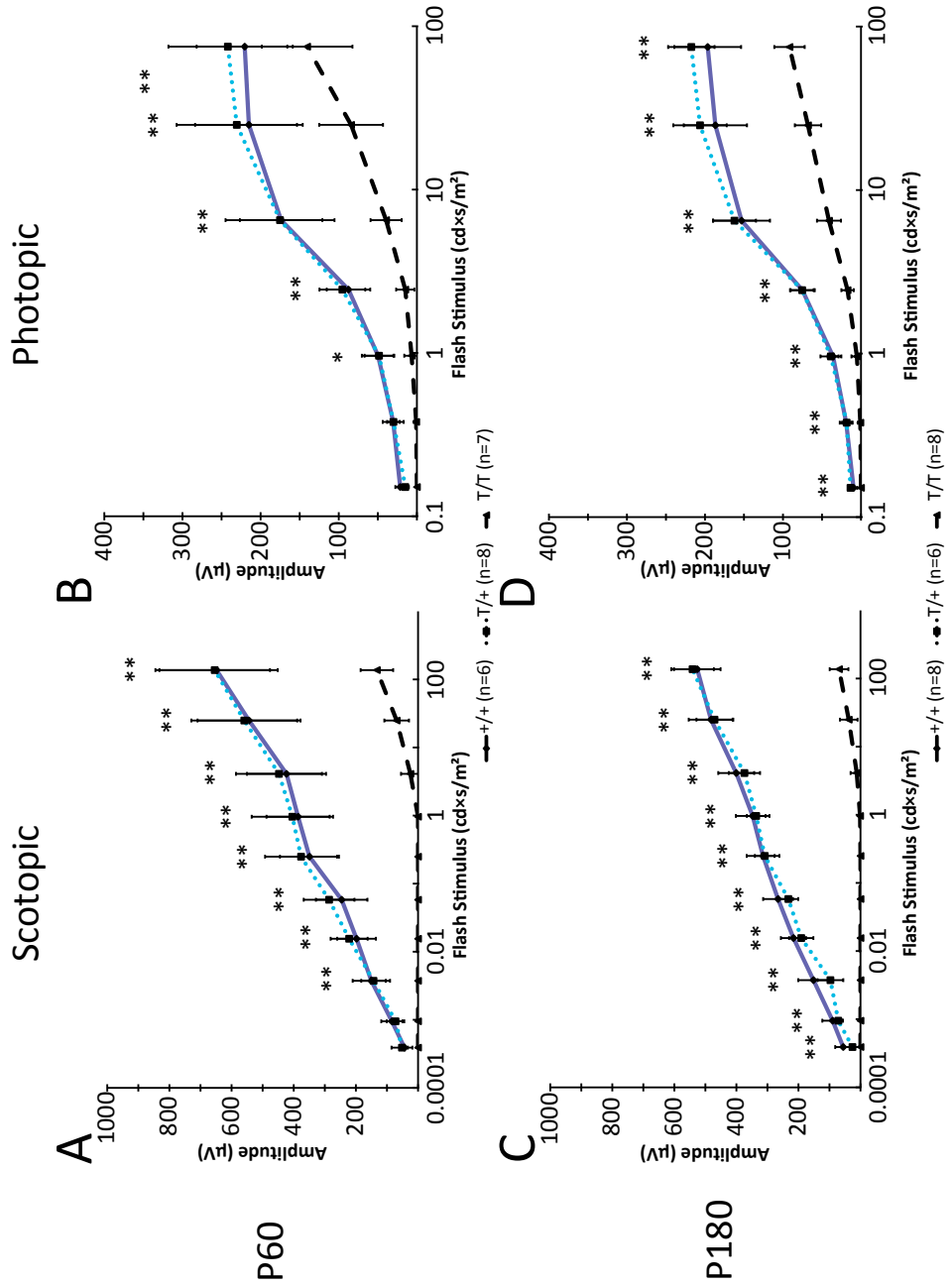

Figure 3.6—tvrm148/tvrm148 mice, but not tvrm148/+ mice, had a loss of ERG response. Dark- and light-adapted b-wave amplitudes, respectively, from +/+, tvrm148/+, and tvrm148/tvrm148 mice at P60 (**A,**

B) and P180 (**C, D**) are shown. * $P < 0.05$ T/T compared with +/+; ** $P < 0.001$ tvrm148/tvrm148 compared with +/+, significance determined through two-way repeated measures ANOVA with post hoc Student-Newman-Keuls testing. There was no difference between +/+ and tvrm148/+ ERG responses. Data are presented as absolute values (mean ± SD).

3.4.5—Visual acuity affected by null mutations

The optokinetic tracking testing, a behavioral measure of visual acuity, was used to determine the effects of the tvrm148 mutation on the visual guided activity of the mouse. A virtual optomotor system (CerebralMechanics) was used to measure visual acuity in +/+, tvrm148/+, and tvrm148/tvrm148 mice. +/+ and tvrm148/+ mice maintained a constant high visual acuity (0.381 ± 0.002 c/d) with little variability from P30 through the end of the study at P210 (Fig. 3.7). tvrm148/+ mice had no detectable reduction in visual acuity. tvrm148/tvrm148 mice, on the other hand, had a significant reduction in visual acuity at P30 (0.318 ± 0.003 c/d), and continued to lose visual acuity until the end of the study (Fig. 3.7). At P210, only a few tvrm148/tvrm148 mice retained measurable visual acuity, which produced the average value of 0.037 ± 0.045 c/d (Fig. 3.7).

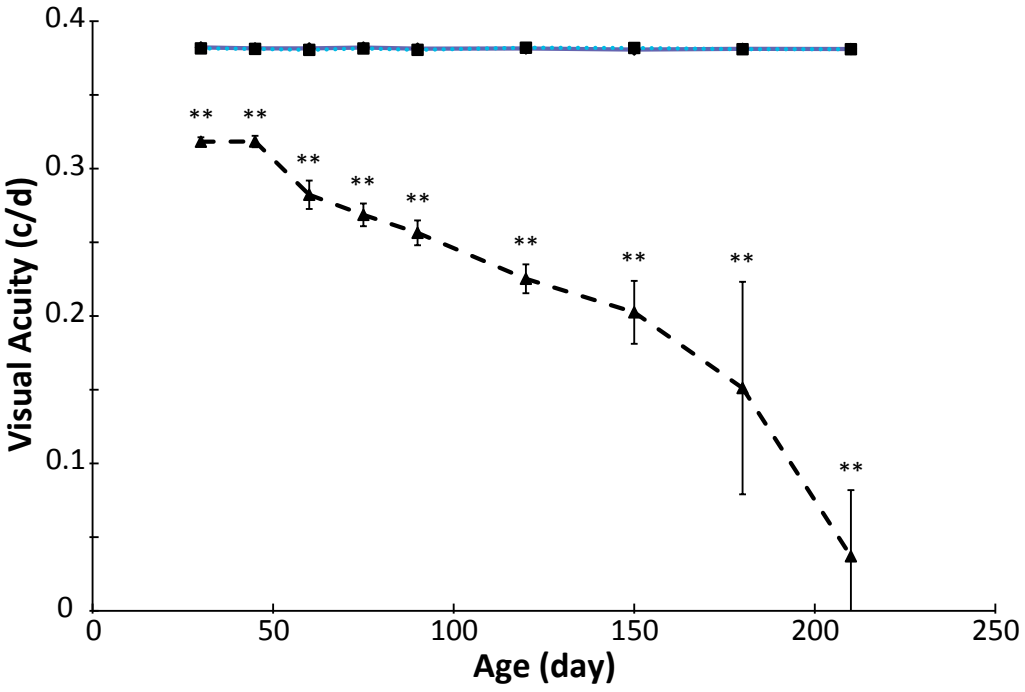

Figure 3.7—tvrm148/tvrm148 mice, but not tvrm148/+ mice, progressively lost visual acuity with age. Visual acuities of +/+ (solid line), tvrm148/+ (dotted line; largely hidden behind the solid line), and tvrm148/tvrm148 mice (dashed line) from P30-P210 are represented on the same graph. ** P <0.001 tvrm148/tvrm148 compared with +/+, significance determined through two-way repeated measures ANOVA with post hoc Student-Newman-Keuls testing. Comparison of tvrm148/+ with +/+ does not reach statistical significance between P30 and P210, and visual acuity measures overlap through the duration of the study. Data are presented as mean ± SD.

3.4.6—Comparison of slow loss of visual acuity in tvrm148/tvrm148 and KO/KO mice

The visual acuities of +/+, tvrm148/tvrm148, and KO/KO mice were compared at P30, P120, and P210 to determine if KO/KO and tvrm148/tvrm148 mice behaved similarly in early, middle, and late stages of the retinal degeneration (Fig 3.8). The slow loss of visual acuity in tvrm148/tvrm148 and KO/KO mice was consistent at each age examined. At P30, tvrm148/tvrm148 visual acuity was 0.318 ± 0.003 c/d, and KO/KO visual acuity was 0.318 ± 0.003 c/d. At P120, tvrm148/tvrm148 visual acuity was 0.225 ± 0.010 c/d, and KO/KO visual acuity was 0.245 ± 0.007 c/d. At P210, tvrm148/tvrm148 visual acuity was 0.037 ± 0.045 c/d, and KO/KO visual acuity was 0.000 ± 0.000 c/d.

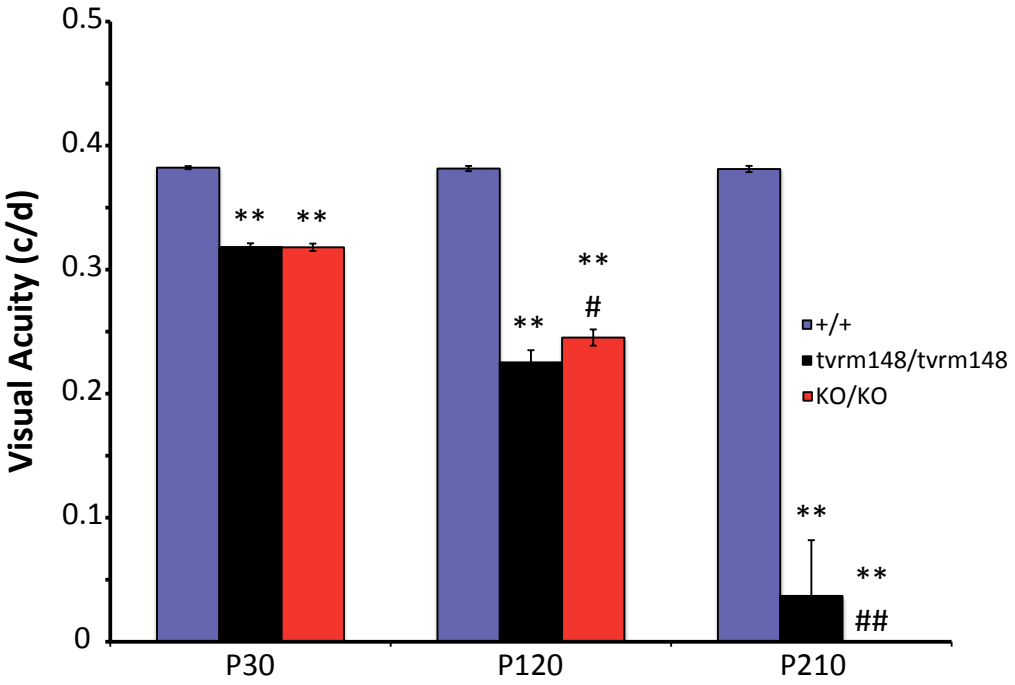

Figure 3.8—tvrm148/tvrm148 mice had residual visual function similar to KO/KO mice. Comparison of visual phenotype measured by visual acuity. tvrm148/tvrm148 mice have a residual visual function similar to KO/KO mice. Visual acuities of +/+ (black bar), tvrm148/tvrm148 (gray bar), and KO/KO (white bar) mice at P30 (+/+ n = 9, KO/KO n = 12, tvrm148/tvrm148 n = 8), P120 (+/+ n = 8, KO/KO n = 8, tvrm148/tvrm148 n = 8), and P210 (+/+ n = 8, KO/KO n = 8, tvrm148/tvrm148 n = 8) are shown on the same graph. Data are presented as mean ± SD. ** P <0.001 compared to wild type; # P <0.05 tvrm148/tvrm148 compared to KO/KO; ## P <0.001 tvrm148/tvrm148 compared to KO/KO.

3.4.7—Histology and morphometrics changes –slight losses in mutants

We sought to determine if loss of visual function correlated with a significant loss of retina layer thickness. Eyes were harvested from P60, P120, P180, and P210 from +/+, tvrm148/+, and tvrm148/tvrm148 mice, and representative sections from P60 and P210 are shown (Fig. 3.9). The tvrm148/tvrm148 retina was thinner than +/+ or tvrm148/+ retinas (Fig. 3.9). Retina architecture was largely intact even at P210, despite some significant outer nuclear layer (ONL) thinning (35.9 ± 2.9 μm in tvrm148/tvrm148 mice compared with 50.9 ± 4.5 μm in +/+ mice) 500 μm on the superior side of the optic nerve ($p<0.001$). Images of +/+, tvrm148/+, and tvrm148/tvrm148 retinas taken at P120 and P180 look similar to P60 and P210 (data not shown).

Quantitative measurements of retina cross-sections from P60 and P210 eyes revealed reduced nuclei counts (Fig. 3.10A-B), thinning of the outer nuclear layer (ONL; Fig. 3.10C-D), inner segment (IS; Fig. 3.10E-F), and outer segment (OS; Fig. 3.10G-H) in tvrm148/tvrm148 mice compared to tvrm148/+ and +/+ mice (Fig. 3.10). tvrm148/tvrm148 retina thinning was apparent as early as P60. The ONLs of +/+ and tvrm148/+ mice were 11-12 nuclei thick at both P60 and P210, but tvrm148/tvrm148 mice had an ONL only 8-9 nuclei thick at P60 and 7-8 nuclei thick at P210 (Fig. 3.10A-B). By P60, tvrm148/tvrm148 retina had lost a significant number of cone nuclei (Fig. 3.11A); +/+ retina had 11.8 ± 3.4 cones per 200 μm segment, but tvrm148/tvrm148 retina had only 6.3 ± 2.3 cone nuclei per 200 μm segment on the superior side of the optic nerve and 3.2 ± 1.4 cone nuclei per 200 μm segment on the inferior side (Fig. 3.11A). By P210, +/+ retina had 10.0 ± 1.8 cone nuclei per 200 μm segment, and tvrm148/tvrm148 retina

had only 2.7 ± 1.4 and 2.0 ± 0.9 cone nuclei per 200 μm segment on the superior and inferior sides of the retina, respectively (Fig. 3.11B).

Retinyl ester accumulations in the RPE are known to correlate with the formation of lipid droplets in RPE65-deficient mice (Redmond, Yu et al. 1998; Samardzija, von Lintig et al. 2008), and we decided to examine the RPE of tvrm148/tvrm148 mice to see if lipid droplet formation in these mice occurred consistent with other *Rpe65* mutant models. TEM images of +/+, tvrm148/+, and tvrm148/tvrm148 RPE show mutant mice have relatively normal morphology with the exception of lipid droplets that are present (Fig. 3.12). Lipid droplets were detected qualitatively in the RPE in tvrm148/tvrm148 mice at P60 (Fig. 3.12C), and lipid droplets appeared larger by P210 (Fig. 3.12F). No lipid droplets were detected in +/+ or tvrm148/+ RPE at P60 or P210 (Fig. 3.12A,B,D,E,G).

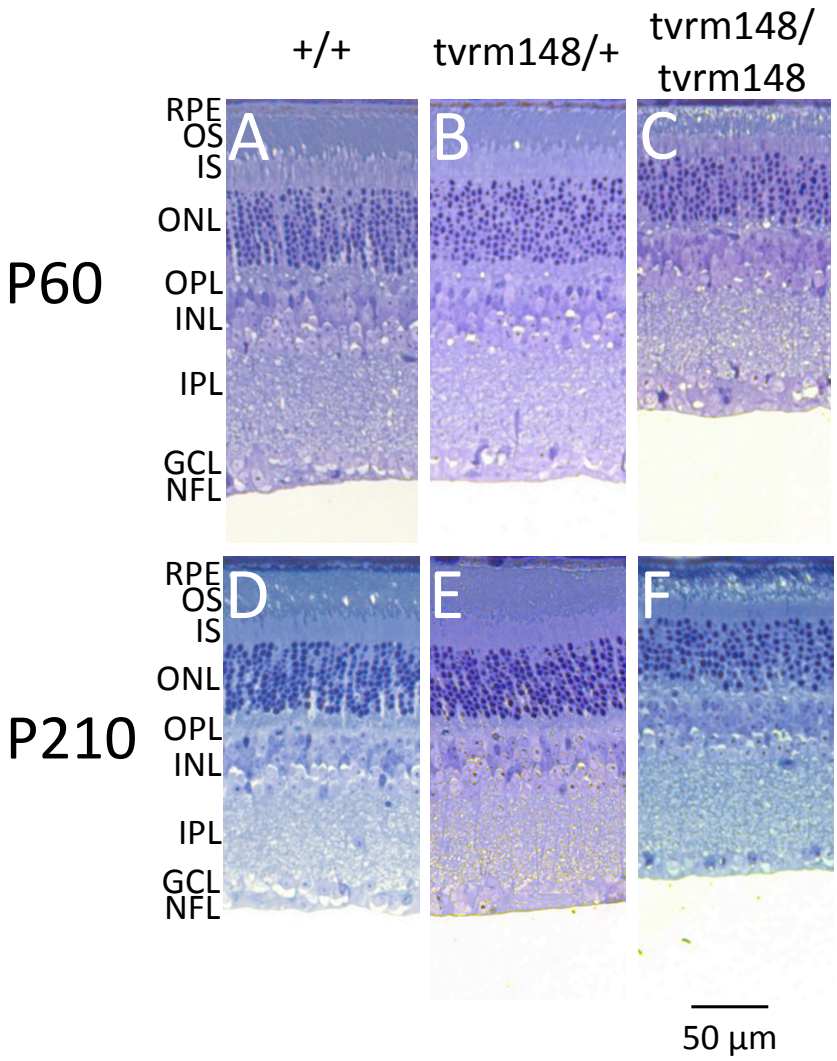

Figure 3.9. tvrm148/tvrm148 mice have a thinner retina than tvrm148/+ or +/+ counterparts. Bright-field images of retina cross-sections stained with toluidine blue are shown. tvrm148/tvrm148 mice experience slight retina thinning but retain normal retina architecture as they age. Representative images of +/+, tvrm148/+, and tvrm148/tvrm148 retina 1 mm superior of the optic nerve at P60 (**A-C**) and P210 (**D-F**) are shown. RPE, retinal pigment epithelium; OS, outer segment; IS, inner segment; ONL, outer nuclear layer; INL, inner nuclear layer; GCL, ganglion cell layer.

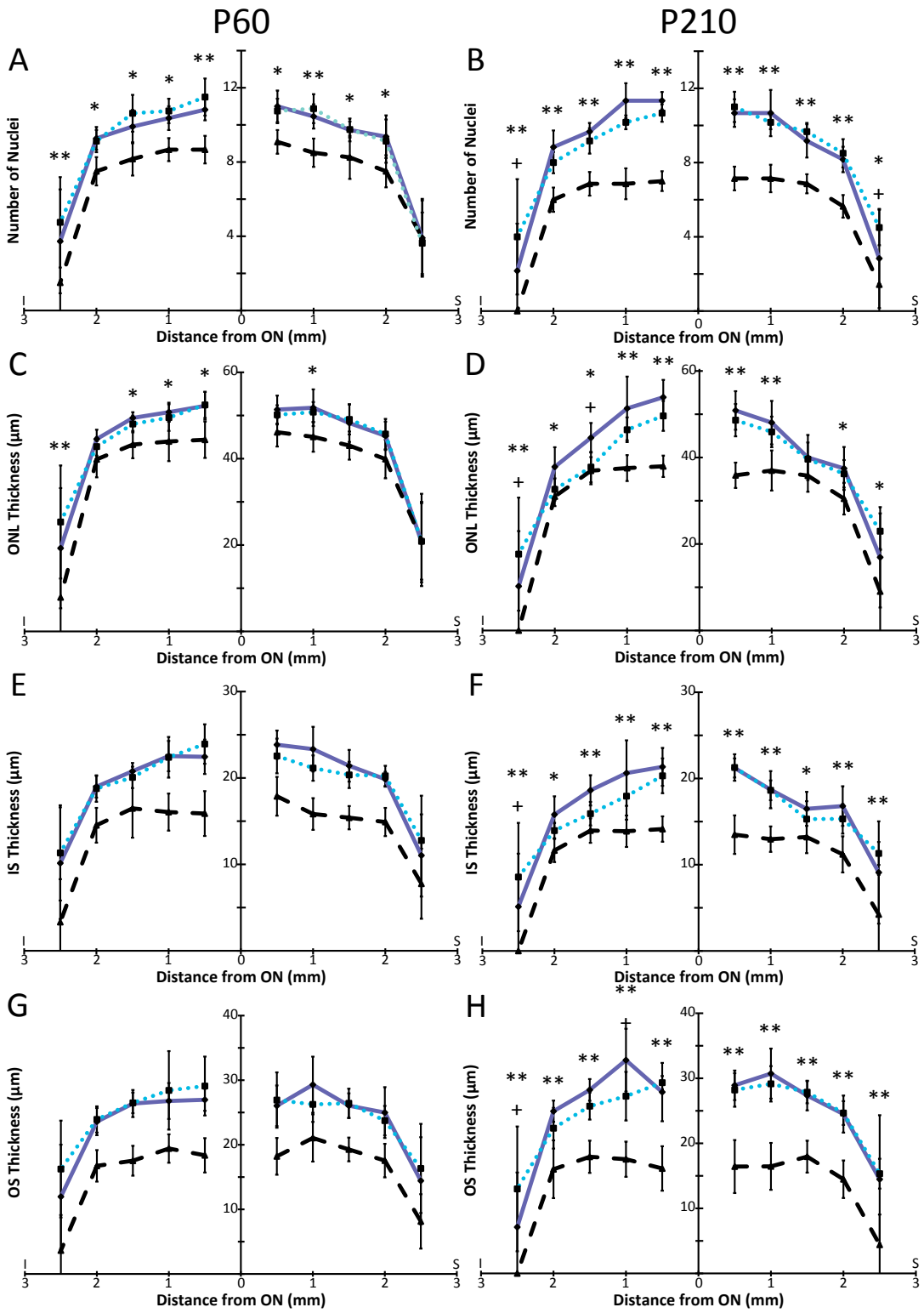
P60
P210
A
B
C
D
E
F
G
H
Number of Nuclei
ONL Thickness (µm)
IS Thickness (µm)
OS Thickness (µm)
Distance from ON (mm)
I
S

Figure 3.10. tvrm148/tvrm148 mouse retina layers progressively thin with age. Quantitative measurements every 500 µm superior and inferior of the optic nerve in +/+ (solid blue line), tvrm148/+ (dotted light blue line), and tvrm148/tvrm148 (dashed black line) retina were taken for the number of stacked nuclei in the outer nuclear layer (ONL) (**A, B**), ONL thickness (**C, D**), inner segment (IS) thickness (**E, F**), and outer segment (OS) thickness (**G, H**) at P60 (+/+ n=11, tvrm148/+ n=8, tvrm148/tvrm148 n=12) and P210 (+/+ n=7, tvrm148/+ n=6, tvrm148/tvrm148 n=14). * $P < 0.05$ tvrm148/tvrm148 compared with +/+; ** $P < 0.001$ tvrm148/tvrm148 compared with +/+, + $P < 0.05$ +/+ compared with tvrm148/+, significance determined through two-way repeated measures ANOVA with post hoc Student-Newman-Keuls testing. Data are presented as mean ± SD.

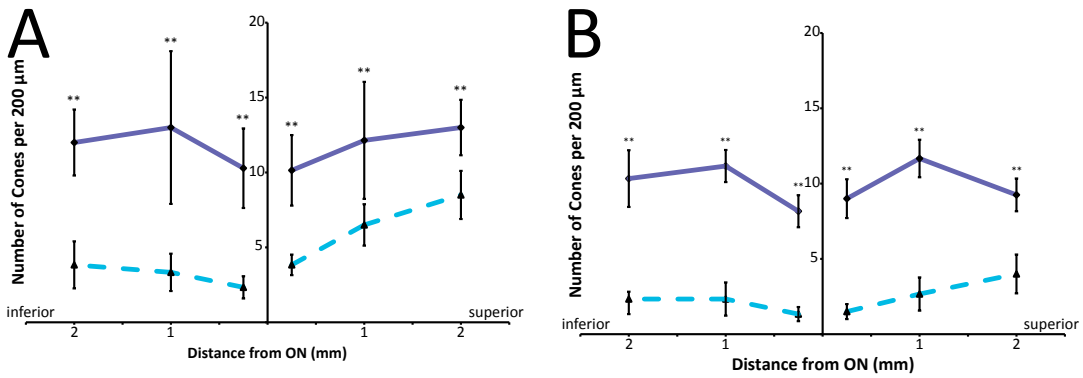

Figure 3.11. tvrm148/tvrm148 mice have significant cone nuclei loss at P60 and P210. Cone nuclei were counted at distances of 0.25, 1, and 2 mm superior and inferior of the optic nerve in a 200 µm segment of the retina at (**A**) P60 and (**B**) P210. ** P <0.001 +/+ compared with tvrm148/tvrm148, significance determined through two-way repeated measures ANOVA with post-hoc Student-Newman-Keuls testing. Data are presented as mean ± SD.

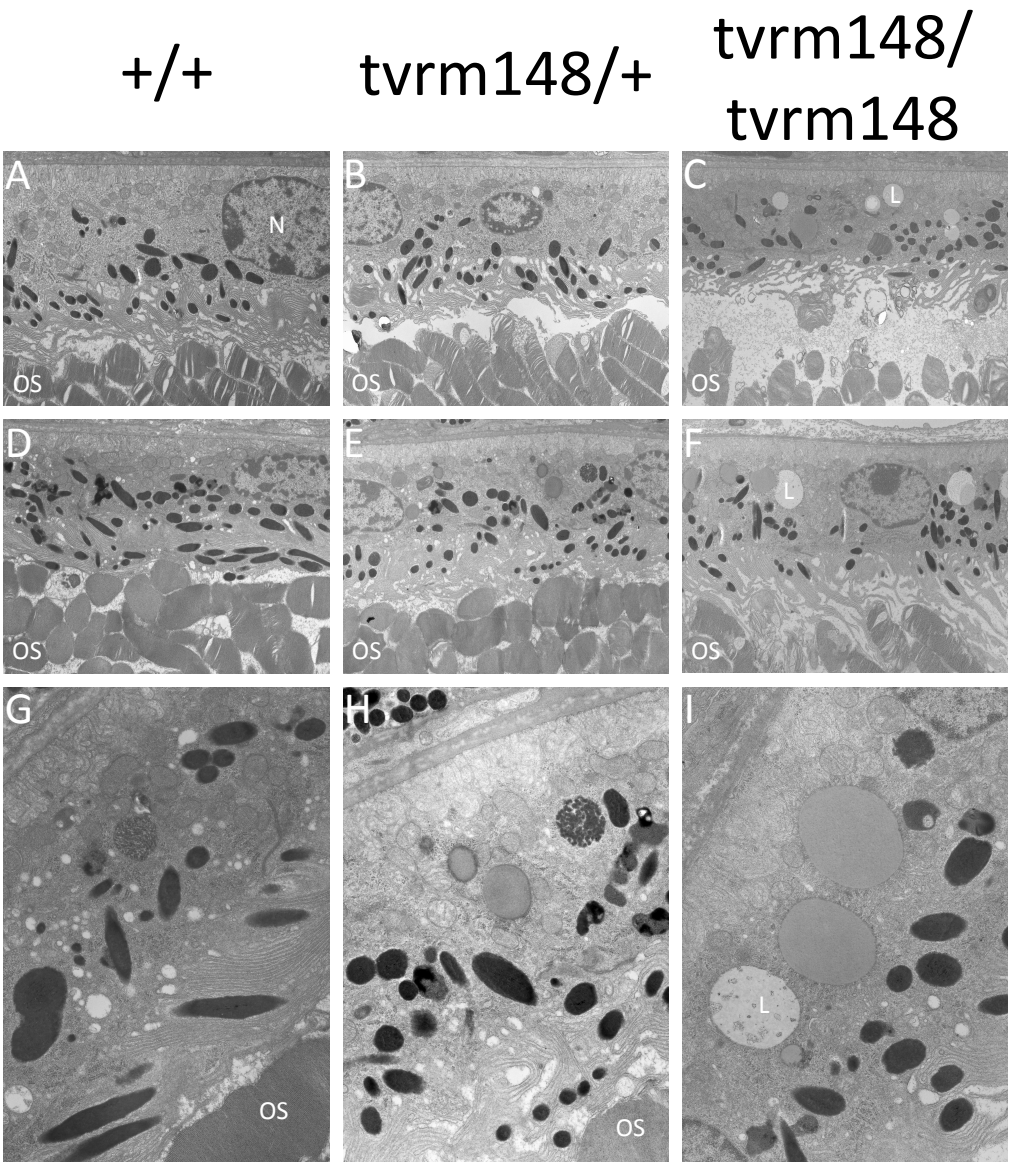

Figure 3.12. TEM shows lipid droplets indicative of retinyl ester accumulation in the RPE of tvrm148/+ and tvrm148/tvrm148 mice. TEM was performed on sections of RPE 1000 μm superior to the optic nerve in +/+, tvrm148/+, and tvrm148/tvrm148 mice at P60 and P210. (**A-C**) TEM images of RPE from +/+, tvrm148/+, and tvrm148/tvrm148 mice at P60, respectively, at 2900X magnification are shown. (**D-F**) TEM images of +/+, tvrm148/+, and tvrm148/tvrm148 mice at P210, respectively, at 2900X magnification are shown. (**G-I**) TEM images of +/+, tvrm148/+, and tvrm148/tvrm148 mice at P210, respectively, at 10000X magnification are shown. N, nucleus; L, lipid droplet; OS, outer segment.

3.4.8—RNA quantitation of tvrm148 mutation

RNA was isolated from the RPE of +/+ and tvrm148/tvrm148 mice to determine if the mutant mice expressed similar levels of *Rpe65* mRNA. qRT-PCR results (Fig. 3.13) indicated insignificant differences in steady-state levels of *Rpe65* mRNA in tvrm148/tvrm148 mice compared to +/+ mice (P=0.617); tvrm148/tvrm148 mice express *Rpe65* mRNA at ~91% of the level in +/+ mice.

3.4.9—RPE65 protein expression in tvrm148/tvrm148 mice

Immunoblotting for RPE65 protein showed the size and abundance of RPE65 protein in +/+, tvrm148/+, and tvrm148/tvrm148 mice (Fig. 3.14A). Immunoblots for RPE65 showed a reduction in RPE65 protein amount in tvrm148/+ and tvrm148/tvrm148 mice (Fig. 3.14A). Densitometry analysis was performed on three immunoblots (Fig. 3.14B). tvrm148/+ mice expressed RPE65 protein at 59.7 ± 4.7% of +/+ levels, and tvrm148/tvrm148 mice expressed RPE65 protein at 14.5 ± 1.5% of +/+ levels (Fig. 3.14B). There did not appear to be any difference in the size of RPE65 protein in tvrm148/tvrm148 mice despite a reduction in the amount of protein (Fig. 3.14A).

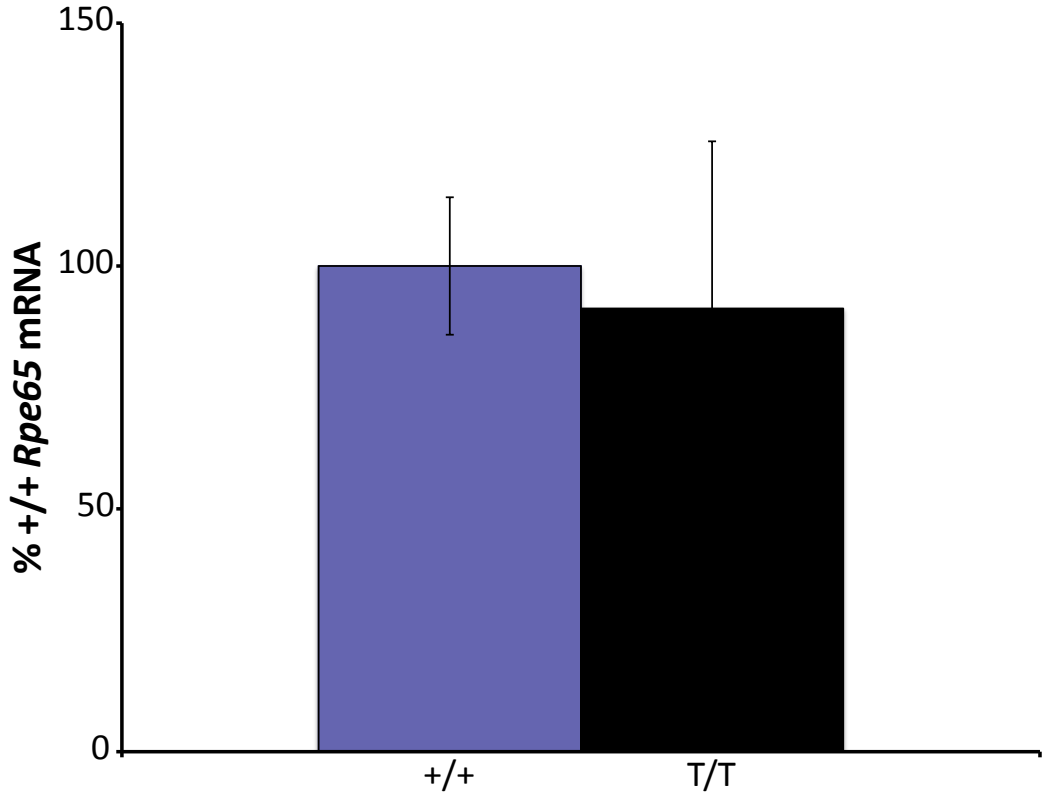

Figure 3.13. tvrm148/tvrm148 mice express *Rpe65* mRNA at the same level as +/+ mice under steady-state conditions. Whole cell RNA from postnatal day (P) 60 +/+ and tvrm148/tvrm148 RPE/choroid extracts was harvested for qRT-PCR. Steady-state *Rpe65* mRNA levels in +/+ mice (n=4) and tvrm148/tvrm148 mice (n=5) show no significant difference ($P = 0.617$).

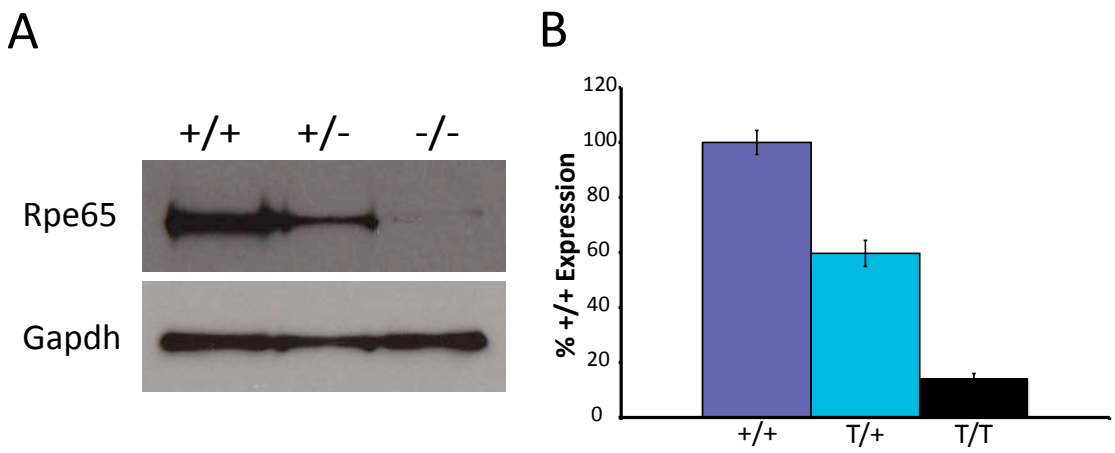

Figure 3.14. Immunoblots and densitometry for RPE65 in +/+, tvrm148/+, and tvrm148/tvrm148 mice show mutant mice have reduced protein levels. 1 µg of RPE/choroid protein extracts harvested from P60 +/+ and tvrm148/tvrm148 RPE. (**A**) Immunoblotting for RPE65 in +/+, tvrm148/+, and tvrm148/tvrm148 protein extracts showed a decrease in RPE65 levels in tvrm148/+ and tvrm148/tvrm148 mice but no change in protein size. GAPDH is shown as a loading control. (**B**) Densitometry of immunoblots (n = 3) showed 60 ± 4.7% +/+ levels of RPE65 protein in tvrm148/+ mice and 14.5 ± 1.5% protein levels in tvrm148/tvrm148 mice (P <0.05 compared to +/+). Data are presented as percentage change from +/+ (mean ± SD).

3.5—DISCUSSION

The KO and tvrm148 mutations do not complement one another, proving that the tvrm148 mutation occurs in the *Rpe65* locus and is the causative lesion driving visual function loss (Fig. 3.5; Table 3.3). The complementation test with the knockout and tvrm148 alleles definitively proves that there is no other mutation contributing to the loss of visual function (Fig. 3.5). This genetic test also resolves concerns associated with discrepancies we found between the genetic and physical maps of chromosome 3 in the region where the *Rpe65* locus and D3Mit147 and D3Mit19 markers reside (Fig. 3.1).

Retinoid analyses of +/+, KO/KO, and tvrm148/tvrm148 mice, showing undetectable amounts of 11-*cis*-retinal (downstream enzymatic product) in retina but large amounts of retinyl esters in RPE/choroid samples (enzymatic substrate) from mutant mice, confirmed that the tvrm148 mutation results in a biochemically null Rpe65 protein product that lacks retinol isomerase activity (Table 3.3). Previous reports of mouse *Rpe65* mutations (Redmond, Yu et al. 1998; Samardzija, von Lintig et al. 2008; Won, Shi et al. 2011) show KO, rd12, and R91W mice have undetectable scotopic responses at dim flash intensities and bright flash intensities in addition to reduced photopic responses (Redmond, Yu et al. 1998; Samardzija, von Lintig et al. 2008; Won, Shi et al. 2011) and these previous findings support the importance of RPE65 in 11-*cis*-retinal production and photoreceptor function. Consistent with other *Rpe65* mutants (Redmond, Yu et al. 1998; Samardzija, von Lintig et al. 2008; Won, Shi et al. 2011), tvrm148/tvrm148 mice at P30 and P180 had poor dark-mediated vision but relatively appreciable light-mediated vision at early ages (Fig. 3.6). LCA2 patients suffer from a similar pathology early in their degenerations (Jacobson, Aleman et al. 2009), so we

sought to determine if tvrm148/tvrm148 and KO/KO mice conform with clinical observations of human patients. tvrm148/tvrm148 mice, but not tvrm148/+ mice, lose visual acuity through P210 (indicating the tvrm148 mutation inherits in a recessive manner) but have appreciable visual function at early ages (Fig. 3.7). KO/KO mice have visual acuity losses that parallel with tvrm148/tvrm148 mice and do not significantly differ from one another (Fig. 3.8). This is the first reported progressive visual acuity loss in *Rpe65* mutant mice (previous measurements have been performed with ERGs) and goes well beyond previous work reporting *Rpe65* mutant mouse visual acuity (Cachafeiro, Bemelmans et al. 2010).

Human LCA2 patients (Jacobson, Aleman et al. 2009; Caruso, Aleman et al. 2010; Pasadhika, Fishman et al. 2010) have mostly intact retina architecture even at late ages (Jacobson, Aleman et al. 2009; Caruso, Aleman et al. 2010; Pasadhika, Fishman et al. 2010), so we sought to qualitatively and quantitatively examine the retina for similar phenotypes. The architecture of the retina in tvrm148/tvrm148 mice relative to +/+ and tvrm148/+ mice was strikingly normal considering the visual function deficits (Fig. 3.9), but these findings were consistent with published literature on RPE65-deficient mouse models (Redmond, Yu et al. 1998; Samardzija, von Lintig et al. 2008; Won, Shi et al. 2011). Droplets (Fig. 3.12) in the RPE in T/T mice are similar to reports in KO, rd12, and R91W mice (Redmond, Yu et al. 1998; Samardzija, von Lintig et al. 2008) that are the result of retinyl ester accumulation (Redmond, Yu et al. 1998). tvrm148/+ and tvrm148/tvrm148 mice experienced significant reductions in RPE65 protein level compared to +/+ (Fig. 3.14) even though there was no reduction in *Rpe65* mRNA levels in tvrm148/tvrm148 mice compared to +/+ (Fig. 3.13). tvrm148/tvrm148 mice had no

detectable 11-*cis*-retinal in neural retina and a 22-fold increases in retinyl esters in RPE samples (Table 3.3), further indicating the mutant protein is a null mutation that possesses no measurable enzymatic activity.

The visual acuity of tvrm148/tvrm148 mice is surprisingly high (almost normal) at early ages (Fig. 3.7) considering the lack of 11-*cis*-retinal generation in KO mice (Redmond, Yu et al. 1998); neither KO nor rd12 mice have detectable amounts of 11-*cis*-retinal in the retina (Redmond, Yu et al. 1998). R91W mice have ~5% the wild type amount of 11-*cis*-retinal in the retina, and this residual enzymatic product is sufficient to preserve vision significantly longer than what is seen in other *Rpe65* mutant mice (Samardzija, von Lintig et al. 2008). We show tvrm148 mice lack 11-*cis*-retinal altogether (Table 3.3). The residual visual function in tvrm148/tvrm148 mice may correspond to residual rod function, not cone function (Chen, Moiseyev et al. 2006) because in the absence of 11-*cis*-retinal, cone opsins in mice mislocalize (Rohrer, Lohr et al. 2005; Zhang, Zhang et al. 2011), and it has been proposed this cone opsin mislocalization may have a toxic effect on cone cells (Zhang, Zhang et al. 2011). Work with rd12 mice shows most cones are lost from the retina by P30 (Cachafeiro, Bemelmans et al. 2010). This is in contrast to most other retinal degenerations reported in mice in which visual function loss is driven primarily by rod photoreceptor loss (Cachafeiro, Bemelmans et al. 2010). Visual acuity measurements are performed in photopic conditions that are dominated by cone photoreceptors in C57BL/6J mice (Umino, Solessio et al. 2008), so it may at first seem counterintuitive that the visual acuity measurements in tvrm148/tvrm148 mice probably rely on residual rod photoreceptor function. Previous work shows the greatly altered kinetics of rod

photoreceptors in KO mice causes them to function exclusively in photopic conditions because of reduced photon quantum-catch capability. This, coupled with the fact that *Rpe65*$^{-/-}$::*Rho*$^{-/-}$ (*Rhodopsin*; pure cone function) mice do not retain visual acuity (Cachafeiro, Bemelmans et al. 2010), suggests the residual visual acuity in tvrm148/tvrm148 mice is driven primarily by rod function. Consistent with previous work (Cachafeiro, Bemelmans et al. 2010; Cachafeiro, Bemelmans et al. 2010; Zhang, Zhang et al. 2011), tvrm148/tvrm148 mice lost 59.9% of cones by P60 (Fig. 3.11); furthermore, many remaining cones are not functional at that age in KO mice, although they can be restored to activity by reintroduction of 11-*cis*-retinal (Tang, Wheless et al. 2011)

The source and identity of chromophore for rod photoreceptors in tvrm148/tvrm148 mice, though, is unclear at this time. However, KO mice may generate and utilize 9-*cis*-retinal to form isorhodopsin (Fan, Rohrer et al. 2003). R91W *Rpe65* knock-in mice generate a small but significant amount of 11-*cis*-retinal (Samardzija, von Lintig et al. 2008). It is possible *Rpe65* mutant mice could obtain enough 11-*cis*-retinal for residual visual function from photoisomerization (Van Hooser, Liang et al. 2002). More recently, evidence is emerging that Müller cells may actually provide small amounts of 11-*cis*-retinal to the retina (Takahashi, Moiseyev et al. 2011; Wang and Kefalov 2011; Kaylor, Yuan et al. 2013), and although this mechanism would not be sufficient to preserve cones, we speculate residual visual function in *Rpe65* mutant mice may be aided by this putative cone visual cycle.

Low RPE65 protein levels in tvrm148/tvrm148 mice could be the result of reduced translation of the *Rpe65* transcript in tvrm148/tvrm148 mice or the result of

RPE65 protein instability. Recent work concerning the three dimensional structure of *B. taurus* RPE65 protein (Kiser, Golczak et al. 2009; Golczak, Kiser et al. 2010; Kiser and Palczewski 2010; Kiser, Farquhar et al. 2012) provides insight into reasons why the $RPE65^{F229S}$ mutant protein may be nonfunctional and possibly unstable. The tvrm148 mutation resides in exon 7 of the *Rpe65* gene (Fig. 3.4) (Won, Shi et al. 2011) and results in a substitution of Ser for Phe at amino acid position 229. Because Phe 229 is conserved in RPE65 from a wide variety of species (Won, Shi et al. 2011), it is possible that a missense mutation at this position could be pathogenic even though the residue is not thought to participate in the active site of RPE65 protein (Kiser, Golczak et al. 2009). The pathogenicity (Table 3.2) of the F229S substitution might be attributed to two other factors. First, RPE65 is a seven-bladed ß-propeller that folds to form a hydrophobic tunnel leading to the active site. Mutations interfering with ß-propeller folding may perturb the formation of the hydrophobic tunnel or the appropriate shape of the active site itself (Kiser, Golczak et al. 2009). A comparison of the location of many of the known pathogenic mutations in human RPE65 with the crystal structure of bovine RPE65 confirm many of these missense mutations reside between the ß-propellers of the protein (Kiser, Golczak et al. 2009). Phe 229 resides between the second and third ß-propellers of RPE65, and because of the different chemical properties of the phenylalanine (large, aromatic, hydrophobic) and serine (small, polar, hydrophilic) sidechains, it would seem possible this amino acid substitution could affect protein folding or shape. The fact that the tvrm148 mutation abolishes 11-*cis*-retinal production, it would seem possible this residue is near the active site of the enzyme and could affect substrate binding and catalysis.

The tvrm148 mutation serves as an interesting contrast to other models of RPE65 deficiency, specifically the R91W mouse. The tvrm148 mutation occurs in a region of *Rpe65* that is rich in pathogenic mutations in the human homolog (Gu, Thompson et al. 1997; Marlhens, Bareil et al. 1997; Morimura, Fishman et al. 1998; Stone 2007; Philp, Jin et al. 2009; Sundaresan, Vijayalakshmi et al. 2009). The R91W mouse, a knock-in model for the most common missense mutation seen in humans, retains residual RPE65 enzymatic activity (Samardzija, von Lintig et al. 2008). The tvrm148 mouse, though, is the first model of RPE65 deficiency to present a null phenotype while retaining the ability to produce a mutant RPE65 protein (albeit low; Fig. 3.14). Because this model has a missense mutation in a region of the protein known for recessively-inheriting, disease-causing missense mutations in human subjects while still retaining a null phenotype, the tvrm148 mutant may have unique utility for studying future treatments for LCA2.

Future work with this mutant mouse model could involve *Rpe65* gene augmentation to see if visual function rescue in these mice resemble rescue seen in other RPE65-deficient mice (Fan, Rohrer et al. 2003). Other future work could examine cone photoreceptor loss in tvrm148/tvrm148 mice to see if the loss resembles that seen in other RPE65-deficient mice (Chen, Moiseyev et al. 2006; Pang, Boye et al. 2010). Like the KO mouse, the tvrm148 mutation acts as an autosomal recessive, null mutation. Compared to the knockout, almost all other properties were very similar based on visual optokinetic testing (Fig. 3.7) and ERGs (Fig. 3.6). Molecular properties of the tvrm148 mRNA are remarkable in its nearly normal abundance (Fig. 3.13), but with little accumulated protein under steady-state conditions that was significantly lower than wild

type (Fig. 3.14). We might speculate that the mRNA is processed normally but that the protein is unstable and rapidly degraded.

In summary, a complementation test proves that tvrm148 is a mutation in the *Rpe65* gene. This mutation results in a null *Rpe65* mouse that makes no 11-*cis*-retinal. The tvrm148 mice have a visual phenotype resembling that found in KO mice, losing visual acuity and ERGs in a similar manner. Protein is present in low amounts and lacks activity, despite wild type levels of mRNA. This work suggests that the tvrm148 mouse may serve as a model for LCA2 and can thus help in the understanding of the basic biology of the visual cycle and aid in the future development of treatment strategies for the disease. Although our work does not resolve the apparent difference in the genetic map and current gene sequence assembly, it does demonstrate the tvrm148 mutation as a causative lesion in *Rpe65*.

Key points presented in this section:

1. The tvrm148 mutation causes a block in the visual cycle by preventing formation of the 11-*cis* double bond in retinoids that is necessary for visual function; homozygous mutant mice had a 22-fold increase in the amount of all-*trans*-RE (substrate) and an undetectable amount of 11-*cis*-RAL (product downstream of RPE65).
2. The tvrm148 mutation inherits and causes a mutant phenotype in an autosomal recessive fashion as supported by OKT, ERG, and histological measurements.
3. When mice have one copy of the tvrm148 mutation, they do not have any detectable visual deficits as measured by OKT and ERG. When mice have two copies of the tvrm148 mutation, they have a 1,000 to 10,000-fold reduction in dark-adapted visual function as measured by ERG and a 90.3% reduction in visual acuity by the time they are seven months old.
4. Mice with two copies of the tvrm148 mutation express wild type levels of *Rpe65* mRNA but only 14.5% the amount of RPE65 protein found in wild type mice.
5. The tvrm148 mutation is damaging to visual function because it results in a lower level of RPE65 protein that cannot make 11-*cis*-retinal, which is needed as a cofactor for light-sensitive proteins of the visual system in the retina.
6. The tvrm148 mutation occurs in a region of the mouse *Rpe65* gene that contains several mutations in the human *RPE65* gene. Because of this, the tvrm148 mouse models a disease phenotype that may accurately reflect what is seen in human patients in the clinic.

IV: The rd12 allele exerts a semidominant negative effect on visual function in mice

This chapter is currently being prepared as a manuscript. It will be submitted imminently.

Key questions to be addressed in this section:

1. Are the ERG and OKT equivalent as functional outcome measurements for *Rpe65* mutations?
2. How is the rd12 mutation inherited in mice (autosomal recessive, autosomal dominant, etc.)?
3. Does the rd12 allele produce a mutant RPE65 protein?
4. Does the rd12 allele express mRNA at detectable levels (i.e. degraded by RNA surveillance pathways at a rate that would make accumulation undetectable in steady state conditions)?
5. Is the mRNA produced by the rd12 allele improperly spliced or containing additional mutations?
6. Is the mutant mRNA predicted to have a significantly altered secondary structure?
7. Does the mutant mRNA localize differently within the RPE cell?
8. Is the mutant mRNA efficiently bound by ribosomes for translation?
9. What relevance does the rd12 mutation have with respect to patients in the clinic?

4.1—ABSTRACT

Purpose. *Rpe65* knockout (KO) and rd12 mice were reported as recessively inherited *Rpe65* mutants. We asked if the rd12 mutation resides in *Rpe65* and how the mutation manifests itself to test whether the rd12 mouse differed significantly from the KO.

Methods. A complementation test was performed by mating KO/KO and rd12/rd12 mice together. Visual function of wild type (+/+), KO/+, rd12/+, KO/KO, rd12/rd12, and KO/rd12 mice was measured by optokinetic tracking (OKT) and electroretinography (ERG). Morphology was assessed by retinal cross section. qRT-PCR was used to measure *Rpe65* mRNA levels. Immunoblotting measured the size and level of RPE65 protein. *Rpe65* mRNA localization was visualized with fluorescence *in situ* hybridization (FISH). Ribosome occupancy of *Rpe65* mRNA was measured by linear sucrose gradient fractionation.

Results. The KO and rd12 alleles did not complement. The rd12 allele induced a semidominant effect on visual function with OKT responses becoming undetectable 120 days earlier in rd12/rd12 mice compared to KO/KO mice. rd12/+ mice lost ~21% visual acuity by P210. rd12/rd12 mice had fewer cone photoreceptor nuclei than KO/KO mice at P60. rd12/rd12 mice expressed 71% wild type levels of *Rpe65* mRNA, but protein was undetectable (lower limit of detection was less than 2.5% wild type). Mutant mRNA was appropriately spliced, exported to the cytoplasm, trafficked, and contained no other mutation except a nonsense mutation (R44X) previously reported. Mutant mRNA was enriched in fractions containing ribosome-free messenger ribonucleoproteins (mRNPs) while wild type mRNA was enriched in fractions containing actively translating polyribosomes.

Conclusions. The rd12 lesion is in *Rpe65* by complementation test. The rd12 allele causes visual function loss in a semidominant manner as measured by OKT. The effects of the rd12 allele on visual function may result from a problem after the mRNA is exported from the nucleus and is either co-incident with a block in initiation of translation or immediately following initiation. This may result in toxic accumulation of mutant mRNA on mRNPs.

4.2—INTRODUCTION

As of October 2013, all 602 pathogenic mutations listed on the NCBI single nucleotide polymorphism (SNP) database identified in human *RPE65* were autosomal recessive mutations (Gu, Thompson et al. 1997; Marlhens, Bareil et al. 1997; Morimura, Fishman et al. 1998; Hanein, Perrault et al. 2004; Chen, Moiseyev et al. 2006; Stone 2007; Philp, Jin et al. 2009; Sundaresan, Vijayalakshmi et al. 2009), **except** $RPE65^{D477G}$ that inherits in an autosomal dominant manner (Bowne, Humphries et al. 2011). To date, all known mouse mutations in *Rpe65* inherit in a recessive manner as well (Redmond, Yu et al. 1998; Pang, Chang et al. 2005; Won, Shi et al. 2011). We studied the retinal degeneration 12 (rd12) mutant because it was thought to be a mutation in *Rpe65*; however, our preliminary studies suggested a dominant characteristic, which is atypical of LCA2 and lesions in *Rpe65*, and called into question whether rd12 was in fact a gene lesion in *Rpe65* or perhaps a nearby gene instead. The differences between the genetic map and the sequence map of the locus for *Rpe65* further caused concern (Wright, Chrenek et al. 2013). Thus, we asked how the rd12 mutation caused disease through a protein-mediated pathway or through some other pathway.

Three mouse models are commonly employed for the study of LCA2 pathology and treatment that are reported as having null *Rpe65* mutations. The first model is the KO mouse that was artificially constructed and contains a deletion of exons 1-3 (Redmond, Yu et al. 1998). The second model, the rd12 mouse, was isolated as a spontaneously occurring mutation in the B6.A-*H2-T18*^{a}/BoyEg strain that was then backcrossed to wild type (C57BL/6J, referred to as +/+ in this study) to make a congenic inbred strain, which the authors referred to as B6-rd12 (Pang, Chang et al. 2005). It mapped genetically near *Rpe65*, and a nonsense mutation (R44X) was found in exon 3 of *Rpe65* (Pang, Chang et al. 2005). tvrm148 was thought be a missense mutation in *Rpe65* (Won, Shi et al. 2011), and this was validated by complementation testing with the KO mouse (Wright, Chrenek et al. 2013). The tvrm148 mutation makes some RPE65 protein and near normal amounts of the mRNA, but has no known dominant negative characteristics. Using a similar approach to reconcile the genetic and sequence maps of *Rpe65* with the tvrm148 mutation (Wright, Chrenek et al. 2013), we performed a complementation test on the rd12 and KO alleles to ask if the rd12 mutation resided in the *Rpe65* locus.

Both the KO and rd12 mouse strains were reported as null *Rpe65* mutants (Redmond, Yu et al. 1998; Pang, Chang et al. 2005). Immunohistochemical staining for RPE65 in both KO and rd12 mouse models show RPE65 protein is undetectable in the eyes of these mice (Pang, Chang et al. 2005; Bemelmans, Kostic et al. 2006; Chen, Moiseyev et al. 2006; Pang, Chang et al. 2006; Li, Kong et al. 2009). KO mice do not express detectable *Rpe65* mRNA (Redmond, Yu et al. 1998), and although previous studies speculated the absence of RPE65 protein was attributable to degradation of the *Rpe65* mRNA by nonsense-mediated decay (NMD) (Pang, Chang et al. 2005), the rd12

allele surprisingly was later reported to produce *Rpe65* mRNA at a level that was similar to wild type C57BL/6J mice (although the data were not shown) (Guerin, Gregory-Evans et al. 2008). We tested whether a truncated 43 amino acid-long RPE65 fragment (the expected size of a protein that would be produced if the nonsense-containing rd12 allele produced a protein) was expressed and whether this small oligopeptide might cause disease. Flowcharts of the various hypotheses and conclusions from these experiments are presented in Fig. 4.1.

4.3—METHODS

4.3.1—Experimental Animals

KO/KO mice (Redmond, Yu et al. 1998) were backcrossed to +/+ mice for 10 generations to make the line fully congenic with the +/+ line housed at Emory University for this study. rd12/rd12 mice (Pang, Chang et al. 2005) congenic to the C57BL/6J mouse strain were purchased from The Jackson Laboratory (Bar Harbor, ME) and were maintained and bred at Emory University. KO/+ mice were bred by crossing +/+ mice with KO/KO mice, rd12/+ mice were bred by crossing +/+ mice with rd12/rd12 mice, and KO/rd12 mice were bred by crossing KO/KO mice with rd12/rd12 mice. Mice were provided food and water ad libitum and maintained in a 12:12 h light-dark cycle. Mice were sacrificed with CO_2 gas. All procedures and care were approved by Emory Institutional Animal Care and Use Committee (IACUC) and followed ARVO guidelines of animal care and use.

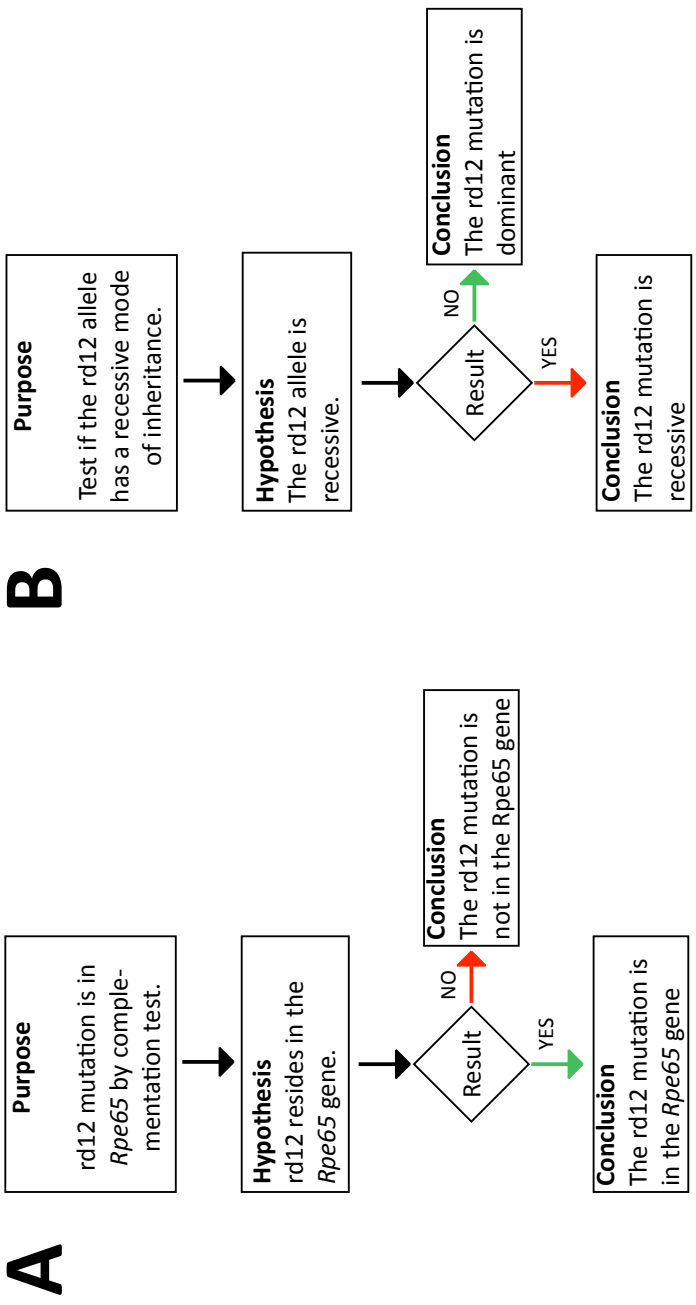
A
Purpose
rd12 mutation is in *Rpe65* by comple-mentation test.
Hypothesis
rd12 resides in the *Rpe65* gene.
Result
NO
YES
Conclusion
The rd12 mutation is not in the Rpe65 gene
Conclusion
The rd12 mutation is in the *Rpe65* gene
B
Purpose
Test if the rd12 allele has a recessive mode of inheritance.
Hypothesis
The rd12 allele is recessive.
Result
NO
YES
Conclusion
The rd12 mutation is dominant
Conclusion
The rd12 mutation is recessive

C

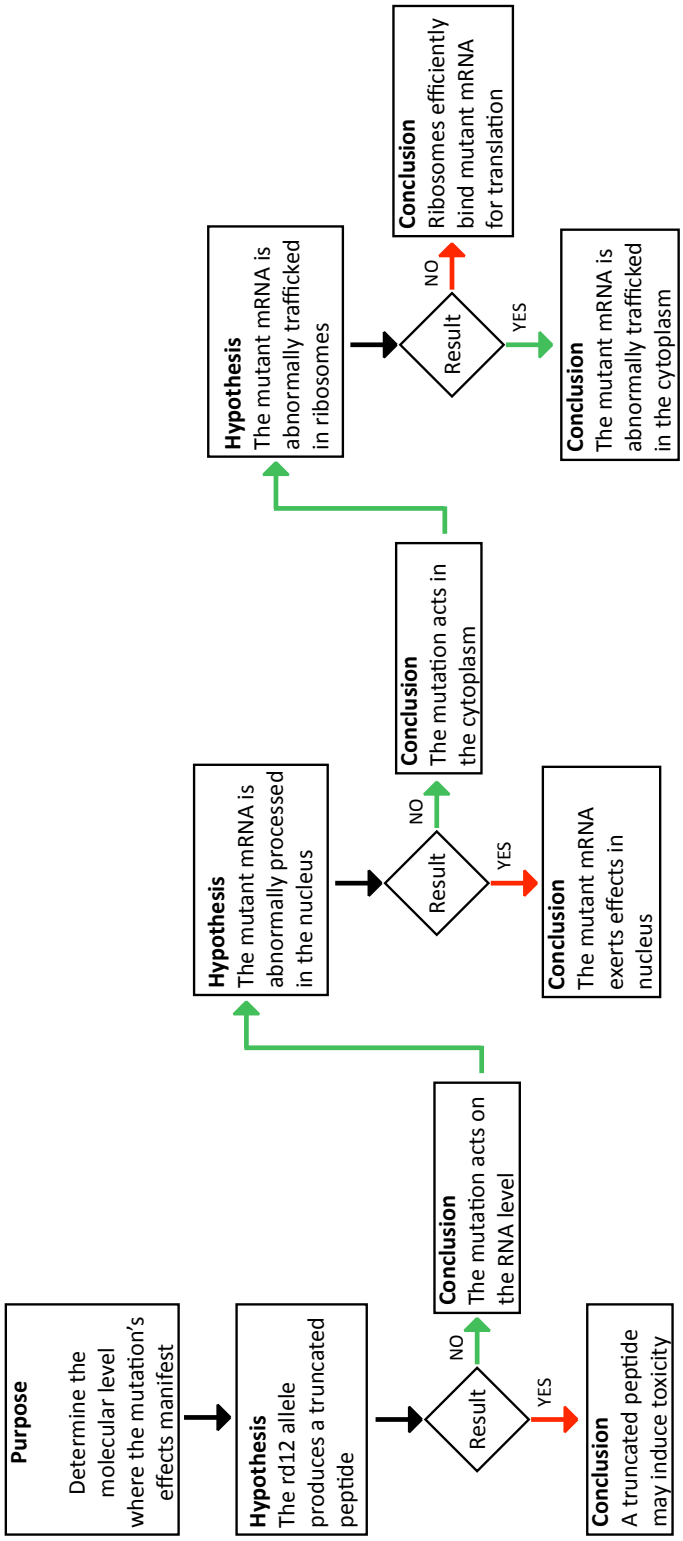
Purpose
Determine the molecular level where the mutation's effects manifest
Hypothesis
The rd12 allele produces a truncated peptide
Result
YES
Conclusion
A truncated peptide may induce toxicity
NO
Conclusion
The mutation acts on the RNA level
Hypothesis
The mutant mRNA is abnormally processed in the nucleus
Result
YES
Conclusion
The mutant mRNA exerts effects in nucleus
NO
Conclusion
The mutation acts in the cytoplasm
Hypothesis
The mutant mRNA is abnormally trafficked in ribosomes
Result
YES
Conclusion
The mutant mRNA is abnormally trafficked in the cytoplasm
NO
Conclusion
Ribosomes efficiently bind mutant mRNA for translation

Figure 4.1—Flowcharts of hypotheses and experiments in Chapter 4. Green arrows denote the experimentally supported conclusions in the study. "Y" refers to "yes," and "N" refers to "no" for the support or rejection of the hypotheses, respectively. (**A**) A complementation test determined whether the rd12 mutation resides in the *Rpe65* locus and (**B**) whether it is inherited in an autosomal recessive or autosomal dominant manner. (**C**) Results presented in this study determined the level at which the mutation manifested itself (i.e. RNA or protein) and where in the cell the mutation manifested itself.

4.3.2—Optokinetic tracking (OKT)

Visual acuities were measured at 100% contrast at postnatal day (P) 30, P45, P60, P75, P90, P120, P150, P180, and P210 using a virtual optomotor system (Prusky, Alam et al. 2004; Douglas, Alam et al. 2005) (OptoMotry 1.7.4; Cerebral Mechanics, Vancouver, BC, Canada). Measurements were taken as previously described (Wright, Chrenek et al. 2013).

4.3.3—Retinoid analysis

Retinoid analyses of mouse retinas and eye cups were performed with normal phase HPLC in adult mice as previously described (Landers and Olson 1988; Garwin and Saari 2000; Wright, Chrenek et al. 2013).

4.3.4—Electroretinography (ERG)

ERG measurements were conducted at P30, P60, and P90 in KO/KO, rd12/rd12, and KO/rd12 mice and at P60, P120, and P180 in +/+, KO/+, and rd12/ + mice using a commercial ERG system (UTAS-E3000, LKC, Gaithersburg, MD), as previously described (Pardue, McCall et al. 1998; Pardue, Phillips et al. 2005; Chang, Hawes et al. 2007; Jablonski, Dalke et al. 2009; Wright, Chrenek et al. 2013). Oscillatory potentials (OPs) were isolated from scotopic waveforms by filtering using a fifth order Butterworth filter and performing a Discrete Fourier Transform (DFT) on the filtered waves (Akula, Hansen et al. 2007; Akula, Mocko et al. 2007; Weymouth and Vingrys 2008). Summed oscillatory potential amplitudes (SOPAs) were calculated by adding amplitudes from OP1-OP6 together (Akula, Hansen et al. 2007; Akula, Mocko et al. 2007; Weymouth and

Vingrys 2008) in +/+, KO/+, and rd12/+ mice. Rod phototransduction parameters were estimated by fitting the Hood and Birch formulation of the Lamb and Pugh model of phototransduction activation to a-waves from scotopic waveforms (Hood and Birch 1993; Hood and Birch 1994).

4.3.5—Histology and morhphometrics

Histology was assessed in +/+, KO/KO, and rd12/rd12 mice at P60 and P210. Retinal sections (prepared by fixing eyes in 2.5% (W/V) gutaraldehyde in 0.1 M sodium cacodylate buffer, pH 7.4 (Electron Microscopy Sciences, Hatfield, PA), embedded in LX-112 (Ladd Research Industries, Williston, VT) and sectioned at 1 μm thickness) were stained and analyzed as previously described (Wright, Chrenek et al. 2013). Cone nuclei were counted in 200 μm areas 250, 1000, and 2000 μm superior and inferior of the optic nerve from sections as previously described (Seeliger, Grimm et al. 2001; Wright, Chrenek et al. 2013).

4.3.6—RNA Extraction and qRT-PCR

Whole cell RNA was isolated from P60 RPE/choroid tissue placed in buffer (Trizol, Life Technologies Corp., Grand Island, NY) and extracted (RNeasy Mini Kit, Qiagen, Valencia, CA) (Wright, Chrenek et al. 2013). RPE cells were fractionated and total RNA from nucleus and cytoplasm were isolated (SurePrep Nuclear or Cytoplasmic RNA Purification Kit, Fisher Scientific, Pittsburgh, PA). mRNA was amplified with a one step reaction (Quantitect SYBR Green RT-PCR Kit, Qiagen) under the following conditions: 30 min at 50 °C, 15 min at 95 °C, 40 cycles at 94 °C for 15 s and 55 °C for 15 s and 72

°C for 40 s, followed by a melt curve analysis for the first run of each primer set. Unless stated otherwise, all *Rpe65* amplification reactions were performed with specific primers that were commercially available (Qiagen product number QT00140140) and normalized to 18S RNA. Primers specific for *Rpe65* exon boundaries were designed and used as previously described (Rozen and Skaletsky 2000; Wright, Chrenek et al. 2013) (Table 4.1). mRNA expression was normalized to 18S ribosomal RNA using the following primers: forward 5′-GTT GGT TTT CGG AAC TGA GGC-3′ and reverse 5′-GTC GGC ATC GTT TAT GGT CG-3′.

4.3.7—qRT-PCR standard curve

Rpe65 cDNA was prepared using qRT-PCR with primers specific to *Rpe65* (forward 5′-TCT TAC CCA TCT GAA CCC ATC -3′ and reverse 5′- CAC ACT CAG AAC CAC ACC AT -3′; Qiagen) on whole RNA extracted from +/+ mouse RPE/choroid. PCR products were purified using a QIAquick PCR Purification Kit (Qiagen) and DNA concentration was calculated by measuring absorbance at 260 nm. Polyacrylamide gel of PCR products is shown in Fig. 4.2. Quantitative PCR was performed on eight ten-fold serial dilutions of the purified *Rpe65* cDNA at the indicated concentrations. Cycle number (the point at which the amplification curve crossed threshold) was plotted against RNA concentration, and a four parameter, sigmoidal logarithmic curve of best fit was calculated in SigmaPlot 12.0 (Systat). The logarithmic curve of best fit is presented alongside the standard curve in Fig. 4.3. This standard curve was used to calculate the amount of *Rpe65* mRNA present in the linear sucrose gradient fractions presented in the text in Fig. 4.22.

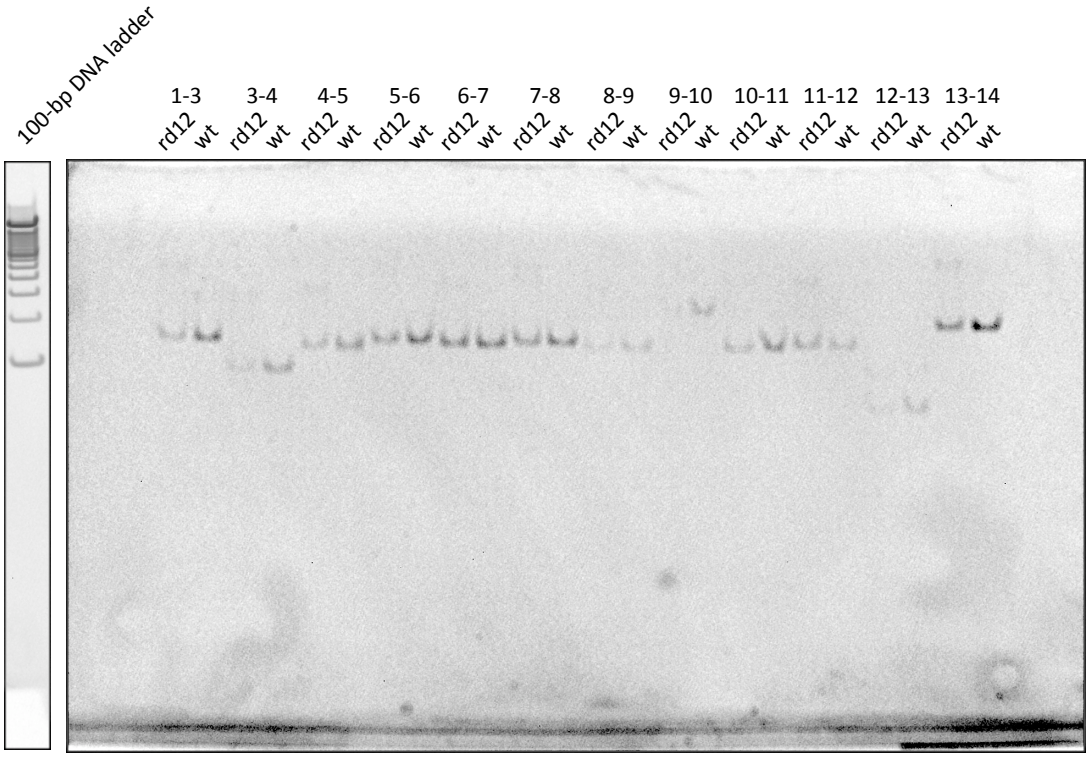

Figure 4.2—qRT-PCR products from *Rpe65* mRNA with primers specific to each exon boundary. A single strong band for each amplified *Rpe65* exon boundary from +/+ and rd12/rd12 mice was observed on polyacrylamide gel electrophoresis (ladder was from the same gel). qRT-PCR products from +/+ and rd12/rd12 mice were directly loaded onto a DNA polyacrylamide gel to check for primer specificity. These same PCR products were also DNA sequenced. Amplified exons are indicated above each set of +/+ and rd12/rd12 samples. Expected sizes of each amplicon are listed in Table 4.1.

Table 4.1—Primer sequences for *Rpe65* exon boundary amplification

Exons Amplified	Size of Expected Amplicon (bp)	Primer Sequence
1-3	188	F: 5′-AAA TTG AAC ACC CTG CTG GT-3′ R: 5′-AGG GCT TGT CCA TGC AAC AG-3′
2-3	180	F: 5′-GGA GGA ACT GTC CTC ACC AC-3′ R: 5′-TAT GTG ACA TGG CCC TCC TT-3′
3-4	121	F: 5′-TGA AGT TGG ATC TGA GCC TT-3′ R: 5′-AAC ATA AGC ATC AGT GCG G-3′
4-5	154	F: 5′-TTC ATC CGC ACT GAT GCT TA-3′ R: 5′-CAA GGG CAT TGT CAG TAA CC-3′
5-6	175	F: 5′-CCC AGA GAC CTT GGA GAC AA-3′ R: 5′-TGC TTT CAG TGG AGG GAT CT-3′
6-7	172	F: 5′-GTC AAT GGT GCC ACT GCT C-3′ R: 5′-AGG GGA ACT GCA CAA CAA CT-3′
7-8	168	F: 5′-CTG CAG TGA TCG TTT CAA GC-3′ R: 5′-CCC ATG CTT TCA TTG GAC TC-3′
8-9	160	F: 5′-TTT CGA GTC CAA TGA AAG CA-3′ R: 5′-CCA GCA ACA GAG ATC CAC AA-3′
9-10	240	F: 5′-CCT GAC TTC AGG CTG AGG AG-3′ R: 5′-TCC CCT TTC AAT CTC TTC CA-3′
10-14	549	F: 5′-AGG CTC CTC AGC CTG AAG TC-3′ R: 5′-AGT CCA TGG AAG GTC ACA GG-3′

These primer sets were designed using web-based Primer3 software for whole-cell amplification of *Rpe65* mRNA exon boundaries (http://biotools.umassmed.edu/bioapps/primer3_www.cgi) with *Rpe65* exon sequences. Oligos were synthesized by MWG Operon.

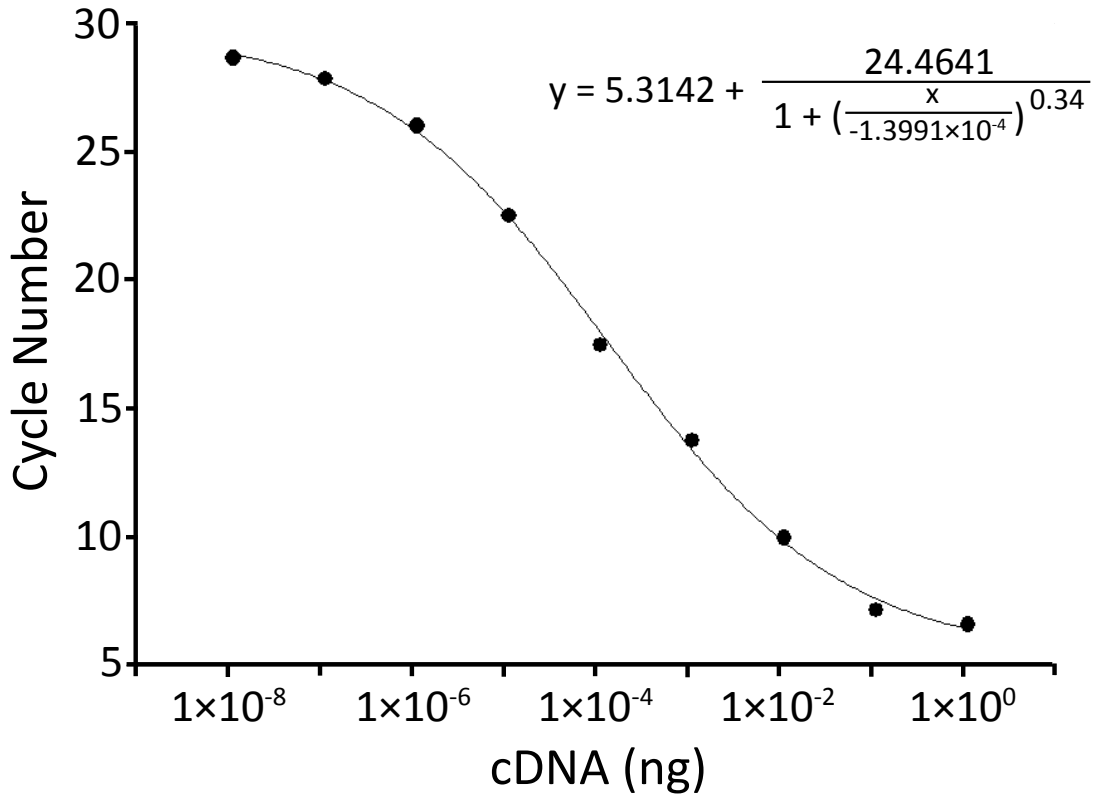

Figure 4.3—Standard curve of *Rpe65* amplification by qRT-PCR. The equation for the fitted curve is shown (n=4 repeats). This equation was used to calculate the amount of RNA that was present in sucrose gradient fractions based on the point at which the amplification curve crossed threshold (n =4; zero cDNA amplifies crosses at ~35 cycles).

4.3.8—DNA sequencing of Rpe65 mRNA

qRT-PCR with primers specific to overlapping regions of *Rpe65* mRNA isolated from +/+ and rd12/rd12 mice (Table 4.1) was performed to create DNA samples for sequencing. The samples were sequenced using the forward primers from each amplification reaction (Eurofins MWG Operon, Louisville, KY). +/+ and rd12/rd12 samples were compared through BLAST (blast.ncbi.nlm.nih.gov/Blast.cgi; Fig. 4.4).

4.3.9—Immunoblotting

Soluble RPE/choroid extracts were collected at P60 as previously described (Wright, Chrenek et al. 2013). Tissue was homogenized in radioimmunoprecipitation assay (RIPA) buffer (Teknova, Hollister, CA) by vortex mixing vigorously with one new stainless steel set screw for five min in a 1.5 ml screw-cap microcentrifuge tube. Samples were then centrifuged at 16,000 ×*g* for 1 min, and supernatant collected and placed into another tube for storage at -80 °C. Pellets left after RIPA-soluble protein removal were then dissolved in 8 M urea and 1 mM dithiothreitol (DTT) in 1% sodium dodecyl sulfate (SDS) for 1 h at 95 °C. Samples were then centrifuged at 16,000 ×*g* for 1 min, and supernatant removed for storage at -80 °C. Protein concentration was determined via bicinchoninic acid (BCA) protein assay (Novagen, Darmstadt, Germany). A total of 10 µg of soluble protein and 20 µg of insoluble protein was resolved by sodium dodecyl sulfate polyacrylamide gel electrophoresis (SDS-PAGE; “Any kD TGX” Criterion gel, BioRad, Hercules, CA) followed by transfer to a nitrocellulose membrane (Invitrogen). A custom-made rabbit polyclonal anti-mouse RPE65 N-terminal specific primary antibody that was raised against the first 43 amino acids of mouse RPE65 protein was incubated at

1:5000 dilution for 1 h at ambient room temperature. Secondary incubation was performed with a goat anti-rabbit-horseradish peroxidase (HRP) conjugate antibody (Invitrogen) at 1:5000 dilution for 1 h at ambient room temperature. Bands were detected by chemiluminescence (ECL Plus; Amersham Biosciences, Piscataway, NJ) as previously described (Wright, Chrenek et al. 2013).

4.3.10—Fluorescence in situ hybridization (FISH)

Mice were sacrificed at P120 and their eyes enucleated. In situ hybridization was performed as per manufacturer's instructions (QuantiGene ViewRNA ISH Tissue 2-Plex Assay; Affymetrix, Santa Clara, CA). The eyes were fixed in a 1:4 dilution of 16% (W/V) paraformaldehyde (Electron Microscopy Sciences) in PBS for 24 h. Eyes were dehydrated and embedded in paraffin (TissuePrep2, Fisher Scientific, Pittsburgh, PA). Paraffin embedded eyes were sectioned at 5 μm thickness and baked on microscope slides (StarFrost, Mercedes Medical, Sarasota, FL) in a hybridization oven at 60 °C for 24 h prior to *in situ* hybridization. RNA *in situ* hybridizations were performed (QuantiGene ViewRNA ISH Tissue 2-Plex Assay kit, Affymetrix, Santa Clara, CA) according to manufacturer's protocol. Probes specific for *Rpe65* (Affymetrix product no. VB6-14045) and β-actin (Affymetrix product no. VB1-10350) mRNAs were purchased from Affymetrix for the assay. Nuclei were counterstained with YO-PRO-1 (Invitrogen). Slides were mounted in (Vectashield Hard Set, Vector Laboratories, Burlingame, CA) and imaged at 240× (with a 60× lens) magnification via confocal microscopy (Fast Blue Substrate excites at 360 nm and emits at 775 nm; Fast Red Substrate excites at 530 nm and emits at 590 nm; YO-PRO-1 excites at 491 nm and emits at 509 nm).

4.3.11—RNA Structure Prediction

Predicted secondary centroid structures from mRNA sequences of wild type, rd12, R91W, and tvrm148 mouse alleles were generated using global RNA structure prediction algorithms (RNAfold v1.4 software, Institute for Theoretical Chemistry, University of Vienna, Vienna, Austria) (Zuker and Stiegler 1981; McCaskill 1990; Schuster, Fontana et al. 1994).

4.3.12—Linear Sucrose Gradient Fractionation

RPE/choroid tissue was isolated from three P60 mice and pooled together per sample. Tissue was isolated from three wild type and three rd12 litters. RPE/choroid was dounce-homogenized and incubated at 4 °C for 15 minutes to arrest polysome migration in either a polysome-preserving gradient buffer (10 mM Tris, pH 7.5, 100 mM KCl, 100 µg/ml cycloheximide, 5 µl/ml RNase inhibitor [Applied Biosystems, Warrington, UK], 5 mM $MgCl_2$) or a polysome-disrupting buffer that contained 10 mM EDTA instead of $MgCl_2$ in gradient buffer (Feng, Absher et al. 1997; Irier, Shaw et al. 2009; Lau, Irier et al. 2010). Triton X-100 (Sigma, St. Louis, MO) was then added to 1% (V/V) final concentration and allowed to incubate on ice for 15 min to lyse cells. Cellular debris was removed by centrifugation at 20,000 ×*g* for 30 minutes. Supernatant was loaded on top of a 15-45% (W/V) linear sucrose gradient for fractionation of mono- and polyribosomes (Feng, Absher et al. 1997; Irier, Shaw et al. 2009; Lau, Irier et al. 2010). Sucrose gradients were centrifuged at 39,000 ×*g* for 90 minutes at 4 ºC in an SW41 rotor. Ten 1 ml fractions from each gradient were collected into microfuge tubes using a gradient

fractionator (Isco, Lincoln, NE). RNA was isolated in Trizol (Invitrogen) as previously described, and *Rpe65* amplified by qRT-PCR using specific primers (Qiagen) and cycle values evaluated against a standard curve (Feng, Absher et al. 1997; Irier, Shaw et al. 2009; Lau, Irier et al. 2010) (Fig. 4.3). This procedure is briefly summarized in Fig. 4.4.

4.3.13—Statistical Analysis

Graphs were constructed by computer (Microsoft Excel 2008, Microsoft Inc., Redmond, WA). All graphs represent data as mean ± standard deviation. Visual acuity, ERG, and morphometric data were analyzed by two-way repeated measures ANOVA (RM-ANOVA) with post-hoc Student-Newman-Keuls testing (SigmaPlot 12, Systat, San Jose, CA). qRT-PCR data were analyzed by one-way ANOVA with post-hoc Student-Newman-Keuls testing (SigmaPlot 12, Systat). Sample sizes are reported in the results, and each sample group contained mice from at least three different litters unless otherwise noted.

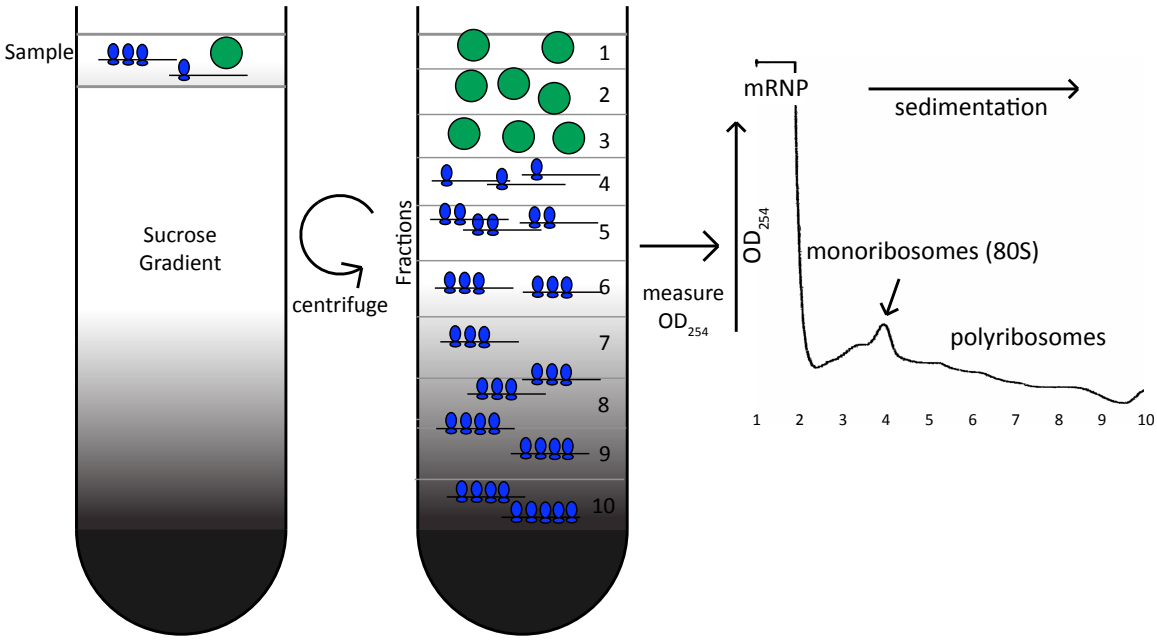

Figure 4.4—Linear sucrose gradient fractionation. Cycloheximide treatment of homogenate pauses translation with any ribosomal proteins (blue ovals) left bound to mRNA so that centrifugation can separate mRNA molecules based on how many ribosomes are bound to them. During centrifugation in the sucrose gradient, mRNA molecules bound by multiple ribosomes will sediment more than mRNAs bound by one or two ribosomes. mRNAs bound by no ribosomes will remain near the top of the gradient, but are bound by ribosome-free messenger ribonucleoporteins (mRNPs; green circles) instead. When the fractions are drawn out of the gradient, absorbance is measured at 254 nm. A higher absorbance corresponds to a greater amount of protein-bound mRNA.

4.4—RESULTS

4.4.1—Complementation test

rd12/rd12 mice were bred to KO/KO mice to determine whether the rd12 and KO alleles complemented each other (Fig. 4.1A) as measured by OKT, a behavioral measure of visual acuity (Prusky, Alam et al. 2004; Douglas, Alam et al. 2005). KO/KO, rd12/rd12, and KO/rd12 mice had significant reductions in visual acuity compared to +/+ mice at P120 (Fig. 4.5). There were also significant differences in the OKT response among KO/KO, rd12/rd12, and KO/rd12 mice, but not between rd12/rd12 and KO/rd12 mice (Fig. 4.5). Retinoid analysis of rd12/rd12 mouse eyes showed no detectable amounts of 11-*cis*-retinal or all-*trans*-retinal (Table 4.2) but showed increased all-*trans*-retinyl ester content (23-24 fold +/+ levels), consistent with previous reports of KO/KO (Redmond, Yu et al. 1998), rd12/rd12 (Pang, Chang et al. 2005), and tvrm148/tvrm148 mice (Won, Shi et al. 2011; Wright, Chrenek et al. 2013).

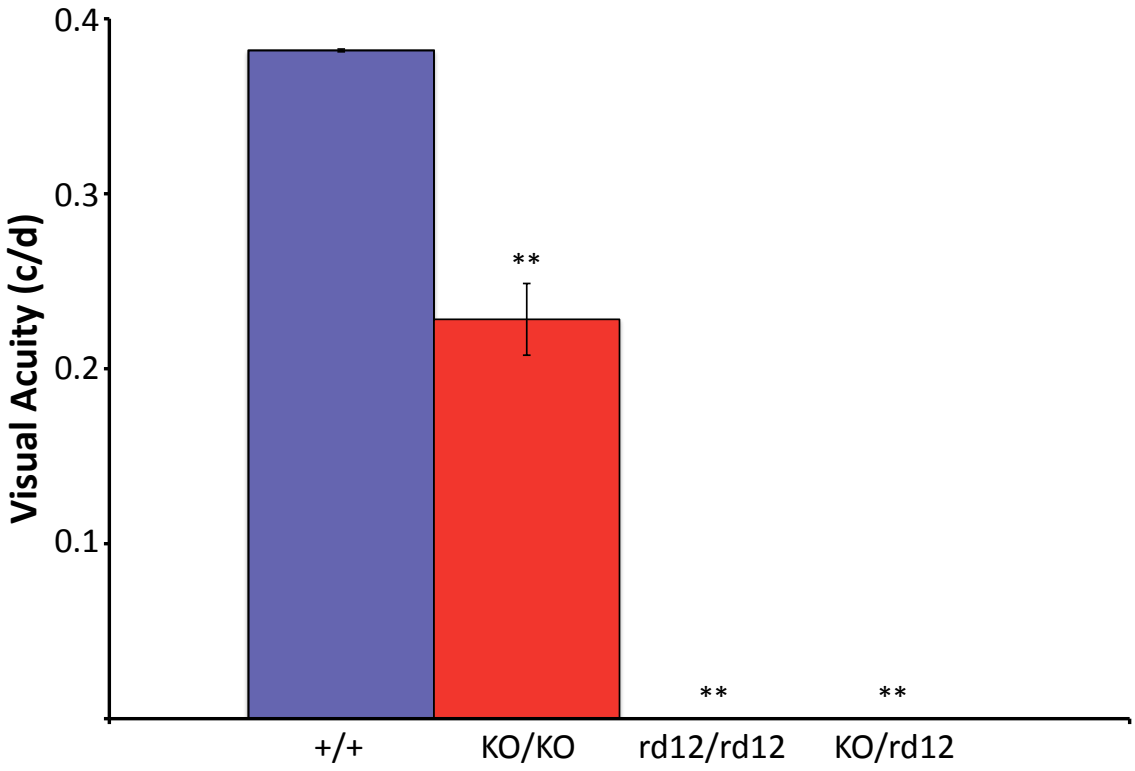

Figure 4.5—The *Rpe65* knockout and rd12 alleles did not complement. KO/rd12 offspring bred from KO/KO and rd12/rd12 parental mice did not have restoration of visual function. OKT measurements in P120 +/+ (n=11), KO/KO (n=9), rd12/rd12 (n=14), and KO/rd12 (n=20) are shown. KO/KO, rd12/rd12, and KO/rd12 mice had significantly reduced visual acuity measures compared to +/+ mice. KO/rd12 and rd12/rd12 mice had significantly reduced responses compared to KO/KO mice but did not differ with respect to one another. $^{**}P < 0.001$ compared with +/+. Data are presented as mean ± SD.

Table 4.2. Retinoid levels in +/+, KO/KO, and rd12/rd12 mice

Genotype[1]	11-*cis*-retinal (pmol/eye)	All-*trans*-retinal (pmol/eye)	Retinyl ester content (pmol/mg protein)
+/+	233.3 ± 125.9	94.1 ± 24.9	54.1 ± 34.1[3]
KO/KO	None detected[2]	None detected	1314 ± 235.8[3]
rd12/rd12	None detected[2]	None detected	1261 ± 394.5[3]

Mice were dark adapted over an hour prior to tissue harvest, and all dissection steps occurred under dim red light. In +/+ mice, 11-*cis*-RAL amounts are much higher than all-*trans*-RE because RPE65 protein is available to convert all-*trans*-RE (RPE65 substrate) into 11-*cis*-ROL, which is then immediately converted to 11-*cis*-RAL by RDH5. All-*trans*-RAL can only form if 11-*cis*-RAL has been recently bound to rhodopsin (because it forms immediately after light exposure); without 11-*cis*-RAL production, all-*trans*-RAL cannot form in appreciable amounts. Please refer back to Fig. 1.1 for a diagram of the visual cycle.

[1]number of animals analyzed per genotype ≥ 3

[2]The lower limit of detection in this assay was 1 pmol.

[3]The lower limit of detection in this assay was 8.8 pmol.

4.4.2—Visual acuity

Because the results of the complementation test suggested the rd12 allele may not inherit in a recessive manner, longitudinal OKT measurements were performed. The differences in visual acuity losses were examined to determine whether the rd12 allele was inherited in a dominant fashion (Fig. 4.1B) and caused an earlier loss of visual function than the KO allele. Figure 4.6 shows that the rd12 allele was inherited in a semidominant manner. Both +/+ and KO/+ mice maintained high visual acuity (0.383 ± 0.001 c/d and 0.381 ± 0.002 c/d, respectively) from P30 until the end of the study at P210 (Fig. 4.6). rd12/+ mice, on the other hand, had a small but significant reduction in visual acuity compared to +/+ mice at P30 (0.354 ± 0.003 c/d; P <0.001 by two-way RM ANOVA; Fig. 4.6) that gradually decreased during the study until P210 (0.299 ± 0.005 c/d; P <0.001). KO/KO mice exhibited a significant reduction in visual acuity (0.317 ± 0.004 c/d; P <0.001, Fig. 4.6) compared to +/+ mice at P30 that became undetectable by the end of the study at P210. rd12/rd12 mice had a similar visual acuity compared to KO/KO mice at P30 (0.303 ± 0.003 c/d; P = 0.145) but lost all measurable visual acuity by P90 (Fig. 4.6) much earlier than the KO/KO mice. KO/rd12 mice had an average visual acuity measure of 0.021 ± 0.038 c/d by P90. rd12/rd12 and KO/rd12 mice had significantly lower visual acuities than KO/KO mice at all time points tested (except at P210, when all homozygous mutant mice had no detectable visual acuity). In summary, rd12/rd12 and KO/rd12 lost visual acuity early, with their progressive visual losses occurring faster than KO/KO mice. Because a single rd12 allele makes the disease progress faster than the KO mutation, we surmise that the rd12 mutation exhibits at least some dominant characteristics.

A

Figure 4.6

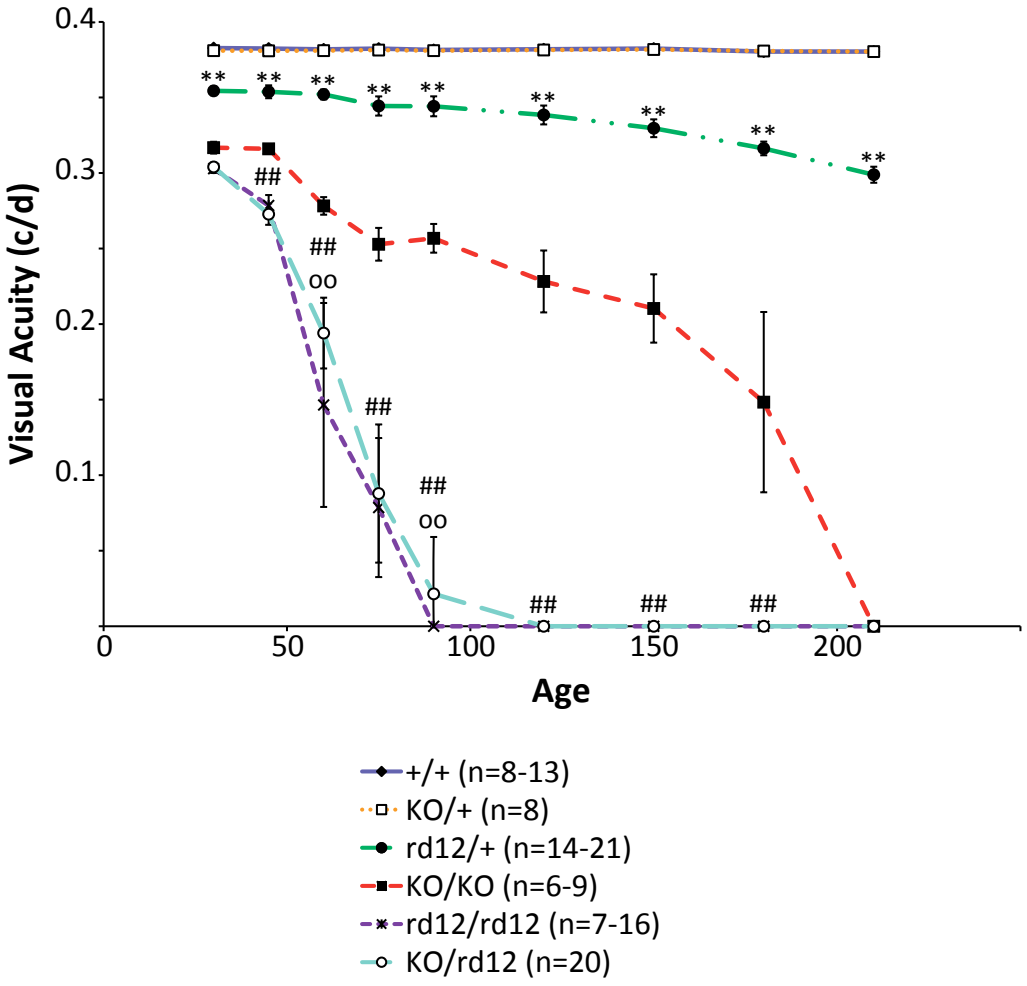
0.4
0.3
0.2
0.1
Visual Acuity (c/d)
0
50
100
150
200
Age
**
##
oo
+/+ (n=8-13)
KO/+ (n=8)
rd12/+ (n=14-21)
KO/KO (n=6-9)
rd12/rd12 (n=7-16)
KO/rd12 (n=20)

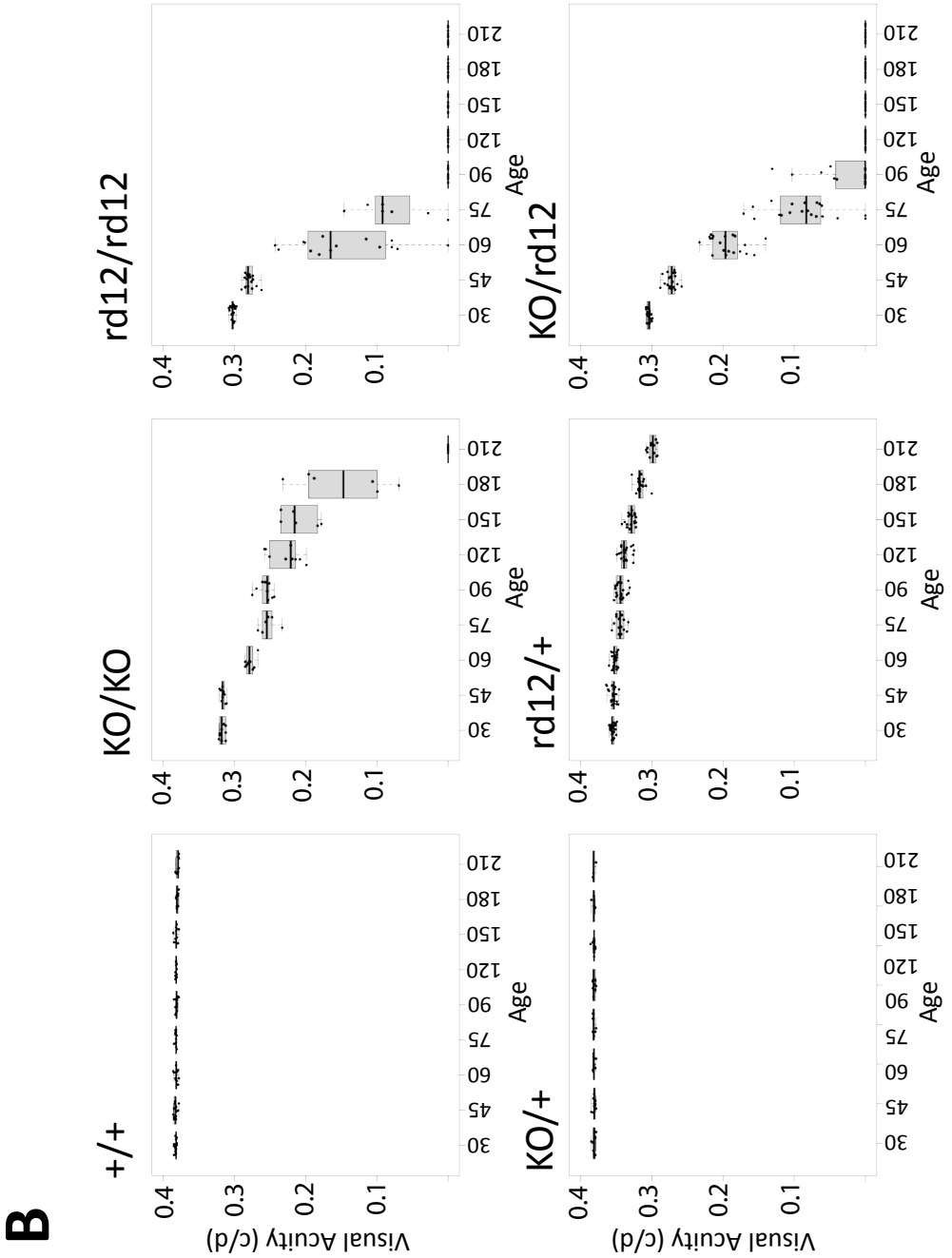
B
+/+
KO/KO
rd12/rd12
KO/+
rd12/+
KO/rd12
Visual Acuity (c/d)
0.4
0.3
0.2
0.1
Age
30
45
60
75
90
120
150
180
210

Figure 4.6—The rd12 allele caused visual acuity loss in a semidominant fashion. Longitudinal OKT measurements were taken on the same mice throughout the duration of the study. Mice harboring at least one copy of the rd12 allele lost visual function at earlier ages than mice that did not harbor the rd12 allele. (**A**) Visual acuities of +/+ (solid line with diamond points; n=8-13), KO/+ (dotted line with square points largely hidden behind the solid line; n=8), rd12/+ (dotted and dashed line with circle points; n=14-21), KO/KO (dashed line with square points; n=6-9), rd12/rd12 (dotted line with asterisk points; n=7-16), and KO/rd12 mice (dashed line with circle points; n=20) from P30-P210 are represented on the same graph. (**B**) Box plots with individual data points of data presented in **A**. ** P <0.001 +/+ compared with rd12/+, ## P <0.001 KO/KO compared with rd12/rd12, oo P <0.001 KO/rd12 compared with rd12/rd12, significance determined through two-way repeated measures ANOVA with post hoc Student-Newman-Keuls testing. There was no difference between +/+ and KO/+ between P30 and P210, and visual acuity measures of the two strains overlap through the duration of the study. Data are presented as mean ± SD.

4.4.3—ERG measurements of homozygous mutant mice

Scotopic (representative scotopic ERG traces are shown in Fig. 4.7) and photopic ERG measurements were conducted on KO/KO, rd12/rd12, and KO/rd12 compound heterozygote mice at P30, P60, and P90 to test whether ERG measurements reflected OKT findings. ERG responses from KO/KO and rd12/rd12 mice were largely consistent with previously published reports (Redmond, Yu et al. 1998; Pang, Chang et al. 2005). These data indicate large reductions in sensitivity (five orders of magnitude) in mutant mice when compared to wild type. There were significant reductions in a-wave amplitudes in rd12/rd12 and KO/rd12 compared to KO/KO as the mice aged (significant at P60 and P90, but not at P30; Fig. 4.8A). Both rd12/rd12 and KO/rd12 mice had scotopic b-wave amplitude reductions compared to KO/KO mice, but only at P60 (Fig. 4.8B). There were subtle differences among KO/KO, rd12/rd12, and KO/rd12 mice. None of these differences was large among rd12, KO, and rd12/KO, but rd12/rd12 trended toward a consistently lower ERG response at most illumination levels (Fig. 4.8). Although there were some differences between KO/KO, rd12/rd12, and KO/rd12 mice, all mutant mice were ~10^3-10^4-fold less sensitive to light than wild type counterparts.

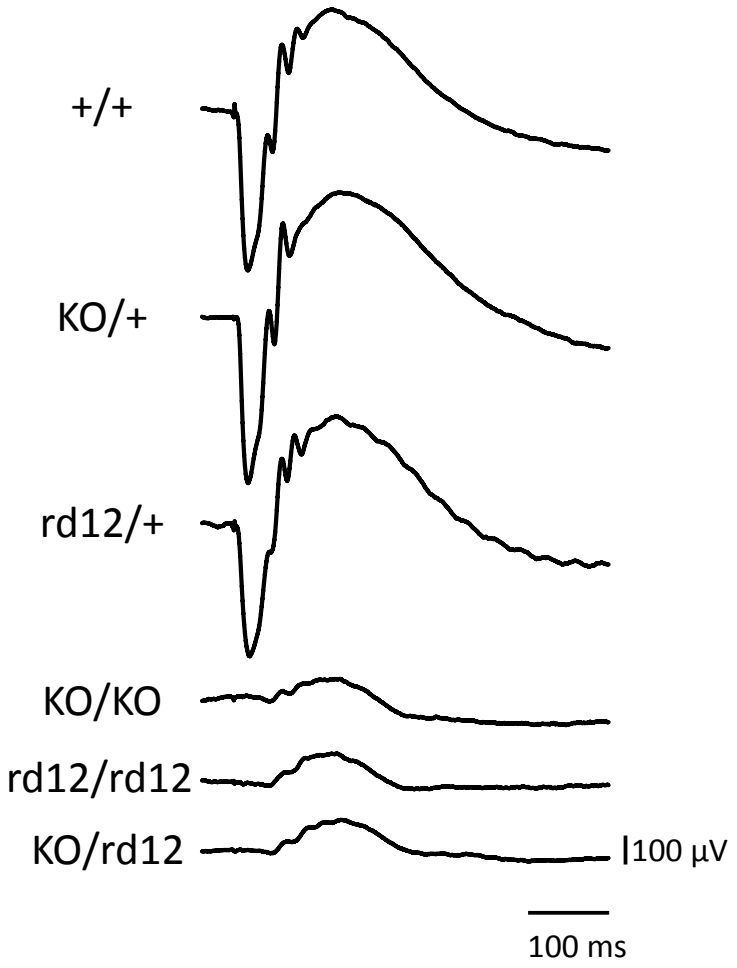

Figure 4.7—Raw ERG traces of genotypes in this study. This figure shows raw scotopic ERG traces of P60 +/+, KO/+, rd12/+, KO/rd12, KO/KO, and rd12/rd12 mice in response to a 137 cd×s/m^2 flash intensity at P30. KO/rd12, KO/KO, and rd12/rd12 mice have responses that are much lower than +/+, KO/+, and rd12/+ counterparts. Features of ERG responses (a-wave, b-wave, and OPs) can be found in Fig. 1.5.

Figure 4.8

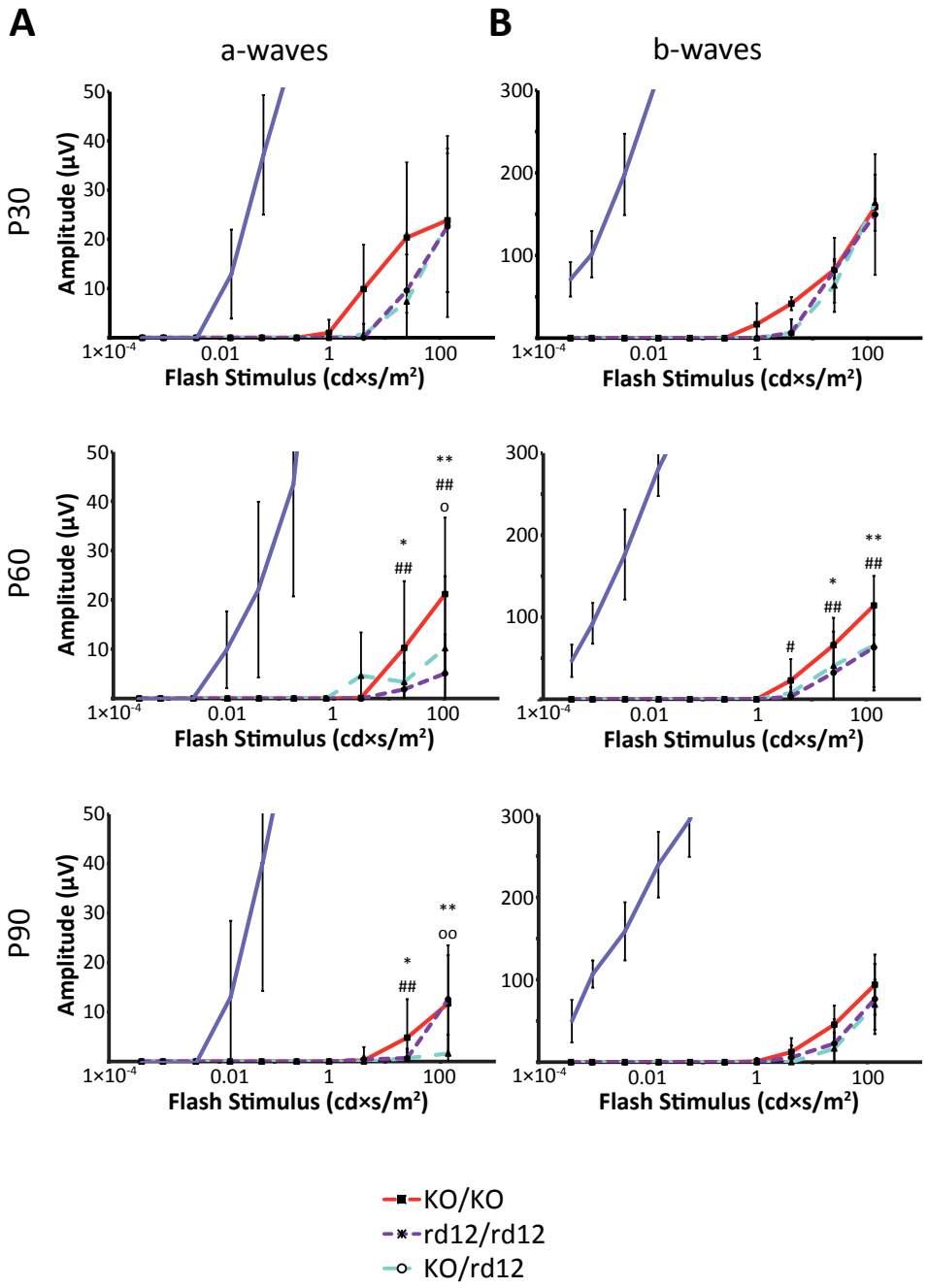
A
a-waves
B
b-waves
P30
P60
P90
Amplitude (µV)
Flash Stimulus (cd×s/m²)
1×10⁻⁴
0.01
1
100
KO/KO
rd12/rd12
KO/rd12

Figure 4.8. Mutant mice had reduced dark-adapted a- and b-wave amplitudes compared to +/+ mice from P30-P90. Based on ERG responses, mutant mice were ~10^3–10^4-fold less sensitive to light than wild type mice. Mice that were either homozygous or compound heterozygous for the rd12 allele trended towards a slightly faster progressive loss of ERG amplitudes than KO/KO mice. Responses from +/+ mice (solid blue line) are shown to provide perspective to response losses observed in mutant mice (solid line to the left of mutant mouse responses). (**A**) Dark-adapted a-wave amplitudes from KO/KO (solid red line; n=8, 9, 9 at P30, P60, and P90, respectively), rd12/rd12 (long teal dashed line; n=7, 7, 6 at P30, P60, and P90, respectively), and KO/rd12 (short purple dashed line; n=16, 19, 19 at P30, P60, and P90, respectively) are shown at P30, P60, and P90. (**B**) Dark-adapted b-wave amplitudes from KO/KO (solid line), rd12/rd12 (long dashed line), and KO/rd12 (short dashed line) are shown at P30, P60, and P90. * P <0.05, ** P <0.001 KO/KO compared to rd12/rd12; # P <0.05, ## P <0.001 KO/KO compared to KO/rd12; o P <0.05, oo P <0.001 KO/rd12 compared to rd12/rd12, significance determined through two-way repeated measures ANOVA with post hoc Student-Newman-Keuls testing. Data are presented as mean ± SD.

4.4.4—ERG measurements of heterozygous mutant mice

Scotopic and photopic ERG measurements (Section 1.2.3, Fig. 1.5) were taken on +/+, KO/+, and rd12/+ mice at P60, P120, and P180 to determine if only one copy of the rd12 allele was sufficient to drive retinal function loss. rd12/+ mice had mild but statistically significant reductions in scotopic a-wave amplitudes when compared to +/+ and KO/+ mice at P60, P120, and P180 (Fig. 4.9A). rd12/+ mice also trended toward slightly reduced summed oscillatory potential amplitudes (SOPAs) when compared to +/+ and KO/+ mice at P60 (Fig. 4.9C). rd12/+ mice had somewhat reduced scotopic b-wave amplitudes at P120 (Fig. 4.9B) and P180 (Fig. 4.9B). Despite reaching statistical significance at some time points, in general and for the most part, rd12/+ mice had only slight reductions in ERG responses. All mice had a progressive loss of b-wave amplitude with age but the loss was slightly more pronounced in rd12/+ mice. In-depth study of a-wave characteristics indicated there were no abnormalities in photoreceptor response (Fig. 4.10) (Akula, Hansen et al. 2007; Akula, Mocko et al. 2007; Weymouth and Vingrys 2008). Raw ERG traces are shown in Fig. 4.8.

Figure 4.9

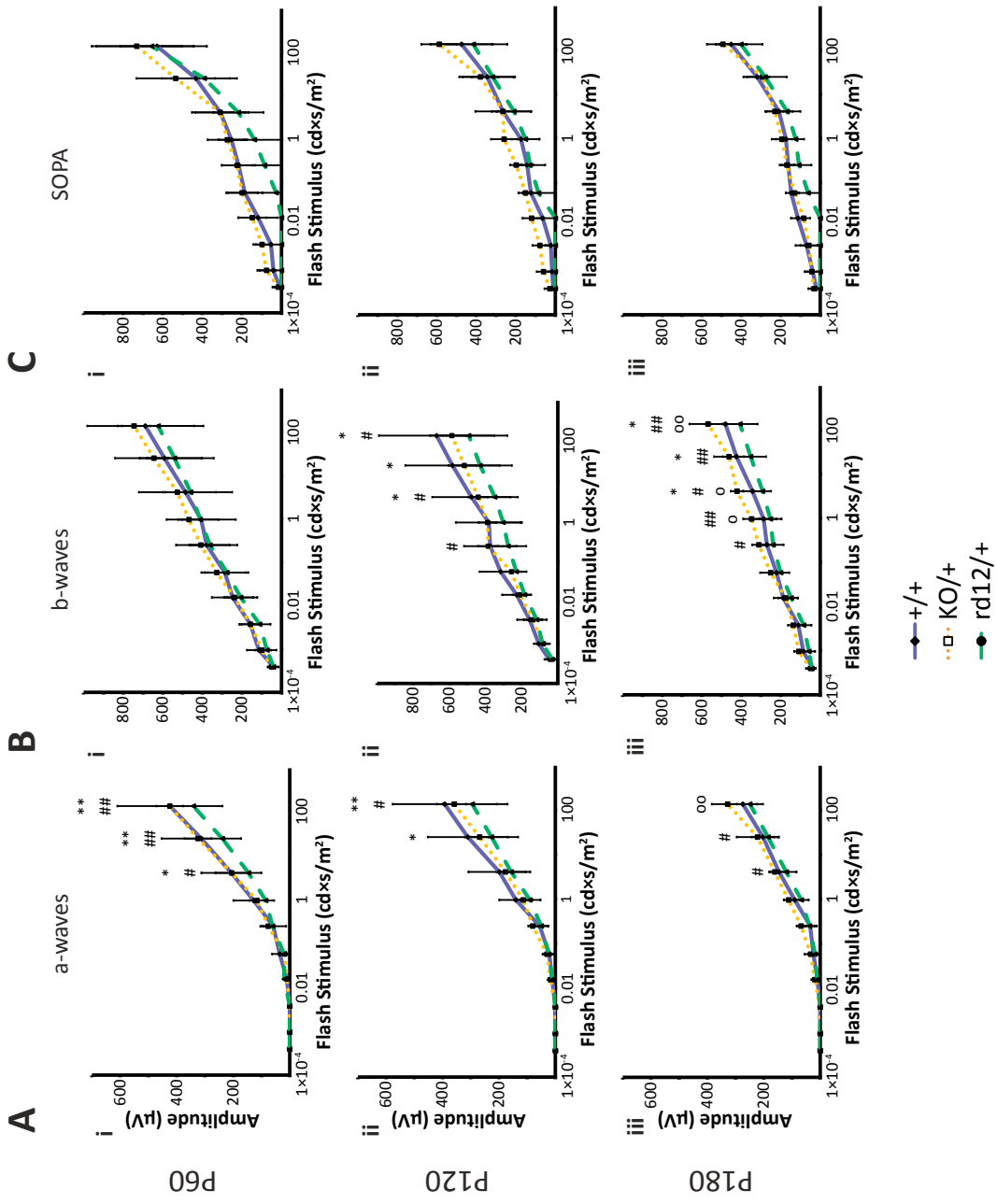
A
B
C
a-waves
b-waves
SOPA
P60
P120
P180
Amplitude (μV)
Flash Stimulus (cd×s/m²)
+/+
KO/+
rd12/+

Figure 4.9. One copy of the rd12 allele causes small reductions in dark-adapted ERG amplitudes. rd12/+ mice trended towards slightly lower a-wave, SOPA, and b-wave amplitudes as they aged, which might be due to a slight toxic effect of the rd12 allele on photoreceptor health and function. (**A**) Dark-adapted a-wave amplitudes from +/+ (solid blue line; n=9, 5, 6 at P60, P120, and P180, respectively), KO/+ (dotted orange line; n=8, 7, 6 at P60, P120, and P180, respectively), and rd12/+ (dashed green line; n=18, 15, 10 at P60, P120, and P180, respectively) are shown at P60, P120, and P180. (**B**) Dark-adapted summed oscillatory potential amplitudes from +/+ (solid line; n=9, 5, 6 at P60, P120, and P180, respectively), KO/+ (dotted line; n=8, 7, 6 at P60, P120, and P180, respectively), and rd12/+ (dashed line; n=18, 15, 10 at P60, P120, and P180, respectively) are shown at P60, P120, and P180. (**C**) Dark-adapted b-wave amplitudes from +/+ (solid line; n=9, 5, 6 at P60, P120, and P180, respectively), KO/+ (dotted line; n=8, 7, 6 at P60, P120, and P180, respectively), and rd12/+ (dashed line; n=18, 15, 10 at P60, P120, and P180, respectively) are shown at P60, P120, and P180. * P <0.05, ** P <0.001 +/+ compared to rd12/+; # P <0.05, ## P <0.001 KO/+ compared to rd12/+; o P <0.05, oo P <0.001 +/+ compared to KO/+, significance determined through two-way repeated measures ANOVA with post hoc Student-Newman-Keuls testing. Data are presented as mean ± SD.

Figure 4.10

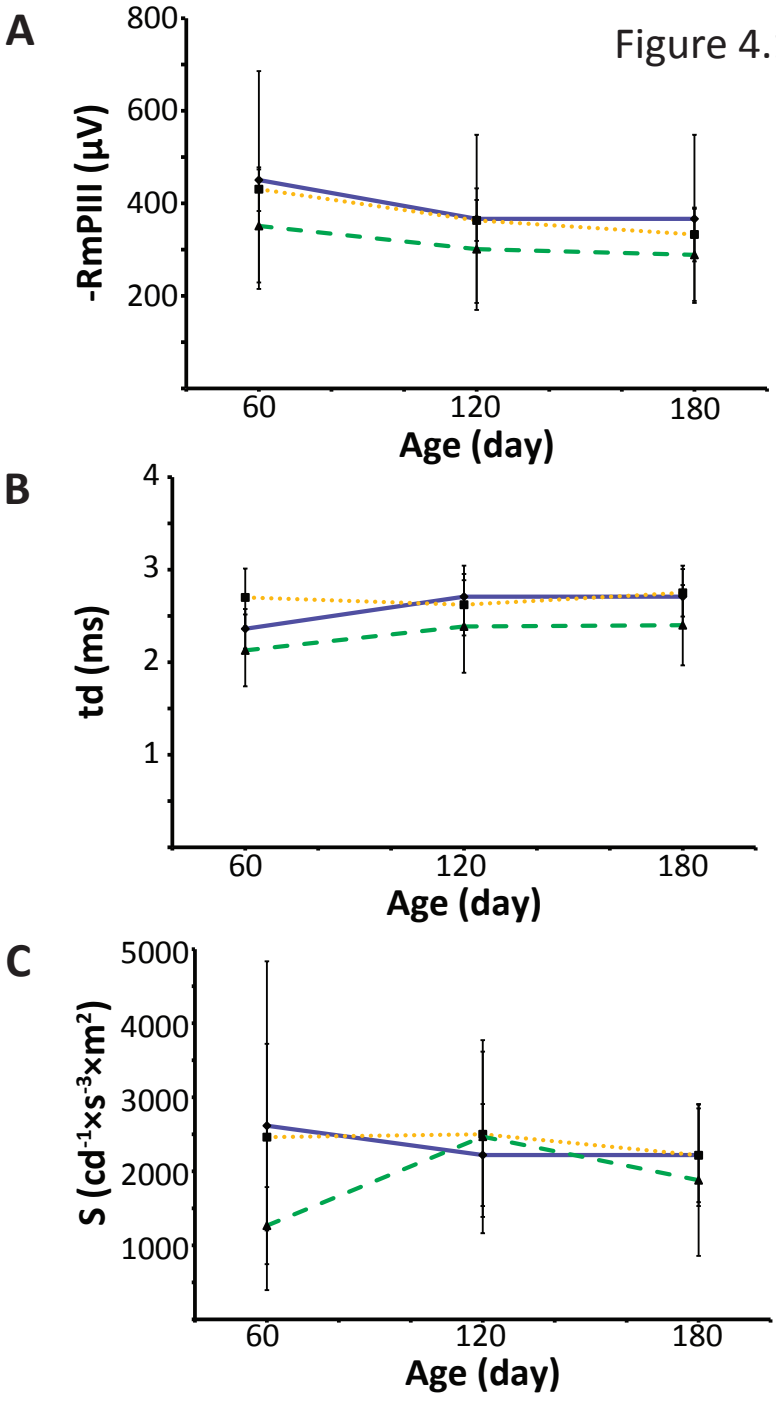
A
800
600
400
200
-RmPIII (µV)
60
120
180
Age (day)
B
4
3
2
1
td (ms)
60
120
180
Age (day)
C
5000
4000
3000
2000
1000
S (cd-1xs-3xm2)
60
120
180
Age (day)

Figure 4.10—Lamb and Pugh modeling of a-wave responses show rd12/+ mice have normal rod phototransduction kinetics. A-wave modeling of scotopic ERG responses in +/+, KO/+, and rd12/+ mice shows rd12/+ mice do not have any significant deficits with respect to the activation of the phototransduction cascade at P60, P120, or P180. (**A**) Maximal a-wave response, R_mPIII. (**B**) Time delay, t_d. (**C**) Phototransduction cascade time constant, S.

4.4.5—Histology and morphometrics

Retina architecture was compared qualitatively by retina cross sections in +/+, KO/KO, and rd12/rd12 mice to determine if there were any overt changes in retina architecture or organization between KO/KO and rd12/rd12 mice (Fig. 4.11). Retina architecture was relatively preserved in both mutant strains compared to +/+ mice despite some slight retinal thinning and gaps in the OS (Fig. 4.11). Quantitative measurements of ONL and OS thicknesses (Fig. 4.12) were taken from the retina cross sections. There were no significant differences of ONL or OS thicknesses between KO/KO and rd12/rd12 mice at either P60 or P210 (Fig. 4.12). KO/KO and rd12/rd12 mice did not have significant reductions in ONL thickness compared to +/+ mice at P60 (49.4 ± 3.7 μm, 52.3 ± 5.1 μm, and 51.2 ± 3.1 μm, respectively) but did by P210 when compared to +/+ mice (41.6 ± 3.0 μm, 39.9 ± 3.7 μm, and 56.3 ± 3.6 μm, respectively). KO/KO and rd12/rd12 mice had significant reductions in OS thicknesses compared to +/+ mice at both P60 (21.3 ± 1.9 μm, 23.2 ± 3.1 μm, and 31.4 ± 4.3 μm, respectively) and P210 (19.4 ± 3.0 μm, 21.5 ± 4.3 μm, and 29.0 ± 3.8 μm, respectively).

Figure 4.11

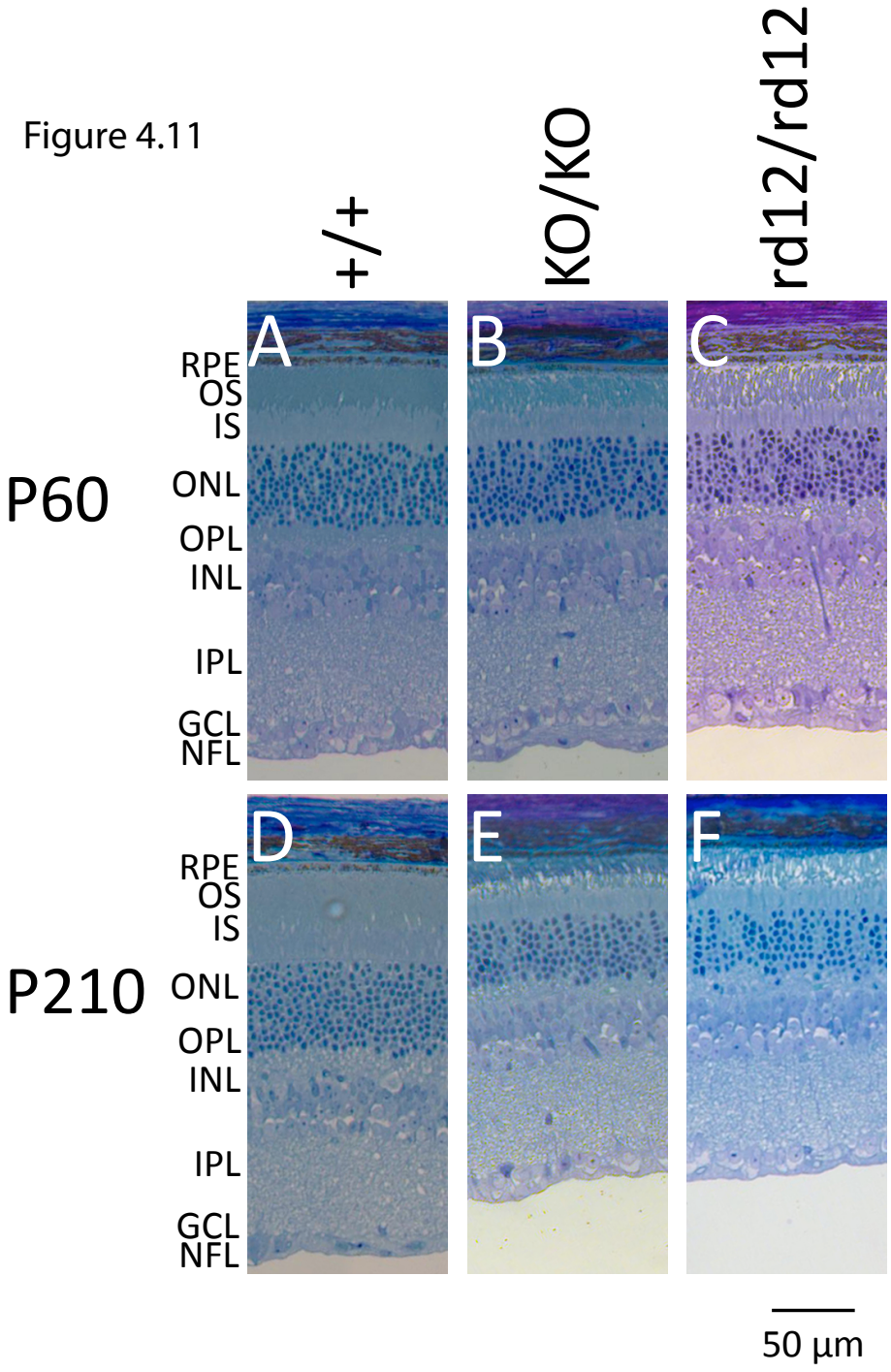
+/+
KO/KO
rd12/rd12
A
B
C
D
E
F
P60
P210
RPE
OS
IS
ONL
OPL
INL
IPL
GCL
NFL
50 µm

Figure 4.11. KO/KO and rd12/rd12 mice had a thinner retina than +/+ mice. KO/KO and rd12/rd12 mice had similar retinal morphology, with only slight retinal thinning compared to wild type mice at P210, mostly in the ONL, IS, and OS (with some slight disorganization in rd12/rd12 OS). Bright-field images of retina cross sections stained with toluidine blue from +/+, KO/KO, and rd12/rd12 mice are shown at P60 (**A-C**) and P210 (**D-F**). No differences in RPE morphology could be detected in these sections. Histopathological changes appear to be localized to photoreceptor cells in the retina. Representative images from retina 1 mm superior of the optic nerve are shown. RPE, retinal pigment epithelium; OS, outer segment; IS, inner segment; ONL, outer nuclear layer; INL, inner nuclear layer; GCL, ganglion cell layer.

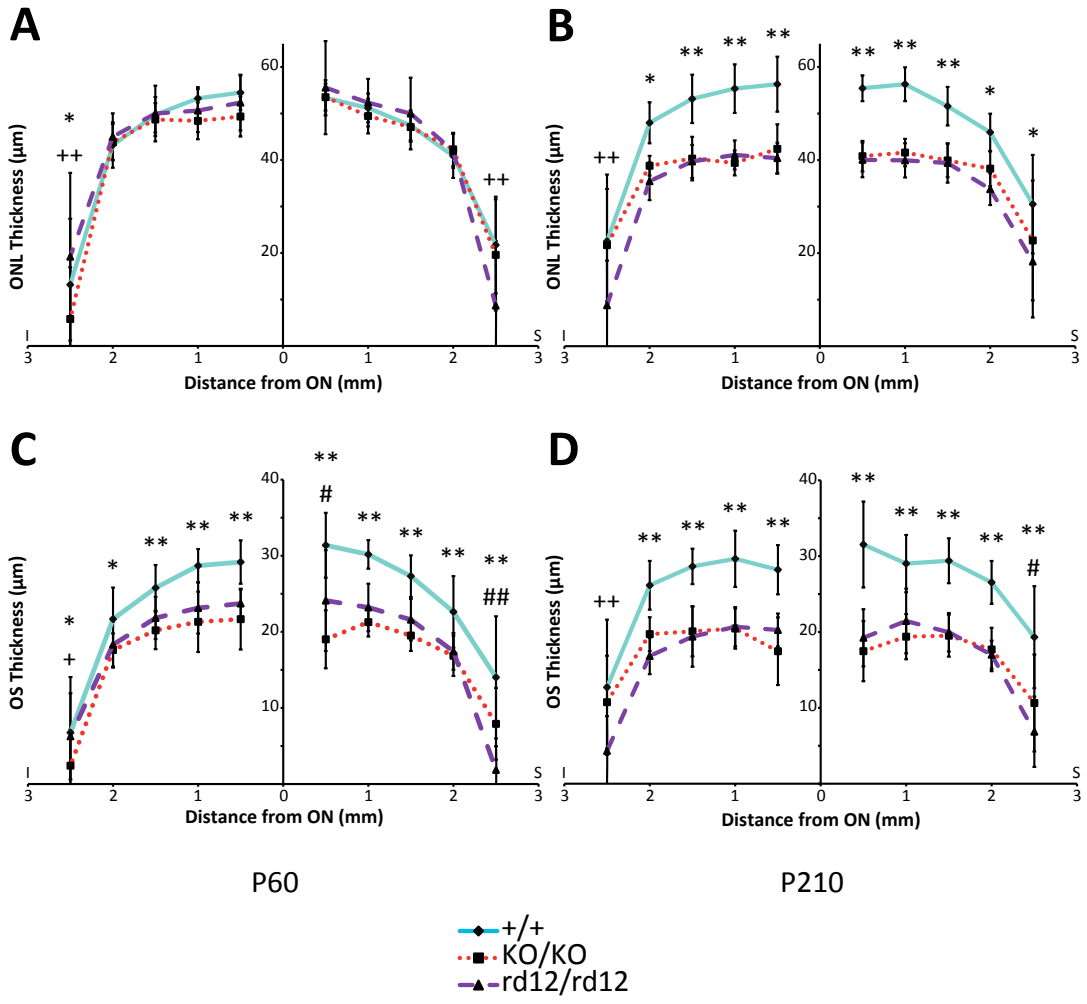

Figure 4.12. KO/KO and rd12/rd12 had similar ONL and OS thinning with age. ONL and OS thicknesses were not significantly different between KO/KO and rd12/rd12 when compared to wild type at either P60 or P210. Quantitative measurements of ONL and OS thicknesses were taken at 500 µm intervals superior and inferior of the optic nerve at P60 and P210 in +/+ (n=17 at P60, n=12 at P210, solid line), KO/KO (n=18 at P60, n=9 at P210, dotted line), and rd12/rd12 (n=7 at P60, n=18 at P210, dashed line) mice. * P <0.05, ** P <0.001 +/+ compared to rd12/rd12; # P <0.05, ## P <0.001 KO/KO compared to rd12/rd12, significance determined through two-way repeated measures ANOVA with post hoc Student-Newman-Keuls testing. Data are presented as mean ± SD.

Cones are particularly susceptible to death when *Rpe65* is mutated, so we sought to test whether cones are lost earlier in rd12/rd12 mice than in KO/KO mice (an important consideration in light of the fact the rd12 mutation seems to drive an earlier loss of visual function than the KO mutation). rd12/rd12 mice had a slight reduction in the number of cone nuclei compared to KO/KO in the superior portion of retinal cross sections at P60 (Fig. 4.13A) despite similar overall ONL thicknesses (Fig. 4.12). rd12/rd12 mice had 2.0 ± 0.8 cones per 200-μm field in the superior central portion of the retina compared to 4.6 ± 0.9 cones per field in KO/KO mice ($P = 0.04$) and 11.1 ± 1.6 cones per field in +/+ mice ($P < 0.001$) at P60. rd12/rd12 mice had 5.8 ± 1.7 cones per field in the superior peripheral portion of the retina compared to 7.6 ± 1.0 cones per field in KO/KO mice ($P = 0.04$) and 12.8 ± 2.8 cones per field in +/+ mice ($P < 0.001$) at P60. The low number of remaining cone cells compared to the relatively large number of remaining rod cells suggests that visual response in mutant mice may be primarily rod-mediated. There were no significant differences in cone nuclei number between KO/KO and rd12/rd12 mice at P210 (Fig. 4.13B).

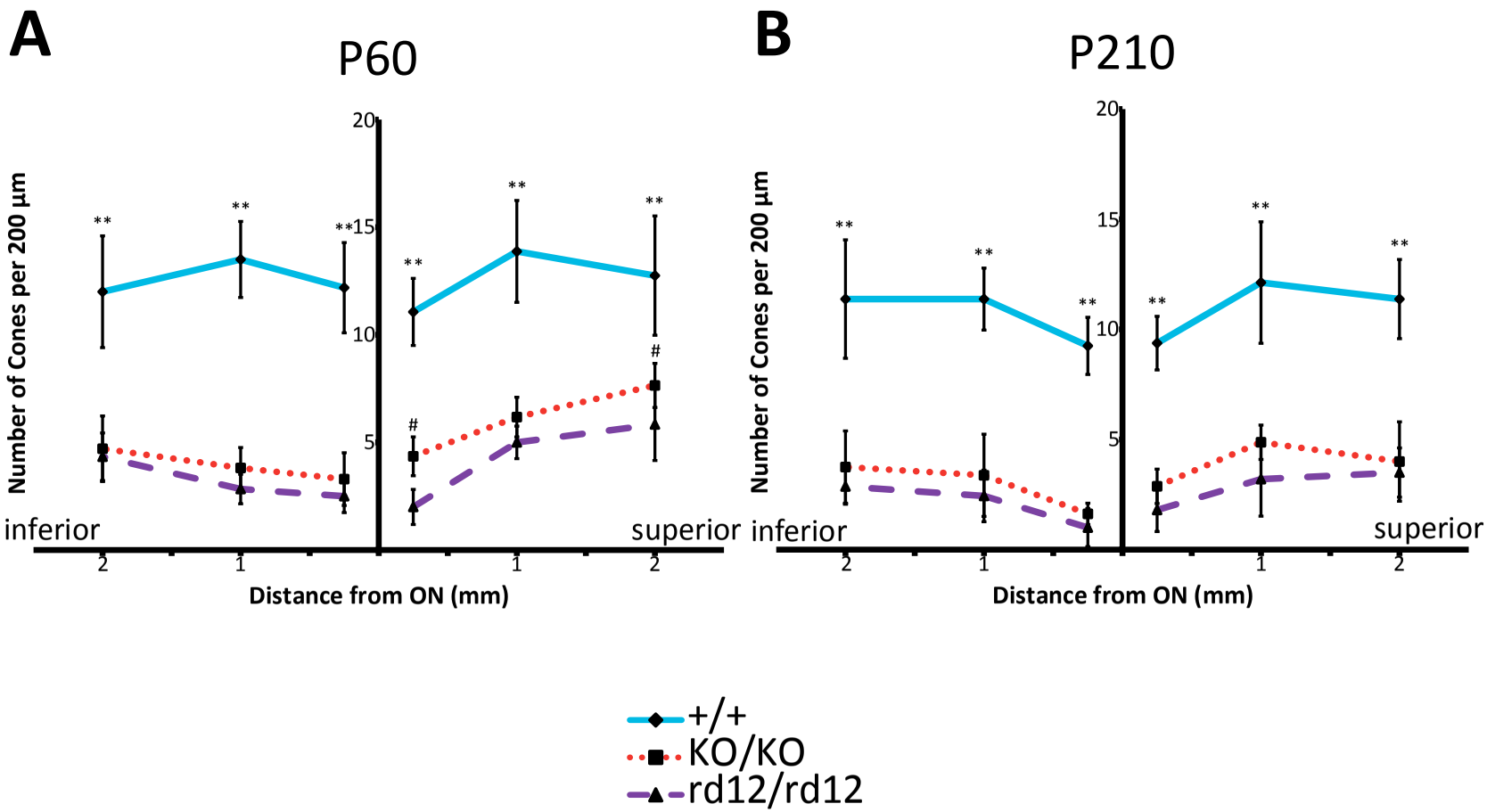
A
P60
B
P210
Number of Cones per 200 µm
20
15
10
5
**
#
inferior
superior
2
1
Distance from ON (mm)
+/+
KO/KO
rd12/rd12

Fig. 4.13—Mice with *Rpe65* mutations had large reductions in the number of cone nuclei. rd12/rd12 mice lost more cones on the superior portion of the retina than KO/KO mice at the same age. Cone nuclei were counted (Carter-Dawson and LaVail 1979) 250 μm, 1000 μm, and 2000 μm superior and inferior of the optic nerve in a 200 μm segment of the retina at P60 (**A**) and P210 (**B**). ***P* <0.001 +/+ compared to rd12/rd12, # P <0.05 KO/KO compared to rd12/rd12, significance determined through two-way repeated measures ANOVA with post hoc Student-Newman-Keuls testing. Data are presented as mean ± SD. The number of samples for each genotype is the same as in Fig. 4.12 because the same slides were analyzed for this experiment.

4.4.6—RPE65 protein levels in rd12 mice

In order to test whether a truncated 43 amino acid RPE65 peptide was being translated in rd12/rd12 mice, we raised a polyclonal antibody against those amino acids. The lower limit of detection for this antibody was found to be 2.5% wild type protein level (Fig. 4.14). RPE65 protein (Fig. 4.15C) was not detected in soluble (Fig. 4.15A) or insoluble RPE/choroid fractions (Fig. 4.15B) isolated from rd12/rd12 mice. The 44-amino acid antigen peptide (a synthetic positive control) was 4.7 kDa in size, the expected size of the truncated protein that could be produced from the nonsense mutant allele. No band of this size was detected (lower limit of detection was 2.5% wild type RPE65 protein level; Fig. 4.14) in rd12/rd12 mice (Fig. 4.15A). A single band was detected at 65 kDa in +/+ soluble protein extracts. Furthermore, preliminary data indicated there was no significant upregulation of endoplasmic reticulum (ER)-associated stress markers (*Xbp1*, *Hspa5*, *Ddit3*) in the RPE of +/+, KO/KO, or rd12/rd12 mice (data not shown).

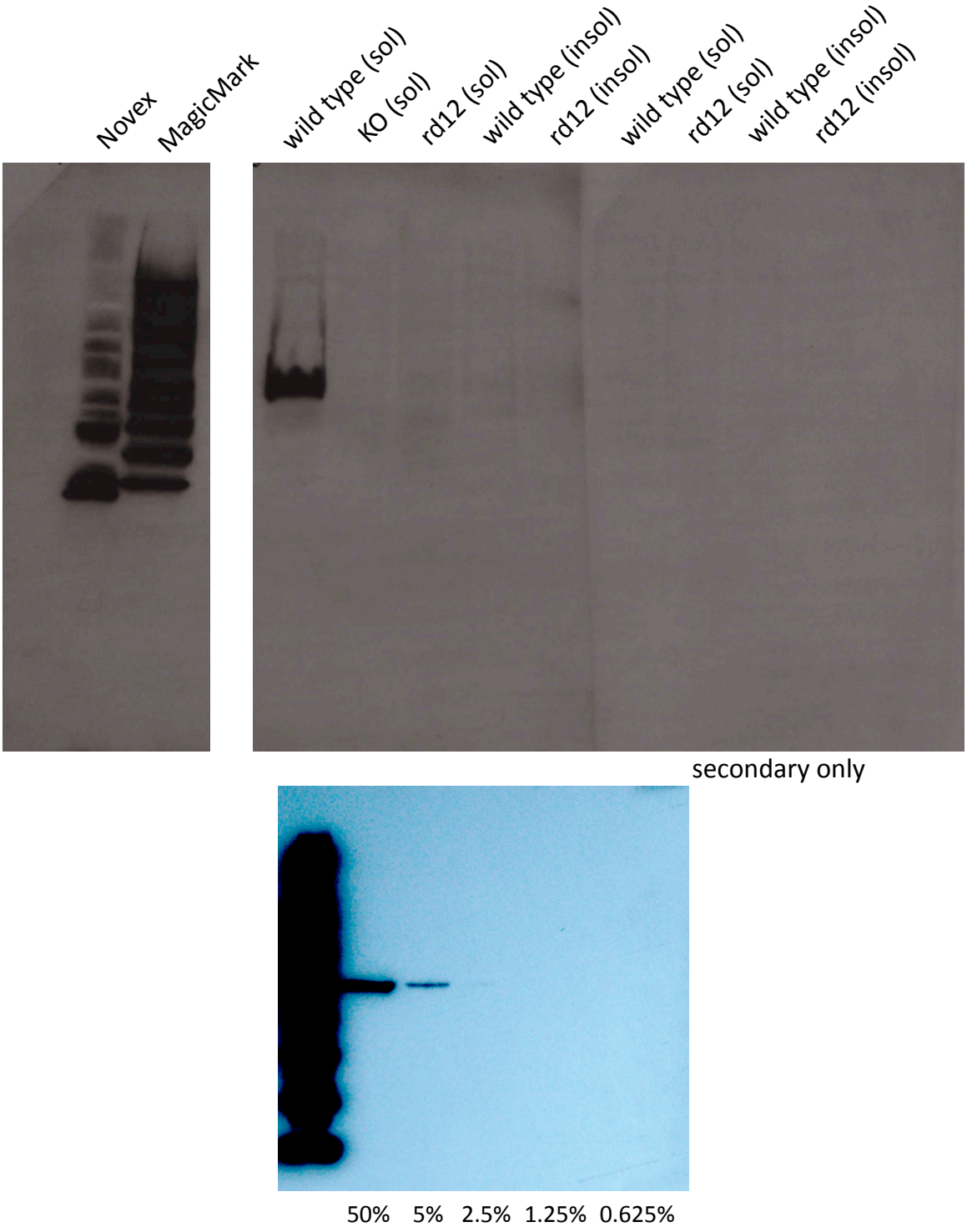

Figure 4.14. The lower limit of detection of the N-terminal specific antibody is 2.5% wild type RPE65 protein level. Serial dilutions of wild type protein were separated by SDS-PAGE and stained with the N-

terminal specific antibody used in this study. Assuming 100% wild type expression at 20 µg of RPE/choroid protein extract, as little as 2.5% that amount is detectable with the antibody.

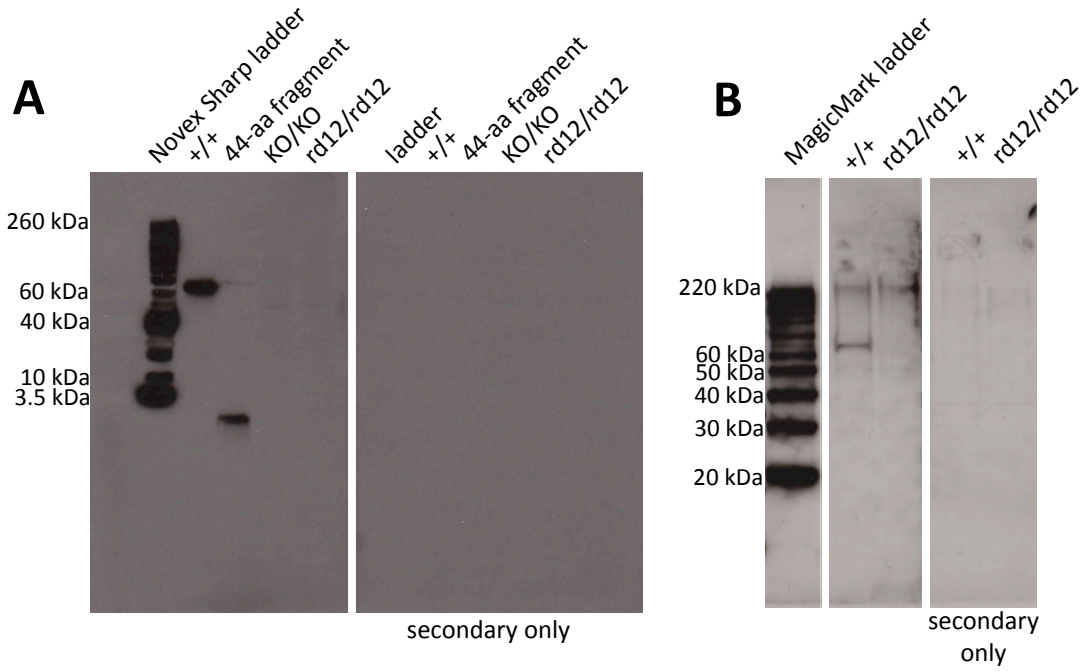

Fig. 4.15—rd12/rd12 mice did not accumulate detectable amounts of RPE65 protein. rd12/rd12 mice did not have detectable amounts of a truncated RPE65 peptide fragment in soluble or insoluble fractions. The antibody could reliably detect RPE65 peptide in amounts as low as 10.0 ng. 10 times the amount of mutant protein extract was added compared to wild type. (**A**) Immunoblotting for RPE65 protein in the soluble RPE protein fraction. 1 µg of soluble +/+ RPE/choroid protein extract, 50 ng of the 44-amino acid antigen, 10 µg of soluble KO/KO RPE/choroid protein extract, and 10 µg of soluble rd12/rd12 RPE/choroid protein extract were loaded. Secondary-only controls are shown. Antigen peptide resolved at a lower molecular weight than 3.5 kDa band on ladder for reasons that are unclear. (**B**) Immunoblotting for RPE65 protein in urea-soluble extracts with 8-day exposure to film. 20 µg protein were loaded in all lanes. Nonspecific binding of primary antibody to molecular weight ladder was noted.

4.4.7—Rpe65 mRNA level in rd12 mice

Rpe65 mRNA was present at 0.007 ± 0.003% of +/+ levels in KO/KO mice, but surprisingly (Fig. 4.16A), *Rpe65* mRNA was present at 70.9 ± 26.9% of +/+ levels in rd12/rd12 mice (Fig. 4.17A)**.** Separation of RPE cells into nuclear and cytoplasmic fractions and relative quantification of *Rpe65* mRNA (Fig. 4.17B) in +/+ and rd12/rd12 mice indicated the mutant mRNA was not sequestered in the RPE nuclei of rd12/rd12 mice. rd12/rd12 mice had 67.4 ± 18.5% of wild type *Rpe65* mRNA levels in the cytoplasm ($P = 0.003$) and 101.1 ± 43.2% wild type *Rpe65* mRNA levels in the nucleus ($P = 0.959$).

4.4.8—Splicing of mutant mRNA

All *Rpe65* exons amplified in both rd12/rd12 and +/+ mice and the levels of *Rpe65* expression for each amplicon are presented in Table 4.3. DNA sequencing of qRT-PCR products showed no cryptic splice sites, skipped exons, or other mutations with the exception of the nonsense mutation that was previously reported (Pang, Chang et al. 2005) (Fig. 4.17).

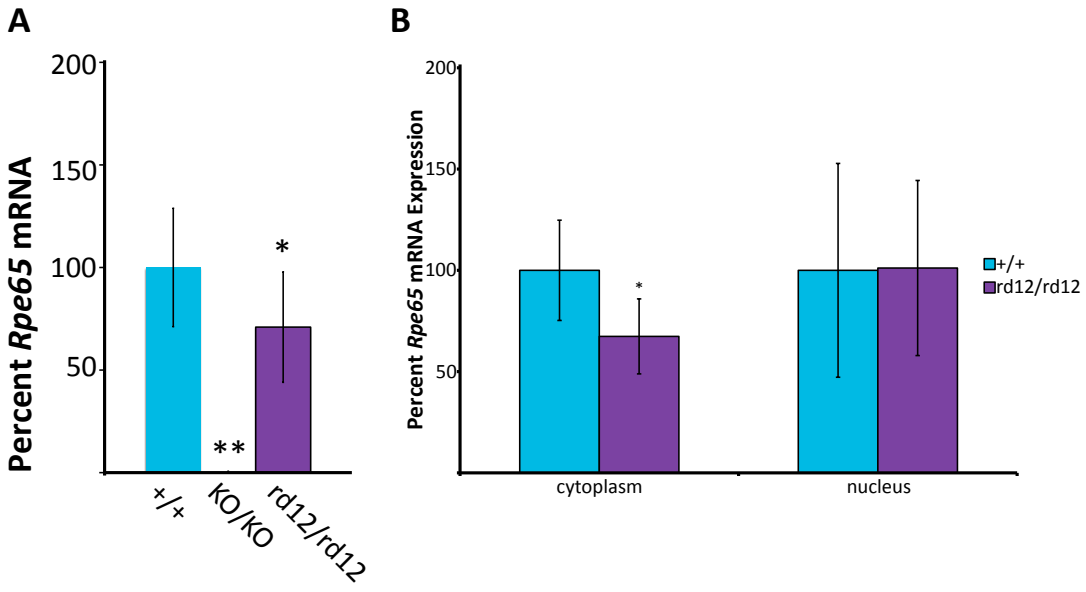

Figure 4.16. rd12 mutant *Rpe65* mRNA was exported to the cytoplasm. rd12/rd12 mice expressed appreciable *Rpe65* mRNA that was exported to the cytoplasm. (**A**) +/+, KO/KO and rd12/rd12 mice *Rpe65* whole-cell mRNA levels. (**B**) Cells from RPE/choroid from P60 +/+ and rd12/rd12 mice were fractionated into their cytoplasmic and nuclear components and the RNA extracted for qRT-PCR. *Rpe65* mRNA was present in similar levels in the nuclear fraction. * P <0.05, ** P <0.001 significance tested through student's unpaired t-test. Data are presented as mean ± SD, n = 10.

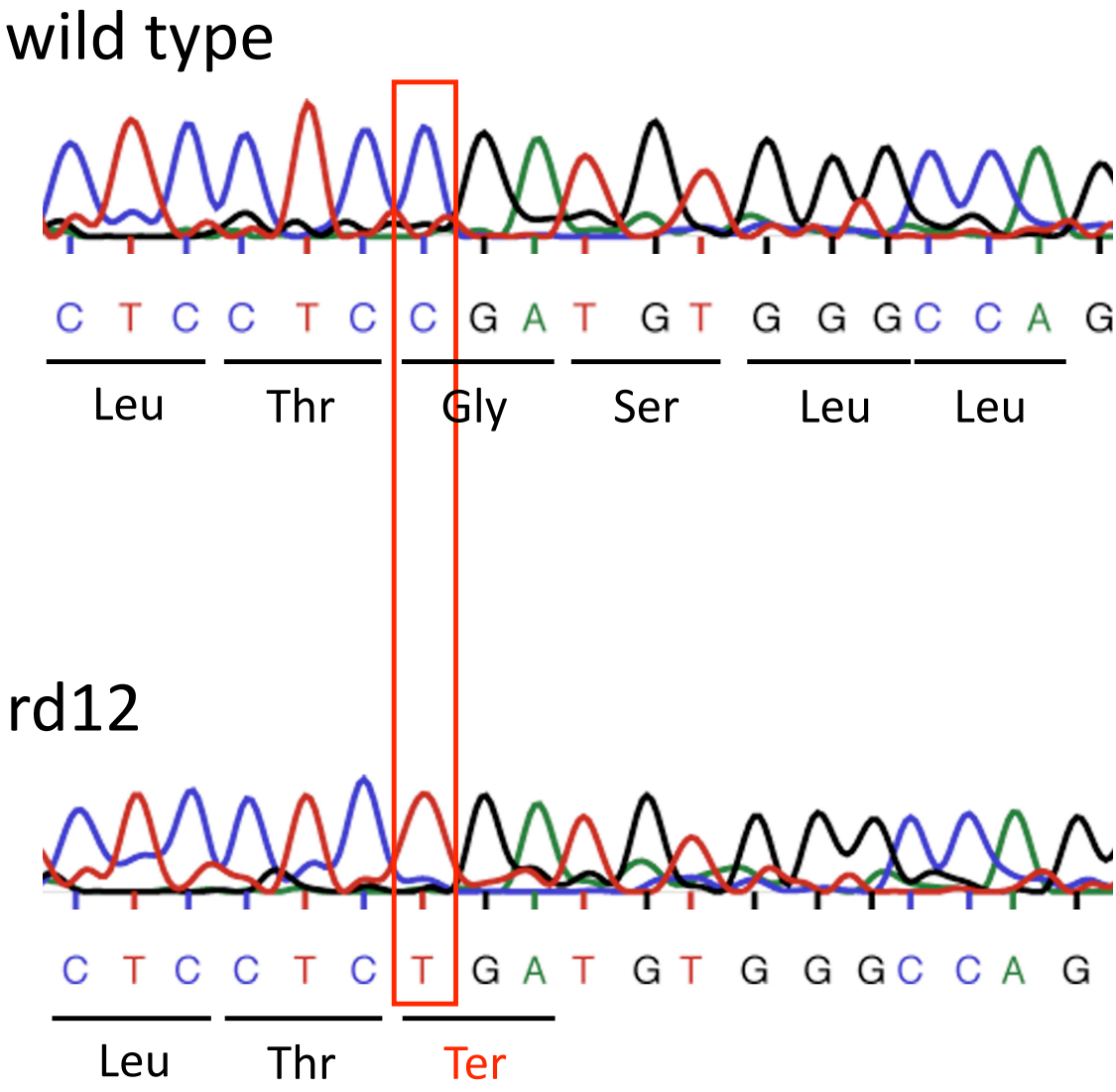

Figure 4.17—Chromatograms of DNA sequences from wild type and rd12 *Rpe65* mRNA showed a nonsense mutation in rd12/rd12 mice. DNA sequencing results from *Rpe65* mRNA isolated from +/+ and rd12/rd12 mice showed the rd12/rd12 mice had only one mutation, a C to T nucleotide substitution (c.130C>T) that created a premature termination codon (PTC). This transition mutation results in an R44X nonsense mutation.

Table 4.3. All *Rpe65* exons were successfully amplified in the mutant rd12 mRNA

Exons Amplified	Percent Wild Type Expression	P-Value (compared to +/+)
1-3	63.7 ± 17.8	0.047*
2-3	65.2 ± 9.3	0.072
3-4	69.2 ± 32.9	0.190
4-5	71.3 ± 7.0	0.070
5-6	72.5 ± 8.3	0.099
6-7	69.5 ± 9.8	0.051
7-8	65.5 ± 9.0	0.073
8-9	52.3 ± 12.0	0.018*
9-10	54.5 ± 9.0	0.014*
10-14	54.7 ± 5.6	0.024*

Exons boundaries in *Rpe65* mRNA were amplified by qRT-PCR in +/+ and rd12/rd12 samples. The percent *Rpe65* mRNA expression in +/+ mice was set to 100% and rd12/rd12 *Rpe65* mRNA expression compared. PCR products were sequenced and their sequences compared to verify there were no sequence changes except for the nonsense mutation in rd12/12rd12 mice. Asterisks next to *P*-values denote statistical significance between +/+ and rd12/rd12 *Rpe65* mRNA expression ($P < 0.05$ as tested by student's t-test).

4.4.9—Predicted Rpe65 mRNA secondary structures

RNAfold (Zuker and Stiegler 1981; McCaskill 1990; Schuster, Fontana et al. 1994) was used to predict the centroid structures that wild type, rd12, R91W, and tvrm148 alleles could adopt (Fig. 4.18). The predicted rd12 mRNA centroid structure was virtually identical to the predicted wild type mRNA structure; tvrm148 and R91W predicted mRNA structures deviated more from wild type mRNA than the rd12 structure (Fig. 4.18). Both wild type and rd12 mRNA structures were predicted to have large regions of both single-stranded RNA (ssRNA) and double-stranded RNA (dsRNA; Fig. 4.18).

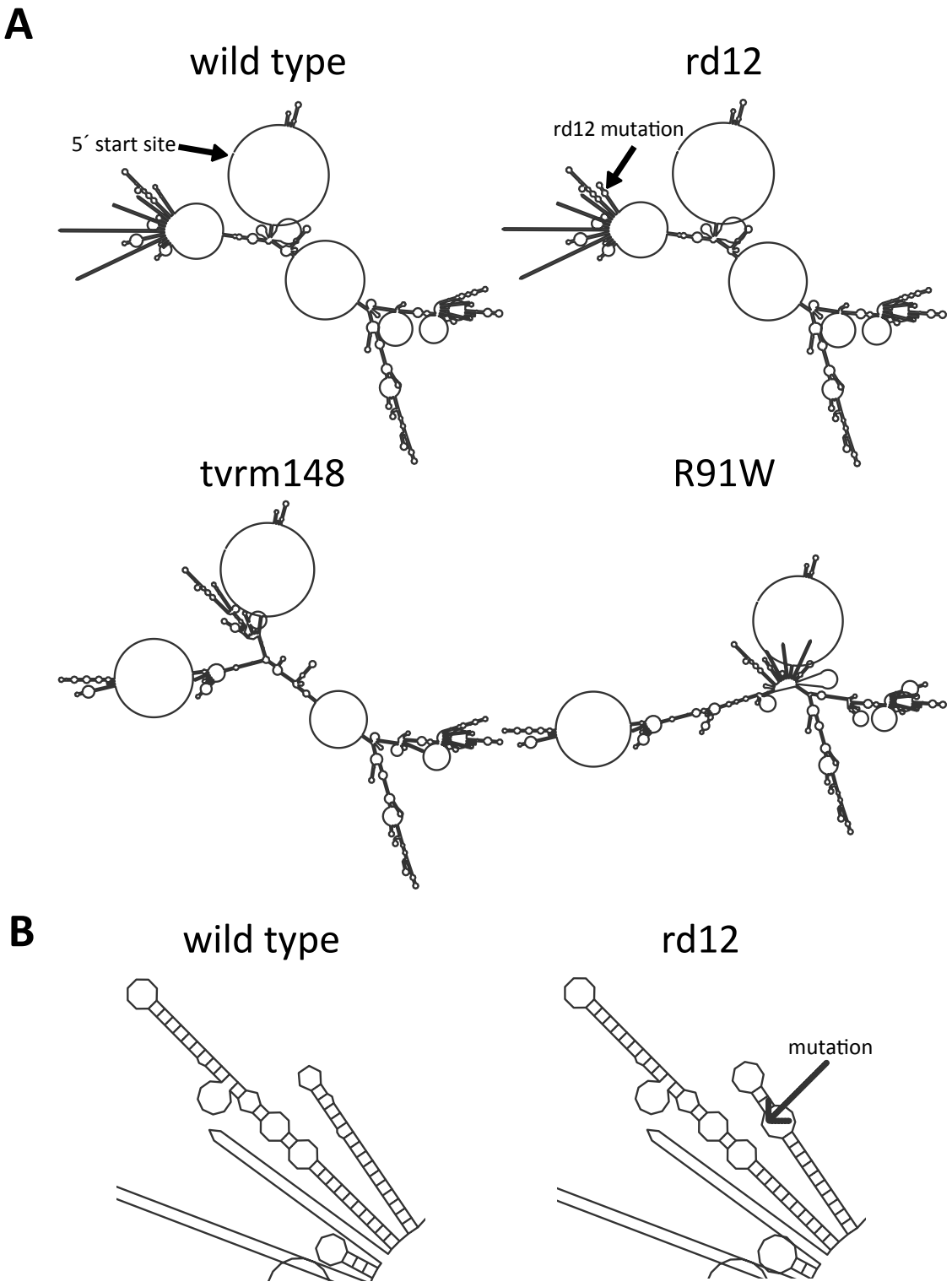
A
wild type
rd12
5´ start site
rd12 mutation
tvrm148
R91W
B
wild type
rd12
mutation

Figure 4.18. rd12 *Rpe65* mRNA had a predicted secondary structure that closely resembled wild type mRNA. Aside from an extra bubble (the size of a single base pairing) in the centroid structure (indicated by arrowhead), wild type and rd12 mRNA structures were predicted to be identical. (**A**) Predicted global centroid structures of *Rpe65* mRNA from wild type, rd12, R91W, and tvrm148 alleles. Predicted mRNA secondary structures from wild type and mutant mouse *Rpe65* alleles predicted rd12 mRNA may adopt a structure that more closely resembled wild type *Rpe65* mRNA than other *Rpe65* alleles. (**B**) Close up of global strcutres presented in **A** show the only noticeable structural abnormality in the rd12 mutant mRNA is an extra bubble in the structure resulting from a loss of base pairing.

4.4.10—FISH of Rpe65 mRNA

In situ hybridization of *Rpe65* mRNA in rd12/rd12 mice qualitatively showed the mutant mRNA localized in similar patterns compared to +/+ mRNA in the RPE cell alone (Fig. 4.19B). *Rpe65* mRNA had staining throughout the RPE cell, with mRNA being preferentially located in the basal regions of the cytoplasm in both +/+ and rd12/rd12 mice (Fig. 4.19B). KO/KO mice showed no *Rpe65* mRNA in any cell by *in situ* hybridization (Fig. 4.19A). No *Rpe65* mRNA was found in cone photoreceptors.

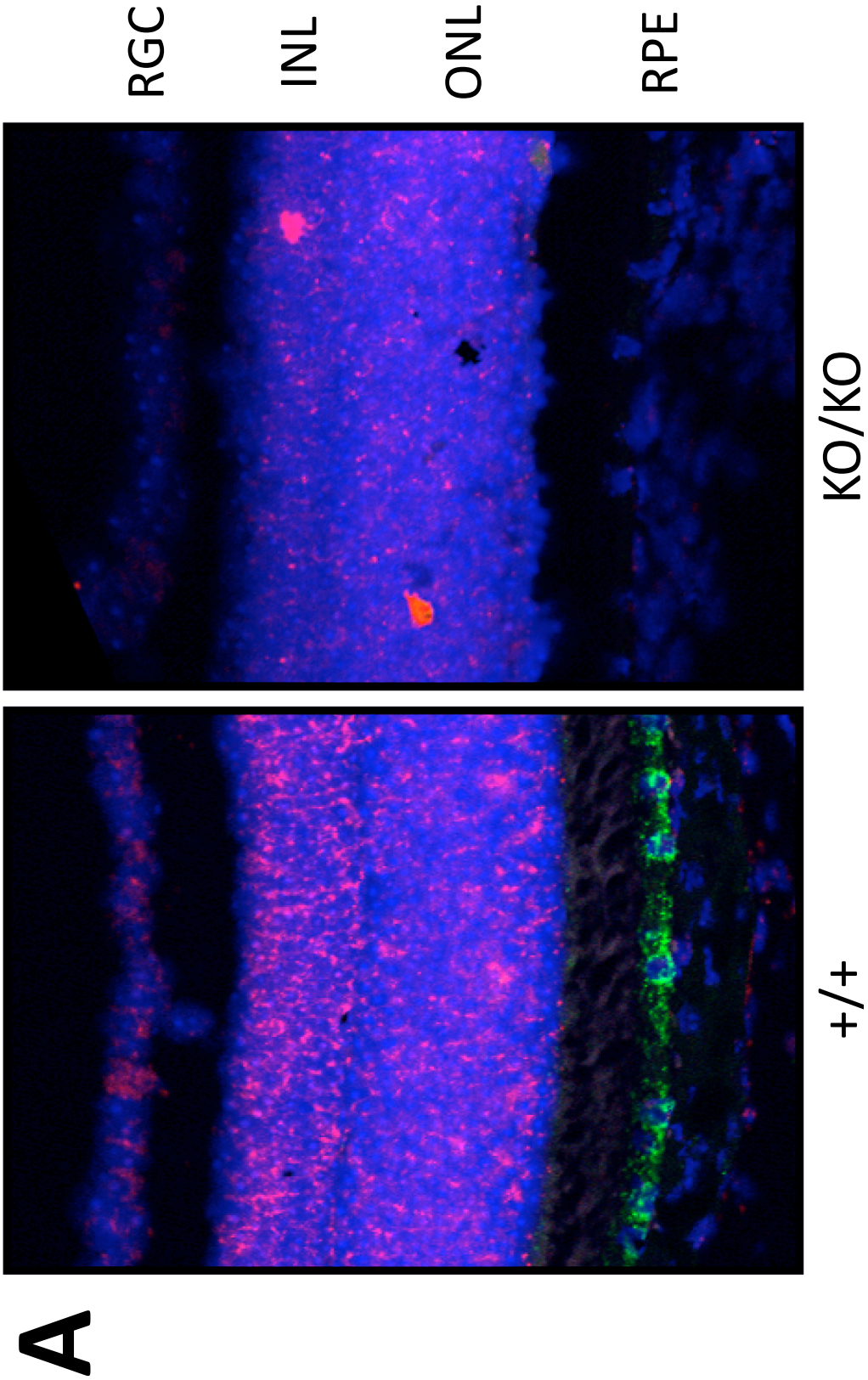
A
RGC
INL
ONL
RPE
KO/KO
+/+

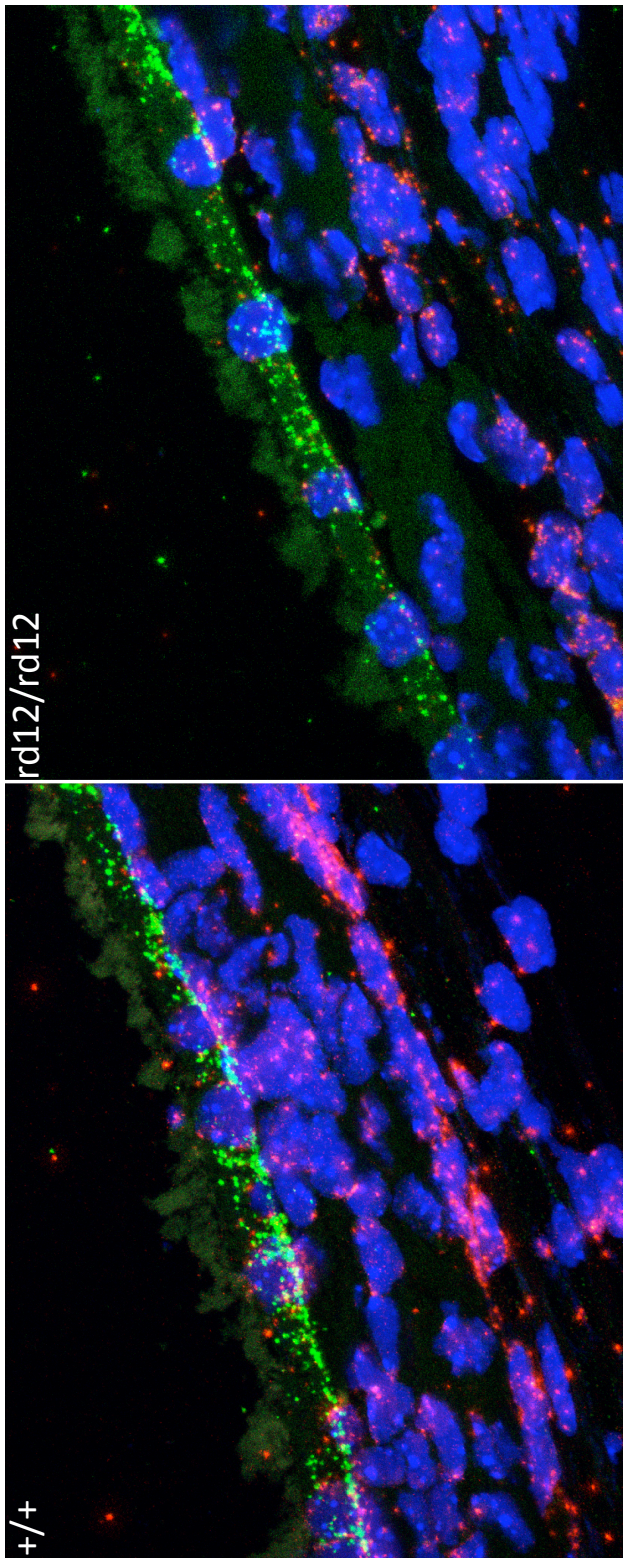

B

Figure 4.19. RNA *in situ* hybridization showed similar localization of *Rpe65* mRNA in both +/+ and rd12/rd12 RPE cells. There were no noticeable differences in the localization of rd12 mRNA with respect to wild type mRNA at P60. No mRNA was found outside of RPE cells in either wild type or mutant mice. *In situ* hybridizations for *Rpe65* (green), β-actin (red) mRNAs and nuclei (blue; YO-RPO 1 idodide) from paraffin sections taken in +/+, KO/KO and rd12/rd12 mice. (**A)** Probes for *Rpe65* mRNA were tested for specificity by staining both +/+ and KO/KO retina. It was expected that *Rpe65* mRNA would be localized to the RPE, and only the RPE, and that there would be no detectable signal in KO/KO mice. KO/KO mice had no detectable *Rpe65* mRNA hybridization, and +/+ mice had signal only in the RPE, supporting the hypothesis that these probes were specific for *Rpe65*. (**B**) *Rpe65* mRNA was found to localize throughout the cell in similar patterns +/+ and rd12/rd12 mice, with much of the signal localized around the basal regions of the RPE. Signal was readily apparent in both the nucleus and cytoplasm of the RPE.

4.4.11—Impaired association of mutant mRNA with ribosomes

We measured the ability of the mutant mRNA to be actively translated by fractionating RPE/choroid cytoplasmic extracts into ribosome-free ribonucleoprotein (mRNP)-, monoribosome-, and polyribosome-containing fractions by linear sucrose gradient centrifugation (Fig. 4.4) (Feng, Absher et al. 1997; Irier, Shaw et al. 2009; Lau, Irier et al. 2010). With the rationale and conditions that we employed (Fig. 4.20), (Feng, Absher et al. 1997; Irier, Shaw et al. 2009; Lau, Irier et al. 2010) fractions near the top of the gradient contained mRNP (fractions 1-3) and monoribosomes (where mRNAs are not actively translated; fraction 4) would be translationally dormant, whereas fractions near the bottom of the gradient contained polyribosomes (fractions 5-10) (Feng, Absher et al. 1997; Irier, Shaw et al. 2009; Lau, Irier et al. 2010). Raw cycle values from qRT-PCR of each fraction in each pool in each genotype are presented in Fig. 4.21. Raw cycle values were then used to calculate the amount of *Rpe65* mRNA in each fraction based on the standard curve in Fig. 4.3. The majority of mutant *Rpe65* mRNAs were detected within mRNP-containing fractions (fractions 1-3), while the majority of wild type *Rpe65* mRNAs were present within polyribosome-containing fractions (fractions 5-10, Fig. 22A). Upon EDTA treatment, polyribosomes were dissociated into subunits (Feng, Absher et al. 1997; Irier, Shaw et al. 2009; Lau, Irier et al. 2010), and the majority of mutant and wild type mRNAs were released into mRNP fractions (fractions 1-3, Fig. 22B). Approximately 80% of *Rpe65* mRNA is found in mRNP-containing fractions (fractions 1-3). Mutant rd12 *Rpe65* mRNA is found in amounts 174.9 ± 9.1% wild type levels in fractions 1-3 (Fig. 4.23). If rd12 mRNA were actively translating a truncated peptide, the majority of mRNA would be found in fractions 4-5 or mostly found in

fraction 4 if translation was stalled during the pioneer round of translation. Also, if mutant rd12 mRNA contained an internal ribosomal entry site (IRES), then there would be greater amounts of rd12 mRNA contained in actively-tranlsating polyribosomes found in fractions 5-10; instead, we see very little mRNA contained in those fractions in rd12/rd12 mice. These results suggest the mutant mRNA does not contain an IRES, which is consistent with the fact that protein is not detectable by antibodies specific for an epitope downstream of the mutation (Redmond, Yu et al. 1998). Also, polyribosome profiles of β-actin mRNA in wild type and rd12 mice are similar (Fig. 4.24), suggesting that the inefficient binding of mutant *Rpe65* mRNA to ribosomes in rd12 mice may not affect other mRNAs and that the profile observed for *Rpe65* mRNA in rd12 is not the result of RNA degradation in ribosome-containing fractions. As a result, it appears as if the majority of mutant rd12 mRNA is found in mRNP fractions and may not efficiently bind ribosomes for translation. It is possible that little *Rpe65* mRNA is observed in the monoribosome fraction in wild type mice because the pioneer round of translation is not a rate-limiting step in the translation of RPE65 protein, but this will need to be confirmed in future work.

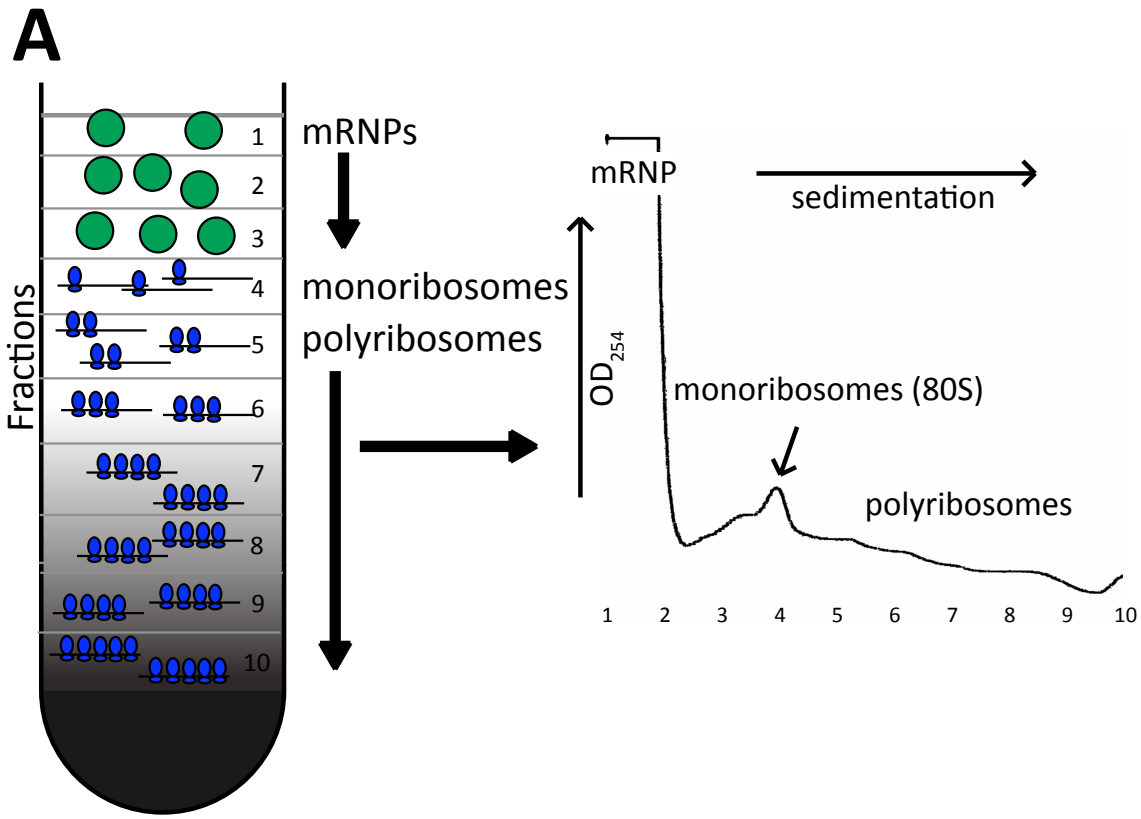
A
Fractions
1
2
3
4
5
6
7
8
9
10
mRNPs
monoribosomes
polyribosomes
mRNP
sedimentation
OD254
monoribosomes (80S)
polyribosomes
1 2 3 4 5 6 7 8 9 10

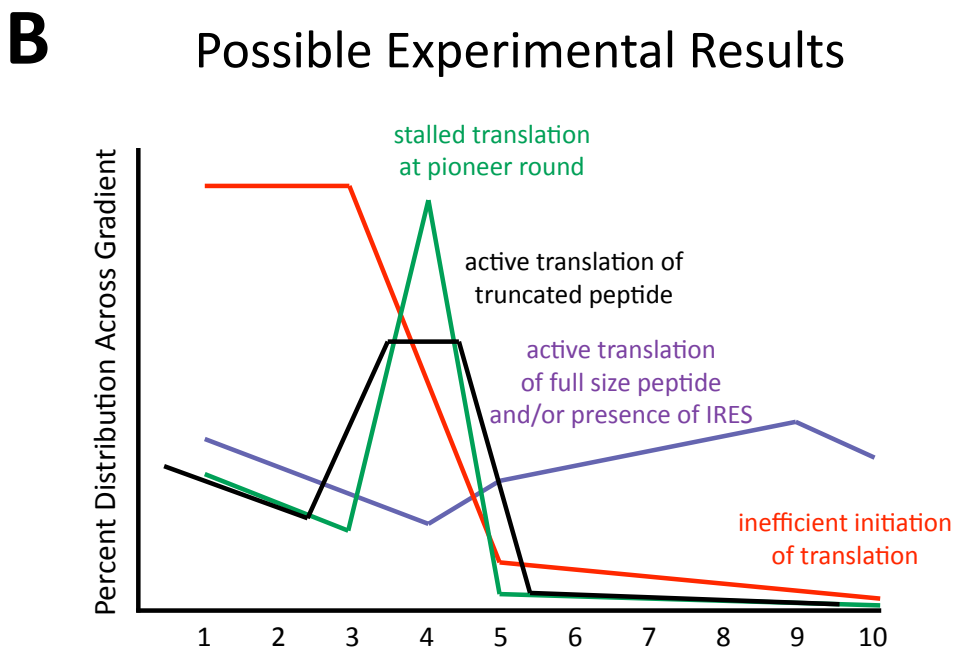
B
Possible Experimental Results
stalled translation
at pioneer round
active translation of
truncated peptide
active translation
of full size peptide
and/or presence of IRES
inefficient initiation
of translation
Percent Distribution Across Gradient
1 2 3 4 5 6 7 8 9 10

Figure 4.20—Possible outcomes of polyribosome profiling. This experimental design could determine whether the mutant rd12 *Rpe65* mRNA could be bound by ribosomes, and if so, how many ribosomes could bind. It required separation of mRNA-bound species on a linear sucrose gradient, followed by isolation of RNA and qRT-PCR of *Rpe65* mRNA from each fraction. (**A**) Sucrose gradient fractionation separated RNA binding protein (RBP)-bound RNAs into three possible species: mRNP-bound RNAs (green circles), monoribosome-bound RNAs (black lines with one blue oval), and polyribosome-bound RNAs (black lines with multiple blue ovals). The first three fractions (1-3) contained RNA species mostly bound by mRNPs, the fourth fraction (4) contained RNA species mostly bound by a single ribosome, and fractions five through ten (5-10) contained RNA species mostly bound by multiple ribosomes. The more ribosomes bound a single mRNA molecule, the further the species migrated down the gradient during centrifugation. (**B**) Because there were detectable amounts of full-size RPE65 protein from +/+ mice, it would be expected that the majority of the wild type *Rpe65* mRNA would be found in fractions 5-10 (this is in fact what was observed). There were four possible outcomes for the mutant mRNA in the cytoplasm: 1) active translation of a full size peptide (which would require ribosomes to read through the PTC, require an IRES, or other require another sequence that would allow read through or suppression of termination in the mutant mRNA); 2) inefficient initiation of translation (the mRNA would only be bound by mRNPs, which we observed in rd12/rd12 mice); 3) stalled translation (a single ribosome would stall on the PTC during the pioneer round of translation); and 4) active translation of a truncated peptide (because of the short length of the read frame in the mutant mRNA with the PTC, only one or two ribosomes would bind to the mRNA at a single time). If there were active translation of a full size RPE65 peptide, the majority of the mRNA would be found in fractions 5-10 (as was the case in +/+ mice). If there was no (or inefficient) initiation of translation, the majority of mRNA would be found in fractions 1-3 (as was the case in rd12/rd12 mice). If there was stalled translation, the majority of mRNA would be found in fraction 4, and if there was active translation of a truncated RPE65 peptide in rd12/rd12 mice, most mRNA would have been found in fractions 4-5.

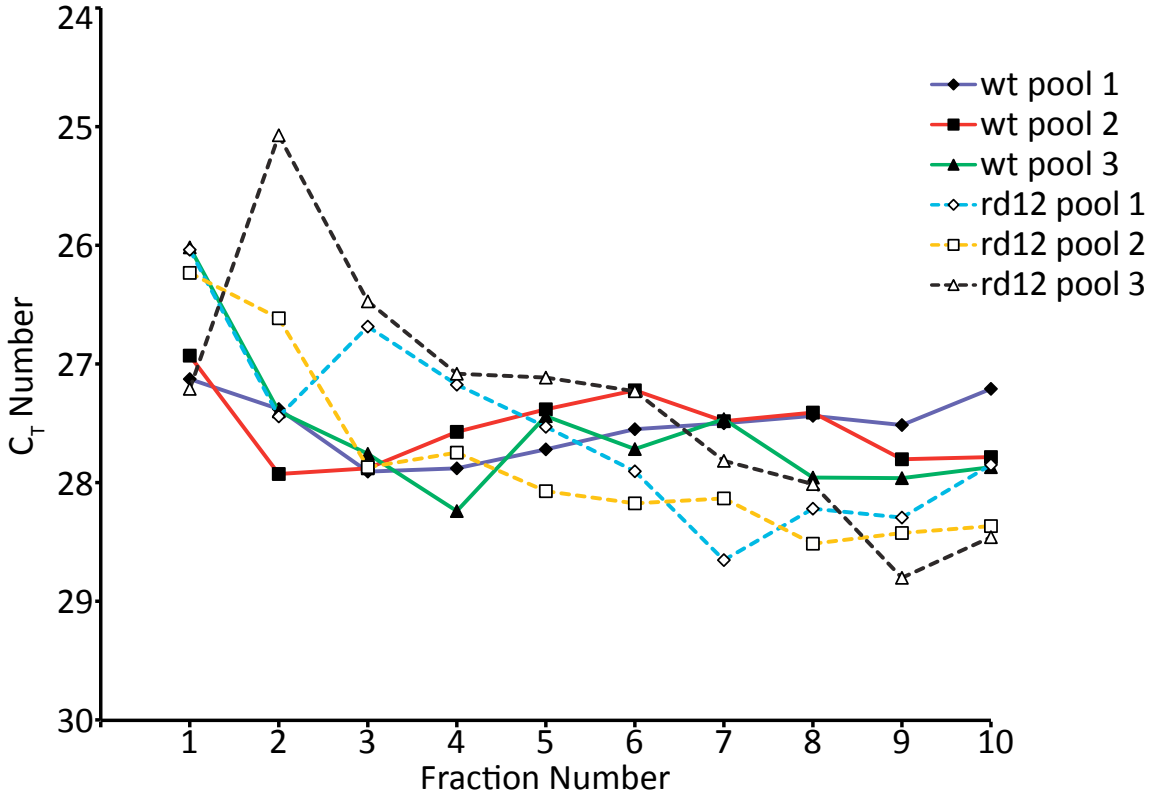

Figure 4.21—Raw cycle values from polyribosome profiling. Cycle values for each sample pool were plotted against fraction number. Please recall from the methods that multiple mice had their RPE/choroid extracts pooled together to create each sample for linear sucrose gradient fractionation and qRT-PCR. Because of this, although there are only three samples for each genotype, at least nine mice from three different litters are represented in these datasets. Cycle values were calculated based upon the point at which the amplification curve crossed threshold.

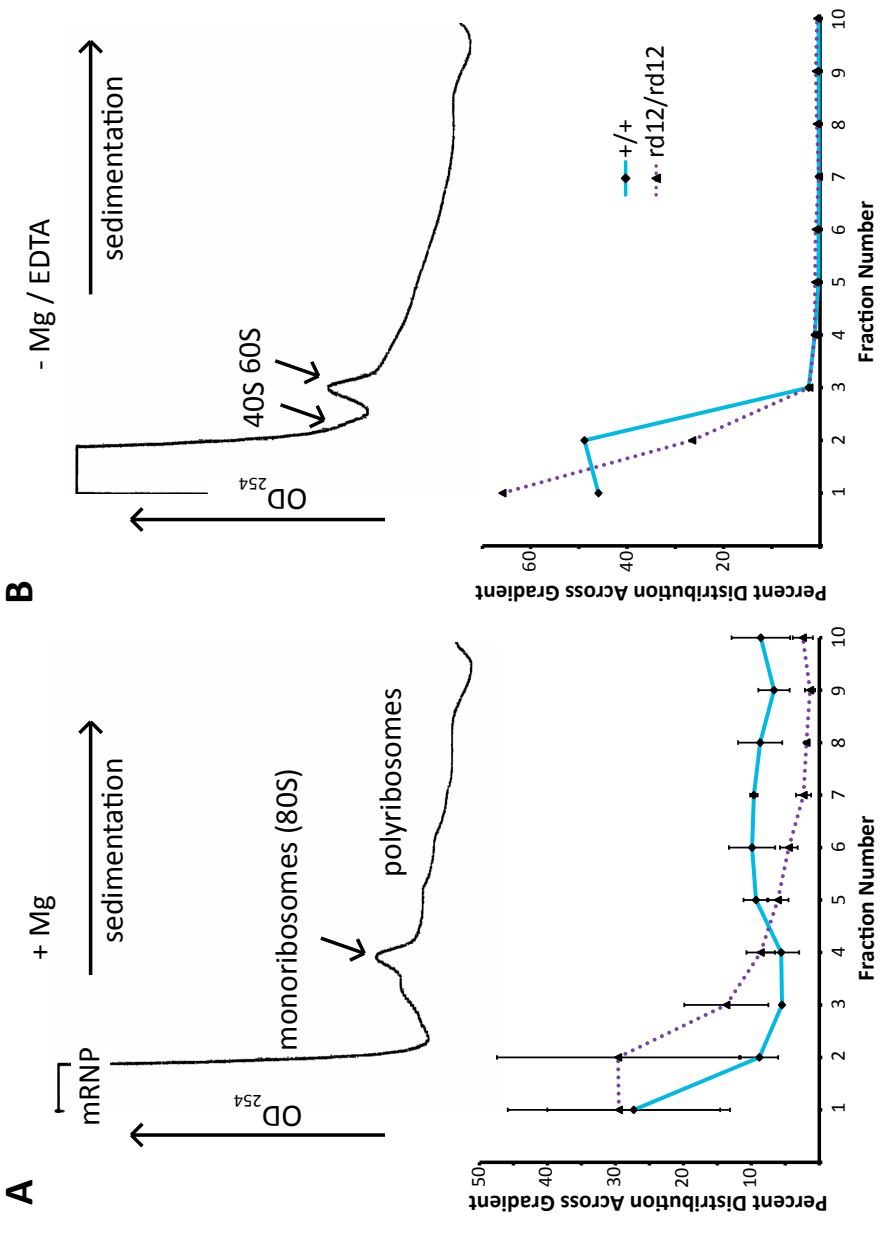
A
+ Mg
sedimentation
mRNP
monoribosomes (80S)
polyribosomes
OD254
Percent Distribution Across Gradient
Fraction Number
B
- Mg / EDTA
sedimentation
40S 60S
OD254
+/+
rd12/rd12
Percent Distribution Across Gradient
Fraction Number

Figure 4.22. rd12 *Rpe65* mRNA was mostly found in ribosome-free mRNPs. Unlike wild type mRNA, mutant rd12 mRNA was mostly contained in ribosome-free ribonucleoprotein (mRNP) fractions. (**A**) Cytoplasmic extracts of RPE/choroid were separated by linear sucrose gradient centrifugation to yield mRNP fractions (1-3), monoribosome fractions (4), and polyribosome fractions (5-10). (**B**) Mono- and polyribosomal complexes disrupted by the addition of EDTA result in all *Rpe65* mRNA being present in mRNP-containing fractions.

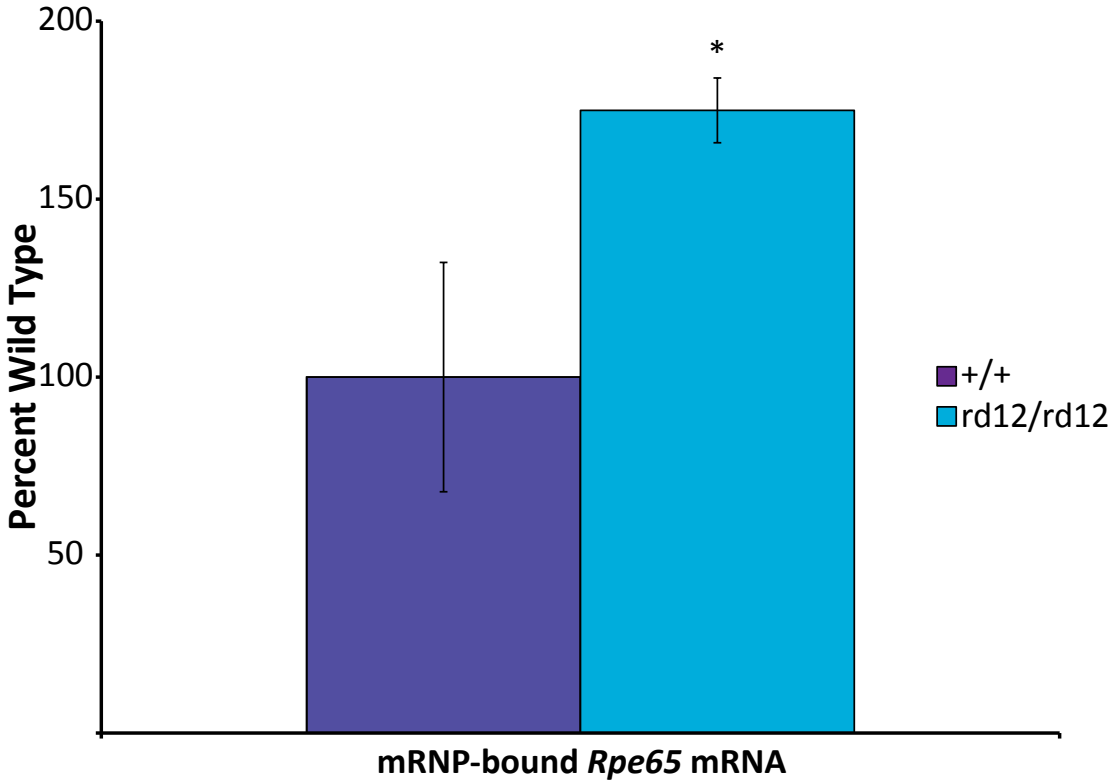

Fig. 4.23—*Rpe65* mRNA is mostly bound by mRNPs in rd12/rd12 mice. The area under the wild type and rd12 curves in fractions 1-3 in the polyribosome profiles of *Rpe65* mRNA were added together to generate the average amount of mRNA present in the mRNP fractions. Because three mRNA-bound species (mRNP-bound, monoribosome-bound, and polyribosome-bound mRNAs) are separated by linear sucrose gradient fractionation in this assay, the area under the polyribosome curves shown in Fig. 4.22 were added together for each species. Mutant mRNA was much more enriched in mRNP-containing fractions and greatly reduced in actively-translating polyribosome fractions in rd12 mice compared to wild type. There were no significant differences between wild type and rd12 mice in monoribosome-bound *Rpe65* mRNAs, which could be due to either insufficient resolution in this experiment or because the mutant mRNA is still capable of binding monoribosomes. **P* <0.05, significance tested through student's unpaired t-test. Data are presented as mean ± SD.

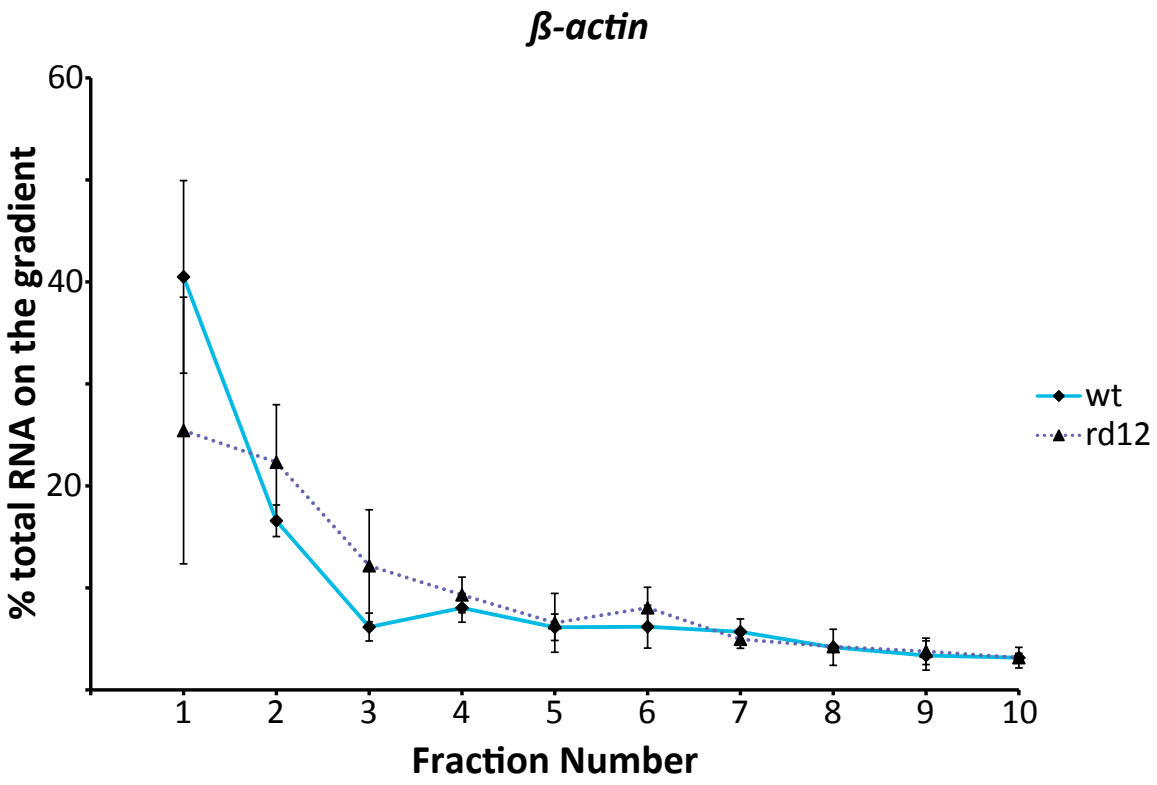

Fig. 4.24. Polyribosome profiles of β-actin are similar between wild type and rd12. Polyribosome profiles of β-actin are similar in both wild type and rd12 mice, indicating that other mRNAs are not affected by the inefficient binding of *Rpe65* mRNA to ribosomes in rd12 mice. This also suggests the lack of *Rpe65* mRNA observed in actively-translating ribsome fractions in rd12 mice is not the result of RNA degradation of samples.

4.5—DISCUSSION

Complementation tests of the rd12 allele with the KO allele showed that the two mutations did not complement, indicating that the rd12 mutation was in the *Rpe65* gene (Fig. 4.5). Also, the rd12 allele induced visual function loss in a semidominant fashion (as illustrated in the OKTs, Fig. 4.6), but in a recessive fashion as indicated by several other metrics including ERGs (Fig. 4.7-4.10), histology (Fig. 4.11), and morphometrics (Fig. 4.12-4.13). The ERG, histology, and morphometrics data are consistent with previous work with these mice (Redmond, Yu et al. 1998; Roman, Boye et al. 2007) that has been reported in the literature across multiple generations and multiple institutions, making it unlikely the semidominant effects in OKT in mice carrying the rd12 mutation are the result of epigenetic inheritance or genetic drift among colonies. Admittedly, none of these other laboratories (or our own) have specifically checked for these possibilities. Thus, the inheritance pattern in rd12/rd12 is more complex than classic autosomal recessive, and we call it semidominant. This complexity extends to the heterozygous states as well: KO/rd12 mice resembled the more severely affected rd12/rd12 mice and not KO/KO mice with respect to visual acuity (Figs. 4.5, 4.6), scotopic a-wave amplitudes (Fig. 4.8A), and scotopic b-wave amplitudes (Fig. 4.8B). A single copy of the rd12 allele was sufficient to drive visual deficits in rd12/+ mice as measured by visual acuity (Fig. 4.6), scotopic a-wave amplitudes (Fig. 4.9A), SOPA (Fig. 4.9C), and scotopic b-wave amplitudes (Fig. 4.9B), although in all these metrics the effect size was small. We speculate that it is possible the rd12/+ mice have some small degree of cone nuclei loss that could account for the trending loss of ERG amplitudes.

The rd12 mutation abolished 11-*cis*-ROL product formation, and resulted in retinyl palmitate (substrate) buildup, as is expected when a mutation causes a loss of retinoid isomerase activity (a loss of function). However, rd12 also exerts an additional semidominant action that harms visual function in a way that may not be directly related to the visual cycle. KO/KO and rd12/rd12 mice have both been reported to be null for 11-*cis*-retinal generation (Redmond, Yu et al. 1998; Pang, Chang et al. 2005), and modeling of phototransduction kinetics from scotopic a-wave recordings indicated rod photoreceptors in rd12/+ mice had similar maximal a-wave responses (Fig. 4.10A), time delays between flash stimuli and photoreceptor response (Fig. 4.10B), and time constants (a measure of rod sensitivity (Akula, Hansen et al. 2007; Akula, Mocko et al. 2007; Weymouth and Vingrys 2008); Fig. 4.10C) when compared to KO/+ mice, suggesting that the phototransduction cascade in rd12/+ mice was normal. Because KO/KO mice possessed no measurable amounts of 11-*cis*-retinal and rd12/+ mice were capable of regenerating functional rhodopsin to the same level as KO/+ mice, these data suggested the separate semidominant action by the rd12 allele might be unrelated to retinoid processing.

Both KO/KO and rd12/rd12 mice have been previously reported to have almost completely intact retina architectures (with a slowly progressive degeneration starting in the photoreceptors) despite severe visual function loss (Redmond, Yu et al. 1998; Pang, Chang et al. 2005), and our findings were consistent with these previous results (Fig. 4.11). Quantitative measurements of ONL and OS thicknesses in KO/KO and rd12/rd12 mice indicated rd12/rd12 mice did not experience an earlier retina thinning than KO/KO mice (Fig. 4.12). Although the overall degrees of retina morphology changes were

comparable in KO/KO and rd12/rd12 mice, rd12/rd12 mice lost cone photoreceptor nuclei earlier than KO/KO mice on the superior side of the retina (Fig. 4.13A). This finding is interesting because the mouse retina is populated almost exclusively by M-cone photoreceptors on the superior side of the retina at the ages that we looked (Szél, Röhlich et al. 1992). S-cones die at earlier ages in both KO/KO and rd12/rd12 mice (Znoiko, Rohrer et al. 2005; Pang, Boye et al. 2010), and this cone cell death is mediated by M- and S-cone opsin mislocalization in the absence of 11-*cis*-RAL (Rohrer, Lohr et al. 2005). S-cone death occurs earlier than M-cone death because of impaired degradation of mislocalized S-opsin (Zhang, Zhang et al. 2011). By P60, most S-cones were gone from the retina of RPE65-deficient mice (Zhang, Zhang et al. 2011), so it is possible earlier cone cell death in rd12/rd12 mice may not be limited only to M-cones. As cone photoreceptors in mouse may have RPE65 protein in the OS (Tang, Buhusi et al. 2011), we speculated that possible expression of the rd12 allele in the M-cone may directly exert a slightly toxic action on cone photoreceptors.

We tested this hypothesis by looking for *Rpe65* mRNA by FISH (Fig. 4.19). We only detected it in RPE cells. There was no signal in cones, rods, or other cells in the neural retina. It is possible that *Rpe65* mRNA is expressed at much lower levels in cones and that this level might be below our limit of detection. Nonetheless, our evidence does not support this hypothesis. Thus, the presence of RPE65 protein in the cones that has been reported in the literature (Tang, Buhusi et al. 2011) does not appear to be result of protein translation in the cone cell, but rather possibly the result of a transport of RPE65 protein from the RPE to the cone OS. It is therefore still a possibility that a truncated

RPE65 protein in rd12/rd12 mice could be transported across in the interphotoreceptor space to cones where they could induce cell stress there.

Previous speculation about the lack of RPE65 protein staining in the RPE suggested that the nonsense rd12 mutation might be subject to degradation by NMD (Pang, Chang et al. 2005). This is logical, given that many RNA surveillance pathways, such as Staufen-mediated mRNA decay (SMD) (Gong, Kim et al. 2009), NMD (Gong, Kim et al. 2009; Schweingruber, Rufener et al. 2013), no-go mRNA decay (Schweingruber, Rufener et al. 2013), and nonsense-associated altered splicing (NAS) (Vuoristo, Pappas et al. 2004; Laimer, Onder et al. 2008) exist in the cell to prevent the potential production of a truncated protein with a deleterious effect by a PTC-containing mRNA (Schweingruber, Rufener et al. 2013). Unfortunately, this speculation was based upon immunocytochemistry data that made use of an antibody that recognized an epitope (an amino acid sequence commonly abbreviated as PETLET, amino acids 157-162 in mouse, bovine, and human RPE65 protein sequence) downstream of the nonsense mutation (Pang, Chang et al. 2005); even if a truncated protein was produced in rd12/rd12 mice, this antibody (Pang, Chang et al. 2005) would not be capable of detecting it. However, the absence of anti-PETLET immunoreactivity importantly shows there is no IRES following the rd12 stop codon (at position 44) in the *Rpe65* mRNA (Pang, Chang et al. 2005). Significantly, a truncated peptide fragment was not detected in our study with the use of an N-terminal specific RPE65 antibody (Fig. 4.15B, C) despite abundant *Rpe65* mRNA being present in rd12/rd12 mice (Fig. 4.17A).

This study demonstrated that the mutant rd12 mRNA is transcribed (Fig. 4.17A), spliced (Table 4.3), exported from the nucleus to the cytoplasm (Fig. 4.17B), and

trafficked within the cell normally (Fig. 4.19), despite having a 29% reduction in mRNA (it is unclear at this time whether this reduction could be the cause or effect of some sort of toxic response). DNA sequencing of PCR products amplified from mutant mRNA (Fig. 4.16) indicated there are no cryptic splice sites, skipped exons, included introns, or any sequence change whatsoever in the mutant mRNA besides the nonsense mutation previously reported (Pang, Chang et al. 2005). The mutant mRNA is still capable of being trafficked normally, because the localization of the mutant mRNA in the cytoplasm does not differ from wild type (Fig. 4.19) and because there is a virtually identical amount of *Rpe65* mRNA in the nuclei of rd12/rd12 RPE cells compared to +/+ RPE nuclei (Fig. 4.17). Because there is no appreciable staining of mRNA in extracellular spaces in either +/+ or rd12/rd12 mice, it is also reasonable to conclude that the mutant mRNA is not exerting a semidominant effect on visual function because of action in the extracellular space. Once at the ribosomes, the mRNA does not efficiently engage with actively translating polyribosomes (Fig. 4.23). Even if the mutant mRNA did engage with actively-translating polyribosomes, we would only expect one or two ribosomes to be able to translate from a single mRNA at once because of the small open reading frame that is created by the nonsense mutation. Because RNA surveillance pathways require nonsense mutation-containing mRNAs to directly interact with ribosomes and stall at the premature stop codon, the sequestration of the mutant mRNA in rd12 mice from ribosomes (Fig. 4.22A) (Imamachi, Tani et al. 2012) may suggest a possibility for the mutant mRNA to evade NMD by evading the pioneer round of translation. It is possible that the 30% reduction in *Rpe65* mRNA in rd12/rd12 mice could be the result of some interaction of mRNA with monoribosomes, which could then allow the mRNA to be

recognized and degraded by NMD at a low level (explaining why 70% is still present in steady-state conditions). This hypothesis is consistent with previous work attempting to restore visual function in rd12 mice by treating them with gentamicin and G418, which were both being tested for their abilities to allow ribosomes to read through PTCs and rescue protein production (Guerin, Gregory-Evans et al. 2008). Although S334ter-4 rats (rats with a nonsense mutation in the rhodopsin gene and an unfavorable PTC for treatment, UAA) were amenable to treatment with both gentamicin and G418, rd12 mice (with a favorable PTC for treatment, UGA) were resistant to treatment (Guerin, Gregory-Evans et al. 2008). We speculate that the reason the rd12 mutant was resistant to gentamicin and G418 treatment was because the mRNA never reached the point where it bound to ribosomes for readthrough of the PTC. We speculate mRNP sequestration of rd12 *Rpe65* mRNA forms the foundation for the semidominant effects on visual function exerted by the rd12 allele (Fig. 4.25). Our polyribosome profiling data are consistent with this interpretation.

Defects in intracellular trafficking and posttranscriptional regulation of various mRNAs have been reported in the eye previously. Deficits in the Tudor Domain Containing 7 (TDRD7) protein are associated with cataract formation in humans and mouse (Lachke, Alkuraya et al. 2011). TDRD7 is a critical component of RNA granules in the lens and may play a role in assisting in the trafficking and storage of target mRNAs encoding critical proteins necessary for lens health (Lachke and Maas 2011). Such a mechanism may not be related to the semidominant pathology induced by the rd12 allele because intracellular transport of the mRNA does not appear to be affected, but there is

precedent in the vision research literature for posttranscriptional mRNA dysregulation as playing a role in human visual dysfunction.

Two other mechanisms might be at play with respect to the rd12 allele. Fragile X-associated tremor ataxia syndrome (FXTAS) (Li and Jin 2012), a gain-of-function RNA-mediated disorder, has been shown to be mediated by an *FMR1* transcript containing a poly-CAG nucleotide expansion (Wojciechowska and Krzyzosiak 2011) present in patients with the fragile X syndrome permutation (Hagerman, Au et al. 2011; Kiliszek, Kierzek et al. 2011). These toxic *FMR1* transcripts can be found in nuclear inclusion bodies; the repeat expansion is able to sequester RNA-binding proteins in the nucleus (Wojciechowska and Krzyzosiak 2011), and this sequestration reduces the pool of splicing factors needed for appropriate splicing of other transcripts (Wojciechowska and Krzyzosiak 2011), leading to the semidominantly inherited negative effects seen in FXTAS patients. By analogy, we wonder if it is possible that the mutant rd12 mRNA could exert its effects through sequestration of RNA binding proteins in the cytoplasm. To the best of our knowledge, only one such case of this mechanism has been reported in the literature. One human *FMR1* mutation, the FRMP^{I304N} mutation, exibits abnormal sequestration of *FMR1* mRNA on mRNPs and is associated with an unusually severe fragile X syndrome phenotype in humans because of reasons that are not clear at this time (Feng, Absher et al. 1997). Attempts to recapitulate this phenotype with this particular mutation in mouse have been unsuccessful, and the exact mechanism-of-action for this phenomenon is not currently understood (Zang, Nosyreva et al. 2009).

Another possible mechanism for the semidominantly-inheriting negative effects seen in mice carrying the rd12 mutation is activation of an innate immune response by

RNA sensors within the RPE. Recent work with *Alu* RNA in human RPE (Kaneko, Dridi et al. 2011; Dridi, Hirano et al. 2012; Tarallo, Hirano et al. 2012) cells indicates *Alu* RNA can induce an innate immune response through activation of the inflammasome via MyD88 (Tarallo, Hirano et al. 2012). Although *Alu* RNA was found to induce an innate immune response through MyD88 in a toll-like receptor (TLR)-independent fashion (Tarallo, Hirano et al. 2012), it is possible that the mutant *Rpe65* mRNA could be recognized by dsRNA and ssRNA sensors TLR3 and TLR7 (Li, Thiele et al. 2009), respectively. Future work could involve breeding rd12/rd12 mice to *MyD88*-, *TLR*, *Nlrp3*-, and *Ifnar*-deficient mice to test for an expected slower loss of visual acuity as in the KO/KO mouse, as the toxic responses of the rd12 mouse would be interrupted by eliminating the mediating inflammasome or interferon pathways.

At the time the rd12 mouse was identified, the R44X mutation had yet to be identified in humans. Recently, the nonsense R44X mutation was identified in humans (refSNP cluster report: rs368088025). Since then, both KO and rd12 mice have been used to develop gene therapy treatments for LCA2 patients (Pang, Boye et al. 2010), and some of these treatments have since moved to clinical trials (Bainbridge, Smith et al. 2008; Cideciyan, Aleman et al. 2008; Hauswirth, Aleman et al. 2008; Maguire, Simonelli et al. 2008), where they have been shown to be both safe and effective up to three years post-treatment (Cideciyan, Hauswirth et al. 2009; Simonelli, Maguire et al. 2010; Jacobson, Cideciyan et al. 2012; Testa, Maguire et al. 2013) despite continuing retinal degeneration (Cideciyan, Jacobson et al. 2013). The work presented in this study might suggest the parents and presumably unaffected family members of LCA2 patients who are known to carry a single copy of the $RPE65^{R44X}$ mutation may need to be monitored for

abnormalities in visual function. The identification of the human R44X mutation makes further study of the rd12 mouse an attractive prospect for the study of LCA2 in a laboratory setting. The rd12/rd12 and rd12/+ mice are models that offer a rare opportunity for future research into RNA-mediated visual deficits, and the implications of future work on the mechanism-of-action of the rd12 allele may have direct impacts on patients seen in the clinic.

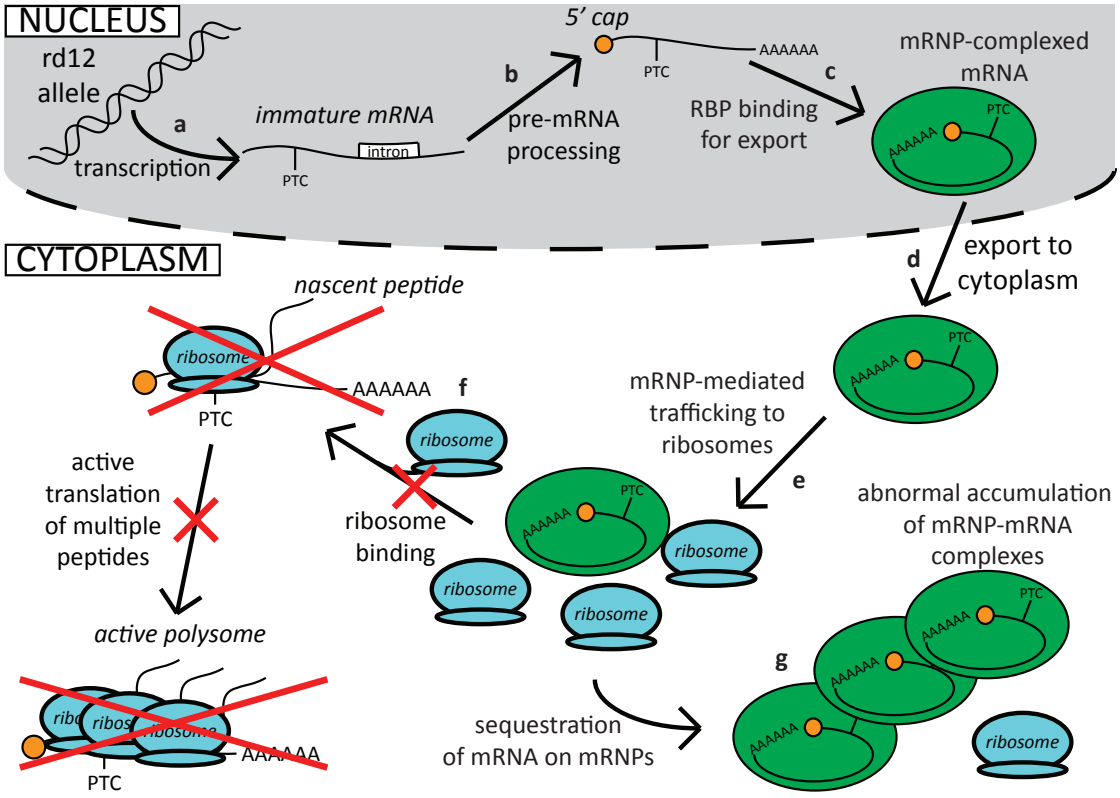

Figure 4.25. Proposed model for the foundation of the negative semidominant effects exerted by the rd12 allele on visual function. The rd12 allele is (**a**) transcribed, (**b**) spliced, (**c**) processed, and (**d**) exported from the nucleus to the cytoplasm like the wild type allele. Once in the cytoplasm, the mutant mRNA is (**e**) trafficked to ribosomes much like the wild type mRNA. Unlike the wild type mRNA, though, the mutant mRNA (**f**) becomes sequestered on mRNPs and are unable to bind to ribosomes for the first round (often called the pioneer round) of translation when nonsense RNA surveillance pathways could recognize the rd12 mRNA and degrade it. Consequently, (**g**) the mutant mRNA-mRNP complexes accumulate and form the foundation for currently unknown downstream mechanisms that cause visual dysfunction in a semidominantly inheriting fashion.

Key points presented in this section:

1. The ERG and OKT are not equivalent forms of measurement. It was expected that ERG and OKT measurements would parallel each other during visual function loss in KO/KO and rd12/rd12 mice. tvrm148/tvrm148 and KO/KO mice lost ERG and OKT measurements in much the same fashion (please refer to **Chapter III**); rd12/rd12 mice lost ERG amplitudes at a slightly faster rate than KO/KO mice but lost OKT response at a much faster rate than KO/KO mice. The data in this Chapter suggest that the OKT may be a much more sensitive form of measurement for mouse strains that are considered to be mostly blind by ERG measurements. Because of the differences in the visual components measured, OKT and ERG measurements should be considered complementary to one another and should both be done when measuring visual responses in mouse.
2. The rd12 mutation inherits and causes visual acuity loss in a semidominant fashion, a novel finding that has not been previously reported. Other effects of the mutation (e.g., most ERG responses, morphology) appear to occur in a recessive fashion, and these findings are consistent with previous reports concerning the rd12 mouse.
3. The rd12 mutant allele does not produce a protein fragment that was present at levels detectable by the antibody used in this study.
4. The rd12 allele produces mRNA that is present at 70% the level found in wild type mice.
5. The mutant *Rpe65* mRNA produced by the rd12 allele is properly spliced and contains no mutations except for the rd12 mutation.

6. The mutant mRNA produced by the rd12 allele is predicted to have a secondary structure that is virtually identical to wild type *Rpe65* mRNA.
7. The rd12 mutant mRNA localizes within the RPE cell in a pattern similar to wild type mRNA.
8. The rd12 mutant mRNA is not efficiently bound by ribosomes for translation. Furthermore, the data do not support the presence of an IRES in the rd12 mutant *Rpe65* mRNA.
9. The rd12 mutation has been identified in humans. It is possible patients with two copies of the $RPE65^{R44X}$ gene mutation may have a more aggressive form of LCA2 and that patients with one copy of the mutation may have a slow progressive visual loss.

V: Discussion and future directions

Key questions to be addressed in this section:

1. What are the novel findings with the tvrm148 mutation?
2. What are the novel findings with the rd12 mutation?
3. What future directions can I take with the research findings from this study?
4. What is the significance of this work with respect to patients in the clinic?

5.1—SUMMARY OF NOVEL FINDINGS

5.1.1—Novel tvrm148 findings

A complementation test of the tvrm148 and KO alleles showed the two alleles did not complement, proving they are in the same locus (Wright, Chrenek et al. 2013). The phenotype of the tvrm148 mouse is similar to the KO mouse. In terms of visual phenotype as measured by OKT, tvrm148 and KO mice both have a progressive loss of visual function from P30 through P210 (Wright, Chrenek et al. 2013) and have a roughly comparable rate of visual function loss (despite some small, but statistically significant, differences at P120 and P210) (Wright, Chrenek et al. 2013). At P60, tvrm148 mice have significant reductions in scotopic and photopic ERG amplitudes that continue to diminish through P180 (Wright, Chrenek et al. 2013). Morphologically, tvrm148 mice have a stable retina architecture despite some thinning in retina layer thicknesses and losses of cone nuclei (Wright, Chrenek et al. 2013). These morphological findings are consistent with the KO mouse (Redmond, Yu et al. 1998) and rd12 mouse (Pang, Chang et al. 2005; Pang, Boye et al. 2010). Mice homozygous for the tvrm148 mutation have lipid droplets in the RPE that are observable by transmission electron microscopy (TEM) (Wright, Chrenek et al. 2013), which is again consistent with what is seen in KO mice (Redmond, Yu et al. 1998). Unlike the KO mouse (Redmond, Yu et al. 1998), the mutant tvrm148 allele is still capable of producing mRNA that is present in steady-state conditions at the same level as in wild type mice (Wright, Chrenek et al. 2013). RPE65 protein is also present, albeit at much reduced levels (Wright, Chrenek et al. 2013); it is still unclear at this time whether the reduction in protein levels is the result of reduced translation of the mutant protein or the result of increased degradation (or otherwise reduced half-life) of

the translated protein. Perhaps most importantly, the tvrm148 mutant mouse has no detectable amounts of 11-*cis*-RAL or all-*trans*-RAL, and has elevated levels of retinyl esters (Wright, Chrenek et al. 2013), all of which do not differ significantly from KO mice (Redmond, Yu et al. 1998; Wright, Chrenek et al. 2013). Taken together, the tvrm148 and KO mice are comparable models of LCA2 in that they both exhibit null phenotypes (i.e. the loss of retinoid isomerase activity). Looking at all the data, the tvrm148 model could also be useful in further development of treatments for LCA2.

5.1.2—Novel rd12 findings

The rd12 mutation differed significantly from the KO mutation at the phenotypic and molecular levels, despite being a single nucleotide substitution like the tvrm148 mutation (Redmond, Yu et al. 1998; Wright, Chrenek et al. 2013). Unlike the KO mouse, rd12 mice have an earlier and faster reduction in visual function as measured by OKT and ERG. Furthermore, crosses of the rd12 mouse with wild type and KO mice indicate that the rd12 mutation inherits in a semidominant manner, a novel finding that has not appeared in the literature to date. OKT measurements showed that rd12/+ mice had a progressive loss of visual function, and KO/rd12 mice were phenotypically similar to rd12/rd12 mice. More cone nuclei are lost at an earlier age in the superior portion of the retina in rd12 mice than KO mice, despite having similar retina architecture and retinal layer thicknesses; this is the first reported difference of cone loss between rd12 and KO mice. This large difference in visual phenotype and small difference in morphological phenotype may be attributable to results found at the molecular level. rd12/rd12 mice produce significant levels of mutant *Rpe65* mRNA, but no truncated protein is detectable;

this is the first report that examines *Rpe65* expression at both the mRNA and protein levels in rd12 mice. Further investigation found that the mutant mRNA trafficks similarly in the cytoplasm as compared to wild type *Rpe65* mRNA, but that the mutant mRNA may be sequestered on ribosome-free messenger ribonucleoproteins (mRNPs) and inefficiently bound by ribosomes for translation. Based on these data, I conclude that the rd12 mutation does not produce visual or molecular effects similar to the KO mutation. Because the rd12 mutation has also been reported in humans, these findings show this is a new model for patients with a specific subtype of LCA2, which may be unusually severe.

5.1.3—Comparisons of the three mouse strains

The KO, tvrm148, and rd12 mutations all resulted in null RPE65 protein function as measured by roughly comparable buildups of all-*trans*-RE (RPE65 substrate) and undetectable amounts of 11-*cis*-RAL that are necessary for visual function (Table 3.3 and Table 4.2). OKT measurements, on the other hand, showed different rates of visual function loss, suggesting that the phenotypic differences observed in rd12 mice with respect to KO and tvrm148 mice were not the result of loss of RPE65 function but because of inefficient binding of the mutant rd12 mRNA to ribosomes. It should be noted that because the only strong differences in visual function are detectable with OKT testing, we cannot rule out an extra defect in the AON or other brain structures associated with vision. This also suggests that the semidominant form of inheritance with the rd12 is not the direct result of isomerase function loss. Interestingly, despite the fact that the tvrm148 mutation can still produce RPE65 protein that is capable of accumulating in detectable amounts in steady-state conditions, it is a nonfunctional protein incapable of

isomerase activity. This suggests that even though two single point mutations can result in no isomerase activity, the gene products themselves (either protein or mRNA) can have diverse and unpredictable effects on visual function that are unrelated to normal gene function. By extension, this implies that there are some aspects to different human *RPE65* gene mutations that may not be modeled in the laboratory at this time.

5.2—LIMITATIONS OF THIS STUDY

Further refinements to the RPE65^{F229S} protein model would need to be done to predict what effects the mutation has on the active site of the enzyme. It is still unclear from the study with the tvrm148 mutation whether the low RPE65 protein levels that were observed in tvrm148/tvrm148 mice are the result of decreased translation efficiency, decreased protein half-life, or both. In the future, the efficiency of *Rpe65* mRNA translation in tvrm148 mice could be addressed by performing a polyribosome profiling experiment in the same way the translation of the mutant rd12 *Rpe65* mRNA was investigated. With respect to the rd12 mutation, counts of cone nuclei in rd12/+ mice compared to +/+ and KO/+ mice were not performed, so it is unknown at this time whether the slow progressive visual function loss in rd12/+ mice is the result of a possible loss of cone photoreceptors. It is also unclear at this time why there is a 30% reduction in mRNA levels in rd12 mice (compared to tvrm148 mice that have no detectable reduction in mRNA levels). The resolution of the sucrose gradient used for polyribosome profiling in this study may not be sufficient to determine whether the rd12 mutant mRNA is incapable of being bound by ribosomes at all or merely inefficiently bound by ribosomes. As a result, it is not definitively known at this time whether there is

a truncated peptide produced by the rd12 allele that could exert some sort of toxic effect but is present in amounts below the limit of detection (i.e. 2.5% wild type level of RPE65 per 20 μg total protein) in this study. It is not entirely understood at this time why inefficient binding of the rd12 mutant mRNA by ribosomes could lead to the observed semidominant effect and whether this is the only mechanistic pathway at play.

It is also not known at this time why +/+, rd12/+, KO/KO, tvrm148/tvrm148, rd12/rd12, and KO/rd12 mice have different visual acuities at P30, the first time point measured in these mice. I can think of three possibilities. First, there could be varying amounts of Müller cell gliosis (a neuropathological process some neurons undergo in response to stress conditions) in these different strains. Second, recent evidence suggests that Müller cell gliosis occurs in KO/KO mice and is associated with ganglion cell death in theses mice (Métrailler, Emery, et al. 2013). Also, mice with rd12 mutations could undergo earlier, or have greater amounts of, cone photoreceptor cell death as compared to other lines by P30. The OKT measurements in these studies were taken in photopic conditions (i.e. cone-mediated visual conditions). If rd12/+ mice and rd12/rd12 mice had increased amounts of cone death, that could account for reduced visual acuity at P30 in these mice with respect to +/+ and KO/KO mice, respectively. Finally, there could be systemic problems in mice with the rd12 mutation. The fact that RPE65 expression has been noted not only in the RPE, but also skin cells and transformed kidney epithelium, suggests that RPE65 could be produced in a wide variety of cells. If the rd12 mutation results in an mRNA with a toxic effect, there could be currently unknown systemic abnormalities that could be contributing to visual acuity in those mice.

5.3—FUTURE DIRECTIONS

5.3.1—Preliminary data for future studies

In the Discussion of the findings with the rd12 mutation presented in Section 4.5, I mentioned that I did not investigate RNA-induced innate immune activation as a possible mechanism to explain the rd12 semidominant effects. Endogenous RNAs (e.g. *Alu* RNA) can induce innate immune activation in the RPE (Kaneko, Dridi et al. 2011; Dridi, Hirano et al. 2012; Tarallo, Hirano et al. 2012) as mediated by MyD88, a toll-like receptor (TLR) adaptor protein (Lai and Gallo 2008; Yu and Levine 2011). Some human geographic atrophy (GA) patients have been shown to have decreased levels of DICER1 (Kaneko, Dridi et al. 2011; Dridi, Hirano et al. 2012; Tarallo, Hirano et al. 2012), a protein that is intimately involved in the processing of immature microRNAs (miRNAs) to mature miRNAs (Tijsterman and Plasterk 2004). Reduced DICER1 levels resulted in higher levels of *Alu* RNA (Kaneko, Dridi et al. 2011), and increased *Alu* RNA levels could in turn induce RPE cell death through activation of the NLRP3 inflammasome (Tarallo, Hirano et al. 2012). Oddly enough, despite the fact that MyD88 was activated, TLR proteins did not appear to play a role in *Alu* RNA-induced RPE cell death (Tarallo, Hirano et al. 2012). It was hypothesized that *Alu* RNA was unable to bind to TLR receptors because of its large size (Tarallo, Hirano et al. 2012); by contrast, endogenous mRNAs (i.e. much smaller than *Alu* RNA) may be small enough to bind. Other RNA sensing pathways can also activate the innate immune response (Li, Thiele et al. 2009; Belgnaoui, Paz et al. 2011; Yu and Levine 2011), but they were not found to play a role in *Alu* RNA toxicity (Tarallo, Hirano et al. 2012). A brief summary of RNA-induced activation of innate immune responses is presented in Fig. 5.1. RNA can induce innate

immune response activation because endogenous sensors may recognize ssRNA or dsRNA structural motifs.

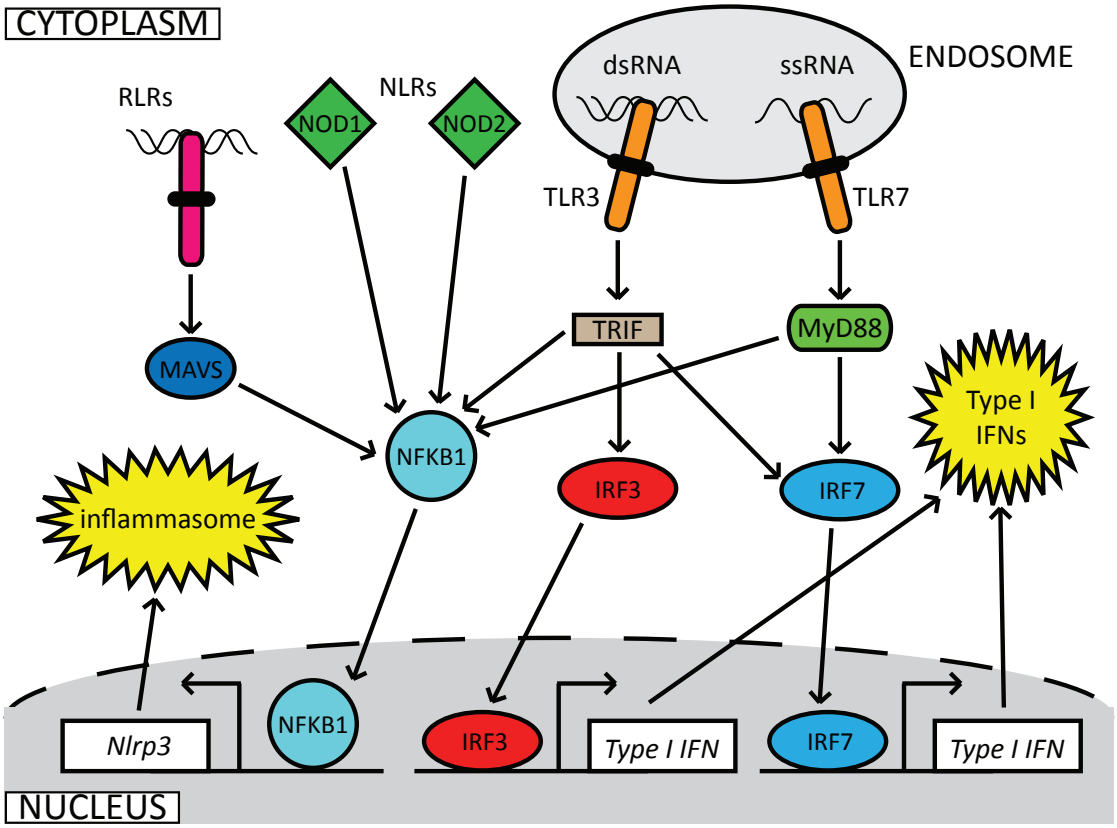

Figure 5.1. RNA-sensing pathways activate Type I interferon (IFNs) and NLRP3 inflammasomes. RNAs can induce the activation and expression of type I IFNs and inflammasome via RIG-I-like receptor (RLR), Nod-like receptor (NLR), and TLR pathways. The mitochondrial anti-viral signaling (MAVS) protein is the adaptor protein for RLRs and can induce the activation and nuclear translocation of nuclear factor kappa B (NFKB1), which can then induce expression of NLRP3. Likewise, NLR pathways can activate NFKB1 through the use of the adaptor proteins NOD1 and NOD2. TLR3 and TLR7 recognize double-stranded RNA (dsRNA) and single-stranded RNA (ssRNA) in endosomes. TLR3 uses TRIF (encoded by *Ticam1*) as an adaptor protein, and TLR7 uses MyD88 as an adaptor protein. TRIF activates interferon response factor 3 (IRF3) and is typically constitutively expressed in most cell types. IRF7, on the other hand, is only activated when both TLR3 and TLR7 are activated. Both IRF3 and IRF7 induce the expression of type I IFNs (e.g. IFN alpha and IFN beta), but not type II IFNs (e.g. IFN gamma) or NLRP3, although MyD88 itself may directly induce type II IFN expression. TRIF and MyD88 may also activate NFKB1 for NLRP3 expression.

RNA secondary structure predictions (Fig 4.17) showed that *Rpe65* mRNA may be capable of adopting large ssRNA and dsRNA motifs and that rd12 mutant *Rpe65* mRNA more closely resembled wild type mRNA than other mutants (Fig. 4.16). Also, there is some evidence in the literature to suggest that mRNP complexes may be trafficked in eukaryotic cells through endosomes (Baumann, Pohlmann et al. 2012; Vollmeister, Schipper et al. 2012), where TLR sensors can also be found (Lai and Gallo 2008). Based on the fact that endogenous RNAs may be capable of activating innate immune responses via MyD88 (Tarallo, Hirano et al. 2012), I hypothesized that genes associated with TLR activation may be upregulated in the RPE of rd12 mice. This would not be the first reported case of such a phenomenon.

Endogenous RNAs have been previously shown to activate innate immune markers in the RPE (Kaneko, Dridi et al. 2011; Dridi, Hirano et al. 2012; Tarallo, Hirano et al. 2012) as mediated by MyD88, so I performed qRT-PCR on innate immune markers associated with TLR, NLR, and RLR signaling (Lai and Gallo 2008; Li, Thiele et al. 2009; Yu and Levine 2011) in P30 wild type, KO, and rd12 mice. Both *MyD88* and *Ticam1* (encoding TRIF) were upregulated in rd12 RPE (311.4 ± 64.4% and 265.9 ± 36.2% wild type levels, respectively) with respect to wild type and KO mice (Fig. 5.2A). *Mavs* and *Nod2* were not significantly upregulated in rd12 RPE (120.2 ± 25.2% and 116.9 ± 35.1% wild type levels, respectively; $P = 0.356$ and $P = 0.557$, respectively). *Nod1* was slightly upregulated in rd12 RPE compared to KO RPE (134.2 ± 42.0% and 64.5 ± 5.2% wild type levels, respectively; $P = 0.011$), but not compared to wild type RPE ($P = 0.104$). *Irf7* was significantly upregulated in rd12 RPE compared to KO and

wild type RPE (168.0 ± 15.6%, 93.1 ± 25.8%, and 100.0 ± 20.5%, respectively; P <0.001; Fig. 5.2B). *Nfkb1* was not significantly upregulated in either KO or rd12 RPE (89.8 ± 24.8% and 102.1 ± 15.2% wild type levels, respectively; $P = 0.723$) with respect to wild type RPE (Fig. 5.2B). Inflammasome markers *Nlrp3* (Grishman, White et al. 2012), *Nlrc4* (Gong and Shao 2012), and *Aim2* (Franchi, Munoz-Planillo et al. 2012) were not upregulated in rd12 RPE (91.0 ± 25.1%, 136.2 ± 39.7%, and 102.1 ± 32.0% wild type levels, respectively; $P = 0.561$, $P = 0.213$, $P = 0.426$, respectively; Fig. 5.2C).

These preliminary data suggest that an innate immune response (Fig. 5.1) could possibly be activated in rd12 mice as mediated by TLR3, TLR7, and IRF7 (Fig. 5.2). The adaptor protein genes for the dsRNA sensor TLR3, *Ticam1* (encoding TRIF) (Lai and Gallo 2008; Yu and Levine 2011), and the ssRNA sensor TLR7, *MyD88* (Lai and Gallo 2008; Yu and Levine 2011), were both upregulated in rd12 mice. Both TLR3 and TLR7/8 activation are necessary for the activation of IRF7 (Li, Thiele et al. 2009), which can then induce the expression of Type I interferons (IFNs) (Lai and Gallo 2008; Yu and Levine 2011). IRF7 is not capable of directly activating the NLRP3 inflammasome (Lai and Gallo 2008; Yu and Levine 2011); in mice, NFKB1 is required to directly activate the NLRP3 inflammasome (Lai and Gallo 2008; Yu and Levine 2011). The lack of *Nfkb1* and *Nlrp3* upregulation in rd12 mice (Fig. 5.2) suggests that the inflammasome may not be a primary target of possible TLR activation.

Based on my data, I propose the negative semidominant effect on visual function exerted by the rd12 allele may be at least in part mediated by TLR signaling pathways, possibly through the activation of Type I IFNs (Fig. 5.3). It should be noted MyD88 can also directly interact with Type II IFN receptors to induce expression of Type II IFNs

(Tsolmongyn, Koide et al. 2013). These preliminary data do not address that possibility. Future planned experiments based on these data are presented in the next section.

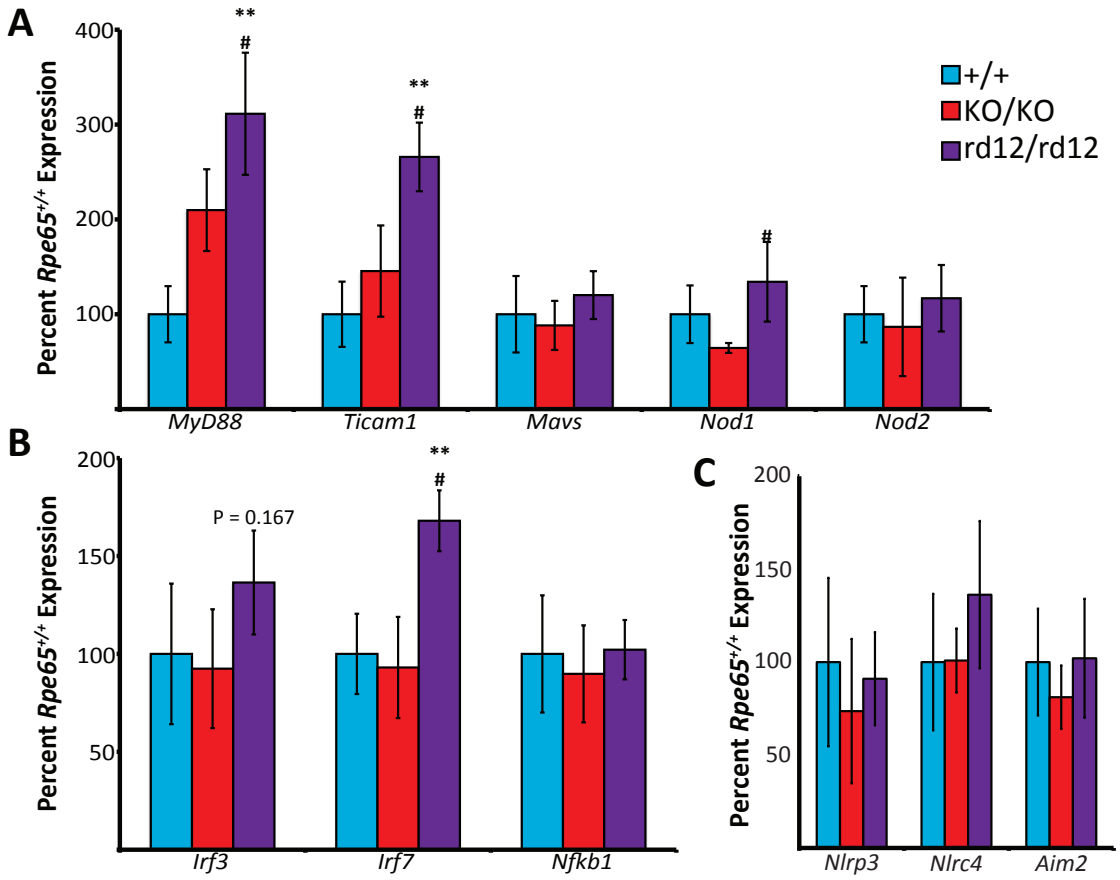

Figure 5.2. TLR receptors may be activated in the RPE of rd12 mice. Whole cell RNA was extracted from the RPE/choroid of P30 wild type, KO, and rd12 mice. (**A**) qRT-PCR of *Ticam1*, *MyD88*, *Mavs*, *Nod1*, and *Nod2*. (**B**) qRT-PCR of *Irf3*, *Irf7*, and *Nfkb1*. (**C**) qRT-PCR of *Nlrp3*, *Nlrc4*, and *Aim2*. * P <0.05, ** P <0.001 wild type compared to rd12; # *P* <0.05 KO/KO compared to rd12, significance determined through one-way ANOVA. Data are presented as mean ± SD.

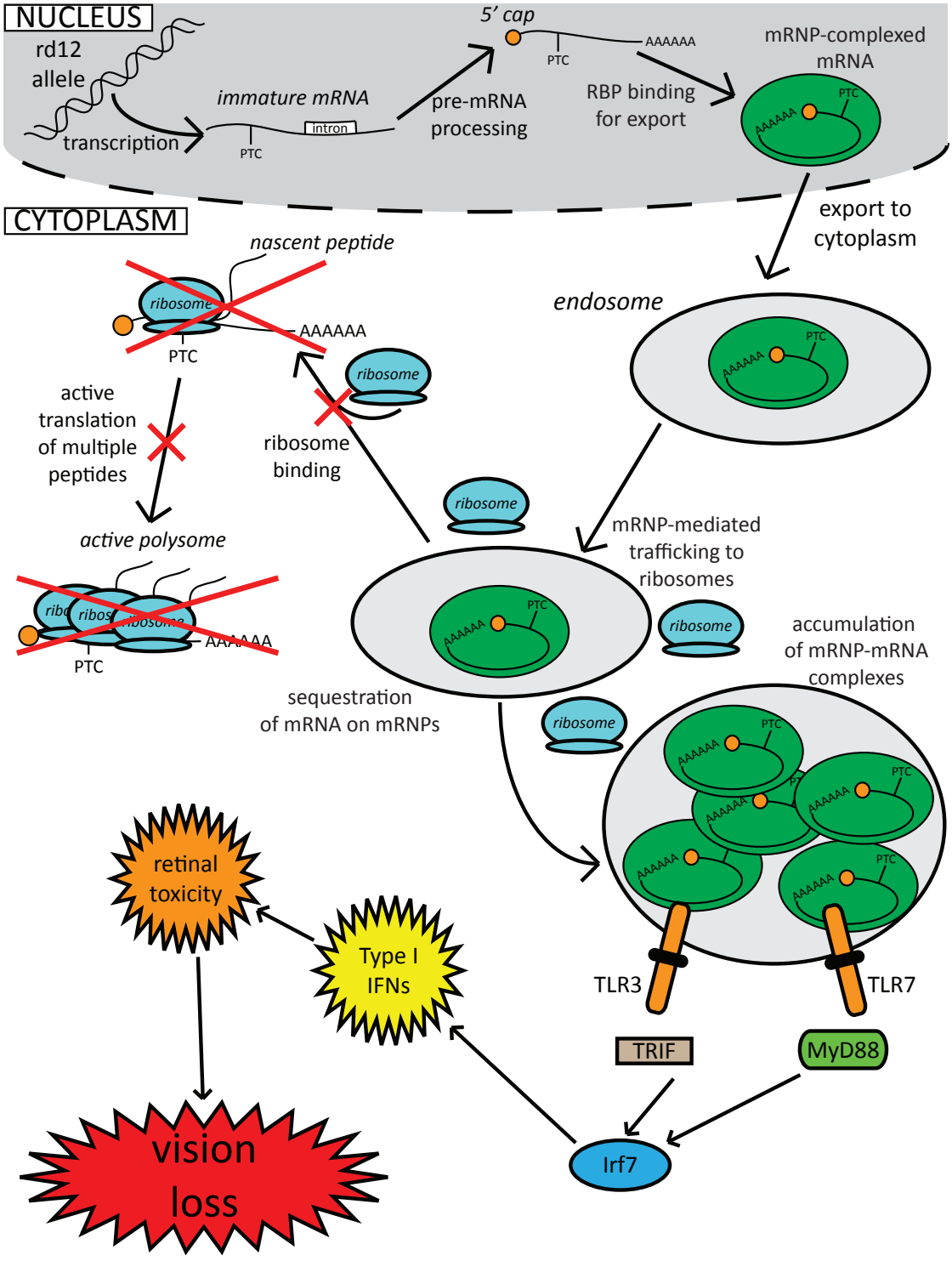
NUCLEUS
rd12
allele
transcription
immature mRNA
intron
PTC
5' cap
AAAAAA
PTC
pre-mRNA
processing
RBP binding
for export
mRNP-complexed
mRNA
PTC
AAAAA
CYTOPLASM
export to
cytoplasm
nascent peptide
ribosome
AAAAAA
PTC
active
translation
of multiple
peptides
ribosome
ribosome
binding
endosome
PTC
AAAAA
active polysome
PTC
ribosome
mRNP-mediated
trafficking to
ribosomes
PTC
AAAAA
ribosome
accumulation
of mRNP-mRNA
complexes
sequestration
of mRNA on mRNPs
ribosome
PTC
AAAAA
retinal
toxicity
Type I
IFNs
TLR3
TLR7
TRIF
MyD88
Irf7
vision
loss

Figure 5.3. Activation of RNA sensors TLR3 and TLR7 are proposed mediators for negative semidominant visual effects induced by the rd12 allele. The rd12 allele is normally transcribed, processed, and exported from the nucleus to the cytoplasm. The mutant mRNA then traffics in an mRNP complex to ribosomes for the pioneer round of translation but cannot bind to them for active translation. The mRNA is recognized by the TLR sensors, TLR3 (sensitive to free dsRNA) and TLR7 (sensitive to free ssRNA), and both then induce activation of the downstream factor IRF7. The inflammasome is not activated during this response, and the semidominant-negative visual function loss may be further mediated by the activation of Type I IFNs.

5.3.2—Future planned experiments

Data presented in "**IV: The rd12 allele exerts a semidominant negative effect on visual function in mice**" suggested the extra detrimental effects of the rd12 allele on visual function were unrelated to the visual cycle (Table 4.2). I hypothesize that if the innate immune response is involved in those extra detrimental effects, then the rd12 visual phenotype will be partially rescued to the KO visual phenotype, if those innate immune pathways are removed from mice carrying the rd12 allele. Fortunately, there are knockout and other mutant mouse models available for studying TLR signaling pathways. I propose breeding the rd12 mouse to each of these mouse models to see if there can be a partial visual preservation with respect to the rd12 phenotype: *Unc93b1*$^{-/-}$ (Tabeta, Hoebe et al. 2006), *Tlr3*$^{-/-}$ (Tabeta, Georgel et al. 2004), *Tlr7*$^{-/-}$ (Lund, Alexopoulou et al. 2004), *Tlr9*$^{-/-}$ (Spies, Hochrein et al. 2003; Tabeta, Georgel et al. 2004), *Mavs*$^{-/-}$ (Subramanian, Natarajan et al. 2013), *Nod1/2* double knockout (DKO) (Stroo, Butter et al. 2012), *Nlrp3*$^{-/-}$ (Tarallo, Hirano et al. 2012), *Ifnar1*^{tm1Agt}, and *Ifngr*$^{-/-}$. These double mutants can then have their visual function measured to assess for any protective effects conferred by the additional mutations.

Data in Fig. 4.6 indicated that the difference between KO and rd12 visual function, as measured by OKT, was largest at P120. I propose a single measurement at P120 may be sufficient in each of these double mutant mice to measure visual preservation. Confirmation of the preliminary data (Fig. 5.2) will address whether visual function loss in rd12 mice is mediated by 1) TLR signaling, 2) NLRP3 inflammasomes, and/or 3) Type I and/or II IFNs (Table 5.1).

Table 5.1—Predicted phenotypes of offspring of rd12 and innate immune deficient mice

Genotype	Locus Name	Visual Preservation Predicted?
rd12/rd12::*Unc93b1*$^{-/-}$	Unc93b1	Y
rd12/rd12::*Tlr3*$^{-/-}$	Toll-like receptor 3	Y
rd12/rd12::*Tlr7*$^{-/-}$	Toll-like receptor 7	Y
rd12/rd12::*Tlr9*$^{-/-}$	Toll-like receptor 9	N
rd12/rd12::*Mavs*$^{-/-}$	Mitochondrial antiviral signaling protein	N
rd12/rd12::*Nod1*$^{-/-}$*::Nod2*$^{-/-}$	Nucleotide-binding oligomerization domain containing 1/2	N
rd12/rd12::Nlrp3$^{-/-}$	NLR family, pyrin domain containing 3	N
rd12/rd12::Ifnar1^{tm1Agt}	Interferon (alpha and beta) receptor 1	Y
rd12/rd12::*Ifngr*$^{-/-}$	Interferon gamma receptor	unknown

Based on preliminary data, I would expect that TLR mutants, but not RLR or NLR mutants, would be partially protective against the rd12 mutant phenotype. UNC93B1, TLR3, and TLR7 are all proteins that are involved in either ssRNA or dsRNA recognition and innate immune pathway activation. TLR9, although it also can be found in endosomes along with TLR3 and TLR7 (Lai and Gallo 2008), would not be expected to be involved in rd12 disease progression because it recognizes CpG-DNA, not RNA (Spies, Hochrein et al. 2003). Likewise, *Nlrp3* and downstream mediators of inflammasome signaling (e.g. *Casp1*, *IL-1*, and *IL-18*) are not expected to be involved in rd12 disease progression based on preliminary data (Fig. 5.2). Because of work with *Alu* RNA in the RPE (Tarallo, Hirano et al. 2012), it remains a possibility that must be addressed in future work.

Irf7 and *MyD88* upregulation, as implicated by preliminary data (Fig. 5.2) points to the direct activation of Type I IFN expression (Lai and Gallo 2008). MyD88 activation, has also been reported to lead to activation of Type II IFN expression because it can interact directly with Type II IFN receptors (Tsolmongyn, Koide et al. 2013). Because of this, the involvement of both Type I and II IFNs must be addressed through crosses of rd12 mice with mice deficient in those signaling pathways. The possible protection of visual function in rd12 mice is expected to be mediated through deficiencies in Type I IFN signaling, but it is entirely possible Type II IFNs could also be involved in disease progression. By contrast, it would be interesting to also perform a series of experiments in KO/KO mice in which interferons were either overexpressed or injected directly into the eye to test if this could mimic the rd12/rd12 phenotype.

5.4—FINAL CONCLUSIONS

The central goal of research in genetics and molecular biology is to improve the health and well being of patients in the clinic. To that end, I worked with mice that have mutations in the *Rpe65* gene to better understand the mechanistic underpinnings of the disease, LCA2, which is caused by mutations in the human *RPE65* gene. Most mouse research concerning LCA2 has focused on the use of the *Rpe65* gene knockout (KO); this model has been demonstrated to accurately model many cases of LCA2 in humans and has been used to develop treatments for patients. Because a wide variety of pathogenic *RPE65* gene mutations are seen in the clinic, I sought to test the tvrm148 and rd12 mutants to see whether these mutations produce phenotypes that are similar to the KO mutation with respect to visual function and molecular biology. I hypothesized that different mutations in the mouse *Rpe65* gene would produce diverse phenotypes with diverse mechanistic underpinnings, and the work I have presented in this dissertation supports this hypothesis. I speculate that because some mutations have effects that are similar to the KO mutant effects while others are not, some patients in the clinic may not respond as well to treatment with therapies currently in development with the KO mutant than others.

Key points presented in this section:

1. The tvrm148 mutation is the first mouse missense mutation reported in the literature that produces a completely nonfunctional protein.
2. The rd12 mutation is the first mutation identified in mouse (and only the second in the literature) that can produce a phenotype in any kind of dominant fashion. OKT measurements may be valuable for detecting variations in visual function in mice with retinal degenerations that are not readily apparent by ERG alone. Because this same gene mutation ($RPE65^{R44X}$) has been identified in humans, the rd12 mutant may be an ideal model for studying what could be an unusually aggressive form of LCA2 in humans.
3. The tvrm148 mouse could be used as a model for the development of novel treatments for human patients. The rd12 mouse could be further investigated to test whether the innate immune response plays a role in the semidominant effects of the allele.
4. This work suggests that different mutations in the *RPE65* gene can produce a variety of mutant phenotypes. Mutations that occur in different regions of the *RPE65* gene may produce variations in disease progression that may directly impact treatment responses in the clinic. Future work may need to be done to further refine treatments for use in the clinic to address all clinical presentations of the disease.

REFERENCES

Abe, T., B. Wiggert, et al. (1977). "Vitamin A receptors. I. Comparison of retinol binding to serum retinol-binding protein and to tissue receptors in chick retina and pigment epithelium." Biochimica et biophysica acta **498**(1): 355-365.

Abecasis, G. R., A. Auton, et al. (2012). "An integrated map of genetic variation from 1,092 human genomes." Nature **491**(7422): 56-65.

Ablonczy, Z., R. K. Crouch, et al. (2002). "11-cis-retinal reduces constitutive opsin phosphorylation and improves quantum catch in retinoid-deficient mouse rod photoreceptors." J Biol Chem **277**(43): 40491-40498.

Acland, G. M., G. D. Aguirre, et al. (2005). "Long-term restoration of rod and cone vision by single dose rAAV-mediated gene transfer to the retina in a canine model of childhood blindness." Mol Ther **12**(6): 1072-1082.

Acland, G. M., G. D. Aguirre, et al. (2001). "Gene therapy restores vision in a canine model of childhood blindness." Nat Genet **28**(1): 92-95.

Adler, A. J. and C. D. Evans (1983). "Rapid isolation of bovine interphotoreceptor retinol-binding protein." Biochim Biophys Acta **761**(3): 217-222.

Adzhubei, I. A., S. Schmidt, et al. (2010). "A method and server for predicting damaging missense mutations." Nat Methods **7**(4): 248-249.

Aguirre, G. D., V. Baldwin, et al. (1998). "Congenital stationary night blindness in the dog: common mutation in the RPE65 gene indicates founder effect." Mol Vis **4**: 23.

Ahmed, E. and J. Loewenstein (2008). "Leber congenital amaurosis: disease, genetics and therapy." Semin Ophthalmol **23**(1): 39-43.

Akula, J. D., R. M. Hansen, et al. (2007). "Rod photoreceptor function predicts blood vessel abnormality in retinopathy of prematurity." Invest Ophthalmol Vis Sci **48**(9): 4351-4359.

Akula, J. D., J. A. Mocko, et al. (2007). "The oscillatory potentials of the dark-adapted electroretinogram in retinopathy of prematurity." Invest Ophthalmol Vis Sci **48**(12): 5788-5797.

Aleman, T. S., S. G. Jacobson, et al. (2004). "Impairment of the transient pupillary light reflex in Rpe65(-/-) mice and humans with leber congenital amaurosis." Invest Ophthalmol Vis Sci **45**(4): 1259-1271.

Altschul, S. F., W. Gish, et al. (1990). "Basic local alignment search tool." J Mol Biol **215**(3): 403-410.

Altschul, S. F., T. L. Madden, et al. (1997). "Gapped BLAST and PSI-BLAST: a new generation of protein database search programs." Nucleic Acids Res **25**(17): 3389-3402.

Amann, P. M., C. Luo, et al. (2012). "Vitamin A metabolism in benign and malignant melanocytic skin cells: importance of lecithin/retinol acyltransferase and RPE65." J Cell Physiol **227**(2): 718-728.

Andrews, J. S. and S. Futterman (1964). "Metabolism of the Retina. V. the Role of Microsomes in Vitamin a Esterification in the Visual Cycle." J Biol Chem **239**: 4073-4076.

Ashtari, M., L. L. Cyckowski, et al. (2011). "The human visual cortex responds to gene therapy-mediated recovery of retinal function." J Clin Invest **121**(6): 2160-2168.

Bainbridge, J. W. B., A. J. Smith, et al. (2008). "Effect of gene therapy on visual function in Leber's congenital amaurosis." N Engl J Med **358**(21): 2231-2239.
Barker, S. E., C. A. Broderick, et al. (2009). "Subretinal delivery of adeno-associated virus serotype 2 results in minimal immune responses that allow repeat vector administration in immunocompetent mice." J Gene Med **11**(6): 486-497.
Baumann, C. (1977). "Boll's phenomenon." Vision Res **17**(11-12): 1325-1327.
Baumann, S., T. Pohlmann, et al. (2012). "Kinesin-3 and dynein mediate microtubule-dependent co-transport of mRNPs and endosomes." J Cell Sci **125**(Pt 11): 2740-2752.
Båvik, C. O., F. Lévy, et al. (1993). "The retinal pigment epithelial membrane receptor for plasma retinol-binding protein. Isolation and cDNA cloning of the 63-kDa protein." J Biol Chem **268**(27): 20540-20546.
Belgnaoui, S. M., S. Paz, et al. (2011). "Orchestrating the interferon antiviral response through the mitochondrial antiviral signaling (MAVS) adapter." Curr Opin Immunol **23**(5): 564-572.
Bemelmans, A.-P., C. Kostic, et al. (2006). "Lentiviral gene transfer of RPE65 rescues survival and function of cones in a mouse model of Leber congenital amaurosis." PLoS medicine **3**(10): e347.
Bemelmans, A. P., C. Kostic, et al. (2008). "Lentiviral gene transfer-mediated cone vision restoration in RPE65 knockout mice." Adv Exp Med Biol **613**: 89-95.
Bernstein, P. S., W. C. Law, et al. (1987). "Biochemical characterization of the retinoid isomerase system of the eye." J Biol Chem **262**(35): 16848-16857.
Bernstein, P. S., W. C. Law, et al. (1987). "Isomerization of all-trans-retinoids to 11-cis-retinoids in vitro." Proc Natl Acad Sci U S A **84**(7): 1849-1853.
Bidou, L., V. Allamand, et al. (2012). "Sense from nonsense: therapies for premature stop codon diseases." Trends in molecular medicine **18**(11): 679-688.
Bowne, S. J., M. M. Humphries, et al. (2011). "A dominant mutation in RPE65 identified by whole-exome sequencing causes retinitis pigmentosa with choroidal involvement." Eur J Hum Genet **19**(10): 1074-1081.
Bridges, C. D., R. A. Alvarez, et al. (1984). "Visual cycle in the mammalian eye. Retinoid-binding proteins and the distribution of 11-cis retinoids." Vision Res **24**(11): 1581-1594.
Bromberg, Y. and B. Rost (2007). "SNAP: predict effect of non-synonymous polymorphisms on function." Nucleic Acids Res **35**(11): 3823-3835.
Buch, P. K., J. W. Bainbridge, et al. (2008). "AAV-mediated gene therapy for retinal disorders: from mouse to man." Gene Ther **15**(11): 849-857.
Cachafeiro, M., A.-P. Bemelmans, et al. (2010). "Remaining rod activity mediates visual behavior in adult Rpe65-/- mice." Invest Ophthalmol Vis Sci **51**(12): 6835-6842.
Cachafeiro, M., A. P. Bemelmans, et al. (2010). "Remaining rod activity mediates visual behavior in adult Rpe65-/- mice." Invest Ophthalmol Vis Sci **51**(12): 6835-6842.
Canada, F. J., W. C. Law, et al. (1990). "Substrate specificities and mechanism in the enzymatic processing of vitamin A into 11-cis-retinol." Biochemistry **29**(41): 9690-9697.
Capriotti, E., R. Calabrese, et al. (2006). "Predicting the insurgence of human genetic diseases associated to single point protein mutations with support vector machines and evolutionary information." Bioinformatics **22**(22): 2729-2734.

Capriotti, E., P. Fariselli, et al. (2005). "Predicting protein stability changes from sequences using support vector machines." Bioinformatics **21 Suppl 2**: ii54-58.

Capriotti, E., P. Fariselli, et al. (2005). "I-Mutant2.0: predicting stability changes upon mutation from the protein sequence or structure." Nucleic Acids Res **33**(Web Server issue): W306-310.

Carter-Dawson, L. D. and M. M. LaVail (1979). "Rods and cones in the mouse retina. I. Structural analysis using light and electron microscopy." The J Comp Neurol **188**(2): 245-262.

Caruso, R. C., T. S. Aleman, et al. (2010). "Retinal disease in Rpe65-deficient mice: comparison to human leber congenital amaurosis due to RPE65 mutations." Invest Ophthalmol Vis Sci **51**(10): 5304-5313.

Chang, B., N. L. Hawes, et al. (2007). "Two mouse retinal degenerations caused by missense mutations in the beta-subunit of rod cGMP phosphodiesterase gene." Vision Res **47**(5): 624-633.

Chen, Y., J. X. Ma, et al. (2003). "Down-regulation of RPE65 protein expression and promoter activity by retinoic acid." Mol Vis **9**: 345-354.

Chen, Y., G. Moiseyev, et al. (2006). "RPE65 gene delivery restores isomerohydrolase activity and prevents early cone loss in Rpe65-/- mice." Invest Ophthalmol Vis Sci **47**(3): 1177-1184.

Chen, Y., G. Moiseyev, et al. (2006). "Impacts of two point mutations of RPE65 from Leber's congenital amaurosis on the stability, subcellular localization and isomerohydrolase activity of RPE65." FEBS Lett **580**(17): 4200-4204.

Chen, Y., G. Moiseyev, et al. (2006). "RPE65 gene delivery restores isomerohydrolase activity and prevents early cone loss in Rpe65-/- mice." Invest Ophthalmol Vis Sci **47**(3): 1177-1184.

Chen, Y., G. Moiseyev, et al. (2003). "Visual cycle retinoid processing proteins are present in HEK293S cells." Vision Res **43**(28): 3037-3044.

Choi, Y., G. E. Sims, et al. (2012). "Predicting the functional effect of amino acid substitutions and indels." PLoS One **7**(10): e46688.

Cideciyan, A. V. (2010). "Leber congenital amaurosis due to RPE65 mutations and its treatment with gene therapy." Prog Retin Eye Res **29**(5): 398-427.

Cideciyan, A. V., T. S. Aleman, et al. (2008). "Human gene therapy for RPE65 isomerase deficiency activates the retinoid cycle of vision but with slow rod kinetics." Proc Natl Acad Sci U S A **105**(39): 15112-15117.

Cideciyan, A. V., W. W. Hauswirth, et al. (2009). "Human RPE65 gene therapy for Leber congenital amaurosis: persistence of early visual improvements and safety at 1 year." Hum Gene Ther **20**(9): 999-1004.

Cideciyan, A. V., S. G. Jacobson, et al. (2013). "Human retinal gene therapy for Leber congenital amaurosis shows advancing retinal degeneration despite enduring visual improvement." Proc Natl Acad Sci U S A **110**(6): E517-525.

Cottet, S., L. Michaut, et al. (2006). "Biological characterization of gene response in Rpe65-/- mouse model of Leber's congenital amaurosis during progression of the disease." FASEB J **20**(12): 2036-2049.

Cremers, F. P., J. A. van den Hurk, et al. (2002). "Molecular genetics of Leber congenital amaurosis." Hum Mol Genet **11**(10): 1169-1176.

Danciger, M., M. T. Matthes, et al. (2000). "A QTL on distal chromosome 3 that influences the severity of light-induced damage to mouse photoreceptors." Mamm Genome **11**(6): 422-427.

Deigner, P. S., W. C. Law, et al. (1989). "Membranes as the energy source in the endergonic transformation of vitamin A to 11-cis-retinol." Science **244**(4907): 968-971.

Dejneka, N. S., E. M. Surace, et al. (2004). "In utero gene therapy rescues vision in a murine model of congenital blindness." Mol Ther **9**(2): 182-188.

Dell'Orco, D., H. Schmidt, et al. (2009). "Network-level analysis of light adaptation in rod cells under normal and altered conditions." Mol Biosyst **5**(10): 1232-1246.

den Hollander, A. I., R. Roepman, et al. (2008). "Leber congenital amaurosis: genes, proteins and disease mechanisms." Prog Retin Eye Res **27**(4): 391-419.

Douglas, R., N. Alam, et al. (2005). "Independent visual threshold measurements in the two eyes of freely moving rats and mice using a virtual-reality optokinetic system." Visual Neurosci. **22**: 677-84.

Doyle, S. E., A. M. Castrucci, et al. (2006). "Nonvisual light responses in the Rpe65 knockout mouse: rod loss restores sensitivity to the melanopsin system." Proc Natl Acad Sci U S A **103**(27): 10432-10437.

Dridi, S., Y. Hirano, et al. (2012). "ERK1/2 activation is a therapeutic target in age-related macular degeneration." Proc Natl Acad Sci U S A **109**(34): 13781-13786.

Ecker, J. L., O. N. Dumitrescu, et al. (2010). "Melanopsin-expressing retinal ganglion-cell photoreceptors: cellular diversity and role in pattern vision." Neuron **67**(1): 49-60.

Ekesten, B., P. Gouras, et al. (2001). "Ultraviolet and middle wavelength sensitive cone responses in the electroretinogram (ERG) of normal and Rpe65 -/- mice." Vision Res **41**(19): 2425-2433.

El Matri, L., A. Ambresin, et al. (2006). "Phenotype of three consanguineous Tunisian families with early-onset retinal degeneration caused by an R91W homozygous mutation in the RPE65 gene." Graefes Arch Clin Exp Ophthalmol **244**(9): 1104-1112.

Fan, J., R. K. Crouch, et al. (2011). "Light prevents exogenous 11-cis retinal from maintaining cone photoreceptors in chromophore-deficient mice." Invest Ophthalmol Vis Sci **52**(5): 2412-2416.

Fan, J., B. Rohrer, et al. (2008). "Rpe65-/- and Lrat-/- mice: comparable models of leber congenital amaurosis." Invest Ophthalmol Vis Sci **49**(6): 2384-2389.

Fan, J., B. Rohrer, et al. (2003). "Isorhodopsin rather than rhodopsin mediates rod function in RPE65 knock-out mice." Proc Natl Acad Sci U S A **100**(23): 13662-13667.

Fan, J., K. Sakurai, et al. (2010). "Deletion of GRK1 causes retina degeneration through a transducin-independent mechanism." J Neurosci **30**(7): 2496-2503.

Fan, J., M. L. Woodruff, et al. (2005). "Opsin activation of transduction in the rods of dark-reared Rpe65 knockout mice." J Physiol **568**(Pt 1): 83-95.

Fan, J., B. X. Wu, et al. (2006). "9-cis Retinal increased in retina of RPE65 knockout mice with decrease in coat pigmentationt." Photochem Photobiol **82**(6): 1461-1467.

Feng, Y., D. Absher, et al. (1997). "FMRP associates with polyribosomes as an mRNP, and the I304N mutation of severe fragile X syndrome abolishes this association." Mol Cell **1**(1): 109-118.

Ferrer-Costa, C., J. L. Gelpi, et al. (2005). "PMUT: a web-based tool for the annotation of pathological mutations on proteins." Bioinformatics **21**(14): 3176-3178.

Fleisch, V. C. and S. C. Neuhauss (2010). "Parallel visual cycles in the zebrafish retina." Prog Retin Eye Res **29**(6): 476-486.

Flicek, P., B. L. Aken, et al. (2008). "Ensembl 2008." Nucleic Acids Res **36**(Database issue): D707-714.

Franchi, L., R. Munoz-Planillo, et al. (2012). "Sensing and reacting to microbes through the inflammasomes." Nat Immunol **13**(4): 325-332.

Fu, Y., H. Zhong, et al. (2005). "Intrinsically photosensitive retinal ganglion cells detect light with a vitamin A-based photopigment, melanopsin." Proc Natl Acad Sci U S A **102**(29): 10339-10344.

Garwin, G. G. and J. C. Saari (2000). "High-performance liquid chromatography analysis of visual cycle retinoids." Methods Enzymol **316**: 313-324.

Gasteiger, E., A. Gattiker, et al. (2003). "ExPASy: The proteomics server for in-depth protein knowledge and analysis." Nucleic Acids Res **31**(13): 3784-3788.

Gearhart, P. M., C. Gearhart, et al. (2010). "Improvement of visual performance with intravitreal administration of 9-cis-retinal in Rpe65-mutant dogs." Arch Ophthalmol **128**(11): 1442-1448.

Golczak, M., P. D. Kiser, et al. (2010). "Importance of membrane structural integrity for RPE65 retinoid isomerization activity." J Biol Chem **285**(13): 9667-9682.

Gong, C., Y. K. Kim, et al. (2009). "SMD and NMD are competitive pathways that contribute to myogenesis: effects on PAX3 and myogenin mRNAs." Genes Dev **23**(1): 54-66.

Gong, Y. N. and F. Shao (2012). "Sensing bacterial infections by NAIP receptors in NLRC4 inflammasome activation." Protein Cell **3**(2): 98-105.

Grantham, R. (1974). "Amino acid difference formula to help explain protein evolution." Science **185**(4154): 862-864.

Grimm, C., A. Wenzel, et al. (2000). "Protection of Rpe65-deficient mice identifies rhodopsin as a mediator of light-induced retinal degeneration." Nat Genet **25**(1): 63-66.

Grishman, E. K., P. C. White, et al. (2012). "Toll-like receptors, the NLRP3 inflammasome, and interleukin-1beta in the development and progression of type 1 diabetes." Pediatr Res **71**(6): 626-632.

Gu, S. M., D. A. Thompson, et al. (1997). "Mutations in RPE65 cause autosomal recessive childhood-onset severe retinal dystrophy." Nat Genet **17**(2): 194-197.

Guerin, K., C. Y. Gregory-Evans, et al. (2008). "Systemic aminoglycoside treatment in rodent models of retinitis pigmentosa." Exp Eye Res **87**(3): 197-207.

Hagerman, R., J. Au, et al. (2011). "FMR1 premutation and full mutation molecular mechanisms related to autism." J Neurodev Disord **3**(3): 211-224.

Hamann, S., D. F. Schorderet, et al. (2009). "Bax-induced apoptosis in Leber's congenital amaurosis: a dual role in rod and cone degeneration." PLoS One **4**(8): e6616.

Hamel, C. P., E. Tsilou, et al. (1993). "Molecular cloning and expression of RPE65, a novel retinal pigment epithelium-specific microsomal protein that is post-transcriptionally regulated in vitro." J Biol Chem **268**(21): 15751-15757.

Hanein, S., I. Perrault, et al. (2004). "Leber congenital amaurosis: comprehensive survey of the genetic heterogeneity, refinement of the clinical definition, and genotype-phenotype correlations as a strategy for molecular diagnosis." Hum Mutat **23**(4): 306-317.

Hauswirth, W. W., T. S. Aleman, et al. (2008). "Treatment of leber congenital amaurosis due to RPE65 mutations by ocular subretinal injection of adeno-associated virus gene vector: short-term results of a phase I trial." Hum Gene Ther **19**(10): 979-990.

Hernández, M., S. E. Pearce-Kelling, et al. (2010). "Altered expression of retinal molecular markers in the canine RPE65 model of Leber congenital amaurosis." Invest Ophthalmol Vis Sci **51**(12): 6793-6802.

Hinterhuber, G., K. Cauza, et al. (2004). "RPE65 of retinal pigment epithelium, a putative receptor molecule for plasma retinol-binding protein, is expressed in human keratinocytes." J Invest Dermatol **122**(2): 406-413.

Hinterhuber, G., K. Cauza, et al. (2005). "Expression of RPE65, a putative receptor for plasma retinol-binding protein, in nonmelanocytic skin tumours." Br J Dermatol **153**(4): 785-789.

Hood, D. C. and D. G. Birch (1993). "Light adaptation of human rod receptors: the leading edge of the human a-wave and models of rod receptor activity." Vision Res **33**(12): 1605-1618.

Hood, D. C. and D. G. Birch (1994). "Rod phototransduction in retinitis pigmentosa: estimation and interpretation of parameters derived from the rod a-wave." Invest Ophthalmol Vis Sci **35**(7): 2948-2961.

Hu, Y., Y. Chen, et al. (2011). "Comparison of ocular pathologies in vitamin A-deficient mice and RPE65 gene knockout mice." Invest Ophthalmol Visual Sci.

Imamachi, N., H. Tani, et al. (2012). "Up-frameshift protein 1 (UPF1): multitalented entertainer in RNA decay." Drug Discov Ther **6**(2): 55-61.

Imanishi, Y., M. L. Batten, et al. (2004). "Noninvasive two-photon imaging reveals retinyl ester storage structures in the eye." J Cell Biol **164**(3): 373-383.

Irier, H. A., R. Shaw, et al. (2009). "Translational regulation of GluR2 mRNAs in rat hippocampus by alternative 3' untranslated regions." J Neurochem **109**(2): 584-594.

Ivert, L., H. Keldbye, et al. (2005). "Age-related changes in the basement membrane of the retinal pigment epithelium of Rpe65 -/- and wild-type mice." Graefes Arch Clin Exp Ophthalmol **243**(3): 250-256.

Jablonski, M. M., C. Dalke, et al. (2009). "An ENU-induced mutation in Rs1h causes disruption of retinal isomerase of the visual cycle." Proc Natl Acad Sci U S A **106**(41): 17325-17330.

Jacobson, S. G., T. S. Aleman, et al. (2007). "Human cone photoreceptor dependence on RPE65 isomerase." Proc Natl Acad Sci U S A **104**(38): 15123-15128.

Jacobson, S. G., T. S. Aleman, et al. (2009). "Defining the residual vision in leber congenital amaurosis caused by RPE65 mutations." Invest Ophthalmol Vis Sci **50**(5): 2368-2375.

Jacobson, S. G., A. V. Cideciyan, et al. (2003). "Crumbs homolog 1 (CRB1) mutations result in a thick human retina with abnormal lamination." Hum Mol Genet **12**(9): 1073-1078.

Jacobson, S. G., A. V. Cideciyan, et al. (2012). "Gene therapy for leber congenital amaurosis caused by RPE65 mutations: safety and efficacy in 15 children and adults followed up to 3 years." Arch Ophthalmol **130**(1): 9-24.

Janecke, A. R., D. A. Thompson, et al. (2004). "Mutations in RDH12 encoding a photoreceptor cell retinol dehydrogenase cause childhood-onset severe retinal dystrophy." Nat Genet **36**(8): 850-854.

Janssen, J. J., E. D. Kuhlmann, et al. (2000). "Retinoic acid delays transcription of human retinal pigment neuroepithelium marker genes in ARPE-19 cells." Neuroreport **11**(7): 1571-1579.

Jin, M., Q. Yuan, et al. (2007). "Role of LRAT on the retinoid isomerase activity and membrane association of Rpe65." J Biol Chem **282**(29): 20915-20924.

Johnson, C. J., L. Berglin, et al. (2008). "Technical brief: subretinal injection and electroporation into adult mouse eyes." Molecular Vision **14**: 2211-2226.

Kaneko, H., S. Dridi, et al. (2011). "DICER1 deficit induces Alu RNA toxicity in age-related macular degeneration." Nature.

Katz, M. L. and T. M. Redmond (2001). "Effect of Rpe65 knockout on accumulation of lipofuscin fluorophores in the retinal pigment epithelium." Invest Ophthalmol Vis Sci **42**(12): 3023-3030.

Katz, M. L., K. D. Wendt, et al. (2005). "RPE65 gene mutation prevents development of autofluorescence in retinal pigment epithelial phagosomes." Mech Ageing Dev **126**(4): 513-521.

Kaylor, J. J., Q. Yuan, et al. (2013). "Identification of DES1 as a vitamin A isomerase in Muller glial cells of the retina." Nat Chem Biol **9**(1): 30-36.

Kiliszek, A., R. Kierzek, et al. (2011). "Crystal structures of CGG RNA repeats with implications for fragile X-associated tremor ataxia syndrome." Nucleic Acids Res **39**(16): 7308-7315.

Kim, S. R., N. Fishkin, et al. (2004). "Rpe65 Leu450Met variant is associated with reduced levels of the retinal pigment epithelium lipofuscin fluorophores A2E and iso-A2E." Proc Natl Acad Sci U S A **101**(32): 11668-11672.

Kiser, P. D., E. R. Farquhar, et al. (2012). "Structure of RPE65 isomerase in a lipidic matrix reveals roles for phospholipids and iron in catalysis." Proc Natl Acad Sci U S A **109**(41): E2747-2756.

Kiser, P. D., M. Golczak, et al. (2009). "Crystal structure of native RPE65, the retinoid isomerase of the visual cycle." Proc Natl Acad Sci U S A **106**(41): 17325-17330.

Kiser, P. D. and K. Palczewski (2010). "Membrane-binding and enzymatic properties of RPE65." Prog Retin Eye Res **29**(5): 428-442.

Koenekoop, R. K. (2008). "Successful RPE65 gene replacement and improved visual function in humans." Ophthalmic Genet **29**(3): 89-91.

Koirala, A., R. S. Makkia, et al. (2013). "S/MAR-containing DNA nanoparticles promote persistent RPE gene expression and improvement in RPE65-associated LCA." Hum Mol Genet.

Kostic, C., S. V. Crippa, et al. (2011). "Gene therapy regenerates protein expression in cone photoreceptors in Rpe65(R91W/R91W) mice." PLoS One **6**(2): e16588.

Kühne, W. (1878). "On the Stable Colours of the Retina." J Physiol **1**(2-3): 109-212 105.
Kühne, W. and H. Sewall (1880). "On the Physiology of the Retinal Epithelium." J Physiol **3**(1): 88-92.
Kumar, P., S. Henikoff, et al. (2009). "Predicting the effects of coding non-synonymous variants on protein function using the SIFT algorithm." Nat Protoc **4**(7): 1073-1081.
Kunchithapautham, K., B. Coughlin, et al. (2009). "Cone outer segment morphology and cone function in the Rpe65-/- Nrl-/- mouse retina are amenable to retinoid replacement." Invest Ophthalmol Vis Sci **50**(10): 4858-4864.
Lachke, S. A., F. S. Alkuraya, et al. (2011). "Mutations in the RNA Granule Component TDRD7 Cause Cataract and Glaucoma." Science **331**(6024): 1571-1576.
Lachke, S. A. and R. L. Maas (2011). "RNA Granules and Cataract." Expert Rev Ophthalmol **6**(5): 497-500.
Lai, Y. and R. L. Gallo (2008). "Toll-like receptors in skin infections and inflammatory diseases." Infect Disord Drug Targets **8**(3): 144-155.
Laimer, M., K. Onder, et al. (2008). "Nonsense-associated altered splicing of the Patched gene fails to suppress carcinogenesis in Gorlin syndrome." Br J Dermatol **159**(1): 222-227.
Landers, G. M. and J. A. Olson (1988). "Rapid, simultaneous determination of isomers of retinal, retinal oxime and retinol by high-performance liquid chromatography." J Chromatogr **438**(2): 383-392.
Lau, A. G., H. A. Irier, et al. (2010). "Distinct 3'UTRs differentially regulate activity-dependent translation of brain-derived neurotrophic factor (BDNF)." Proc Natl Acad Sci U S A **107**(36): 15945-15950.
Leskov, I. B., V. A. Klenchin, et al. (2000). "The gain of rod phototransduction: reconciliation of biochemical and electrophysiological measurements." Neuron **27**(3): 525-537.
Li, F., I. Thiele, et al. (2009). "Identification of potential pathway mediation targets in Toll-like receptor signaling." PLoS Comput Biol **5**(2): e1000292.
Li, W., F. Kong, et al. (2009). "Gene therapy following subretinal AAV5 vector delivery is not affected by a previous intravitreal AAV5 vector administration in the partner eye." Mol Vis **15**: 267-275.
Li, X., W. Li, et al. (2011). "Gene therapy rescues cone structure and function in the 3-month-old rd12 mouse: a model for midcourse RPE65 leber congenital amaurosis." Invest Ophthalmol Vis Sci **52**(1): 7-15.
Li, Y. and P. Jin (2012). "RNA-mediated neurodegeneration in fragile X-associated tremor/ataxia syndrome." Brain Res **1462**: 112-117.
Liu, S. Y. and T. M. Redmond (1998). "Role of the 3'-untranslated region of RPE65 mRNA in the translational regulation of the RPE65 gene: identification of a specific translation inhibitory element." Arch Biochem Biophys **357**(1): 37-44.
Livrea, M. A., L. Tesoriere, et al. (1991). "All-trans to 11-cis retinol isomerization in nuclear membrane fraction from bovine retinal pigment epithelium." Exp Eye Res **52**(4): 451-459.
Lorenz, B., P. Gyurus, et al. (2000). "Early-onset severe rod-cone dystrophy in young children with RPE65 mutations." Invest Ophthalmol Vis Sci **41**(9): 2735-2742.

Lund, J. M., L. Alexopoulou, et al. (2004). "Recognition of single-stranded RNA viruses by Toll-like receptor 7." Proc Natl Acad Sci U S A **101**(15): 5598-5603.
Lyubarsky, A. L., A. B. Savchenko, et al. (2005). "Mole quantity of RPE65 and its productivity in the generation of 11-cis-retinal from retinyl esters in the living mouse eye." Biochemistry **44**(29): 9880-9888.
Ma, J., L. Xu, et al. (1998). "Cloning and localization of RPE65 mRNA in salamander cone photoreceptor cells1." Biochim Biophys Acta **1443**(1-2): 255-261.
Ma, J., J. Zhang, et al. (2001). "Expression, purification, and MALDI analysis of RPE65." Invest Ophthalmol Vis Sci **42**(7): 1429-1435.
Ma, J. X., D. Zhang, et al. (1999). "Identification of RPE65 in transformed kidney cells." FEBS Lett **452**(3): 199-204.
Maeda, A., T. Maeda, et al. (2005). "Role of photoreceptor-specific retinol dehydrogenase in the retinoid cycle in vivo." J Biol Chem **280**(19): 18822-18832.
Maeda, T., A. V. Cideciyan, et al. (2009). "Loss of cone photoreceptors caused by chromophore depletion is partially prevented by the artificial chromophore pro-drug, 9-cis-retinyl acetate." Hum Mol Genet **18**(12): 2277-2287.
Maeda, T., Z. Dong, et al. (2012). "QLT091001, a 9-cis-retinal analog, is well-tolerated by retinas of mice with impaired visual cycles." Invest Ophthalmol Vis Sci **54**(1): 455-466.
Maeda, T., A. Maeda, et al. (2009). "Evaluation of 9-cis-retinyl acetate therapy in Rpe65-/- mice." Invest Ophthalmol Vis Sci **50**(9): 4368-4378.
Maguire, A. M., K. A. High, et al. (2009). "Age-dependent effects of RPE65 gene therapy for Leber's congenital amaurosis: a phase 1 dose-escalation trial." Lancet **374**(9701): 1597-1605.
Maguire, A. M., F. Simonelli, et al. (2008). "Safety and efficacy of gene transfer for Leber's congenital amaurosis." N Engl J Med **358**(21): 2240-2248.
Maiti, P., J. Kong, et al. (2006). "Small molecule RPE65 antagonists limit the visual cycle and prevent lipofuscin formation." Biochemistry **45**(3): 852-860.
Marlhens, F., C. Bareil, et al. (1997). "Mutations in RPE65 cause Leber's congenital amaurosis." Nat Genet **17**(2): 139-141.
Marmor, M. F. and L. J. Martin (1978). 100 years of the visual cycle.
Masland, R. H. (2012). "The neuronal organization of the retina." Neuron **76**(2): 266-280.
Mata, N. L., W. N. Moghrabi, et al. (2004). "Rpe65 is a retinyl ester binding protein that presents insoluble substrate to the isomerase in retinal pigment epithelial cells." J Biol Chem **279**(1): 635-643.
Matthews, R. G., R. Hubbard, et al. (1963). "Tautomeric Forms of Metarhodopsin." J Gen Physiol **47**: 215-240.
McBee, J. K., V. Kuksa, et al. (2000). "Isomerization of all-trans-retinol to cis-retinols in bovine retinal pigment epithelial cells: dependence on the specificity of retinoid-binding proteins." Biochemistry **39**(37): 11370-11380.
McCaskill, J. S. (1990). "The equilibrium partition function and base pair binding probabilities for RNA secondary structure." Biopolymers **29**(6-7): 1105-1119.
Métrailler S, Emery M, et al. (2013) "ERK1/2 pathway is activated in degenerated Rpe65-deficient mice." **116C**:86-95.

Métrailler, S., D. F. Schorderet, et al. (2012). "Early apoptosis of rod photoreceptors in Rpe65(-/-) mice is associated with the upregulated expression of lysosomal-mediated autophagic genes." Exp Eye Res **96**(1): 70-81.

Mi, H., A. Muruganujan, et al. (2013). "PANTHER in 2013: modeling the evolution of gene function, and other gene attributes, in the context of phylogenetic trees." Nucleic Acids Res **41**(Database issue): D377-386.

Moiseyev, G., Y. Chen, et al. (2005). "RPE65 is the isomerohydrolase in the retinoid visual cycle." Proc Natl Acad Sci U S A **102**(35): 12413-12418.

Moiseyev, G., O. Nikolaeva, et al. (2010). "Inhibition of the visual cycle by A2E through direct interaction with RPE65 and implications in Stargardt disease." Proc Natl Acad Sci U S A **107**(41): 17551-17556.

Moiseyev, G., Y. Takahashi, et al. (2006). "RPE65 is an iron(II)-dependent isomerohydrolase in the retinoid visual cycle." The Journal of biological chemistry **281**(5): 2835-2840.

Morimura, H., G. A. Fishman, et al. (1998). "Mutations in the RPE65 gene in patients with autosomal recessive retinitis pigmentosa or leber congenital amaurosis." Proc Natl Acad Sci U S A **95**(6): 3088-3093.

Mowat FM, Breuwer AR, et al. (2013) "RPE65 gene therapy slows cone loss in Rpe65-deficient dogs." Gene Ther **20**(5): 545-55.

Narfström, K., M. L. Katz, et al. (2003). "In vivo gene therapy in young and adult RPE65-/- dogs produces long-term visual improvement." J Hered **94**(1): 31-37.

Ng, P. C. and S. Henikoff (2001). "Predicting deleterious amino acid substitutions." Genome Res **11**(5): 863-874.

Ng, P. C. and S. Henikoff (2003). "Accounting for human polymorphisms predicted to affect protein function." Nucleic Acids Res **31**(13): 3812-3814.

Ng, P. C. and S. Henikoff (2003). "SIFT: Predicting amino acid changes that affect protein function." Nucleic Acids Res **31**(13): 3812-3814.

Ng, P. C. and S. Henikoff (2006). "Predicting the effects of amino acid substitutions on protein function." Annu Rev Genomics Hum Genet **7**: 61-80.

Nicoletti, A., D. J. Wong, et al. (1995). "Molecular characterization of the human gene encoding an abundant 61 kDa protein specific to the retinal pigment epithelium." Hum Mol Genet **4**(4): 641-649.

Nikolaeva, O., G. Moiseyev, et al. (2011). "Binding to lipid membrane induces conformational changes in RPE65: implications for its isomerohydrolase activity." J Biochem.

Nikolaeva, O., Y. Takahashi, et al. (2009). "Purified RPE65 shows isomerohydrolase activity after reassociation with a phospholipid membrane." Febs J **276**(11): 3020-3030.

Nusinowitz, S., W. H. Ridder, 3rd, et al. (2006). "Cortical visual function in the rd12 mouse model of Leber Congenital Amarousis (LCA) after gene replacement therapy to restore retinal function." Vision Res **46**(22): 3926-3934.

Pang, J., S. E. Boye, et al. (2010). "Self-complementary AAV-mediated gene therapy restores cone function and prevents cone degeneration in two models of Rpe65 deficiency." Gene Ther **17**(7): 815-826.

Pang, J.-J., B. Chang, et al. (2005). "Retinal degeneration 12 (rd12): a new, spontaneously arising mouse model for human Leber congenital amaurosis (LCA)." Mol Vis **11**: 152-162.

Pang, J. J., B. Chang, et al. (2006). "Gene therapy restores vision-dependent behavior as well as retinal structure and function in a mouse model of RPE65 Leber congenital amaurosis." Mol Ther **13**(3): 565-572.

Pardue, M. T., M. A. McCall, et al. (1998). "A naturally occurring mouse model of X-linked congenital stationary night blindness." Invest Ophthalmol Vis Sci **39**(12): 2443-2449.

Pardue, M. T., M. J. Phillips, et al. (2005). "Neuroprotective effect of subretinal implants in the RCS rat." Invest Ophthalmol Vis Sci **46**(2): 674-682.

Parker, R. O. and R. K. Crouch (2010). "Retinol dehydrogenases (RDHs) in the visual cycle." Exp Eye Res **91**(6): 788-792.

Pasadhika, S., G. A. Fishman, et al. (2010). "Differential macular morphology in patients with RPE65-, CEP290-, GUCY2D-, and AIPL1-related Leber congenital amaurosis." Invest Ophthalmol Vis Sci **51**(5): 2608-2614.

Perlman, J. I., B. R. Nodes, et al. (1982). "Utilization of retinoids in the bullfrog retina." J Gen Physiol **80**(6): 885-913.

Philp, A. R., M. Jin, et al. (2009). "Predicting the pathogenicity of RPE65 mutations." Hum Mutat **30**(8): 1183-1188.

Poehner, W. J., M. Fossarello, et al. (2000). "A homozygous deletion in RPE65 in a small Sardinian family with autosomal recessive retinal dystrophy." Mol Vis **6**: 192-198.

Pollard, K. S., M. J. Hubisz, et al. (2010). "Detection of nonneutral substitution rates on mammalian phylogenies." Genome Res **20**(1): 110-121.

Porto, F. B. O., I. Perrault, et al. (2002). "Prenatal human ocular degeneration occurs in Leber's congenital amaurosis (LCA2)." J Gene Med **4**(4): 390-396.

Prusky, G., N. Alam, et al. (2004). "Rapid quantification of adult and developing mouse spatial vision using a virtual optomotor system." Invest Ophthalmol Vis Sci **45**(12): 4611-4616.

Qtaishat, N. M., T. M. Redmond, et al. (2003). "Acute radiolabeling of retinoids in eye tissues of normal and rpe65-deficient mice." Invest Ophthalmol Vis Sci **44**(4): 1435-1446.

Rakoczy, P. E., C. M. Lai, et al. (2003). "Assessment of rAAV-mediated gene therapy in the Rpe65-/- mouse." Adv Exp Med Biol **533**: 431-438.

Ramensky, V., P. Bork, et al. (2002). "Human non-synonymous SNPs: server and survey." Nucleic Acids Res **30**(17): 3894-3900.

Redmond, T. M., S. Gentleman, et al. (2001). "Identification, expression, and substrate specificity of a mammalian beta-carotene 15,15'-dioxygenase." J Biol Chem **276**(9): 6560-6565.

Redmond, T. M., E. Poliakov, et al. (2010). "RPE65, visual cycle retinol isomerase, is not inherently 11-cis-specific: support for a carbocation mechanism of retinol isomerization." J Biol Chem **285**(3): 1919-1927.

Redmond, T. M., E. Poliakov, et al. (2005). "Mutation of key residues of RPE65 abolishes its enzymatic role as isomerohydrolase in the visual cycle." Proc Natl Acad Sci U S A **102**(38): 13658-13663.

Redmond, T. M., C. H. Weber, et al. (2007). "Effect of Leu/Met variation at residue 450 on isomerase activity and protein expression of RPE65 and its modulation by variation at other residues." Mol Vis **13**: 1813-1821.

Redmond, T. M., S. Yu, et al. (1998). "Rpe65 is necessary for production of 11-cis-vitamin A in the retinal visual cycle." Nat Genet **20**(4): 344-351.

Reese, M. G., F. H. Eeckman, et al. (1997). "Improved splice site detection in Genie." J Comput Biol **4**(3): 311-323.

Rohrer, B., Z. Ablonczy, et al. (2003). "Does constitutive phosphorylation protect against photoreceptor degeneration in Rpe65-/- mice?" Adv Exp Med Biol **533**: 221-227.

Rohrer, B., H. R. Lohr, et al. (2005). "Cone opsin mislocalization in Rpe65-/- mice: a defect that can be corrected by 11-cis retinal." Invest Ophthalmol Vis Sci **46**(10): 3876-3882.

Roman, A. J., S. L. Boye, et al. (2007). "Electroretinographic analyses of Rpe65-mutant rd12 mice: developing an in vivo bioassay for human gene therapy trials of Leber congenital amaurosis." Mol Vis **13**: 1701-1710.

Rozen, S. and H. Skaletsky (2000). "Primer3 on the WWW for general users and for biologist programmers." Methods Mol Biol **132**: 365-386.

Saari, J. C. (2012). "Vitamin A metabolism in rod and cone visual cycles." Annu Rev Nutr **32**: 125-145.

Sagara, H. and K. Hirosawa (1991). "Monoclonal antibodies which recognize endoplasmic reticulum in the retinal pigment epithelium." Exp Eye Res **53**(6): 765-771.

Samardzija, M., N. Tanimoto, et al. (2009). "In conditions of limited chromophore supply rods entrap 11-cis-retinal leading to loss of cone function and cell death." Hum Mol Genet **18**(7): 1266-1275.

Samardzija, M., J. von Lintig, et al. (2008). "R91W mutation in Rpe65 leads to milder early-onset retinal dystrophy due to the generation of low levels of 11-cis-retinal." Hum Mol Genet **17**(2): 281-292.

Sato, K., M. Nakazawa, et al. (2010). "S-opsin protein is incompletely modified during N-glycan processing in Rpe65(-/-) mice." Exp Eye Res **91**(1): 54-62.

Sato, K., T. Ozaki, et al. (2012). "M-opsin protein degradation is inhibited by MG-132 in Rpe65(-)/(-) retinal explant culture." Mol Vis **18**: 1516-1525.

Schatz, P., M. Preising, et al. (2011). "Fundus albipunctatus associated with compound heterozygous mutations in RPE65." Ophthalmol **118**(5): 888-894.

Schuster, P., W. Fontana, et al. (1994). "From sequences to shapes and back: a case study in RNA secondary structures." Proc Biol Sci **255**(1344): 279-284.

Schweingruber, C., S. C. Rufener, et al. (2013). "Nonsense-mediated mRNA decay - Mechanisms of substrate mRNA recognition and degradation in mammalian cells." Biochim Biophys Acta **1829**(6-7): 612-623.

Seeliger, M. W., C. Grimm, et al. (2001). "New views on RPE65 deficiency: the rod system is the source of vision in a mouse model of Leber congenital amaurosis." Nat Genet **29**(1): 70-74.

Simonelli, F., A. M. Maguire, et al. (2010). "Gene therapy for Leber's congenital amaurosis is safe and effective through 1.5 years after vector administration." Mol Ther **18**(3): 643-650.

Spies, B., H. Hochrein, et al. (2003). "Vaccination with plasmid DNA activates dendritic cells via Toll-like receptor 9 (TLR9) but functions in TLR9-deficient mice." J Immunol **171**(11): 5908-5912.

Stieger, K. and B. Lorenz (2008). "[The treatment of inherited dystrophies and neovascular disorders of the retina by rAAV-mediated gene therapy]." Klin Monbl Augenheilkd **225**(12): 1009-1023.

Stone, E. M. (2007). "Leber congenital amaurosis - a model for efficient genetic testing of heterogeneous disorders: LXIV Edward Jackson Memorial Lecture." Am J Ophthalmol **144**(6): 791-811.

Strauss, O. (2005). "The retinal pigment epithelium in visual function." Physiological reviews **85**(3): 845-881.

Stroo, I., L. M. Butter, et al. (2012). "Phenotyping of Nod1/2 double deficient mice and characterization of Nod1/2 in systemic inflammation and associated renal disease." Biol Open **1**(12): 1239-1247.

Subramanian, N., K. Natarajan, et al. (2013). "The adaptor MAVS promotes NLRP3 mitochondrial localization and inflammasome activation." Cell **153**(2): 348-361.

Sundaresan, P., P. Vijayalakshmi, et al. (2009). "Mutations that are a common cause of Leber congenital amaurosis in northern America are rare in southern India." Mol Vis **15**: 1781-1787.

Sunyaev, S. R., F. Eisenhaber, et al. (1999). "PSIC: profile extraction from sequence alignments with position-specific counts of independent observations." Protein Eng **12**(5): 387-394.

Szél, A., P. Röhlich, et al. (1992). "Unique topographic separation of two spectral classes of cones in the mouse retina." J Comp Neurol **325**(3): 327-342.

Tabaska, J. E. and M. Q. Zhang (1999). "Detection of polyadenylation signals in human DNA sequences." Gene **231**(1-2): 77-86.

Tabeta, K., P. Georgel, et al. (2004). "Toll-like receptors 9 and 3 as essential components of innate immune defense against mouse cytomegalovirus infection." Proc Natl Acad Sci U S A **101**(10): 3516-3521.

Tabeta, K., K. Hoebe, et al. (2006). "The Unc93b1 mutation 3d disrupts exogenous antigen presentation and signaling via Toll-like receptors 3, 7 and 9." Nat Immunol **7**(2): 156-164.

Takahashi, Y., Y. Chen, et al. (2006). "Two point mutations of RPE65 from patients with retinal dystrophies decrease the stability of RPE65 protein and abolish its isomerohydrolase activity." J Biol Chem **281**(31): 21820-21826.

Takahashi, Y., G. Moiseyev, et al. (2009). "Identification of a novel palmitylation site essential for membrane association and isomerohydrolase activity of RPE65." J Biol Chem **284**(5): 3211-3218.

Takahashi, Y., G. Moiseyev, et al. (2005). "Identification of conserved histidines and glutamic acid as key residues for isomerohydrolase activity of RPE65, an enzyme of the visual cycle in the retinal pigment epithelium." FEBS Lett **579**(24): 5414-5418.

Takahashi, Y., G. Moiseyev, et al. (2006). "The roles of three palmitoylation sites of RPE65 in its membrane association and isomerohydrolase activity." Invest Ophthalmol Vis Sci **47**(12): 5191-5196.

Takahashi, Y., G. Moiseyev, et al. (2011). "An alternative isomerohydrolase in the retinal Müller cells of a cone-dominant species." FEBS J **278**(16): 2913-2926.
Takahashi, Y., G. Moiseyev, et al. (2011). "An alternative isomerohydrolase in the retinal Muller cells of a cone-dominant species." Febs J **278**(16): 2913-2926.
Tang, P. H., M. C. Buhusi, et al. (2011). "RPE65 is present in human green/red cones and promotes photopigment regeneration in an in vitro cone cell model." J Neurosci **31**(50): 18618-18626.
Tang, P. H., M. C. Buhusi, et al. (2011). "RPE65 is present in human green/red cones and promotes photopigment regeneration in an in vitro cone cell model." J Neurosci **31**(50): 18618-18626.
Tang, P. H., L. Wheless, et al. (2011). "Regeneration of Photopigment Is Enhanced in Mouse Cone Photoreceptors Expressing RPE65 Protein." J Neurosci **31**(28): 10403-10411.
Tarallo, V., Y. Hirano, et al. (2012). "DICER1 loss and Alu RNA induce age-related macular degeneration via the NLRP3 inflammasome and MyD88." Cell **149**(4): 847-859.
Testa, F., A. M. Maguire, et al. (2013). "Three-Year Follow-up after Unilateral Subretinal Delivery of Adeno-Associated Virus in Patients with Leber Congenital Amaurosis Type 2." Ophthalmol **120**(6): 1283-1291.
Thompson, D. A., P. Gyurus, et al. (2000). "Genetics and phenotypes of RPE65 mutations in inherited retinal degeneration." Invest Ophthalmol Vis Sci **41**(13): 4293-4299.
Thompson, S., A. Recober, et al. (2010). "Light aversion in mice depends on nonimage-forming irradiance detection." Behav Neurosci **124**(6): 821-827.
Tijsterman, M. and R. H. Plasterk (2004). "Dicers at RISC; the mechanism of RNAi." Cell **117**(1): 1-3.
Trehan, A., F. J. Canada, et al. (1990). "Inhibitors of retinyl ester formation also prevent the biosynthesis of 11-cis-retinol." Biochemistry **29**(2): 309-312.
Trudel, E., S. Beaufils, et al. (2006). "Binding of RPE65 fragments to lipid monolayers and identification of its partners by glutathione S-transferase pull-down assays." Biochemistry **45**(10): 3337-3347.
Tsolmongyn, B., N. Koide, et al. (2013). "A toll-like receptor 2 ligand, Pam3CSK4, augments interferon-gamma-induced nitric oxide production via a physical association between MyD88 and IFN-gamma receptor in vascular endothelial cells." Immunology.
Tu, D. C., L. A. Owens, et al. (2006). "Inner retinal photoreception independent of the visual retinoid cycle." Proc Natl Acad Sci U S A **103**(27): 10426-10431.
Umino, Y., E. Solessio, et al. (2008). "Speed, spatial, and temporal tuning of rod and cone vision in mouse." J Neurosci **28**(1): 189-198.
Van Hooser, J. P., T. S. Aleman, et al. (2000). "Rapid restoration of visual pigment and function with oral retinoid in a mouse model of childhood blindness." Proc Natl Acad Sci U S A **97**(15): 8623-8628.
Van Hooser, J. P., Y. Liang, et al. (2002). "Recovery of visual functions in a mouse model of Leber congenital amaurosis." J Biol Chem **277**(21): 19173-19182.
Veske, A., S. E. Nilsson, et al. (1999). "Retinal dystrophy of Swedish briard/briard-beagle dogs is due to a 4-bp deletion in RPE65." Genomics **57**(1): 57-61.

Vollmeister, E., K. Schipper, et al. (2012). "Microtubule-dependent mRNA transport in the model microorganism Ustilago maydis." RNA Biol **9**(3): 261-268.
Vuoristo, M. M., J. G. Pappas, et al. (2004). "A stop codon mutation in COL11A2 induces exon skipping and leads to non-ocular Stickler syndrome." Am J Med Genet A **130A**(2): 160-164.
Wachtmeister, L. (1998). "Oscillatory potentials in the retina: what do they reveal." Prog Retin Eye Res **17**(4): 485-521.
Wald, G. (1935). "Carotenoids and the Visual Cycle." J Gen Physiol **19**(2): 351-371.
Wald, G. (1968). "The molecular basis of visual excitation." Nature **219**(5156): 800-807.
Wald, G. and P. K. Brown (1953). "The molar extinction of rhodopsin." J Gen Physiol **37**(2): 189-200.
Wald, G. and A. B. Clark (1937). "Visual Adaptation and Chemistry of the Rods." J Gen Physiol **21**(1): 93-105.
Wang, J.-S. and V. J. Kefalov (2011). "The cone-specific visual cycle." Prog Ret Eye Res **30**(2): 115-128.
Wenzel, A., C. E. Reme, et al. (2001). "The Rpe65 Leu450Met variation increases retinal resistance against light-induced degeneration by slowing rhodopsin regeneration." J Neurosci **21**(1): 53-58.
Weymouth, A. E. and A. J. Vingrys (2008). "Rodent electroretinography: methods for extraction and interpretation of rod and cone responses." Prog Retin Eye Res **27**(1): 1-44.
Wojciechowska, M. and W. J. Krzyzosiak (2011). "CAG repeat RNA as an auxiliary toxic agent in polyglutamine disorders." RNA Biol **8**(4): 565-571.
Won, J., L. Y. Shi, et al. (2011). "Mouse model resources for vision research." J Ophthalmol **2011**: 391384.
Woodruff, M. L., Z. Wang, et al. (2003). "Spontaneous activity of opsin apoprotein is a cause of Leber congenital amaurosis." Nat Genet **35**(2): 158-164.
Wright, C. B., M. A. Chrenek, et al. (2013). "Complementation test of Rpe65 knockout and tvrm148." Invest Ophthalmol Vis Sci. **54**(7): 5111-22.
Xu, F., Q. Dong, et al. (2012). "Novel RPE65 mutations associated with Leber congenital amaurosis in Chinese patients." Mol Vis **18**: 744-750.
Yamamoto, H., A. Simon, et al. (1999). "Mutations in the gene encoding 11-cis retinol dehydrogenase cause delayed dark adaptation and fundus albipunctatus." Nat Genet **22**(2): 188-191.
Yu, M. and S. J. Levine (2011). "Toll-like receptor, RIG-I-like receptors and the NLRP3 inflammasome: key modulators of innate immune responses to double-stranded RNA viruses." Cytokine Growth Factor Rev **22**(2): 63-72.
Yue, P., Z. Li, et al. (2005). "Loss of protein structure stability as a major causative factor in monogenic disease." J Mol Biol **353**(2): 459-473.
Yue, P., E. Melamud, et al. (2006). "SNPs3D: candidate gene and SNP selection for association studies." BMC Bioinformatics **7**: 166.
Yue, P. and J. Moult (2006). "Identification and analysis of deleterious human SNPs." J Mol Biol **356**(5): 1263-1274.
Zang, J. B., E. D. Nosyreva, et al. (2009). "A mouse model of the human Fragile X syndrome I304N mutation." PLoS Genet **5**(12): e1000758.

Zhang, H., J. Fan, et al. (2008). "Trafficking of membrane-associated proteins to cone photoreceptor outer segments requires the chromophore 11-cis-retinal." J Neurosci **28**(15): 4008-4014.

Zhang, T., N. Zhang, et al. (2011). "Cone opsin determines the time course of cone photoreceptor degeneration in Leber congenital amaurosis." Proc Natl Acad Sci U S A **108**(21): 8879-8884.

Zimmerman, W. F. (1974). "The distribution and proportions of vitamin A compounds during the visual cycle in the rat." Vision Res **14**(9): 795-802.

Znoiko, S. L., R. K. Crouch, et al. (2002). "Identification of the RPE65 protein in mammalian cone photoreceptors." Invest Ophthalmol Vis Sci **43**(5): 1604-1609.

Znoiko, S. L., B. Rohrer, et al. (2005). "Downregulation of cone-specific gene expression and degeneration of cone photoreceptors in the Rpe65-/- mouse at early ages." Invest Ophthalmol Vis Sci **46**(4): 1473-1479.

Zuker, M. and P. Stiegler (1981). "Optimal computer folding of large RNA sequences using thermodynamics and auxiliary information." Nucleic Acids Res **9**(1): 133-148.

Appendix

Protocols

This section contains protocols that I have adapted from publicly available protocols for personal use. This is not to say that the original manufacturer's protocols or the Nickerson lab protocols are inadequate in any way. These protocols simply contain alterations that I may have introduced in the event any troubleshooting needs to be done by future users if they are having difficulties reproducing my results. UNLESS EXPLICITLY STATED OTHERWISE, ALL STEPS ARE PERFORMED AT ROOM TEMPERATURE.

A.1—Electroretinography (ERG)

The purpose of this protocol is to measure the raw electrical response of the mouse retina to light stimulus. For analysis of the raw data, please see **A.2—ERG data analysis**.

A.1.1—Reagents and equipment

- UTAS-E3000 ERG system (LKC, Gaithersburg, MD)
- Ganzfeld dome (LKC)
- DTL fiber electrodes (wire-loop electrodes can also be used; these electrodes are constructed in-house by Micah Chrenek)
- Heating pad set to 37 ºC
- Ket/Xy mix (320 µl 50 mg/ml ketamine, Putney Inc., Portland, ME, 24 µl 100 mg/ml xylazine, Lloyd Inc, Shenandoah, IA, 656 µl 1X Dulbecco's phosphate buffered saline, Mediatech, Manasses, VA)
- 0.5% carboxymethylcellulose sodium (a.k.a. Refresh Tears you can buy in a corner pharmacy)
- 0.5% proparacaine hydrochloride ophthalmic solution USP (Bausch and Lomb, Rochester, NY)
- 2.5% phenylephrine hydrochloride solution USP (Bausch and Lomb)
- Kimwipes (Kimberly-Clark, Irving, TX)
- Vaseline (or other petroleum jelly product)
- Q-tips (or equivalent for applying Vaseline)

A.1.2—Preparations for ERG measurement

1. Mice must be placed in a completely dark environment overnight prior to ERG measurement. All steps must be performed under dim red light. A red light filter LED head lamp can be helpful for working with the mice under these conditions.
2. Anesthetize a mouse with Ket/Xy mix by intraperitoneal (IP) injection at a dose of 80 mg/kg ketamine and 16 mg/kg xylazine. Typically, I would give 200 µl of Ket/Xy mix to a mouse at P60. Always weigh the mouse prior to injection to determine dose. You can inject 50 µl more anesthetic after 10 min if the mouse is still not anesthetized.
3. Wait approximately 5 min for the mouse to become anesthetized.
4. Once the mouse is anesthetized, place it on a heating pad. While the mouse is under the influence of Ket/Xy, it must never leave a heating pad until it is completely recovered.
5. Place a drop of proparacaine on the each mouse eye and let sit for 1-2 min so the cornea is no longer sensitive to stimuli.
6. Use a Kimwipe to wipe absorb excess proparacaine away from the eye (but do not directly touch the eye with the Kimwipe).
7. Place a drop of phenylephrine on each mouse eye and let sit for 1-2 min to dilate the pupil.
8. Place the mouse in the ERG apparatus.
9. Insert grounding electrodes into the left and right cheeks of the mouse and into the base of the tail. Electrodes are labeled so they are not confused with one another.

10. Swivel DTL fiber electrodes until the fiber is just in contact with the cornea.
11. Place a single drop of methylcellulose solution onto each eye. This will aid in recording of the electrical response and help keep the mouse eye moistened (eye drying is a problem for mice as they cannot blink while anesthetized with Ket/Xy).
12. Position the Ganzfeld dome directly in front of the mouse.

A.1.3—Scotopic ERG measurement

1. On the computer, select the Pardue 10-7 protocol (outlined in Pardue, et al. *Invest Ophthalmol Vis Sci* 1998, Jablonski, et al. *Mol Vis* 2005, Chang, et al. Vision Res 2007). This protocol consists of ten dark-adapted steps (to assess rod and mixed rod-cone responses) and seven light-adapted steps (to assess cone responses).
2. After performing each step of the protocol, save the data. If you move on to the next step before saving the data, the raw data for the step that was just completed will be lost.
3. Once you complete and save the data from step 10, place another drop of methylcellulose on each eye if needed. In my experience, after step 10, the mouse eye is beginning to look somewhat dry.
4. Proceed to light level 11. The Ganzfeld will now project light into the ERG apparatus where the mouse is on the heating pad. Do not record data.

A.1.4—Photopic ERG measurement

1. Data cannot be recorded for step 11 until the mouse is light-adapted. The mouse needs to be exposed to the bright light field projected by the Ganzfeld for 10 min prior to taking measurements from step 11-17.
2. After 10 min has passed, performing steps 11-17. Make sure you save data after completing each step before moving to the next step.

A.1.5—Recovery

1. Most likely, the mouse will begin moving shortly after completing step 17. The mouse should be transferred to another heating pad outside of the ERG apparatus so it can recover from anesthesia.
2. Place petroleum jelly product on the mouse eye using a Q-tip (but do not directly touch the mouse eye with the Q-tip).
3. When the mouse begins to more fully recover from anesthesia, it may begin to try moving off the heating pad. Place the mouse in an extra mouse cage (with bedding) until the mouse is fully recovered from anesthesia (60-90 minutes).
4. While the mouse is recovering (or while preparing another mouse for ERG measurement), use the GrabData macro on the computer to collect the raw data for ERG data analysis. Data can be saved directly onto the lab file server.

A.2—Optokinetic tracking (OKT)

The purpose of this protocol is to measure the visual acuity of the mouse. Please refer to section for my personal notes about this procedure. *A.2.3—Notes and important considerations*

A.2.1—Reagents and equipment

- OKT apparatus (OptoMotry, CerebralMechanics, Vancouver, BC)
- OptoMotry software (I used version 1.7.4)

A.2.2—Protocol

1. Unless stated otherwise, all software settings are left on default.
2. Under Testing tab on OptoMotry Controller, select Options. Make sure the "Yes/No" and "Prompt" boxes are checked.
3. Place the mouse on the center platform and close the lid to the OKT apparatus.
4. Use the computer mouse to center the virtual gradient crosshairs between the mouse eyes.
5. If you see tracking, press F1 (shortcut keyboard key for "Yes" response). If you do not see tracking, press F2 (shortcut keyboard key for "No" response). If for any reason the gradient needs to be paused, press F6.
6. Keep monitoring and scoring the mouse's responses to the virtual gradient stimulus until the computer says, "Done."

7. Once you are finished testing, go to the Results tab on the OptoMotry Controller. Record results for each eye and the Combined (i.e. average) visual threshold for the mouse. I typically recorded measurements on paper and then typed them into Microsoft Excel.
8. Remove the mouse from the platform and press F3 to reset the test for the next mouse.

A.2.3—Notes and important considerations

1. Having the "Prompt" box checked (A.2.2 step 1) will help ensure you are accurately recording tracking response movements instead of random head movements. Because this test relies on an involuntary reflex response to a visual stimulus, the head tracking response will occur within seconds of the mouse's exposure to visual stimulus. The computer prompt marks the end of the period of time after exposure to visual stimulus in which a mouse could be reasonably expected to track movement if the mouse can detect it. If you are unsure whether the mouse can see the stimulus and is simply not paying attention to the stimulus, pause the gradient (F6 key), wait a few moments, re-center the virtual gradient between the mouse's eyes, and try again.
2. At first, the mouse may fall off the platform multiple times, particularly if this is the first time the mouse is being tested. If this happens, simply put the mouse back on the platform and try taking measurements again. Do not be discouraged if this takes several attempts.

3. Tracking is positively identified by movement of the mouse head at the same rate as the virtual gradient rotation. It should be a smooth, continuous motion that occurs for a 1-2 second period. Sporadic movements, movement of the nose or ears alone, smooth continuous head motion at the same rate as the virtual gradient but in the opposite direction of the gradient, or head movement after the computer prompt says “Waiting” should not be scored as a positive tracking response.
4. As of OptoMotry software version 1.7.4, if a mouse does not see and respond to the virtual gradient at the first frequency (0.056 c/d), then the program makes a gradient with frequency 0.003 c/d. In my experience, even mice with normal vision do not respond to this gradient frequency because the dark portion of the gradient is simply too large for them to take interest. So, if I continuously saw a mouse that would not respond to a 0.056 c/d gradient frequency for three times in each eye, I recorded the mouse visual threshold as 0.000 c/d (i.e. the mouse does not have a detectable visual threshold). I have spoken with representatives from CerebralMechanics about this before, and they suggested that I score positive tracking at 0.003 c/d so the program will increase the frequency to a level the mice might respond. I have not followed this advice because I believe it introduces an unacceptable degree of user bias into the experiment and to maintain consistency throughout my experiments.
5. Some mice may be uncooperative on a testing day for unknown reasons. If the experiment permits, wait until the following day to try to test again.
6. ERG and OKT measurements cannot be taken on the same day. ERGs require overnight dark-adaptation of mice (precluding taking ERG measurements

immediately following OKT testing), and in my experience, mice cannot recover from anesthesia quickly enough for OKT testing following ERGs.

7. Be aware of genetic background confounds. For example, Balb/c mice cannot track the gradient because of axon patterning defects in the accessory optic system (the required center for processing of the optokinetic response). As this procedure becomes more widely used in the vision research community, the literature may accumulate valuable information about the applicability of this test to different strains. Do not allow an incomplete reading of the literature to distort the interpretations of your data.
8. I highly recommend reading the works of Prusky and Douglas. Please refer to Section 1.3 of the dissertation for citation information.

A.3—Fluorescence in situ hybridization (FISH)

The purpose of this protocol is to determine the localization of specific mRNAs in the retina and RPE. I have personally optimized this protocol for use in retina and RPE cross-sections. Please be aware these protocols may need to be adjusted or reworked if attempted in different tissue types. Also, it is important for the user to realize this protocol cannot be used for absolute quantitation of mRNA signal in samples; because this protocol makes use of technologies that amplifies the signal produced by a probe binding to an individual RNA strand, there is not linear amplification of signal with RNA content. This protocol is adapted from the QuantiGene ViewRNA ISH Tissue 2-Plex Assay kit. RNA degredation is of particular concern with this protocol. Follow this protocol EXACTLY. Use fresh reagents for EVERYTHING.

A.3.1—Reagents and equipment

- Accu-Cut SRM 200 microtome (Sakura, The Netherlands)
- 37% formaldehyde (Fisher Scientific, Pittsburgh, PA)
- 16% W/V Paraformaldehyde (Electron Microscopy Sciences, Hatfield, PA)
- QuantiGene ViewRNA ISH Tissue 2-Plex Assay (Affymetrix, Santa Clara, CA)
- ThermoBrite Denaturation/Hybridization System 110/120 VAC (Abbott Molecular, Des Plaines, IL)
- RNase Zap spray (Sartorius, Göttengen, Germany)
- Mercedes StarFrost Platinum P/N MER 7255 slides (Mercedes Medical, Sarasota, FL)

- Gene Roller GRH10 hybridization oven (Savant, Midland, MI)
- Phosphate Buffered Saline (Mediatech, Manasses, VA)
- Stock ethanol
- Stock xylene
- YO-PRO-1 (Life Technologies, Grand Island, NY)
- Vectashield Hard Set (Vector Laboratories, Burlingame, CA)
- Wet and Wild nail polish (cheap nail polish from corner pharmacy)

A.3.2—Day 1—Sample collection

1. Sacrifice mice. Use a Sharpie or other method to mark the superior portion of the eye prior to enucleating.
2. Place the enucleated eye in a 4:1 V/V dilution of 16% W/V paraformaldehyde (PFA) in 1X PBS.
3. Let the eye fix at room temperature for 16-24 hr.

A.3.3—Day 2—Sample dehydration and paraffin embedding

1. Wash fixed eyes 3× in 1X PBS.
2. Puncture eyes on the temporal side with a 30 gauge needle.
3. Transfer eyes to an embedding cassette.
4. Prepare the following solutions for dehydration (all V/V): 50% ethanol, 60% ethanol, 70% ethanol, 80% ethanol, 90% ethanol, 95% ethanol, 100% ethanol (2×), 50%-50% ethanol-xylene mix, 100% xylene (2×). All solutions need to be

prepared fresh with stock solution and dH_2O. DO NOT, FOR ANY REASON, USE OLD SOLUTIONS. Paraffin for embedding does not to be fresh.

5. Transfer cassettes to 50% ethanol solution and let sit for 20 min.
6. Transfer cassettes to 60% ethanol solution and let sit for 20 min.
7. Transfer cassettes to 70% ethanol solution and let sit for 20 min.
8. Transfer cassettes to 80% ethanol solution and let sit for 20 min.
9. Transfer cassettes to 90% ethanol solution and let sit for 20 min.
10. Transfer cassettes to 95% ethanol solution and let sit for 20 min.
11. Transfer cassettes to 100% ethanol solution and let sit for 20 min.
12. Repeat step 11 with the second 100% ethanol solution.
13. Transfer cassettes to 50%-50% ethanol-xylene mix and let sit for 20 min.
14. Transfer cassettes to a hot (60 ºC) paraffin bath and let sit for 60 min.
15. Transfer cassettes to a second hot (60 ºC) paraffin bath and let sit overnight.

A.3.4—Day 3—Paraffin embedding of samples

1. Embed eyes in cassettes using paraffin embedding station in Boatright lab.
2. Orient the cornea to the left with the optic nerve to the right. The temporal puncture should be facing up.
3. Once the paraffin has set, wait until the next day to section.

A.3.5—Day 4—Sectioning of samples

1. Set hot water bath next to microtome 38 ºC with RNase free water. Spray the bath dish with liberal amounts of RNase Zap spray until it is covered. Rinse the spray

off with dH_2O and dry with a Kimwipe. Fill with dH_2O and let the water bath come to 38 ºC.

2. Prepare to section by cutting through the paraffin until you reach the optic nerve.
3. Prepare a room temperature dish to soak the eye. Spray the dish liberally with RNase Zap spray and rinse with dH_2O. Fill with dH_2O and let the eye soak in the block for 2.5-3.5 hr.
4. Set Gene Roller hybridization oven to 60 ºC.
5. Section the eye at 5-µm thickness. Let the sections sit in the hot water bath for 2 min before transferring them onto a StarFrost slide. Fit 2-3 sections onto a single slide.
6. Transfer the slides to a slide rack and place in the hybridization oven to let sit overnight (or 16-24 hr).

A.3.6—Day 5—Sample preparation and target probe hybridization

1. Set ThermoBrite to 60 ºC and bake the slides for 30 min with the lid open.
2. Prepare 2 L of 1X PBS.
3. Prepare 10% formaldehyde in 1X PBS in a fume hood by adding 146 mL 1X PBS to 54 mL 37% formaldehyde and mixing well.
4. Prepare 4% formaldehyde in 1X PBS in a fume hood by adding 178 mL 1X PBS to 22 mL 37% formaldehyde and mixing well.
5. Prepare 3× bottles of 1 L of Wash Buffer by adding 9 mL Wash Comp 1 and 2.5 mL Wash Comp 2 to 988.5 mL dH_2O.

6. Dilute 5 mL of 100X Pretreatment Solution in 495 mL dH_2O. Heat on a hot plate to 95-100 ºC.
7. Prepare 200 mL Storage Buffer by adding 60 mL Wash Comp 2 to 140 mL dH_2O and mixing well.
8. Prewarm 40 mL of 1X PBS and Probe Set Diluent QF to 40 ºC in hybridization oven.
9. After the slides have baked on the ThermoBrite for 30 min, pour 10% formaldehyde into a staining dish. Insert slides into a slide rack and let fix under a fume hood in 10% formaldehyde for 1 hr at room temperature.
10. Remove the slide rack from the 10% formaldehyde and was 2× in 1X PBS for 1 min with frequent agitation.
11. Remove each slide and flick to remove 1X PBS. Let slides dry on a paper towel to dry, and make sure they are completely dry before proceeding to the next step.
12. In a fume hood, pour fresh xylene solution into 2 staining dishes.
13. Place the slides back in a slide rack and wash in staining dish containing xylene with frequent agitation at room temperature for 5 min.
14. Repeat step 13 in the second xylene-containing staining dish.
15. Remove the slide rack from xylene and wash the slides 2× in 95% ethanol for 1 min.
16. Remove the slides from the slide rack and let dry on a paper towel for 15 min. Make sure the slides are completely dry before proceeding to the next step.

17. Create a hydrophobic barrier on each slide with a hydrophobic pen (Vecto Laboratories) 2-3 mm from the outer edge of the section. Let the hydrophobic barrier dry for 30 min.
18. Load the slides onto the slide rack and transfer the slide rack to the hot Pretreatment Solution (prepared in step 6).
19. Let the slides incubate at 95-100 ºC in Pretreatment Solution for 15 min.
20. Wash the slides 2× in dH_2O for 1 min with frequent agitation. Transfer the slides to a dish containing 1X PBS. DO NOT LET SLIDES DRY AFTER THIS STEP FOR ANY REASON.
21. Set the ThermoBrite to 40 ºC and insert humidity strips.
22. For each sample, prepare protease sample: 4 µl Protease QF in 396 µl 1X PBS (prewarmed to 40 ºC).
23. Remove slides from slide rack and tap to remove excess 1X PBS. Place the slides on the ThermoBrite.
24. Add 400 µl of the protease solution to each sample.
25. Close the lid to the ThermoBrite and let the samples incubate for 10 min.
26. Decant the protease solution from the slides and wash the slides in a slide rack 2× in 1X PBS.
27. Transfer the slides to a staining dish containing 4% formaldehyde and fix for 5 min at room temperature.
28. Wash the slides 2× in 1X PBS for 1 min with frequent agitation.
29. Save the 4% formaldehyde solution for the next day.

30. Prepare Probe Set Solution for each slide by adding 10 µl QuantiGene ViewRNA TYPE 1 Probe Set (user defined) and 10 µl QuantiGene ViewRNA TYPE 6 Probe Set (user defined) to 380 µl 40 ºC prewarmed 1X PBS.
31. Remove the slides from the slide rack and tap to remove excess 1X PBS.
32. Place the slides in the 40 ºC ThermoBrite and add 400 µl of Probe Set Solution to each slide.
33. Close the lid and let incubate at 40 ºC for 2 hr.
34. Decant Probe Set Solution and place the slides in a slide rack.
35. Wash slides 3× in Wash Buffer for 2 min with frequent agitation.
36. Store slides in Storage Buffer overnight (for a maximum of 24 hr).

A.3.7—Day 6—Signal amplification and detection

1. Prewarm PreAmplifier Mix QT, Amplifier Mix QT, and Label Probe Diluent QF buffers to 40 ºC in hybridization oven.
2. Place Label Probe 1-AP, Label Probe 6-AP, and Blue reagents on ice.
3. Bring Fast Red Tablets, Naphthol Buffer, AP Enhancer Solution, and Blue Buffer to room temperature.
4. Ensure availability of YO-PRO-1 for nuclei staining.
5. Remove the slides from Storage Buffer and wash 2× in Wash Buffer for 2 min with constant agitation.
6. Set the ThermoBrite to 40 ºC and insert humidity strips.
7. Swirl PreAmplifier Mix QT bottle briefly to ensure the solution is properly mixed.

8. Remove each slide and flick it to remove Wash Buffer.
9. Place slides in ThermoBrite, add 400 µl of PreAmplifier Mix QT, and close the lid to incubate slides at 40 ºC for 25 min.
10. Decant PreAmplifier Mix QT, place slides in a slide rack, and wash 3× in Wash Buffer for 2 min with constant agitation.
11. Swirl Amplifier Mix QT bottle briefly to ensure the solution is properly mixed.
12. Place slides in ThermoBrite and add 400 µl Amplifier Mix QT to each slide.
13. Close the lid and let incubate at 40 ºC for 15 min.
14. Decant Amplifier Mix QT from slides and wash 3× in Wash Buffer for 2 min with constant agitation.
15. Vortex mix and spin down Label Probe 6-AP before using. This is important.
16. Prepare 400 µl of Working Label Probe 6-AP Solution for each slide by adding 0.4 µl of Label Probe 6-AP to 399.6 µl prewarmed Label Probe Diluent QF.
17. Remove slides and flick to remove Wash Buffer.
18. Place the slides on ThermoBrite and incubate at 40 ºC for 15 min.
19. Decant Working Label Probe 6-AP Solution from the slides and insert them into a slide rack, washing 3× in Wash Buffer for 3 min with constant agitation.
20. I highly recommend turning the lights off in the lab at this point and keeping them off until the procedure is finished to prevent photobleaching of the dyes.
21. Prepare the Fast Blue Substrate. It is important that you add the reagents IN THIS EXACT ORDER to prevent precipitation in solution. Be sure to vortex mix each reagent and spin down briefly in a centrifuge before using. Add 5 mL of Blue Buffer to a 15 mL conical tube. Add 105 µl Blue Reagent 1 and VORTEX MIX

for 10 seconds. Add 105 µl Blue Reagent 2 and VORTEX MIX for 10 seconds. Add 105 µl Blue Reagent 3 and VORTEX MIX for 10 seconds. After making Fast Blue Substrate, keep the tube in the dark until use.

22. Remove each slide from the slide rack and flick to remove any remaining Wash Buffer. Place the slides in a box (not the ThermoBrite) and add 400 µl Fast Blue Substrate. Let incubate at room temperature for 30 min.
23. Decant Fast Blue Substrate, place slides into slide rack, and wash 2× with Wash Buffer for 2 min with frequent agitation.
24. Remove slides from slide rack and flick to remove excess Wash Buffer. Place the slides back in a dark box and add 400 µl AP Stop QT to slides. Incubate in the dark box at room temperature for 30 min.
25. Decant AP Stop QT from slides and wash slides in a slide rack 2× in 1X PBS for 1 min.
26. Wash slides 1× in Wash Buffer for 1 min with constant agitation.
27. Vortex mix and spin down Label Probe 1-AP before using. This is important because improper mixing will cause variations in signal strength.
28. Prepare 400 µl of Working Label Probe 1-AP Solution for each slide by adding 0.4 µl of Label Probe 1-AP to 399.6 µl prewarmed Label Probe Diluent QF.
29. Remove slides and flick to remove Wash Buffer.
30. Place the slides on ThermoBrite and incubate at 40 ºC for 15 min.
31. Decant Working Label Probe 1-AP Solution from the slides and insert them into a slide rack, washing 3× in Wash Buffer for 3 min with constant agitation.

32. Flick slides to remove Wash Buffer. Add 400 µl AP Enhancer Solution to each slide and incubate in the dark at room temperature for 5 min.
33. While the slides incubate, prepare the Fast Red Substrate. Add 5 mL of Naphthol Buffer to a 15 mL conical tube along with a single Fast Red Tablet. Vortex mix until the tablet is completely dissolved in buffer and store in the dark until use.
34. Decant AP Enhancer Solution and place the slides in the ThermoBrite. Add 400 µl of Fast Red Substrate to each slide. Close the lid and let incubate at 40 ºC for 30 min.
35. After incubation, decant Fast Red Substrate from slides and was the slides in a slide rack 1× in 1X PBS for 1 min with constant agitation.
36. Fix the slides in a slide dish containing 4% formaldehyde (saved from the *Day 5*) for 5 min in a fume hood at room temperature.
37. Wash the slides in 1X PBS for 1 min with frequent agitation.
38. Place the slides flat on the bench top and add a single drop of YO-PRO-1 stain to each section to stain nuclei. Let incubate at room temperature for 5 min.
39. Decant YO-PRO-1 stain flick to remove excess stain. Add a single drop of Vectashield Hard Set to each slide and carefully add cover slip.
40. Place the slides in the dark to let the mounting media set overnight.
41. The slides can be imaged the next day with a confocal microscope. At the end of the next day, make sure you add Wet and Wild nail polish to the edge of the cover slips so the slides do not dry. I have noticed there is not much signal loss for up to 1 month following staining. Slides should be stored at 4 ºC in a dark box when not being imaged.

A.4—Whole cell RNA extraction

The purpose of this protocol is to extract whole cell RNA from RPE/choroid for qRT-PCR. This protocol contains a modified homogenization (so there are no residual sclera chunks) and modified phenol-chloroform extraction using the Qiagen RNeasy kit. It is important to note that not all buffers from the kit are used during this procedure, so please be aware of this. In my experience, this procedure yields a relatively large amount of high-quality RNA. The homogenization portion of this protocol has been adapted from Micah Chrenek's protocol available on the EEC Research Forum webpage.

A.4.1—Reagents and equipment

- Trizol reagent (Life Technologies, Grand Island, NY)
- Stock chloroform (Fischer Scientific, Pittsburgh, PA)
- 100% ethanol (Fisher Scientific)
- MO-BIO Vortex Adaptor (MO-BIO, Carlsbad, CA)
- ¼-in #10-24 stainless steel set screws (ordered from Amazon)
- RNeasy Mini Kit with spin columns (Qiagen, Valencia, CA)
- Microcentrifuge set to 4 ºC.
- Molecular Grade Water (distilled, deionized, DNase, RNase, and protease free) (Mediatech, Manasses, VA)

A.4.2—Homogenization

1. Dissect fresh RPE/choroid/sclera tissue by puncturing the limbus with a 30-gauge needle and cutting around the limbus to remove cornea, iris, and lens. Cut the eyecup in one or two places to help flatten it, and use the dissecting scissors to gently sweep away the retina.
2. Place dissected RPE/choroid (add both from each eye to a single tube) in a 1.5-mL snap cap tube containing 900 µl Trizol reagent.
3. Add a single set screw to each tube. Make sure caps are securely sealing each tube before continuing.
4. Add tubes to MO-BIO Vortex Adaptor screwed onto the top of a vortex mixer.
5. Vortex mix continuously for 5 min or until tissue is completely homogenized.

A.4.3—RNA purification

1. Add 180 µl chloroform to each tube.
2. Vortex mix for 10 seconds (on a normal vortex mixer, NOT one with the adaptor).
3. Centrifuge at full speed (defined as no more than 13,000 ×*g* for all steps) at 4 ºC for 15 min.
4. Transfer 500 µl of aqueous layer to new tubes (the aqueous layer is the top, colorless layer). When removing the aqueous layer, do not disturb the organic layer.
5. Add 500 µl chloroform to each tube containing the aqueous layer. Vortex mix for 10 seconds.
6. Centrifuge tubes at full speed (defined above) at 4 ºC for 5 min.

7. Transfer 400 µl of aqueous (i.e. upper) layer to new tubes.
8. Add 300 µl 100% ethanol to each tube and vortex mix for 20 seconds.
9. Transfer the entire contents of the tube to RNeasy spin column.
10. Centrifuge at full speed at 4 ºC for 1 min.
11. Add 700 µl RW1 buffer (from RNeasy kit) to each column.
12. Centrifuge at full speed at 4 ºC for 1 min.
13. Add 500 µl RPE buffer (from RNeasy kit) to each column.
14. Centrifuge at full speed at 4 ºC for 1 min.
15. Add another 500 µl RPE buffer to each column.
16. Centrifuge at full speed at 4 ºC for 3 min to remove any residual buffer.
17. Add 60 µl molecular grade water to each tube.
18. Centrifuge at full speed at 4 ºC for 1 min.
19. Store tubes with purified RNA at -80 ºC.

A.4.4—Troubleshooting

1. Although you can treat your samples with DNase to remove any contaminating DNA, I've never noticed any problem with DNA contamination of my samples. Trizol preps are usually clean in my experience. You can also avoid concerns about contaminating DNA in your samples by using properly designed primers (e.g. primers that span exon-exon boundaries).
2. Yield can be variable, depending on the quality of dissection. In my experience, it can range between 10-30 ng/µl. The quality of the sample itself, though, should be constant.

A.5—Cell fractionation and RNA extraction of nuclear/cytoplasmic fractions

The purpose of this protocol is to separate RPE/choroid cells into nuclear and cytoplasmic fractions for RNA extraction for qRT-PCR. For the most part, this protocol follows the manufacturer's protocol in the SurePrep Nuclear or Cytoplasmic RNA Purification Kit sold by Fisher Scientific. I have made some modifications for working with RPE/choroid tissue, and those steps are included in the protocol. The homogenization portion of this protocol has been adapted from Micah Chrenek's protocol available on the EEC Research Forum webpage.

A.5.1—Reagents and equipment

- MO-BIO Vortex Adaptor (MO-BIO, Carlsbad, CA)
- ¼-in #10-24 stainless steel set screws (ordered from Amazon)
- dry ice
- SurePrep Nuclear or Cytoplasmic RNA Purification Kit (Fisher Scientific, Pittsburgh, PA)
- 100% ethanol (Fisher Scientific)
- 1 M dithiothreitol (DTT, Sigma-Aldrich, St. Louis, MO) solution (1 M DTT in 0.1 M sodium acetate, Fisher Scientific, Pittsburgh, PA)Molecular Grade Water (distilled, deionized, DNase, RNase, and protease free) (Mediatech, Manasses, VA)

A.5.2—Tissue preparation

1. Place 1.5 mL snap cap tubes into a tub of dry ice to cool them. This is necessary because the tissue needs to be flash-frozen immediately after dissection.
2. Dissect fresh RPE/choroid/sclera tissue by puncturing the limbus with a 30-gauge needle and cutting around the limbus to remove cornea, iris, and lens. Cut the eyecup in one or two places to help flatten it, and use the dissecting scissors to gently sweep away the retina.
3. Place the tissue (both RPE/choroid samples from the same mouse) into the snap cap tube and return it to the dry ice bucket. Wait 10-15 min.
4. While the sample freezes, prepare Lysis Solution. Lysis Solution is prepared by mixing 1 mL of Lysis Solution provided in the kit with 10 µl 1 M DTT.
5. Add 200 µl Lysis Solution to each frozen sample and add a single set screw to each sample.
6. Add tubes to MO-BIO Vortex Adaptor screwed onto the top of a vortex mixer.
7. Vortex mix continuously for 5 min or until tissue is completely homogenized.
8. The samples will appear frothy following homogenization. Remove the set screw with tweezers and briefly spin down to remove all bubbles.

A.5.3—Cytoplasmic RNA preparation

1. Spin lysate for 3 min at full speed. This is the step that separates the nuclei from the cytosol. The pellet has to be saved for nuclear RNA extraction.

2. Transfer supernatant (containing cytoplasmic RNA) to another tube. Keep the tube with the pellet (containing nuclear RNA) on ice for later steps.
3. Continuing with the tube containing the supernatant, add 200 µl Binding Solution (provided in the kit). Vortex mix for 10 seconds.
4. Add 200 µl 100% ethanol to the mixture and vortex mix for 10 seconds.
5. Transfer the mixture to a spin column (provided by the kit), and centrifuge at maximum speed for 1 min.
6. Discard the flowthrough.
7. Add 400 µl Wash Solution to the column and centrifuge at maximum speed for 1 min. Discard the flowthrough.
8. Repeat step 7.
9. Add another 400 µl Wash Solution to the column. Centrifuge for 2 min to remove any residual buffer.
10. Add 50 µl molecular grade water to column and centrifuge at 200×*g* for 2 min to elute.
11. Centrifuge at maximum speed for 1 min to elute RNA.
12. Store RNA samples at -80 ºC. RNA concentration is measured at 260 nm.

A.5.3—Nuclear RNA preparation

1. Add 400 µl Binding Solution to the lysate tube containing the pellet. Vortex mix for 10 seconds.
2. Add 200 µl 100% ethanol, and vortex mix for 10 seconds.
3. Transfer the solution to a spin column (provided in the kit).

4. Centrifuge at 13,000 ×*g* (max speed) for 1 min and discard the flowthrough.
5. Add 400 µl Wash Solution to the column and centrifuge at maximum speed for 1 min. Discard the flowthrough.
6. Repeat step 7.
7. Add another 400 µl Wash Solution to the column. Centrifuge for 2 min to remove any residual buffer.
8. Add 50 µl molecular grade water to column and centrifuge at 200×*g* for 2 min.
9. Centrifuge at maximum speed for 1 min to elute RNA.
10. Store RNA samples at -80 ºC.

A.5.4—Troubleshooting

1. Yield will most likely be low when compared to the yield expected from whole-cell RNA extraction (<50%).
2. If you want to check for the purity of each fraction, I would recommend checking for the presence of nuclear-specific RNA species factors (e.g. snoRNAs). These should only be found in the nucleus. They should be abundant in the nuclear fraction and at much lower levels in the cytoplasmic fraction.

A.6—Extraction of soluble and insoluble protein for SDS-PAGE

The purpose of this protocol is to prepare soluble and insoluble protein for SDS-PAGE from RPE/choroid samples. Because of the extremely limited amount of starting material (i.e. RPE cells) in a single mouse (approximately 100,000 cells), I recommend pooling RPE/choroid samples from the same mouse litter into the same tube. The homogenization portion of this protocol has been adapted from Micah Chrenek's protocol available on the EEC Research Forum webpage.

A.6.1—Reagents and equipment

- MO-BIO Vortex Adaptor (MO-BIO, Carlsbad, CA)
- ¼-in #10-24 stainless steel set screws (ordered from Amazon)
- dry ice
- 1 M dithiothreitol (DTT, Sigma-Aldrich, St. Louis, MO) solution (1 M DTT in 0.1 M sodium acetate, Fisher Scientific, Pittsburgh, PA)
- 1% sodium dodecyl sulfate (SDS)
- Radioimmunoprecipitation assay (RIPA) buffer (Teknova, Hollister, CA)
- cOMPLETE mini protease inhibitor tablet (Roche Applied Sciences, Indianapolis, IN)

A.6.2—Buffer preparation

1. Prepare Buffer A by dissolving a cOMPLETE mini tablet in 10 mL of RIPA buffer in a conical tube by vortex mixing at maximum speed. It may take a few minutes to dissolve the tablet.
2. Prepare Buffer B by dissolving 4.8 g urea, 100 µl 1 M DTT, and a cOMPLETE mini tablet in 10 mL 1% SDS to give a final concentration of 8 M urea.

A.6.3—Tissue dissection

1. Dissect fresh RPE/choroid tissue by puncturing the limbus with a 30-gauge needle and cutting around the limbus to remove cornea, iris, and lens. Cut the eyecup in one or two places to help flatten it, and use the dissecting scissors to gently sweep away the retina.
2. Place the tissue (both RPE/choroid samples from the same mouse) into a snap cap tube containing 200 µl Buffer A (expected yield for 10 mouse eyes is roughly 1 mg/ml).

A.6.4—Extraction of soluble proteins

1. Add a set screw to each sample pool tube, fasten top securely, and vortex mix on Vortex Adaptor for 5 min.
2. Use tweezers to remove set screw.
3. Centrifuge tube at full speed for 1 min to pellet insoluble material.

4. Remove supernatant and transfer to a new tube. Keep the tube containing the insoluble pellet for the next step. Store soluble protein extract at -80 ºC.

A.6.5—Extraction of insoluble proteins

1. Add 200 µl Buffer B to tube containing insoluble pellet.
2. Incubate in a 95 ºC water bath for 1 hr to dissolve pellet.
3. Centrifuge tube at full speed for 1 min to pellet insoluble material.
4. Remove supernatant and transfer to a new tube. Store insoluble protein extract at -80 ºC.
5. Store pellet from this extraction for further use if necessary.

A.7—Linear sucrose gradient fractionation and RNA extraction

The purpose of this protocol is to separate ribosome-free messenger ribonucleoproteins (mRNPs), monoribosome-bound mRNAs, and polyribosome-bound mRNAs into different fractions. Multiple RPE/choroid samples from multiple mice need to be pooled together so there is enough starting material for the assay. For my work, three mice were pooled together in a single sample. The protocol below is EXACTLY THE SAME PROTOCOL FROM THE YUE FENG LAB on Emory University's campus. My personal modifications to the protocol are at the end and involve RNA extraction from the sucrose gradient and generation of the qRT-PCR standard curve. Any questions regarding the fractionation itself should be directed toward Dr. Feng's laboratory. Because of the sensitive nature of mRNA-ribosome complexes, tissue dissections should be performed in the Feng laboratory immediately before fractionation, all of which is conducted in the Feng laboratory.

A.7.1—Reagents and equipment

- Polysome-preserving gradient buffer (10 mM Tris, pH 7.5, 100 mM KCl, 100 µg/ml cycloheximide, 5 µl RNase inhibitor [from Applied Biosystems])
- Polysome-dissociating gradient buffer (10 mM Tris, pH 7.5, 100 mM KCl, 10 mM EDTA, 5 µl RNase inhibitor [from Applied Biosystems])
- Triton X-100 (Sigma-Aldrich, St. Louis, MO)
- 15-45% (W/W) linear sucrose gradient prepared in either polysome-preserving or –dissociating gradient buffer

- Trizol (Life Technologies, Grand Island, NY)
- Trizol reagent (Life Technologies)
- Stock chloroform (Fisher Scientific, Pittsburgh, PA)
- 100% ethanol (Fisher Scientific)
- RNeasy Mini Kit with spin columns (Qiagen, Valencia, CA)
- Microcentrifuge set to 4 ºC.
- Molecular Grade Water (distilled, deionized, DNase, RNase, and protease free) (Mediatech, Manasses, VA)

A.7.2—Tissue dissection and homogenization

1. Dissect fresh RPE/choroid tissue by puncturing the limbus with a 30-gauge needle and cutting around the limbus to remove cornea, iris, and lens. Cut the eyecup in one or two places to help flatten it, and use the dissecting scissors to gently sweep away the retina.
2. Scrape away RPE/choroid with dissection scissors. Place the dissected RPE/choroid tissue into a tube containing either polysome-preserving or –dissociating gradient buffer and gently homogenize with a dounce homogenizer.
3. Incubate tissue at 4 ºC for 15 minutes to allow cycloheximide to arrest polysome migration along mRNA (or to dissociate mRNA from ribosomes if using buffer containing EDTA).
4. Add Triton X-100 to a final concentration of 1% (V/V) concentration.
5. Incubate on ice 15 min to lyse cells.
6. Pellet membranous cell structures by centrifuging at 20,000 ×*g* for 30 min.

A.7.3—Fractionation

1. Load supernatant (750 µl) into tube containing 11 mL of the sucrose gradient and centrifuge at 39,000×*g* for 90 min in an SW41 rotor at 4 ºC.
2. Fractionate using an Isco fractionating system (upward replacement fraction collection), measuring ribosome sedimentation by recording fraction absorbance at 254 nm.
3. Separate into 10 separate 1.1 mL fractions.
4. Keep samples on ice until RNA extraction.

A.7.4—RNA purification

1. Remove 300 µl of each sucrose fraction from each sample and transfer to a new tube. Store the remaining fraction at -80 ºC.
2. Add 600 µl Trizol to each fraction sample.
3. Add 180 µl chloroform to each tube.
4. Vortex mix for 10 seconds (on a normal vortex mixer, NOT one with the adaptor).
5. Centrifuge at full speed (13,000 ×*g* for all steps) at 4 ºC for 15 min.
6. Transfer 500 µl of aqueous layer to new tubes (the aqueous layer is the top, colorless layer). When removing the aqueous layer, do not disturb the organic layer.
7. Add 500 µl chloroform to each tube containing the aqueous layer. Vortex mix for 10 seconds.

8. Centrifuge tubes at 4 ºC for 5 min.
9. Transfer 400 µl of aqueous (i.e. upper) layer to new tubes.
10. Add 300 µl 100% ethanol to each tube and vortex mix for 20 seconds.
11. Transfer the entire contents of the tube to RNeasy spin column.
12. Centrifuge at full speed at 4 ºC for 1 min.
13. Add 700 µl RW1 buffer (from RNeasy kit) to each column.
14. Centrifuge at full speed at 4 ºC for 1 min.
15. Add 500 µl RPE buffer (from RNeasy kit) to each column.
16. Centrifuge at full speed at 4 ºC for 1 min.
17. Add another 500 µl RPE buffer to each column.
18. Centrifuge at full speed at 4 ºC for 3 min to remove any residual buffer.
19. Add 60 µl molecular grade water to each tube.
20. Centrifuge at full speed at 4 ºC for 1 min.
21. Store tubes with purified RNA at -80 ºC.

A.7—qRT-PCR

The purpose of this protocol is to quantify the amount of mRNA that is produced by a gene of interest relative to 18S RNA. The mastermix recipe presented in the protocol can be scaled up for 25 µl, but I prefer performing 10 µl reactions to conserve RNA samples that may be difficult to obtain from experiments that might not be easily repeatable. Use this protocol with the Eppendorf Realplex^2 machine located in the Boatright lab. This protocol has been adapted from Micah Chrenek's protocol available on the EEC Research Forum webpage.

A.7.1—Reagents and Equipment

- Realplex^2 thermal cycler (Eppendorf, Hauppauge, NY)
- QuantiTect SYBR Green PCR Kits (Qiagen, Valencia, CA)
- Primers specific for genes of interest
- Molecular grade water (Mediatech, Manasses, VA)
- RNA (harvested from tissue and diluted to 2 ng/µl)
- AB-1400/W Flat Deck Thermo-Fast 96 detection plate (Thermo Scientific, Waltham, MA)
- MSB-1001 Microseal B Adhesive Sealer (Bio-Rad, Hercules, CA)

A.7.2—Reaction Preparation

1. Prepare mastermixes (1 and 2) with the following recipes:

Component	Volume Per Reaction (µl)	Mastermix 1 Volume
Water	2.9	(Number of target genes × 4 + 3) × 2.9
SYBR green 2X mix (included in Qiagen kit)	5.0	(Number of target genes × 4 + 3) × 5.0
RNA	1.0	(Number of target genes × 4 + 3) × 1.0
RT mix (included in Qiagen kit)	0.1	(Number of target genes × 4 + 3) × 0.1

Component	Volume Per Reaction (µl)	Mastermix 2 Volume
Water	2.54	2.54 × 5
SYBR green 2X mix	5.0	5.0 × 5
RT mix	0.1	0.1 × 5
Mastermix 1 Volume	0.36	0.36 × 5

2. The mastermix recipes will allow for 4 technical repeats of each reaction.
3. Vortex mix each mastermix for 10 seconds and then briefly spin down in a centrifuge.
4. Add 9 µl of mastermix 1 to plate wells.
5. Add 1 µl primer to each well.

6. Add 9 µl mastermix 2 to four other wells.
7. Add 1 µl 18S primers to wells.
8. Seal plate with adhesive sealer.
9. Vortex mix plate for 10 seconds.
10. Spin down plate in centrifuge briefly at 3000 ×*g* (just until it stops accelerating).

A.7.3—Reaction Run

1. Program the following protocol into the Realplex^2 machine:
    a. Hold at 50.0 ºC for 30 minutes (for reverse transcription)
    b. Hold at 95 ºC for 15 minutes (for activation of *Taq* polymerase)
    c. Program 40 repeats of the following:
        i. 94.0 ºC for 15 seconds (DNA melting)
        ii. 55.0 ºC for 15 seconds (primer annealing)
        iii. 72.0 ºC for 40 seconds (polymerase extension)
    d. Melt curve analysis (to help determine primer specificity)
2. Place the plate into the machine and close it. Lock the top into place.
3. Run the reaction. This should take ~3 hours to complete.
4. View the melt curves. If the primers are specific, there should be a tight peak at the melting temperature (this means there is a loss of fluorescence at the same temperature in all PCR products, and this typically only happens if all the PCR products are identical, i.e., the primers are specific)
5. Set threshold to 200.
6. Save data to a Microsoft Excel file (this is the default option for saving data)

7. Save protocol.
8. Close out of the program.
9. Transfer data to a data stick for analysis.
10. Save the plate at -20 ºC.

A.7.4—Data Analysis

1. Average Ct values from the four technical repeats together.
2. Subtract average 18S Ct value from average Ct value from gene of interest to produce dCt values for each gene. This is known as normalization.
3. When comparing multiple samples of the same genotype, subtract all dCt values from all samples from the first sample dCt value. This will give the ddCt value. For other genotypes, subtract all dCt values from the first dCt value in the first genotype to give ddCt values.
4. Calculate 2^(-ddCt) values for each sample in the experiment.
5. Average 2^(-ddCt) values from four technical repeats together.
6. Plot the data.

A.7.5—Notes and important considerations

1. Although the melt curve analysis can determine if a homogenous product is produced by amplification, it still does not provide information about whether the gene of interest is actually the DNA segment being amplified. I recommend DNA sequencing of the PCR product to verify whether the gene of interest is actually what is being amplified in the reaction.

2. I typically use Eurofins MWG Operon for this. In my personal opinion, they produce cleaner sequence than GeneWiz or other companies. Also, there is the added benefit of the fact that Eurofins MWG Operon will actually send you the chromatogram data from their Sanger sequencing. This can be especially useful if the DNA sequence in the text files that are sent back to you in the results have "N" in the sequence. If that occurs, it's usually because the chromatogram was not clear enough for their computers to identify what nucleotide was sequenced. You might be able to make a better call, and if nothing else, I would consider it good practice to verify that the nucleotides being sequenced were identified correctly throughout the entire sequence.
3. Qiagen primer sequences are proprietary, and they will not issue a Certificate of Analysis for them. Their primers are pre-mixed with both forward and reverse primers, so you will not be able to perform DNA sequencing on the PCR products (Sanger sequencing uses forward primer only). I would recommend subcloning the PCR products into a TA cloning vector (I did this in Chapter 4 of my dissertation) and using T7 primers to sequence the PCR insert.

A.8—Immunoblotting

The purpose of this protocol is to identify whether a peptide of interest is present in cells or tissue, and if the peptide is of the expected molecular weight. This protocol makes use of Micah Chrenek's immunoblotting protocol that is found on the EEC Research Forum webpage. This protocol makes use of the Bio-Rad Criterion system. For the purposes of this protocol, I will not be listing a specific gel or running buffer that was used. That information can be found in the Methods sections of Chapters 3 and 4 of the dissertation.

A.8.1—Reagents and Equipment

- Gene Roller GRH10 hybridization oven (Savant)
- Criterion gel (Bio-Rad, Hercules, CA)
- Criterion running buffer (Bio-Rad)
- Methanol (Fischer Scientific, Pittsburgh, PA)
- Primary antibody specific to peptide of interest
- HRP-conjugated secondary antibody
- Western Blocking Reagent (Roche Applied Science, cat no 11 921 681 001, Indianapolis, IN)
- ECL Plus (Amersham Biosciences, Piscataway, NJ)
- 1 M dithiothreitol (DTT, Sigma-Aldrich, St. Louis, MO) solution (1 M DTT in 0.1 M sodium acetate, Fisher Scientific, Pittsburgh, PA)
- 4X loading dye (Life Technologies, Grand Island, NY)
- Saran wrap

- Criterion blotter filter paper (Bio-Rad)
- Criterion nitrocellulose membrane (Bio-Rad)
- Tris-buffered saline buffer (Mediatech, Manasses, VA)
- Tween-20 (Sigma Aldrich)
- Criterion gel box (Bio-Rad)
- Criterion transfer box (Bio-Rad)
- Tris (Sigma-Aldrich)
- Glycine (Sigma-Aldrich)

A.8.2—SDS-PAGE

1. Prepare protein samples for SDS-PAGE by adding protein sample, 1X 1M DTT, and 1X loading dye (and water, if needed to make all the samples the same volume).
2. Heat the samples in a 70 ºC water bath for 10 min.
3. Remove precast Criterion gel from storage.
4. Remove the comb and bottom tape from the gel.
5. Insert gel into one of the slots in the Criterion gel box with the upper chamber of the gel facing towards the center of the box.
6. Repeat for a second gel if using 2 gels.
7. Fill the upper buffer chamber in each gel with 60 ml running buffer.
8. Fill the bottom of the gel box with 800 ml running buffer.
9. Clean the wells of the gel with loading buffer and gel loading tips.
10. Add samples to wells.

11. Run at 200V for 50 min.

A.8.3—Protein Transfer

1. Prepare transfer buffer by mixing 6.06 g Tris, 28.8 g Glycine, 1600 ml water, and 400 ml methanol together.
2. Break the plates of the Criterion gel apart using the lid from the gel box.
3. Equilibrate both gel and nitrocellulose membrane in transfer buffer for 5 min.
4. Fill the Criterion transfer box with transfer buffer until it is half full.
5. Place a magnetic stir bar in the buffer tank.
6. Place a frozen ice pack in the back of the cell.
7. Flip down the transfer box lever to hold the ice pack in place.
8. Place the transfer box onto a magnetic stir plate and set to a slow stir speed.
9. Set up the gel/membrane sandwich plate (included with Criterion transfer box).
    a. Pour transfer buffer into each compartment of the gel/blot assembly tray (included with the transfer box).
    b. Place the cassette in the large compartment of the tray with the black portion of the cassette submerged.
    c. Place a piece of filter paper on top of the black side of the cassette.
    d. Place the gel on top of the filter paper. Remove any bubbles that may have been trapped using a roller.
    e. Transfer the membrane from the small tank and place on top of gel. Be careful not to trap any air bubbles. The membrane should not be moved or adjusted once it touches the gel.

f. Place a piece of filter paper on top of the membrane.

g. Place another piece of filter paper on top.

h. Clamp the cassette and transfer to transfer box. Align the red side of the cassette with the red plate.

10. Add the remaining transfer buffer to the fill level marked on the tank.
11. Attach the lid and plug in the power supply.
12. Run at 300 mA for 90 minutes.
13. Once the transfer is complete, disassemble, and place the membrane between dry blotting paper for storage at room temperature until ready for use. Do not use until it has dried.

A.8.4—Immunoblotting

1. Prepare 1X TBS by diluting 100 ml 10X stock TBS in 900 ml of water.
2. Prepare TBST by adding 1 ml Tween-20 to 1 L 1X TBS.
3. Prepare 1% blocking solution by diluting 10 ml of Western blotting reagent in 90 ml TBS.
4. Prepare 0.5% blocking solution by diluting 50 ml 1% blocking solution with 50 ml TBS.
5. Block unspecific binding of primary antibody by incubating the membrane for 1 h in 1% blocking solution in hybridization oven at room temperature.
6. Incubate membrane for 1 h with primary antibody diluted in 0.5% blocking solution at room temperature.

7. Was twice in TBST for 10 min each, then twice with 0.5% blocking solution for 10 min each.
8. Incubate membrane for 1 h with secondary antibody diluted in 0.5% blocking solution.
9. Was four times in TBST for 15 min each.
10. Detect bands using ECL kit and X-ray film in the dark.

A.8.5—Troubleshooting

1. It is important to expose the blot to x-ray film as soon as possible after adding the ECL substrate. The signal will begin to inhibit itself within a few minutes after treatment. To get the best signal possible, I would highly recommend not waiting longer than five minutes to expose the blot to film.
2. Make sure you watch the loading dye when performing SDS-PAGE. Different gels will run at different speeds, so make sure you do not run the gel for too long or smaller molecular weight proteins will run off the bottom.
3. If you have concerns about the efficiency of your transfer of protein from gel to nitrocellulose membrane, stain the gel with Coomassie blue after transfer. There should be nothing left in the gel if the transfer is efficient.